CONSENSUS OVER NETWORKED DYNAMICAL SYSTEMS

CONTROL, DESIGN, & INTERACTION

MATHIAS HUDOBA DE BADYN

A dissertation submitted in partial fulfillment of the requirements for the degree of

DOCTOR OF PHILOSOPHY

University of Washington

June 2019

READING COMMITTEE:

Mehran Mesbahi, Chair
Kristi Morgansen
Lillian Ratliff

PROGRAM AUTHORIZED TO OFFER DEGREE:

William E. Boeing Department of Aeronautics and Astronautics

University of Washington

ABSTRACT

CONSENSUS OVER NETWORKED DYNAMICAL SYSTEMS

CONTROL, DESIGN, & INTERACTION

MATHIAS HUDOBA DE BADYN

CHAIR OF THE SUPERVISORY COMMITTEE:

Mehran Mesbahi

William E. Boeing Department of Aeronautics and Astronautics

This dissertation focuses on three main aspects of control theory applied to networked dynamical systems – how to control networked systems, how to design networks to facilitate control and estimation for such systems, and how to reason about interacting with them. We examine how network symmetries and how the distribution of cooperative and antagonistic interactions facilitate control of the seminal consensus protocol, as well as measures that indicate how well a network facilitates consensus. Various tools for designing complex networks are developed in this dissertation, including decentralized update schemes for improving network edge weights and the time scales on which the agents in the network operate. The crux of the analysis of these algorithms lies in a beautiful connection between electrical network theory, the paradigm of series-parallel networks, and multi-agent consensus. Lastly, we examine how to design feedforward and feedback controllers for consensus networks that have state-dependent edge switching. The key tool is a continuum approximation of the agent dynamics, which allows for an optimal transport approach for feedforward control, and a density gradient feedback scheme.

Dedicated to my parents and my grandmother.

PUBLICATIONS

Some ideas and figures have appeared previously in the following publications:

INCLUDED PUBLICATIONS

[2] M. H. Matheny, J. Emenheiser, W. Fon, A. Chapman, M. Rohden, A. Salova, J. Li, M. Hudoba de Badyn, L. Duenas-Osorio, M. Mesbahi, J. P. Crutchfield, M. C. Cross, R. M. D'Souza, and M. L. Roukes, "Exotic states in a simple network of nanoelectromechanical oscillators," *Science*, vol. 363, no. 6431, pp. 1–10, 2019. DOI: 10.1126/science.aav7932.

[22] M. Hudoba de Badyn and M. Mesbahi, "Growing controllable networks via whiskering and submodular optimization," in *Proc. 55th IEEE Conference on Decision and Control*, Las Vegas, USA, 2016, pp. 867–872, ISBN: 9781509018369. DOI: 10.1109/CDC.2016.7798376.

[23] M. Hudoba de Badyn, *On the Control of Consensus Networks: Theory and Applications*. Seattle, USA: Master's Thesis, 2017.

[60] M. Hudoba de Badyn and M. Mesbahi, "Large-scale distributed Kalman filtering via an optimization approach," *IFAC-PapersOnLine*, vol. 50, no. 1, pp. 10 742–10 747, 2017.

[61] M. Hudoba de Badyn, U. Eren, B. Açıkmeşe, and M. Mesbahi, "Optimal mass transport and kernel density estimation for state-dependent networked dynamic systems," in *Proc. 57th IEEE Conference on Decision and Control*, Miami Beach, USA, 2018.

[62] S. Alemzadeh, M. Hudoba de Badyn, and M. Mesbahi, "Controllability and stabilizability analysis of signed consensus networks," in *Proc. IEEE Conference on Control Technology and Applications*, Kohala Coast, USA, 2017, pp. 55–60.

[63] M. Hudoba de Badyn, S. Alemzadeh, and M. Mesbahi, "Controllability and data-driven identification of bipartite consensus on nonlinear signed networks," in *Proc. 56th IEEE Conference on Decision and Control*, Melbourne, Australia, 2017.

[71] M. Hudoba de Badyn, A. Chapman, and M. Mesbahi, "Network entropy: A system-theoretic perspective," in *Proc. 54th IEEE Conference on Decision and Control*, Osaka, Japan, 2015, pp. 5512–5517.

[77] D. R. Foight, M. Hudoba de Badyn, and M. Mesbahi, "Time Scale Design for Network Resilience," in *Submitted to Proc. 58th IEEE Conference on Decision and Control*, Nice, France, 2019, pp. 1–8.

[78] M. Hudoba de Badyn, D. R. Foight, and M. Mesbahi, "Time Scale and Edge Weight Design for H2 Performance on Consensus Networks," *To be submitted to the IEEE Transactions on Control of Network Systems*, vol. XX, no. X, pp. 1–10, 2019.

[96] B. Barzgaran, M. Hudoba de Badyn, and M. Mesbahi, "Growing Controllable Networks via Single and Multi-Node Attachments," in *In prep*, Chicago, USA, 2019, pp. 1–6.

[98] M. Hudoba de Badyn and M. Mesbahi, "Efficient Computation of Performance on Series-Parallel Networks," in *Proc. American Control Conference*, Philadelphia, USA, 2019, pp. 1–6.

[99] ——, "H2 Performance of Series-Parallel Networks : A Compositional Perspective," *Submitted to the IEEE Transactions on Automatic Control*, vol. XX, no. X, pp. 1–13, 2019.

I've never seen the Icarus story as a lesson about the limitations of humans.
I see it as a lesson about the limitations of wax as an adhesive.

— Randall Munroe

ACKNOWLEDGMENTS

I would first like to thank my parents for raising me, and for being scientific role models. I also would like to apologize to my mother for asking if I could replace her with Ms. Frizzle at the tender age of 3. She was really the true Ms. Frizzle all along, except with a Subaru Forester instead of a nonphysical school bus. Although the amount of clutch replacements on that vehicle does make me suspect it was used for some sort of offroad scientific exploration.

Secondly, I want thank the staff at the William E. Boeing Department of Aeronautics and Astronautics. From even my undergraduate days when I was applying to the AA department, Ed Connery and Wanda Frederick treated me with the same friendliness and respect that carried over when I eventually joined the university as a doctoral student. I wish Wanda all the best in her retirement. The other members of the staff were also fantastic to work with over the years. I'd like to thank Victor Aque, Jenny Park, Winnie Lin, Leah Panganiban, Pam McGrath, and all the other staff members whom I didn't interact with personally, but I'm sure still contributed strongly to my success here.

I am incredibly grateful to Mehran Mesbahi for being my advisor, mentor, and for helping me travel the world. His hard work behind (literal) closed doors allowed me to pursue my dreams of becoming a scientist (a rocket one, at that!), and his calm, friendly demeanour was a great blanket, filling me with solace in the face of the soul-crushing academic world. I also want to thank the members of my qualifying exam, general exam, and dissertation commitees. Mehran Mesbahi, Christopher Lum, Setthivoine You, Kristi Morgansen, Jon Wellner and Lillian Ratliff all helped me enourmously in my growth as a student of control theory.

To the Canadian and American taxpayer, I thank you for giving me money. In particular, I was generously funded by the National Sciences and Engineering Research Council of Canada under grant CGSD2-502554-2017, the U.S. Army Research Lab and U.S. Army Research Office under contract number W911NF-13-1-0340, and the U.S. Air Force Office of Scientific Research under grant number FA9550-16-1-0022. This work could not have been completed with your help. In this list, I also have to thank the project managers and coordinators on the Network Control MURI Grant, which include Alfredo Garcia, Purush Iyer, and Ananthram Swami. I'm also very grateful to the Erwin Schrödinger International Institute for hosting me from May 3–May 19 of 2019 during the Optimal Transport Workshop.

For the Network Control MURI Grant, I have to thank all of my collaborators, and especially Raissa D'Souza for doing a fantastic job organizing this massive scientific endeavour. The team of course includes Mehran, but also Michael Roukes, Jim Crutchfield, Leonardo Duenas-Osorio, Anastasiya

Salova, Martin Rohden, Airlie Chapman, Matt Matheny, Jeff Emmenheiser, Warren Fon, Jordan Snyder, Kelly Finn, Siavash Alemzadeh, Afshin Mesbahi, Brianne Beisner, Brenda McCowan, and many others.

From the University of Washington library system, I would like to thank Lisa Bacis and all of the librarians that found books and scanned old articles for me through the online request portal. The UW Libraries are truly world-class, in great part due to the work of the staff.

I've made many friends at the University of Washington, some of whom contributed to my success, and some of whom may or may not have de-contributed to my success. The members of the Robotics, Aerospace and Information Networks lab have most definitely been the former – Dillon Foight, Siavash Alemzadeh, Taylor Reynolds, Bijan Barzgaran, Jingjing Bu, Tom Miesen, Aditya Deole, Dian-Jing Chen, Soumya Vasisht, Caroline Schlemmer, Airlie Chapman, Afshin Mesbahi, Unsik Li, Eric Schoof, Robert Vasil, Kerney Wu, Pietro Pierpaoli, Saghar Hosseini, Will Howerton, Dave Besson, Shariar Talebi, Newsha Rahimi, and Mengyuan Wang. My collaborators in the other control labs have also been instrumental to my success. I'd like to thank Utku Eren, Adam Tahir, Miki Szmuk, Sarah Li, Yue Yu, Sierra Adibi, Armand Awad, Emma Hansen, Max Spetzler, Alison Zongolowicz, Dan Calderone, Doris Voina, Skye Mceowen, Elliot Claveau, Chris Everson, Alice Liu, Ena Hodzic, Pablo Posada, Gustavo Fujiwara, Sean Phenisee, Tony Deleo, Jithin George, Ellie Forbes, Abhiram Aiwal, Dawei Lu, Osazonamen Igbinosun, Danylo Malyuta, Sean Rice and everyone else that I forgot here. A special place in my heart goes out to Armin Mortazavi, the Sports Champion; and Michael Grudich, the Fortran master – the two brothers I never had.

There are far too many professors to list who have significantly impacted my success, but I will try nonetheless to do this justice. Back in my early undergraduate days, Mark Van Raamsdonk was one of the first who taught me how the academic career path looked like, and helped me land my first research job. In that job, I must thank James Owen for being my advisor and helping me get my first paper published, and for introducing me to fine ales. My second research job was with Richard Marchand and Richard Sydora, who helped me author my first first-author paper, and I will be forever grateful. Joanna Karczmarek taught me so many things while I did my undergraduate physics thesis with her, but most of all she believed in me more than I did. Greg Martin's patience and guidance as I did my undergraduate mathematics thesis with him helped me mature as a mathematician, at least a little bit.

When I entered graduate school, the faculty at the Aeronautics & Astronautics departments were the key to any success I have achieved. Apart from Mehran Mesbahi, the remainder of the controls faculty including Kristi Morgansen, Christopher Lum, and Behçet Açıkmeşe all helped me in my transition to a new field, and propelled me in a direction that helped me publish a number of papers. In electrical engineering, Maryam Fazel and Sam Burden taught me a great deal about optimization and reinforcement learning. These tools I will take with me for the rest of my career. I owe a huge debt of gratitude to Lillian Ratliff for being a constant source of advice about research goals, and the academic job market. Her comments on my application packet were paramount in my success in obtaining a job after graduating.

In my dual life in the mathematics department, I received a warm welcome, despite being a practitioner of the forbidden arts of engineering, from many of the students and faculty. In particular, I would like to thank Sara Billey for her aid in understanding combinatorics, as well as Dmitriy Drusvyatskiy and Soumik Pal for their work as my *de facto* advisors during my mathematics Master's. Ioanna Dumitriu cemented my knowledge of linear algebra, which of course is the basis of all of control theory, and Jim Burke taught me about line search methods. I'm especially grateful to Jack Lee and John Palmieri for admitting me to the Master's program in the first place.

I'm grateful to Si-Gung John Leong, Sifu Alan Houp and Si-Jie Lotus Houp at the Seattle Kung Fu Club for the wonderful time learning martial arts throughout the later years of my PhD. The Civil Air Patrol, Seattle Squadron, had the patience to sit through several of my presentations, appropriately titled "Droning About Drones". They taught me a lot about how many of the formation control algorithms presented in this work can be used in practice in search-and-rescue operations, and hopefully one day save lives. I would like to thank the bartenders at Big Time Brewing and the Toronado, especially the late Matt Bonney. I'd pour one out in celebration of our times together, but given your former profession, that seems inappropriate. I only wish I had the chance to say goodbye.

Contents

List of Figures

List of Tables

Part I

NETWORKS

1

CONSENSUS ON NETWORKS

1.1 NETWORKS AND NETWORKED DYNAMICAL SYSTEMS

Humans as a species are, by nature, social. From the dawn of civilization, humans have banded together and formed social groups, with complex interactions both between groups and between individual human beings. As civilization and technology progressed over time, this instrinsic desire to create bonds between each other and to stay connected has been reflected in the very core of things we have created. The wonders of the modern age encompass miraculous technologies such as the Internet, wireless communication, and global transportation in the form of roads and airline traffic. Although not all of the effects of these technologies on human society and the planet at large are positive, their very existence is the result of a desire to understand the physical laws of the world, and to close the the distance between individual humans.

At the core of human interaction is the notion of a social network – pairwise interactions between humans. Such interactions can be considered friendly or antagonistic, or something more akin to the (in)famous Facebook relationship status "It's Complicated". Humans are clearly not the only socially interacting living beings, nor the only natural or synthetic system that is described by a network. The goal of this dissertation is to exposit a general framework for studying interactions of dynamic agents on networks – how the structure of the network affects the dynamics and behaviour of people, processes and information propaging over the networks.

Networks are comprised of a system of individual agents, and interactions among those agents. In recent years, a paradigm of studying distributed systems as an emergent structure out of a network has attracted significant research interest. The individual agents in a network can make local, autonomous, and decentralized decisions in order to coordinate to some global objective. For large networks, this allows for distributing out computational resources across many agents, thus requiring lower computational power in each agent. Furthermore, large networks are also robust to individual agent failures – many agents means greater redundancy.

Such networked dynamical systems can be synthetic – for example, cyber-physical systems such as power grids or the Internet, or even the Internet of Things. A topic of significant interest and potential impact is autonomous robotics, ranging from swarms of unmanned aerial vehicles for disaster response or space exploration, to autonomous cars coordinating together on a traffic network. Natural networked dynamical systems include the flocking of animals, such as geese, fish or buffalo, or abstract notions of distributed systems such as genetic regulatory networks.

All of these networked dynamical systems share the key feature of having several notions of dynamics. Each agent has their own decision-making dynamics, but this is influenced by a higher-order protocol that dictates a

dynamical interaction, or information sharing, between agents. As a mathematical object, networks are a powerful analysis tool for separating these two notions.

In this thesis, we examine the latter – the notion of information-sharing protocols over networks that agents use to augment their internal decision-making, or their self-dynamics. The most common and useful such protocol is called *consensus*. This begs the question addressed in the next section.

1.2 WHY CONSENSUS?

Consensus is a popular algorithm for allowing a networked dynamical system to agree on a common value of some parameter utilized in their self-dynamics. It is a simple protocol in principle – each agent averages the value of the parameter that they hold with that of their neighbours. However, consensus has a rich theoretical literature. Despite its simplicity, it is a protocol that is very much affected by the instrinsic structure of the network it is running on, and is thus amenable to analysis using graph theory.

Because of its control-theoretic pedigree, it is one of the premier protocols of choice when attempting to study the interplay between dynamics, or the study of differential equations, with the discrete world – that of combinatorics, graph theory and network science. Furthermore, many natural systems actually have dynamics that are captured by consensus as a first-order approximation.

As part of the motivation of the work in this thesis, we outline some common examples below.

1.2.1 *Consensus in Coordination [1]*

Consider the problem of n agents trying to *flock*, i.e. move in the same heading and velocity. Suppose, for simplicity, that the agents are double-integrator Newton particles:

$$\begin{aligned}\dot{q}_i &= p_i \\ \dot{p}_i &= u_i,\end{aligned}$$

where $1 \leq i \leq n$ denotes the agent, and each $q_i, p_i \in \mathbb{R}^3$. A choice of control that will achieve flocking is the following:

$$u_i = -\nabla V(q) - \mathcal{L}_{\mathcal{G}} p,$$

where $\mathcal{L}_{\mathcal{G}}$ is the *graph Laplacian*, and $V(q)$ is a potential function of the form

$$V(q) = \frac{1}{2} \sum_i \sum_{j \neq i} \psi_\alpha \left(\|q_j - q_i\| \right).$$

Here, ψ_α is a function describing the interaction between agents – it may increase or decrease as a function of distance $\|q_j - q_i\|$ between agents i and j.

The term $-\mathcal{L}_{\mathcal{G}}p$ is what is known as *consensus*. The graph Laplacian $\mathcal{L}_{\mathcal{G}}$ both encodes the connectivity structure of the network, but also encapsulates the notion of distributed averaging – the quantity p_i is averaged continuously over time with the neighbours of i.

1.2.2 *Consensus in Oscillator Networks [2]*

A *nanoelectromechanical oscillator* is a small, piezoelectric membrane approximately 100μm in size, consisting of a clamped aluminum nitride ultrathin plate. Such oscillators can be electrically coupled, and tuned to precise resonant frequencies with high quality factors. Consider a system of nanoelectromechanical oscillators, electrically coupled in a ring (each oscillator is connected to two others). Then, the dynamics of the jth oscillator can be described by a complex-valued amplitude A_j satisfying

$$\frac{dA_j}{dt} = -\frac{A_j}{2} + \frac{A_j}{2|A_j|} + i\left[\omega_j A_j + \alpha|A_j|^2 A_j\right] - i\beta A_j + \frac{i\beta}{2}\left(A_{j-1} + A_{j+1}\right). \tag{1.1}$$

The coupling between oscillator j, and its neighbours $(j-1)$ and $(j+1)$ is given by the last term $\frac{i\beta}{2}(A_{j-1} + A_{j+1})$.

By considering the phasor $A_j = a_j e^{i\phi_j}$, Equation (1.1) can be decomposed into *amplitude* (a_j) and *phase* (ϕ_j) dynamics:

$$\begin{aligned}\frac{da_j}{dt} &= \frac{1-a_j}{2} - \frac{\beta}{2}\left[a_{j+1}\sin\left(\phi_{j+1}-\phi_j\right) + a_{j-1}\sin\left(\phi_{j-1}-\phi_j\right)\right] \qquad (1.2)\\ \frac{d\phi_j}{dt} &= \omega_j + \alpha a_j^2 - \beta + \frac{\beta}{2a_j}\left[a_{j+1}\cos\left(\phi_{j+1}-\phi_j\right) + a_{j-1}\cos\left(\phi_{j-1}-\phi_j\right)\right].\end{aligned}$$

In Equation (1.2), the term

$$\left[a_{j+1}\sin\left(\phi_{j+1}-\phi_j\right) + a_{j-1}\sin\left(\phi_{j-1}-\phi_j\right)\right]$$

is known as *Kuramoto coupling*, after the famed Kuramoto oscillator model.

If oscillator j is connected to more than two other oscillators, we can write this term as

$$\sum_{k\in N_j}\left[a_k\sin\left(\phi_k-\phi_j\right)\right],$$

where N_j is the set of neighbours of oscillator j. When the oscillators are *phase synchronized*, in that $\phi_j \approx \phi_i$, then $\sin(\phi_k - \phi_j) \approx \phi_k - \phi_j$, and so this term becomes

$$\sum_{k\in N_j}\left[a_j\left(\phi_k-\phi_j\right)\right] = -\mathcal{L}_{\mathcal{G}}\phi,$$

where ϕ is the stacked vector of the phases. Thus, in the natural dynamics of certain physical oscillator networks, the graph Laplacian captures the

steady-state notion of synchronization – one dynamic interpretation of 'agreement'.

1.2.3 *Consensus in Opinions [3]*

Suppose that n individuals are discussing their opinion on a certain topic. For example, some individuals may prefer cats over dogs, and others dogs over cats, and some may be neutral[1]. One way of encoding this is by assigning a numerical value x_i over a *spectrum* of opinions to each agent, with one extreme representing cat people, and the other dog people.

One model of studying how opinions propagate in such a circumstance is known as the *opinion dynamics with bounded confidence*. This is a discrete-time process, in which each agent only averages their opinion with neighbours whose opinions are ϵ_i-close to theirs:

$$x_i(t+1) = \frac{1}{|N_i(t)|} \sum_{j \in N_i(t)} x_j(t). \tag{1.3}$$

Here, $N_i(t)$ is the set of neighbours of agent i, which is given by

$$N_i(t) = \{j \ : \ |x_i(t) - x_j(t)| \leq \epsilon_i\}.$$

Note that this set of neighbours is time-dependent: as opinions change over time, two agents who find themselves at too large of a disagreement will cease contact with each other. This causes them to no longer share information, and thus they no longer influence each other.

The dynamics in Equation (1.3) can be interpreted as a discrete-time consensus protocol. Since Equation (1.3) is nothing but a linear combination of some of the agent states x_j, this can be interpreted as a matrix-vector multiplication. The matrix will have a zero-structure corresponding to the connection structure of a dynamic graph – two agents are connected if and only if their opinions are ϵ_i (or ϵ_j) close.

1.2.4 *Consensus in Natural Systems [4]*

In an earlier subsection, we introduced the flocking problem – what control signals should agents compute and actuate in order to achieve consensus on heading and velocity? The inverse question is also appropriate: given a natural system that flocks, say of birds or fish, what dynamics accurately capture the observed behaviour?

1 Such an example may sound contrived, but there are many other pressing discussions of this form that include some notion of bipartisanship. For example, politics, or the debate between `vim` versus `emacs`.

Cucker and Smale proposed a flocking model based on distributed averaging – at time t, each bird i does a discrete-time averaging process on velocity (here v_i is a scalar):

$$v_i(t+1) - v_i(t) = \sum_{k=1}^{k} a_{ij} \left(v_j(t) - v_i(t) \right). \tag{1.4}$$

The *weight* a_{ij} is computed as a function of the distance between birds – a bird may wish to average with its closer neighbours more readily than neighbours farther away, both for deconfliction purposes as well as the simple fact that velocity is likely judged more accurately at close distances.

Cucker and Smale proposed the function

$$a_{ij} = \frac{K}{(\sigma^2 + |x_i - x_j|)^{\beta}},$$

where $\sigma > 0, \beta \geq 0$ and K are all tuning parameters.

The dynamics in Equation (1.4) can then be written in terms of the graph Laplacian and the stacked velocity vector v:

$$\begin{aligned} x(t+1) - x(t) &= v \\ v(t+1) - v(t) &= -\mathcal{L}_{\mathcal{G}}(x)v. \end{aligned}$$

A continuous-time process may be inferred by taking appropriate limits between timesteps as:

$$\begin{aligned} \dot{x} &= v \\ \dot{v} &= -\mathcal{L}_{\mathcal{G}}(x)v. \end{aligned}$$

This is, again, a consensus algorithm, albeit with a *state-dependent* graph Laplacian.

1.3 OVERVIEW OF THESIS

In this thesis, we use consensus as a prototypical example of a networked dynamical system on which the effects of the network topology on the dynamics becomes apparent. The research discussed in this thesis all relates to answering questions regarding how the network can be used, abused or tuned when designing distributed control systems.

The structure of the network allows for a combinatorial number of additional parameters to tune when considering control design for distributed systems. For example, one can consider the choice of the actual network structure as a design choice, as well as the strength or type of interaction between individual agents. The notion of feedback control now can take into account the state of neighbouring agents. Even individual parameters for how the agent takes the information from its neighbours into account when computing its control action can be considered a control design problem.

As such, it is easy to lose focus in the large breadth of questions one can ask in this research area. In this thesis, we separate the task of examining the effect of the network on the system into three questions.

1. How does the network structure affect the controllability of a networked dynamical system?
2. How can one design a network *a priori* to facilitate control? What are the right metrics on which to measure this performance?
3. How can one interact with a networked dynamical system? How do you hand a joystick to an unskilled operator and tell them to guide a swarm of robots?

1.4 CONTRIBUTIONS

The three questions above are each addressed in a separate part of this thesis – control, design and interaction. The motivations for each part, and the contributions and publications therein are discussed below.

1.4.1 *Part 2 – Control*

The most natural question to ask is if given a network, does that network render a networked dynamical system controllable, or uncontrollable. This question of course relies on how one intends the network to be influenced. One way to influence a network is to identify a certain number of agents near the boundary of the network, and either take over some part of their state, or simply inject some control signal into the system represented by that agent. Previous work in the literature has identified that for consensus networks, symmetries fixing control input nodes renders the system uncontrollable.

The first contribution of this part is to examine how this controllability condition changes when you consider new classes of interagent interactions. The motivation behind these interactions is the study of social networks. In social networks, one (hopefully) has some friends, and also potentially some enemies. One can draw a graph representing such a social network by assigning each interaction edge a scalar weight, with a positive weight denoting a friendly (cooperative, or excitatory) interaction, and a negative weight denoting an unfriendly (anti-cooperative, or inhibitory) interaction. The consensus protocol on such a network exhibits interesting behaviour, in particular the network will 'cluster' into two groups each achieving consensus on their own.

We show that a certain distribution of negative edge weights, coupled with a network symmetry fixing the input node, renders the resulting system uncontrollable. The distribution is referred to as 'structural balance', and essentially means that for any three agents that have existing relationships, either the mathematical encodings of the phrases 'the friend of a friend is a friend', or the 'enemy of an enemy is a friend' is satisfied. We also derive a similar uncontrollability condition for nonlinear variants of consensus.

In structurally balanced networks, the signed consensus protocol exactly achieves the aforementioned clustering. It turns out that the two clusters

that are formed all have positive (friendly) interactions between agents in the same cluster, but only negative (unfriendly) interactions exist across clusters. Given some time-series data of a nonlinear signed networked dynamical system, it is of interest to be able to identify the exact agents in each cluster. We use novel algorithms related to the Koopman operator that allow one to reduce the problem of community detection to some simple linear algebra calculations on the data stream. In particular, we show that the sign structure of what is known in context as a *Koopman mode* exactly encodes which agents are in which cluster. This can be used, for example, to identify friend-enemy relationships in complex social networked systems.

Lastly, we examine the problem of state estimation on high-dimensional systems. For example, consider the problem of identifing the pressure or density of a weather system over a large geographical area from data collected by stations across that area. By discretizing the system into a grid, one can consider the pressure or density in each grid cell to be one element of a large state-space. State-estimation algorithms, such as Kalman filtering, are computationally intractable due to matrix inverses on high-dimensional systems. We expand on a method of Sutton to find the best diagonal matrix estimate of the covariance matrix used to compute the Kalman filter, allowing this computation to become tractable. We employ a consensus-based algorithm to allow each station to agree on the value of the state estimate, given that each station can only measure a finite region of the state space.

INCLUDED PUBLICATIONS

[23] M. Hudoba de Badyn, *On the Control of Consensus Networks: Theory and Applications*. Seattle, USA: Master's Thesis, 2017.

[60] M. Hudoba de Badyn and M. Mesbahi, "Large-scale distributed Kalman filtering via an optimization approach," *IFAC-PapersOnLine*, vol. 50, no. 1, pp. 10 742–10 747, 2017.

[62] S. Alemzadeh, M. Hudoba de Badyn, and M. Mesbahi, "Controllability and stabilizability analysis of signed consensus networks," in *Proc. IEEE Conference on Control Technology and Applications*, Kohala Coast, USA, 2017, pp. 55–60.

[63] M. Hudoba de Badyn, S. Alemzadeh, and M. Mesbahi, "Controllability and data-driven identification of bipartite consensus on nonlinear signed networks," in *Proc. 56th IEEE Conference on Decision and Control*, Melbourne, Australia, 2017.

1.4.2 *Part 3 – Design*

The majority of this thesis focuses on the question of *design* – how do you build up a network from scratch to ensure that it 'performs' well? What does it even mean to 'perform' well?

One metric of performance is simply controllability – is the network controllable? This is a binary performance measure. The first contribution of this part is a algorithm called 'whiskering' which looks at a certain kind of

rooted graph product to build up a network from scratch so that controllability is preserved. We also examine the case where a few agents are being added to a network – which agents in the already existing network can you attach them to, and what is the best way to do this?

One measure of how a system 'performs' is known as the $\mathcal{H}_2$ performance. Roughly speaking, this measures how much 'energy' the system accumulates as it is being driven by random noise. A system that performs 'well' has a low $\mathcal{H}_2$ norm – for example, a swarm of UAVs can coordinate better if their positions and velocities are not disturbed much when they encounter turbulence. We examine the $\mathcal{H}_2$ norm in several contexts.

First, we use the paradigm of *series-parallel networks*. These are a class of networks that lack a homeomorphism to K_4, the complete graph on 4 nodes. Many difficult (read – NP-hard) combinatorial problems, such as the minimum vertex cover and maximum matching problems, have linear-time solutions on series-parallel networks. The key is a $O(\log n)$ decomposition algorithm that takes a series-parallel network and decomposes it into small atomic elements, and 'series' & 'parallel' operations on those elements – think of adding resistors in series or parallel.

This allows us to do two things. First, we can compute the $\mathcal{H}_2$ norm of a consensus network very quickly by exploiting this decomposition. The standard solution of computing the $\mathcal{H}_2$ norm requires a matrix inverse, making this calculation $O(n^\omega)$ where ω is the matrix multiplication complexity (roughly 2.3 as of now). Our method allows us to do this in $O(kn)$ to $O(k \log n)$ complexity, where k is the number of input nodes. Secondly, a similar algorithm also allows the network to distributively update the edge weights in order to optimize the $\mathcal{H}_2$ norm.

The second context in which we study the $\mathcal{H}_2$ norm is on networks with multiple *time scales*. These are systems in which some states are 'faster' than others – in the context of consensus networks, this 'speed' is the rate at which an agent integrates information from its neighbours. We consider *edge consensus*, which is a decomposition of the consensus problem into examining information flow along edges between agents, rather than on the agents themselves. The reason we do this is because we cannot analytically work with the $\mathcal{H}_2$ norm of time scaled consensus on the agent states – the effective graph Laplacian in this case is not a symmetric matrix, and there are no standard techniques (other than looking at edge consensus) to deal with this additional complexity.

What we show is that the $\mathcal{H}_2$ norm satisfies a separation principle – when the noise takes a certain form, the contribution of the time scales and the contribution of the edge weights are completely decoupled from each other. When considering the design problem – what edge weights and what time scales optimize the $\mathcal{H}_2$ norm –, this means we can design parameters of the agent independently from the parameters of its interconnections (given a constant graph structure).

The last contribution of this part is to examine a notion of complexity of graphs, which we call 'network entropy' (although strictly speaking, it is not formally 'entropy' in the information-theoretic sense – it is better called pseudoentropy). We show that this notion of entropy encodes some notion of 'signal mixing' in consensus – as information flows from agent to agent,

cycles in the network increase the mixing of the signal. This is related to some of the performance measures discussed above, in particular the $\mathcal{H}_2$ norm.

INCLUDED PUBLICATIONS

[22] M. Hudoba de Badyn and M. Mesbahi, "Growing controllable networks via whiskering and submodular optimization," in *Proc. 55th IEEE Conference on Decision and Control*, Las Vegas, USA, 2016, pp. 867–872, ISBN: 9781509018369. DOI: 10.1109/CDC.2016.7798376.

[23] M. Hudoba de Badyn, *On the Control of Consensus Networks: Theory and Applications*. Seattle, USA: Master's Thesis, 2017.

[71] M. Hudoba de Badyn, A. Chapman, and M. Mesbahi, "Network entropy: A system-theoretic perspective," in *Proc. 54th IEEE Conference on Decision and Control*, Osaka, Japan, 2015, pp. 5512–5517.

[77] D. R. Foight, M. Hudoba de Badyn, and M. Mesbahi, "Time Scale Design for Network Resilience," in *Submitted to Proc. 58th IEEE Conference on Decision and Control*, Nice, France, 2019, pp. 1–8.

[78] M. Hudoba de Badyn, D. R. Foight, and M. Mesbahi, "Time Scale and Edge Weight Design for H2 Performance on Consensus Networks," *To be submitted to the IEEE Transactions on Control of Network Systems*, vol. XX, no. X, pp. 1–10, 2019.

[96] B. Barzgaran, M. Hudoba de Badyn, and M. Mesbahi, "Growing Controllable Networks via Single and Multi-Node Attachments," in *In prep*, Chicago, USA, 2019, pp. 1–6.

[98] M. Hudoba de Badyn and M. Mesbahi, "Efficient Computation of Performance on Series-Parallel Networks," in *Proc. American Control Conference*, Philadelphia, USA, 2019, pp. 1–6.

[99] ——, "H2 Performance of Series-Parallel Networks : A Compositional Perspective," *Submitted to the IEEE Transactions on Automatic Control*, vol. XX, no. X, pp. 1–13, 2019.

1.4.3 *Part 4 – Interaction*

In the final part of this thesis, we examine some notions of controlling networked dynamical systems. The original motivation for this work was to look at state-dependent networked dynamical systems – systems in which the graph itself evolves as a function of the underlying process. It turns out that such systems are amenable to controller design if we allow some uncertainty in their states.

In particular, if you start to care about the overall behaviour of the networked system as a whole rather than the individual agent states, you can do something called *density control*. Here, you assign a density function in space that describes the overall distribution of agents in that space. We then examine notions of feedback and feedforward control, as well as an density

estimation procedure, that allows the agents in a networked dynamical system to coordinate among themselvse to distribute themselves according to this target density.

The tool we use is *optimal mass transport*, or the rigorous study of moving one pile of dirt to another under minimal effort. Jokes aside, consider two measures in some ambient probability space, and then consider all maps T whose pushforward under one measure is the other measure. One can assign a cost to this map by integrating over the initial measure, and then the task is to find the map T which is optimal under this cost.

For quadratic costs and absolutely continuous measures, one can pose an equivalent formulation discussed by Brenier and Benamou that seeks to find an incompressible flow that takes one measure to the other in finite time. The incompressible flow constraint is essentially the continuity equation – or the Liouville equation of a single integrator! For an arbitrary system, one just swaps out the continuity equation with the appropriate Liouville equation, and one gets an optimal control problem as a result. We discuss this in the context of networked dynamical systems.

INCLUDED PUBLICATIONS

[61] M. Hudoba de Badyn, U. Eren, B. Açıkmeşe, and M. Mesbahi, "Optimal mass transport and kernel density estimation for state-dependent networked dynamic systems," in *Proc. 57th IEEE Conference on Decision and Control*, Miami Beach, USA, 2018.

1.5 PRELIMINARIES

In this section, we outline the mathematical notation, as well as some elementary algebraic graph theory. Further notation and mathematics will be developed in the subsequent chapters; this section simply provides the universal notation used in every chapter of this thesis.

1.5.1 *Notation*

We consider $\mathbb{R}_+$ and $\mathbb{R}_{++}$ as the sets of nonnegative and positive real numbers, respectively. A column vector with n elements is referred to as $v \in \mathbb{R}^n$ where v_i or $[v]_i$ both represent the ith element in v. The matrix $M \in \mathbb{R}^{p\times q}$ contains p rows and q columns with $[M]_{ij}$ denoting the element in the ith row and jth column of M. The square matrix $N \in \mathbb{R}^{n\times n}$ is *symmetric* if $N^T = N$. The identity matrix, I_n, is the diagonal $n \times n$ square matrix with ones on its diagonal and zeros otherwise. For $w \in \mathbb{R}^n$ the $\mathrm{diag}(w)$ is an $n \times n$ matrix with w on its diagonal and zero elsewhere. The unit vector e_i is the column vector with all zero entries except $[e_i]_i = 1$. The column vector of all ones is denoted as $\mathbf{1}$. The *cardinality* of a set S is denoted as $|S|$. The *annihilator* of a set S is defined as

$$S^\perp = \{v^* \in \mathbb{R}^n : \langle v, v^* \rangle = 0 \text{ for all } v \in S\},$$

where $\langle \cdot, \cdot \rangle$ is the inner product in the Euclidean space. The column space of a matrix M is denoted by $\mathcal{R}(M)$. We define $\mathcal{R}(P)$ to be *A-invariant* if there exists C such that $AP = PC$. We say A is similar to B if there is an invertible matrix R such that $R^{-1}AR = B$; two similar matrices share the same spectral properties. The *leading principal submatrix* of order k of X is the square submatrix of X formed by deleting the last $n-k$ rows and columns; let $A[K]$ denote the principal submatrix of A obtained by deleting the rows and columns of A corresponding to the elements in the set $[m] \setminus K$. We denote the Moore-Penrose pseudoinverse of a matrix A as $A^{\dagger}$. The symbol '$\succeq$' defines the *positive semi-definite ordering*: for $n \times n$ PSD matrices A, B we have that

$$A \succeq B \iff A - B \succeq 0_{n \times n}.$$

The function h is *even* if $h(-x) = h(x)$ and is *odd* if $h(-x) = -h(x)$. The function f is of class C^r if the derivatives $f, f', \ldots, f^{(r)}$ exist and are continuous. The function $g \in C^{\infty}$, otherwise called *smooth*, has derivatives of all order. Let $F : \mathbb{R}^n \to \mathbb{R}^n$ be a vector field and let $\varphi : \mathbb{R}^n \to \mathbb{R}^n$ be a smooth mapping. Then, F is *φ-invariant* if $(D\varphi(x))F(x) = F(\varphi(x))$ for all $x \in \mathbb{R}^n$ with $D\varphi(x)$ the Jacobian matrix of φ at x. The Lie bracket of two vector fields f and g is denoted by $[f, g]$. Given a mapping $\gamma : \mathcal{M} \to \mathcal{M}$, the fixed point set of γ is denoted by $\mathrm{Fix}(\gamma) = \{x \in \mathcal{M} | \gamma(x) = x\}$. The operator $\pi_{n-1} : \mathbb{R}^n \to \mathbb{R}^{n-1}$ is defined to be the projection onto the first $(n-1)$-coordinates.

1.5.2 *Consensus and Algebraic Graph Theory*

A multi-agent system with n agents is characterized by a *graph* $\mathcal{G} = (\mathcal{V}, \mathcal{E}, \mathcal{W})$ where $\mathcal{V} = \{v_1, v_2, \ldots, v_n\}$ is the set of nodes, $\mathcal{E} \subseteq \mathcal{V} \times \mathcal{V}$ denotes the set of edges, and $\mathcal{W} \in \mathbb{R}_{+}^{n \times n}$ consists of weights assigned to edges. We call $A \in \mathbb{R}_{+}^{n \times n}$ the *adjacency matrix* where $A_{ij} = W_{ij} \neq 0$. The *degree matrix* $D \in \mathbb{R}^{n \times n}$ is a square diagonal matrix where $D_{ii} = \sum_{j \in \mathcal{N}(i)} A_{ij}$. The *graph Laplacian* is then defined as $\mathcal{L}_{\mathcal{G}} = D - A$. Then the *consensus dynamics*, with $x \in \mathbb{R}^n$ the state vector, is defined as

$$\dot{x}_i = -\sum_{j \in \mathcal{N}_i} W_{ij} (x_i - x_j),$$

or in matrix-vector form, as

$$\dot{x} = -\mathcal{L}_{\mathcal{G}} x.$$

A *path* of length r in $\mathcal{G}$ is given by a sequence of different nodes $v_{i_0}, v_{i_1}, \ldots, v_{i_r}$ such that for $k = 0, 1, \ldots, r-1$, the nodes v_{i_k} and $v_{i_{k+1}}$ are neighbors. When the terminal nodes are equal, the path is called a *cycle* [5]. A *leaf*, or *whisker*, is a node with degree 1.

Part II

CONTROL

2

SIGNED CONSENSUS NETWORKS

Networked dynamical systems have been the forefront of active research for the past two decades. Some well-studied examples of networked systems are social networks and dynamics of opinions [3], flocking [6], autonomous robotics [7], [8], quantum networks [9], autonomous flight [10], traffic control [11],multi-agent systems [12], [13], and gene networks [14]. Several networked systems include both cooperative and antagonistic interactions, such as certain classes of social dynamics [15], [16].

Consensus algorithms have been used in many scientific and engineering applications, including those listed above. A large amount of research has been dedicated to looking at the control of consensus [5]. The work by Rahmani *et al.* showed that certain symmetries of networks characterized by automorphisms of the topology of the network cause uncontrollability [17]. This was generalized by Chapman and Mesbahi who showed signed fractional automorphisms generate necessary and sufficient conditions for uncontrollability and unstabilizability of linear systems [18]. Further work examined methods of generating network topologies, for either performance improvements, as in [19] and [20], or those that are controllable for consensus, such as in [21] and [22], [23].

Consensus algorithms on networks with antagonistic interactions were first considered by Altafini [24], [25]. The network property of *structural balance*, first considered in the study of social networks ([15], [26], [27]) was identified in Altafini's work as the property inducing bipartite consensus in which the agents converge to two disjoint clusters instead of a uniform consensus. Graph-theoretic properties of signed Laplacian dynamics were studied by Pan *et al.* [28]. Further research by Pan *et al.* has looked at identifying the bipartite structure of structurally balanced graphs using data from signed Laplacian dynamics and dynamic mode decomposition [29], adding to the works done by Harary and Kabell [30], and Facchetti *et al* [31]. Recent contributions by Clark *et al.* have studied the leader selection problem in signed consensus [32].

The generalization to nonlinear consensus algorithms has been studied in numerous settings. Behaviour of nonlinear consensus protocols was considered by Srivastava *et al.* [16]. The extension of these consensus protocols to signed networks was studied by Altafini [24]. Moreover, the generalization of symmetry arguments for controllability was examined by by Aguilar and Gharesifard [33].

The (literal) dual side of control is estimation. One of the most successful estimation algorithms is called the *Kalman filter*. The Kalman filter is an algorithm that uses the known dynamics of a system to remove noise from measurements of that system. When considering large-scale dynamical systems, implementation of the standard or extended Kalman filters can be computationally difficult. In such cases, the Kalman filter requires the inversion of very large matrices at each timestep. This may cause the Kalman

filter to run slower than the dynamical process it is trying to measure, or to severely reduce the temporal resolution of the measurements.

There are many systems for which measurements are taken by a network of sensors and are of high dimension; examples of such systems include weather models and can be found in [34] and [35]. Previous methods for circumventing this problem include decomposing the dynamical system being measured into several subsystems and distributing the subsystems over the sensor network as in [34], or using Monte-Carlo methods for estimating the error covariance, such as in [36]. Previously, Sutton proposed to modify the Kalman filter error covariance update with a gradient descent method for the purpose of mimimizing memory consumption, albeit for a specific instantiation of a SISO linear system [37].

Distributed Kalman filtering seeks to estimate the state of a system by distributing the tasks of measuring the system and subsequently filtering the data to many agents, who then collectively assemble the state estimate. Such algorithms utilizing consensus to provide a global estimate were presented by [38] and [39], and later extended by [40]. Performance of distributed Kalman filters using graph-theoretic quantities were studied by [41].

There has been a recent interest in applying data-driven methods to control of networks, for example the Koopman operator. The Koopman operator is a dynamical framework in which one considers the propagation of observables of the state, rather than the state itself. The Koopman operator is linear, even for a non-linear system, but the trade-off is that the vector space of observables is generally infinite dimensional [42]. This formalism lends itself well to a data-driven approach, allowing one to approximate the Koopman operator by collecting data [43]. Research by Pan *et al.* has looked at identifying the bipartite structure of signed networks using data-driven methods [29], furthering work done by Facchetti *et al.* [31], and Harary and Kabell [30].

The contributions of the chapters in this part are as follows. We conduct a controllability analysis of signed Laplacian consensus using symmetry arguments developed by Rahmani *et al.* [17], for the individual single-input-single-output (SISO) and multi-input-multi-output (MIMO) cases of consensus dynamics with leader nodes. In particular, we identify the property of structural balance that when combined with symmetry causes uncontrollability of signed consensus dynamics. The key feature of structurally balanced graphs that allows this analysis is that they admit a *gauge transformation* that allows the permutation matrix corresponding to the graph symmetry to be extended to a signed permutation matrix, which we show leads to uncontrollability when corresponding to a symmetry about input nodes. We then use tools developed by Chapman and Mesbahi in [18] to derive controllability and stablilizability conditions for influenced signed consensus dynamics.

Next, we show that the property of structural balance, when combined with symmetries in the underlying graph, as well as certain symmetries of the nonlinear dynamics, causes uncontrollability in the context of the accessibility problem. In particular, we consider the same network flows studied in [16], [24], [33]; however we extend the controllability analysis to signed dynamics. Subsequently, we extend the bipartite identification problem considered by Pan *et al.* in [29] to the case of signed nonlinear consensus net-

works. In particular, we use a Koopman operator-theoretic approach alongside Extended Dynamic Mode Decomposition (EDMD) to extract a 'Koopman mode' whose sign structure reveals the bipartite structure.

Lastly, we examine estimation problems on large sensor networks. In particular, we extend the gradient descent algorithm for estimating the Kalman filter error covariance to the general MIMO linear system as a proposed solution to the problem of running a Kalman filter on a high-dimensional system. We improve the gradient descent using Nesterov acceleration and adaptive learning rate methods. We apply the methods above to distributed Kalman filtering on a sensor network.

This part is organized as follows. We outline the problem statements in §3.1. In §3.2, we show that structural balance combined with symmetry about inputs leads to uncontrollability, and derive the corresponding stabilizability conditions. The nonlinear case is discussed in §3.3.

In Chapter 4, we outline the basics of Koopman operator theory, and how we apply it for community detection in nonlinear structurally-balanced networked dynamical systems. We discuss distributed Kalman filtering in §6.1. Relevant examples are shown in Chapter 5, and the paper is concluded in §6.5.

2.1 MATHEMATICAL BACKGROUND

2.1.1 *Signed Networks*

A *signed graph* $\mathcal{G}_s$ is a graph that admits negative weights. We define the *signed graph Laplacian* as $\mathcal{L}_{\mathcal{G}_s} = D_s - A_s$, where $[A_s]_{ij} = \pm A_{ij}$, and where the degree matrix is given by $D_{ii} = \sum_{j\in\mathcal{N}(i)} |A_{ij}| = \sum_{j\in\mathcal{N}(i)} |W_{ij}|$. The generalization of consensus dynamics to signed graphs was introduced in [25], and the corresponding dynamical system is given by $\dot{x} = -\mathcal{L}_{\mathcal{G}_s} x$, i.e.

$$\dot{x}_i = -\sum_{j\in\mathcal{N}(i)} |W_{ij}| \left(x_i - \operatorname{sgn}(W_{ij}) x_j\right),$$

where sgn represents the sign function. A *gauge transformation* is a change of orthant order via a matrix $G_t \in \left\{\operatorname{diag}(\sigma) : \sigma = [\sigma_1, \ldots, \sigma_n],\ \sigma_i = \pm 1\right\}$. We know $G_t = G_t^T = G_t^{-1}$. Let the *gauge-transformed Laplacian* be given by $\mathcal{L}_{\mathcal{G}_t} = G_t \mathcal{L}_{\mathcal{G}_s} G_t = D - G_t A_s G_t$ where

$$\left(\mathcal{L}_{\mathcal{G}_t}\right)_{ij} = \begin{cases} \sum_{k\in\mathcal{N}(i)} |A_{ik}| & j = i \\ -\sigma_i \sigma_j A_{ij} & j \neq i. \end{cases}$$

2.1.2 *Automorphisms/Interlacing/Equitable Partitions*

An *automorphism* of the graph $\mathcal{G}$ is a permutation ψ of its nodes such that $\psi(i)\psi(j) \in \mathcal{E}$ if and only if $ij \in \mathcal{E}$. Let the *permutation matrix* Ψ be such that $[\Psi]_{ij} = 1$ if $\psi(i) = j$ and zero otherwise. Then ψ is an automorphism of $\mathcal{G}$ if and only if $\Psi A(\mathcal{G}) = A(\mathcal{G})\Psi$ (see [5]). The permutation ψ *induces* a mapping $\varphi : \mathbb{R}^n \to \mathbb{R}^n$ such that $[\varphi(x)]_i = x_{\phi(i)}$. Let the permutation

matrix J be such that $[J]_{ij} = 1$ if $\psi(i) = j$ and zero otherwise. Therefore, the permutation matrix J is simply the Jacobian matrix of φ, in that $J = D\varphi$.

Suppose $A \in \mathbb{R}^{n\times n}$ and $B \in \mathbb{R}^{m\times m}$ are both symmetric and $m \leq n$. Then the eigenvalues of B *interlace* the eigenvalues of A if for $i = 1, 2, \ldots, m$, $\lambda_{n-m+i}(A) \leq \lambda_i(B) \leq \lambda_i(A)$ where $\lambda_1(A) \geq \lambda_2(A) \geq \cdots \geq \lambda_n(A)$ are the eigenvalues of A in a non-increasing order [44].

In a similar way that we defined the functions ϕ and φ for the graph automorphism, consider the function $\mathfrak{g} : \mathcal{V} \to \mathcal{V}$ encoding the action of the gauge on the nodes. This induces a function $g : \mathbb{R}^n \to \mathbb{R}^n$ such that $[g(x)]_i = \sigma_i x_i$. The gauge transformation is then the Jacobian of this function, in that $G_t = Dg$.

The *cell* C is a subset of the graph nodes $\mathcal{V}$. A *nontrivial cell* is a cell with more than one node. A *partition* is a grouping of $\mathcal{V}$ into different cells. An *r-partition* π of $\mathcal{V}$ with cells $\{C_i\}_{i=1}^r$ is *equitable* if each node in C_j has the same number of neighbors in C_i, for all i, j. We call π a *nontrivial equitable partition* (NEP) if it contains at least one nontrivial cell. Let b_{ij} be the number of neighbors in C_j of a node in C_i. The *quotient* of $\mathcal{G}$ over π, denoted by $\mathcal{G}/\pi$, is the directed graph with the cells of an equitable *r-partition* π as its nodes and b_{ij} edges directed from C_i to C_j. The adjacency matrix of the quotient is specified by $[A(\mathcal{G}/\pi)]_{ij} = b_{ij}$. A *characteristic vector* $p_i \in \mathbb{R}^n$ of a nontrivial cell C_i has 1's in components associated with C_i and 0's elsewhere. A *characteristic matrix* $P \in \mathbb{R}^{n\times r}$ of a partition π of $\mathcal{V}$ is defined as $[p_i]_{i=1}^r$.

For example, for the equitable partition in figure 2.1a we get

$$A(\mathcal{G}/\pi) = \begin{bmatrix} 0 & 2 & 0 \\ 1 & 1 & 1 \\ 0 & 2 & 0 \end{bmatrix} \quad \text{and} \quad P = \begin{bmatrix} 1 & 0 & 0 \\ 0 & 1 & 0 \\ 0 & 1 & 0 \\ 0 & 0 & 1 \end{bmatrix}.$$

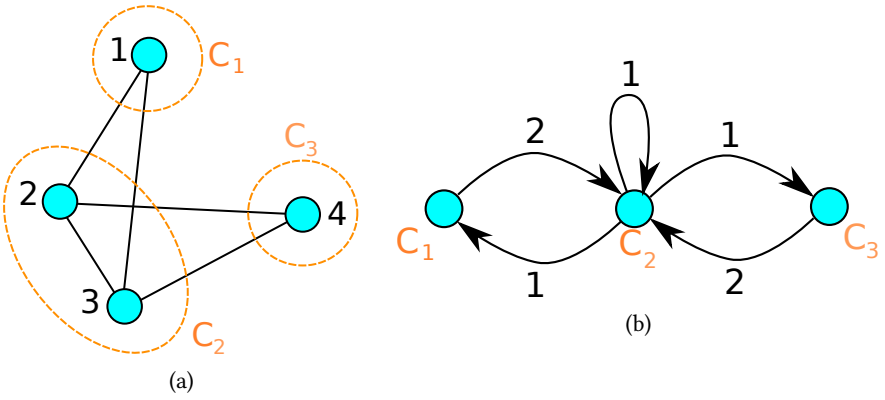

Figure 2.1: (a) Equitable partition of a sample graph, (b) quotient of the graph in (a)

3

SIGNED CONTROL

3.1 PROBLEM STATEMENT

The analysis of this paper consists of several main parts, which examine two different notions of influencing control on networks, as well as linear and nonlinear controllability. In the first part, we examine the notion of uncontrollability due to symmetry and interlacing which was initially derived in [17] for signed consensus networks. The notion of control in this case is taking over the state of one or several nodes in the network, and using their edges to inject signals into the system. In the second part, we consider the case where the nodes are controlled by injecting a single-integrator signal to some nodes of the graph.

Signed consensus networks are of interest because the negative weights induce a phenomenon known as *clustering*, where agents will not converge to an agreement subspace, but rather converge to opposite equilibria (an example of clustering is shown in Section 5.1). The condition that causes clustering was identified by [24] as *structural balance*. Surprisingly, we show that this topological feature is exactly the condition that produces uncontrollability of signed networks.

Lemma 1. *(See [24]) The following statements are equivalent:*

1. *The signed graph $\mathcal{G}$ is structurally balanced;*
2. *There exists a gauge G_t such that $G_t A_s G_t$ has only positive entries (i.e. the transformed graph becomes* unsigned*);*
3. *All cycles in $\mathcal{G}$ are positive;*
4. *The signed Laplacian $\mathcal{L}_{\mathcal{G}_s}$ has a zero eigenvalue;*
5. *There exists a bipartition of $\mathcal{V}$ such that the edge weights on the edges within the same set are positive, and the edges connecting the two sets are negative.*

One may recall that the unsigned consensus dynamics have an agreement subspace spanned by the eigenvector $\mathbf{1}$ corresponding to the zero eigenvalue. For signed consensus, the zero eigenvalue explicitly corresponds to disagreement. Then one may think that structural balance is therefore not a desireable quality for signed consensus, but it turns out that if the graph is not structurally balanced, the consensus dynamics become trivial in some sense, and converge to zero.

Theorem 1. *(See [24]) If $\mathcal{L}_{\mathcal{G}_s}$ is structurally unbalanced in a signed graph $\mathcal{G}_s$, then $\lim_{t\to\infty} x(t) = 0$ where $x \in \mathbb{R}^n$ is the state vector with the corresponding dynamics $\dot{x} = -\mathcal{L}_{\mathcal{G}_s} x$. Otherwise, if $\mathcal{L}_{\mathcal{G}_s}$ is structurally balanced, then $\lim_{t\to\infty} x(t) = (1/n)\left(\mathbf{1}^T G_t x(0)\right) G_t \mathbf{1}$.*

Previous work by Rahmani *et al.* in [17] showed that symmetry with respect to a single input and interlacing for multiple input are sufficient for uncontrollability, and this was generalized by Chapman and Mesbahi in [18] to show that fractional symmetry with respect to the inputs is sufficient and necessary for uncontrollability.

In this paper, we aim to show that structural balance is the property that combined with symmetry and interlacing leads to uncontrollability. There are examples of signed networks that are input symmetric but controllable, and we will discuss these in Section 5.3. Before proceeding to our main results, we summarize the various dynamics considered in the paper.

There are several variants of consensus dynamics with respect to how inputs are injected into nodes. Given a connected signed graph $\mathcal{G}_s$, we can select one node and use that specific node to inject our input signal u. This corresponds to partitioning the Laplacian as follows (see, for example, [5]):

$$\mathcal{L}_{\mathcal{G}_s} = \left[\begin{array}{c|c} A_s^f & B_s^f \\ \hline B_s^{f\,T} & A_s^i \end{array}\right],$$

where f and i denote the *floating* and *input* parts of the network respectively. Then, the dynamical system for signed consensus networks is

$$\dot{x} = -A_s^f x - B_s^f u\,, \tag{3.1}$$

where for a single-input-single-output (SISO) system we have $A_s^f \in \mathbb{R}^{(n-1)\times(n-1)}$, $B_s^f \in \mathbb{R}^{(n-1)\times 1}$, and A_s^i is a scalar. Similarly, one can define the same dynamics as (3.1) for the multiple-input-multiple-output (MIMO) system. In that case, $A_s^f \in \mathbb{R}^{n_f\times n_f}$ and $B_s^f \in \mathbb{R}^{n_f\times n_i}$ where n_f and n_i are the numbers of the nodes in floating and input subgraphs respectively. The *floating signed graph* is denoted by $\mathcal{G}_s^f$.

Lemma 2. *[**Popov-Belevitch-Hautus (PBH) Test**] The system described in (3.1) is controllable if and only if none of the eigenvectors of A_s^f are simultaneously orthogonal to all columns of B_s^f.*

We use lemma 2 further to discuss controllability of the SISO case in Section 3.2.1.1, and the MIMO case in Section 3.2.1.2.

The second variant of controlling consensus networks is to simply inject signals into nodes, without taking over the state of the node. We can therefore define the *influenced signed consensus dynamics* with q inputs and p outputs as

$$\dot{x} = -\mathcal{L}_{\mathcal{G}_s} x + B(I)u,\ y = C(O)x, \tag{3.2}$$

where $I \subseteq N$ is the set of input nodes, $O \subseteq N$ the set of output nodes, and $B(I), C(I)$ are the matrices

$$B(I) = \begin{bmatrix} | & & | \\ e_{i_1} & \cdots & e_{i_q} \\ | & & | \end{bmatrix}, C(O) = \begin{bmatrix} | & & | \\ f_{j_1} & \cdots & f_{j_p} \\ | & & | \end{bmatrix}^T,$$

in which e_i is the indicator vector for nodes $i \in I$, and f_j for nodes $j \in O$. The control signal vector is $u \in \mathbb{R}^q$. Both (output) controllability and (output) stabilizability of these dynamics is considered in Section 3.2.2.

For examining nonlinear consensus, we follow the same conventions as in [33]. Consider the controlled dynamical system

$$\dot{x} = F(x, u) \tag{3.3}$$

where $F : \mathbb{R}^n \times \mathbb{R}^m \to \mathbb{R}^n$ is a smooth mapping. The *accessible set* $\mathcal{A}(x_0, T)$ of the system (3.3) from x_0 at time T is the set of all end-points $\theta(T)$ where $\theta : [0, T] \to \mathbb{R}^n$ is a trajectory of (3.3). The accessible set of (3.3) from x_0 up to T is defined as $\mathcal{A}(x_0, \leq T) := \cup_{0 \leq \tau \leq T} \mathcal{A}(x_0, \tau)$. Then, the nonlinear dynamical system (3.3) is said to be *accessible* from the initial point x_0 if for every $T > 0$ the set $\mathcal{A}(x_0, \leq T)$ contains a non-empty interior.

3.2 METHODS

3.2.1 *Signed Graph Controllability*

3.2.1.1 *The SISO Case*

A standard result by [17] shows that for a SISO consensus network, a symmetry about the input node is sufficient for uncontrollability. We extend this result for the signed consensus networks considered by [24] and [29]. In particular, we show that structural balance and input symmetry for the unsigned graph is sufficient for uncontrollability.

Remark 1. *This result shows signed Laplacian is in some sense more robust to symmetries about the input nodes. In particular, there are examples of unsigned graphs that are symmetric about an input and therefore uncontrollable, but whose signed counterparts exhibit controllability despite the symmetry. Therefore, there is not enough conditions to claim the uncontrollability of the system.*

Now, we state and prove a lemma which helps us provide the main result of this section.

Lemma 3. *Assume the unsigned graph $\mathcal{G}$ enjoys input symmetry and the signed network $\mathcal{G}_s$ is structurally balanced. Then, the following statements hold*

1. *There exists J' such that $J' A_s^f = A_s^f J'$*

2. *For the same J' as part 1, $J'^T B_s^f = B_s^f$*

3. *If v is the eigenvector corresponding to the eigenvalue λ of A_s^f. Then, $J'v$ (and hence $v - J'v$) would also be the eigenvectors corresponding to λ*

Proof. From the second statement of lemma 1 there exists G_t such that

$$G_t \mathcal{L}_{\mathcal{G}_s} G_t = \mathcal{L}_{\mathcal{G}}, \tag{3.4}$$

and hence

$$\begin{aligned} A_s^f &= G' A^f G' \\ B_s^f &= \sigma_n G' B^f . \end{aligned}$$

It follows

$$\begin{aligned} G_t \left[\begin{array}{c|c} A_s^f & B_s^f \\ \hline B_s^{f\,T} & A_s^i \end{array}\right] G_t &= \left[\begin{array}{c|c} G' A_s^f G' & G' B_s^f \sigma_n \\ \hline \sigma_n B_s^{f\,T} G' & \sigma_n A_s^i \sigma_n \end{array}\right] \\ &= \left[\begin{array}{c|c} A^f & B^f \\ \hline B^{f\,T} & A^i \end{array}\right], \end{aligned}$$

where $G' = \operatorname{diag}(\sigma_1, \sigma_2, \ldots, \sigma_{n-1})$. Without loss of generality, we can assume $\sigma_n = 1$ since (3.4) also holds for $-G$. This gives

$$B^f = G' B_s^f .$$

From [17] we know that if $\mathcal{G}$ has the input symmetry structure, then there exists the permutation matrix J such that

$$J A^f = A^f J .$$

Let $J' = G' J G'$,

$$\begin{aligned} J' A_s^f &= G' J G' G' A^f G' = G' J A^f G' \\ &= G' A^f J G' = G' A^f G' G' J G' = A_s^f J', \end{aligned}$$

which proves part (1).

We also have

$$\begin{aligned} J'^T B_s^f &= J'^T G' B^f = G' J^T G' G' B^f = G' J^T B^f \\ &= -G' J^T A^f \mathbf{1} = -G' A^f J^T \mathbf{1} = B_s^f, \end{aligned}$$

which gives the result of part (2).

For the last part of the proof by definition we know $A_s^f v = \lambda v$. Then

$$A_s^f J' v = J' A_s^f v = \lambda J' v,$$

implying that $J'v$ is also an eigenvector for the same eigenvalue. Hence, assuming orthonormal eigenvectors for A_s^f, then $v - J'v$ would also be an eigenvector corresponding to λ. □

The matrix J' introduced for a signed floating graph in lemma 2 is in some sense correspondent to the permutation matrix J in the unsigned case. In fact, the only difference between J and J' are the elements with the same rows or columns as the negative elements in G'. For example, for the graph of Figure 3.1, with node 5 as the input node, the matrices J, J', and G' are found to be

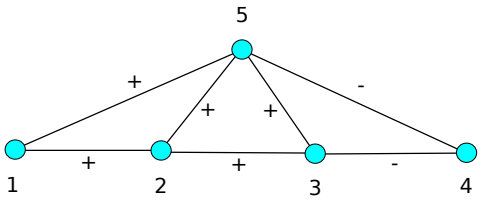

Figure 3.1: A network topology with input symmetry

$$J = \begin{bmatrix} 0 & 0 & 0 & 1 \\ 0 & 0 & 1 & 0 \\ 0 & 1 & 0 & 0 \\ 1 & 0 & 0 & 0 \end{bmatrix}, \; G' = \begin{bmatrix} 1 & 0 & 0 & 0 \\ 0 & 1 & 0 & 0 \\ 0 & 0 & 1 & 0 \\ 0 & 0 & 0 & -1 \end{bmatrix}$$

$$J' = \begin{bmatrix} 0 & 0 & 0 & -1 \\ 0 & 0 & 1 & 0 \\ 0 & 1 & 0 & 0 \\ -1 & 0 & 0 & 0 \end{bmatrix}.$$

Therefore, the first two parts of lemma 3 demonstrate the correlation between the signed and unsigned consensus networks using the gauge transformation G_t.

Now we have all the tools we need to provide the main theorem of this part.

Theorem 2. *The signed network system $\mathcal{G}_s$ is uncontrollable if it is input symmetric and structurally balanced*

Proof. We use the results of lemma 3 and the PBH test to show the uncontrollability of $\mathcal{G}_s$.

Let (λ, v) be a pair of eigenvalue and eigenvector for A_s^f so that $A_s^f v = \lambda v$. Then, from part 3 of lemma 3 we know that $v - J'v$ is also and eigenvector for A_s^f. Then, from part 2 of lemma 3 we have

$$(v - J'v)^T B_s^f = v^T B_s^f - v^T J'^T B_s^f = v^T B_s^f - v^T B_s^f = 0,$$

which implies that the system is not controllable according to the PBH test of controllability. □

Remark 2. *A signed symmetry implies the existence an unsigned symmetry of $\mathcal{G}$. The converse is true when $\mathcal{G}$ is structurally balanced.*

3.2.1.2 *The MIMO Case*

In this section, we examine how the notion of structural balance is interposed in the controllability analysis of multiple input signed networks. The results in this section are extensions to [17]. To this end, we leverage the machinery of interlacing and equitable partitions on graphs.

First, we restate and modify two fundamental lemmas from [44] to the signed case and then provide the analysis which leads to sufficient conditions on the uncontrollability of the system.

Definition 1. *Let G_t be the gauge transformation as in (3.4). Then, P' is the* signed characteristic matrix *defined as $P' = G_t P$.*

Lemma 4. *Let π be a parition of the structurally balanced signed graph $\mathcal{G}_s$, with adjacency matrix A_s and signed characteristic matrix P'. Then, π is equitable if and only if the column space of P' is A_s-*invariant.

Proof. (Necessity) assume π is equitable. From lemma 9.3.1 in [44] if π is equitable then $AP = P\hat{A}$ with $\hat{A} = A(\mathcal{G}_s/\pi)$. Then, it follows from the second statement in lemma 1

$$P\hat{A} = AP = G_t A_s G_t P \quad \Rightarrow \quad A_s P' = P'\hat{A}.$$

(Sufficiency) From lemma 9.3.2 in [44], π is equitable if there exists B such that $AP = PB$. Then, if such B exists, we get

$$PB = AP = G_t A_s G_t P \quad \Rightarrow \quad A_s P' = P'B.$$

□

Lemma 4 shows how the gauge transformation is injected into the analysis of signed networks. Indeed, based on the knowledge of the second statement in lemma 1, we use the structural balance to turn the signed system into the extensively developed un-signed consensus dynamics.

The next lemmas are provided for the sake of completeness.

Lemma 5. *(See [17]) Given a symmetric matrix $A \in \mathbb{R}^{n\times n}$, let S be a subspace of $\mathbb{R}^n$. Then, $S^\perp$ is A-*invariant *if and only if S is A-*invariant.

Lemma 6. *(See [44] Theorem 9.5.1) Let $\Phi \in \mathbb{R}^{n\times n}$ be a real symmetric matrix, and let $R \in \mathbb{R}^{n\times m}$ be such that $R^T R = I_m$. Set $\Theta = R^T \Phi R$ and let $v_1, v_2, \ldots, v_m$ be an orthogonal set of eigenvectors for Θ such that $\Theta v_i = \lambda_i(\Theta) v_i$, where $\lambda_i(\Theta) \in \mathbb{R}$ is an eigenvalue of Θ. Then, $\Phi R = R\Theta$ if the interlacing between Φ and Θ is tight.*

Remark 3. *As discussed in [17], we can now find an orthogonal decomposition of $\mathbb{R}^n$ using the signed characteristic matrix P' as*

$$\mathbb{R}^n = \mathcal{R}(P') \oplus \mathcal{R}(Q'),$$

where $\mathcal{R}(Q') = \mathcal{R}(P')^{\perp}$. Then, an orthonormal basis for $\mathbb{R}^n$ can be formed as

$$T = [\, \bar{P}' \mid \bar{Q}' \,], \tag{3.5}$$

where $\bar{P}'$ and $\bar{Q}'$ represent normalized P' and Q' respectively and satisfy $\bar{P}'^T \bar{Q}' = 0$ and $\bar{Q}'^T \bar{Q}' = I_{n-r}$.

Lemma 7. *Given a connected signed graph $\mathcal{G}_s$, the system (3.1) is uncontrollable if and only if $\mathcal{L}_{\mathcal{G}_s}$ and A_s^f share at least one common eigenvalue.*

Lemma 7 is a derivation from lemma 7.9 in [17]. Since this is a general result depending on the Laplacian and its leading principal submatrix (floating graph), and the PBH test, the same holds for the signed case.

From this point, the goal is to show that for some specific graph partition and the structural balance of the network, L_s and A_s^f share similar eigenvalues which leads to uncontrollability. The next two lemmas assert that $\mathcal{L}_{\mathcal{G}_s}$ and A_s^f are similar to some block diagonal matrices.

Lemma 8. *Suppose a structurally balanced signed graph $\mathcal{G}_s$ has an NEP π with $\bar{P}'$ and $\bar{Q}'$ as in (3.5). Then, the signed Laplacian $\mathcal{L}_{\mathcal{G}_s}$ is similar to the block diagonal matrix*

$$\bar{\mathcal{L}}_{\mathcal{G}_s} = \begin{bmatrix} \mathcal{L}_{P'} & \mathbf{0} \\ \mathbf{0} & \mathcal{L}_{Q'} \end{bmatrix},$$

where $\mathcal{L}_{P'} = \bar{P}'^T \mathcal{L}_{\mathcal{G}_s} \bar{P}'$ and $\mathcal{L}_{Q'} = \bar{Q}'^T \mathcal{L}_{\mathcal{G}_s} \bar{Q}'$.

Lemma 9. *Let $\mathcal{G}_s^f$ be a signed floating graph, and A_s^f be defined as in (3.1) and $\bar{P}'$ and $\bar{Q}'$ be as in (3.5). If there exists an NEP π_f in $\mathcal{G}_s^f$ and a π in the original structurally balanced signed graph $\mathcal{G}_s$ such that all the nontrivial cells in π_f are also cells in π, then A_s^f is similar to the block diagonal matrix*

$$\bar{A}_s^f = \begin{bmatrix} A_{P'}^f & \mathbf{0} \\ \mathbf{0} & A_{Q'}^f \end{bmatrix},$$

with $A_{P'}^f = \bar{P}_f'^T A_s^f \bar{P}_f'$ and $A_{Q'}^f = \bar{Q}_f'^T A_s^f \bar{Q}_f'$.

The proofs are similar to lemmas 7.11, 7.12, and 7.14 in [17] and is skipped for succinctness. One just needs to consider the role of structural balance and the fact that the signed characteristic matrix P' needs to be replaced for P due to the insertion of gauge transformation.

We are now well-equipped to address the main result of the section. In the following theorem, we see that in certain circumstances, the two block diagonal matrices share identical blocks and thus‘ common eigenvalues. This leads to the uncontrollability of the system by lemma 7.

Theorem 3. *Given a connected structurally balanced signed graph $\mathcal{G}_s$ with the floating graph $\mathcal{G}_s^f$, the system (3.1) is uncontrollable if there exist NEPs on $\mathcal{G}_s$ and $\mathcal{G}_s^f$, π and π_f, such that π_f contains all nontrivial cells of π.*

The main scheme of the proof is similar to theorem 7.15 in [17]. We repeat the proof to show how the new orthogonal basis formed by $\bar{P}'$ and $\bar{Q}'$ work in the new setup of signed networks.

Proof. As a result of structural balance, let $\bar{P}'$ and $\bar{Q}'$ be defined as in (3.5). Following the convention in [17], let $\pi \cap \pi_f = \{C_1, C_2, \dots, C_{r_1}\}$ with $|C_i| \geq 2,\ i = 1, 2, \dots, r_1$. Let the nontrivial cells contain the first n_1 nodes. Since π_f contains all nontrivial cells of π, it follows

$$P' = \begin{bmatrix} P_1' & \mathbf{0} \\ \mathbf{0} & I_{n-n_1} \end{bmatrix}_{n\times r} \quad \text{and} \quad P_f' = \begin{bmatrix} P_1' & \mathbf{0} \\ \mathbf{0} & I_{n_f-n_1} \end{bmatrix}_{n_f\times r_f},$$

where $P_1' \in \mathbb{R}^{n_1\times r_1}$ contains the nontrivial part of the signed characteristic matrices. Let $\bar{P}'$ and $\bar{P}_f'$ be the normalization of P' and P_f' and define $\bar{Q}'$ and $\bar{Q}_f'$ as in (3.5). Then

$$\bar{Q}' = \begin{bmatrix} Q_1' \\ \mathbf{0} \end{bmatrix}_{n\times(n_1-r_1)}, \quad \bar{Q}_f' = \begin{bmatrix} Q_1' \\ \mathbf{0} \end{bmatrix}_{n_f\times(n_1-r_1)},$$

where $Q_1' \in \mathbb{R}^{n_1\times(n_1-r_1)}$ satisfies $Q_1'P_1 = 0$. It follows that $\bar{Q}_f' = R^T\bar{Q}'$ with $R = [I_{n_f}, \mathbf{0}]^T$. Then, by lemmas 8 and 9, we get

$$\mathcal{L}_{Q'} = \bar{Q}'^T\mathcal{L}_{\mathcal{G}_s}\bar{Q}' = \bar{Q}_f'^T R^T\mathcal{L}_{\mathcal{G}_s}R\bar{Q}_f' = \bar{Q}_f'^T A_s^f\bar{Q}_f' = \mathcal{A}_{Q'}^f$$

This implies that $\mathcal{L}_{\mathcal{G}_s}$ and A_s^f share a block matrix and thus have at least one equal eigenvalue. Therefore, by lemma 7 the system is uncontrollable. □

Theorem 3 gives sufficient conditions for uncontrollability of the signed network system. However, this by no means is a necessary condition. e.g. a system can be uncontrollable and structurally unbalanced simultaneously.

3.2.2 *Stabilizability and Output Controllability*

Recent developments in controllability have extended the idea of using symmetry to characterize controllability of linear systems.

Theorem 4 (Symmetry Controllability Test [18]). *Consider the general linear dynamics*

$$\dot{x} = Ax + Bu,\ y = Cx,$$

with $A \in \mathbb{R}^{n\times n}$, $B \in \mathbb{R}^{n\times m}$ and $C \in \mathbb{R}^{p\times n}$. For A diagonalizable and C full row rank, consider the conditions on a square matrix P:

a. *$P \neq I, AP = PA$ and $PB = B$*

b. *$CP = ZC$ for some $Z \neq I$*

c. *$\frac{1}{2}(P + P^T) \preceq I$ and $PA + (PA)^T \preceq A + A^T$*

Then, there exists $P \in \mathbb{C}^{n\times n}$ such that

1. *(a) $\iff$ (A, B) uncontrollable*
2. *(a) & (b) $\iff$ (A, B, C) is output uncontrollable*
3. *(a) & (c) $\iff$ (A, B) is unstabilizable*
4. *(a) & (b) & (c) $\iff$ (A, B, C) is output unstabilizable*

Using Theorem 2 in [18], we can now characterize the controllability, output controllability, stabilizability and output stabilizability of the *influenced signed consensus dynamics*

$$\dot{x} = -\mathcal{L}_{\mathcal{G}_s} x + B(I)u,\ y = C(O)x,$$

where $I \subseteq N$ is the set of input nodes, $O \subseteq N$ the set of output nodes, and $B(I), C(I)$ are the matrices

$$B(I) = \begin{bmatrix} | & & | \\ e_{i_1} & \cdots & e_{i_q} \\ | & & | \end{bmatrix}, C(O) = \begin{bmatrix} | & & | \\ f_{j_1} & \cdots & f_{j_p} \\ | & & | \end{bmatrix}^T,$$

in which e_i is the indicator vector for nodes $i \in I$, and f_j for nodes $j \in O$.

Our main result is the following theorem, which identifies structural balance as the key feature for uncontrollability of the dynamics (3.2), on top of symmetry of the underlying unsigned graph. The crux of the argument is that the gauge transformation allows a signed symmetric automorphism to satisfy the criteria in Theorem 2 of [18], allowing a variant of the result in Corollary 5 of [18].

Theorem 5. *Let J be a non-trivial signed fractional automorphism of $\mathcal{L}_{\mathcal{G}}$. Suppose further that $\mathcal{L}_{\mathcal{G}_s}$ is structurally balanced with gauge G_t. Consider dynamics (3.2), and the following conditions on $J_s := G_t J G_t$ with $B_s := G_t B(I)$ and $C_s := C(O)G_t$*

a. $J_s B_s = B_s$

b. $C_s(R) J_s C_s(\mathcal{V} \setminus R)^T = 0, C_s(R) J_s C_s(R)^T = Z \neq I.$

c. $J_s v_i = v_i$ *for all* $v_i \sim \lambda_i(\mathcal{L}_{\mathcal{G}_s}) > 0.$

Then,

1. *(a)* $\iff$ $(-\mathcal{L}_{\mathcal{G}_s}, B)$ *uncontrollable*
2. *(a) & (b)* $\iff$ $(-\mathcal{L}_{\mathcal{G}_s}, B, C)$ *is output uncontrollable*
3. *(a) & (c)* $\iff$ $(-\mathcal{L}_{\mathcal{G}_s}, B, C)$ *is output unstabilizable*
4. *(a) & (b) & (c)* $\iff$ $(-\mathcal{L}_{\mathcal{G}_s}, B, C)$ *is output unstabilizable*

The results hold when $B \to B_s$ *or* $C \to C_s$.

The proof of Theorem 5 is similar to the proof of Corollary 5 in [18], with several technical differences which we discuss here. In particular, our result only requires a fractional automorphism J of the underlying unsigned graph; the matrix J_s does not need to be a signed fractional automorphism, which in this sense generalizes Corollary 5 of [18].

The following lemmas establish the equivalence of controllability under a gauge transformation of the B and C matrices for structurally balanced $\mathcal{L}_{\mathcal{G}_s}$, and some useful identities that will elucidate the role of the gauge transformation in Theorem 5.

Lemma 10. *Let* $(\mathcal{L}_{\mathcal{G}_s}, B(I))$ *be the pair in the dynamics* (3.2)*, and let* $B_s(I) = G_t B(I)$ *for any gauge transformation* G_t *(regardless of whether* $\mathcal{L}_{\mathcal{G}_s}$ *is structurally balanced). Then,* $(-\mathcal{L}_{\mathcal{G}_s}, B(I))$ *is controllable if and only if* $(-\mathcal{L}_{\mathcal{G}_s}, B_s(S))$ *is controllable.*

Furthermore, letting $C_s(O) = C(O) G_t$*, we have that* $(-\mathcal{L}_{\mathcal{G}S}, B(I), C(O))$ *is output controllable if and only if* $(-\mathcal{L}_{\mathcal{G}}, B_s(I), C_s(O))$ *is output controllable.*

Lemma 11. *Consider the dynamics in* (3.2)*. Suppose* $\mathcal{L}_{\mathcal{G}_s}$ *is structurally balanced with gauge* G_t.

1. *Suppose that there is an automorphism* J *such that* $J\mathcal{L}_{\mathcal{G}_s} = \mathcal{L}_{\mathcal{G}_s} J$*. Then,* $J_s \mathcal{L}_{\mathcal{G}_s} = \mathcal{L}_{\mathcal{G}_s} J_s$*, where* $J_s = G_t J G_t$.
2. *Suppose* J *is input symmetric. Then,* $J_s B_s = B_s$.
3. *Suppose that there exists* $Z \neq I$ *such that* $ZC(O) = C(O)J$*. Then,* $ZC_s(O) = C(O)J_s$.

Proof. By Lemma 10, $J_s B_s = B_s$ is equivalent to Theorem 4(a).

Suppose that there exists $Z \neq I$ such that $ZC(O) = C(O)J$ to establish condition Theorem 4(b). Note that $C(O)C(O)^T = I$ and $C(O)C(N \setminus O)^T = 0$, and $[C(O)^T,\ C(N \setminus O)^T]$ is unitary. We can compute

$$\begin{aligned}
0 &= C(O)J - ZC(N \setminus O) \\
&= (C(O)J - ZC(N \setminus O))[C(O)^T,\ C(N \setminus O)^T] \\
&= [C(O)JC(O)^T - ZC(R)C(R)^T, \\
&\quad C(O)JC(N \setminus O)^T - ZC(R)C(N \setminus O)^T] \\
&= [C(O)JC(O)^T - Z,\ C(O)JC(N \setminus O)^T],
\end{aligned}$$

yielding $C(R)JC(N \setminus R)^T = 0$, $C(R)JC(R)^T = Z \neq I$. By Lemma 11(3), this is equivalent if we interchange $J \to J_s$ and $C \to C_s$.

Now, lets assume 5(a), and assume that

$$\begin{aligned}
&-J_s\mathcal{L}_{\mathcal{G}_s} - (\mathcal{L}_{\mathcal{G}_s}J_s)^T \succeq -\mathcal{L}_{\mathcal{G}_s} - \mathcal{L}_{\mathcal{G}_s}^T \\
\implies &\frac{1}{2}\left(J_s\mathcal{L}_{\mathcal{G}_s} + (J_s\mathcal{L}_{\mathcal{G}_s})^T\right) \preceq \mathcal{L}_{\mathcal{G}_s},
\end{aligned}$$

in order to establish Theorem 4(c). Since $(J_s + J_s^T)/2 \preceq I$, we can see that

$$\frac{\lambda_i(\mathcal{L}_{\mathcal{G}_s})}{2} v_i^T(J_s + J_s^T)v_i \geq v_i^T\mathcal{L}_{\mathcal{G}_s}v_i = \lambda_i(\mathcal{L}_{\mathcal{G}_s}),$$

with equality if $J_s v_i = v_i$, and hence $\lambda_i(\mathcal{L}_{\mathcal{G}_s}) > 0$, which holds for the stable modes of $-\mathcal{L}_{\mathcal{G}_s}$. □

We now prove Lemma 10.

Proof. Note that the column space of the controllability matrix of $(-\mathcal{L}_{\mathcal{G}_s}, B)$

$$C(B(I)) := \begin{bmatrix} B & -\mathcal{L}_{\mathcal{G}_s}B & \cdots & (-\mathcal{L}_{\mathcal{G}_s})^{n-1}B \end{bmatrix}$$

is spanned by columns of the form $(-\mathcal{L}_{\mathcal{G}_s})^m e_i$ for $0 \leq m \leq n-1$. The action of a gauge G_t on $B(I)$ is to multiply each column of $B(I)$ by ± 1, and so the column space of the controllability matrix of $(-\mathcal{L}_{\mathcal{G}_s}, B_s)$

$$C(B(I)) := \begin{bmatrix} G_tB & \cdots & (-\mathcal{L}_{\mathcal{G}_s})^{n-1}G_tB \end{bmatrix}$$

is spanned by columns of the form $\sigma_i(-\mathcal{L}_{\mathcal{G}_s})^m e_i$ for $0 \leq m \leq n-1$, and $\sigma_i = \pm 1$. Clearly,

$$\operatorname{span}\{(-\mathcal{L}_{\mathcal{G}_s})^m e_i\} = \operatorname{span}\{\sigma_i(-\mathcal{L}_{\mathcal{G}_s})^m e_i\}$$

and so $\operatorname{rank}[C(B(I))] = \operatorname{rank}[C(B_s(I))]$. The same argument applies for output controllability, considering the output controllability matrix

$$C(B(I), C(O)) := \begin{bmatrix} CB & \cdots & C(-\mathcal{L}_{\mathcal{G}_s})^{n-1}B \end{bmatrix}.$$

□

We now prove Lemma 11.

Proof.

$$\begin{aligned} J_s\mathcal{L}_{\mathcal{G}_s} &= G_tJG_tG_t\mathcal{L}_{\mathcal{G}}G_t \\ &= G_tJ\mathcal{L}_{\mathcal{G}}G_t \\ &= G_t\mathcal{L}_{\mathcal{G}}JG_t \\ &= G_t\mathcal{L}_{\mathcal{G}}G_tG_tJG_t \\ &= \mathcal{L}_{\mathcal{G}_s}J_s. \end{aligned}$$

We know $JB = B$. Hence, $J_sB_s = G_sJG_sG_sB = G_sJB = G_sB = B_s$.

$$ZC(O)G_t = C(O)JG_t = C(O)G_tG_tJG_t = C_s(O)J_s$$

□

Using the equivalences established in these two lemmas, the proof of Theorem 5 follows as the proof of Corollary 5 in [18], but using J_s instead of the signed fractional automorphism P.

3.3 NONLINEAR CONTROLLABILITY OF SIGNED NETWORKS

In this section, we extend previous work [33] to analyze the controllability of nonlinear consensus protocols to the case where these protocols run on a signed network. We consider three types of nonlinear consensus protocols, following the nomenclature in [16], [24], [33].

- **Absolute Nonlinear Flow**

$$\dot{x}_i = -\sum_{j\in N_i}[f(x_i) - \mathrm{sgn}(a_{ij})f(x_j)] \tag{3.6}$$

- **Relative Nonlinear Flow**

$$\dot{x}_i = -\sum_{j\in N_i} f\left(x_i - \mathrm{sgn}(a_{ij})x_j\right) \tag{3.7}$$

- **Disagreement Nonlinear Flow**

$$\dot{x}_i = -f\left(\sum_{j\in N_i} x_i - \mathrm{sgn}(a_{ij})x_j\right) \tag{3.8}$$

To make this section self-contained, we provide two main theorems from [33] which we use later to demonstrate uncontrollability.

Theorem 6. *Let $\mathcal{G} = (\mathcal{V}, \mathcal{E})$ and $F : \mathbb{R}^n \to \mathbb{R}^n$ be a flow on $\mathcal{G}$. Assume φ is a non-identity symmetry on F. Then, for any leader l, the leader-follower network flow on $\mathcal{G}$ induced by l is not accessible from the origin in $\mathbb{R}^{n-1}$.*

Theorem 7. *Let $\mathcal{G} = (\mathcal{V}, \mathcal{E})$ and let $F : \mathbb{R}^n \to \mathbb{R}^n$ be the dynamics in any of (3.6)-(3.8). Also, assume φ be an automorphism of $\mathcal{G}$. Then F is φ-invariant.*

Remark 4. *The more general case of* (3.6)-(3.8) *holds when each node has its own smooth nonlinear function* $f_i : \mathbb{R} \to \mathbb{R}$. *However, as shown in [33],* $f_i = f_{\phi(i)}$ *is a necessary and sufficient condition for all the subsequent controllability analysis to work. Since we assume the general function* f *for all nodes, this condition is automatically satisfied.*

The behavior of the dynamics (3.6)-(3.8) clearly depends on the choice of $f : \mathbb{R} \to \mathbb{R}$. In [24], several classes of functions were considered. First, the class of *translated positive, infinite sector nonlinearities* $\mathcal{S}$ is defined as

$$\mathcal{S} := \Big\{ f : [f(x) - f(x^*)](x - x^*) > 0 \text{ for } x \neq x^*, f(0) = 0, \int_{x^*}^{x} f(t)dt \to \infty \text{ as } |x| \to \infty \Big\}.$$

See [27] for properties of this class of functions. A subset $\mathcal{S}_0 \subset \mathcal{S}$ of these functions that will be used later is the *untranslated* ($x^* = 0$) *positive, infinite sector nonlinearities* given by

$$\mathcal{S}_0 := \Big\{ f : f(x^*)x > 0 \text{ for } x \neq 0, f(0) = 0, \int_{0}^{x} f(t)dt \to \infty \text{ as } |x| \to \infty \Big\}.$$

The reason these classes of functions are interesting is that when combined with the dynamics introduced in (3.6)-(3.8), *clustering* occurs in a structurally balanced graph. This is summarized in the following theorem.

Theorem 8. *(*Theorems 3 & 4 in [24]*) Consider a graph* $\mathcal{G}$. *Assume either the dynamics* (3.6) *with* $f \in \mathcal{S}$ *or the dynamics* (3.7) *with* $f \in \mathcal{S}_0$ *running on* $\mathcal{G}$. *Then,*

$$\lim_{t\to\infty} x(t) = \frac{1}{n}\left(\mathbf{1}^T G_t x(0)\right) G_t \mathbf{1}$$

if and only if $\mathcal{G}$ *is structurally balanced (with gauge transformation* G_t*).*

According to this theorem, for certain classes of functions, the dynamics will converge to two different clusters. These clusters are exactly those corresponding to the bipartite consensus condition in Lemma 1(5).

In the following subsections, we elaborate on the controllability of the dynamics (3.6)-(3.8) and show that a notion of symmetry about the input node, as well as structural balance, lead to uncontrollability. For each case we consider even (symmetric) and odd (anti-symmetric) functions f. From [24] we know if the underlying signed graph $\mathcal{G}$ is structurally balanced, then there exists a gauge transformation G_t that acts as a similarity transformation on the adjacency matrix of $\mathcal{G}$ in that $G_t A_s(\mathcal{G}) G_t = A$ where A is the adjacency matrix of unsigned $\mathcal{G}$. We will show that G_t defines a useful coordinate transformation that allows an immediate application of the uncontrollability test derived by Aguilar and Gharesifard [33].

Before that, we need the following definition to extend the notion of a graph symmetry to signed graphs.

Definition 2. *Let φ be a non-identity automorphism on graph $\mathcal{G}$. Suppose that this graph is structurally balanced, with gauge transformation G_t induced by the function $g : \mathbb{R}^n \to \mathbb{R}^n$ defined by $[g(x)]_i = \sigma_i x_i$. Then, we define* signed automorphism *operator as $\varphi' = g \circ \varphi \circ g$. Moreover, assume that J is the matrix representation of the permutation operator φ, in that $J = D\varphi$. Then, the analogous matrix $J' = G_t J G_t$ is the matrix representation of the signed permutation operator φ', in that $J' = D(g \circ \varphi \circ g)$.*

Definition 2 implies that unlike the unsigned case, the signed automorphism contains sign alterations of edge weights while permuting the nodes. Hence, if $\varphi(x_i) = x_r$, then $\varphi'(x_i) = \sigma_i \sigma_r x_r$. For example, consider the graph in Figure 3.2.

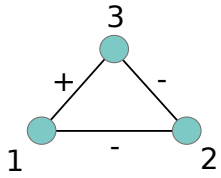

Figure 3.2: Example of a signed automorphism

The corresponding gauge transformation and automorphisms are defined as

$$G_t = \begin{bmatrix} 1 & 0 & 0 \\ 0 & -1 & 0 \\ 0 & 0 & 1 \end{bmatrix}, \; J = \begin{bmatrix} 0 & 1 & 0 \\ 1 & 0 & 0 \\ 0 & 0 & 1 \end{bmatrix}$$

$$J' = G_t J G_t = \begin{bmatrix} 0 & -1 & 0 \\ -1 & 0 & 0 \\ 0 & 0 & 1 \end{bmatrix}.$$

One can note that while the structures of J and J' are similar, the signs of the elements are different. This also implies

$$\varphi'(x_1, x_2, x_3) = (-x_2, -x_1, x_3) \;\Rightarrow\; \begin{cases} \varphi'(x_1) = \sigma_1 \sigma_2 x_2 \\ \varphi'(x_2) = \sigma_1 \sigma_2 x_1 \\ \varphi'(x_3) = \sigma_3 \sigma_3 x_3 \end{cases}$$

Recall that we use $\phi(i)$ as the action of the automorphism on the index of a node rather than the more obscure notation $\varphi(v_i)$. For example, in Figure 3.2 we have that $\phi(1) = 2$ and $\phi(2) = 1$.

3.3.0.1 *Absolute Nonlinear Flow*

The original definition of this kind of flow allows the function f to vary across the nodes [16]. In our problem setup, however, all such functions are assumed to be equal, and thus the dynamics resemble linear consensus in

that we can write $\dot{x} = -\mathcal{L}_{\mathcal{G}_s} f(x)$, where $f(x)$ is the function f applied entry-wise to the vector x.

In the following theorem, we will show that for absolute nonlinear flow with odd functions f, structural balance directly generalizes the uncontrollability conditions in [33]. For the case of even functions, we need to impose additional topological structure on the edge weights of the underlying graph.

Theorem 9. *Consider a structurally balanced graph $\mathcal{G}$ with gauge transformation G_t and* absolute nonlinear flow *dynamics* (3.6). *Further suppose $\mathcal{G}$ has a non-trivial signed automorphism φ'. Let $f : \mathbb{R}^n \to \mathbb{R}$ be a smooth odd function (for example, odd $f \in \mathcal{S}_0$ with f smooth). Then, for any vertex $j \in \mathrm{Fix}(\varphi')$ chosen as the leader, the leader-follower network is not accessible from the origin in $\mathbb{R}^{n-1}$. Moreover, the same results holds for smooth even functions f if φ' preserves edge signs, in that* $\mathrm{sgn}(a_{ij}) = \mathrm{sgn}(a_{\phi(i)\phi(j)})$.

Proof. Following Equation (3.3), let F denote the network flow and assume the dynamics in (3.6). We will first note that for smooth odd functions f, the dynamics of the system can become unsigned by a convenient coordinate transformation. Let $z = G_t x$, or $z_i = \sigma_i x_i$. Then, following [25] we get the equivalent dynamics

$$\begin{aligned}\dot{z}_i &= -\sigma_i \sum_{j\in\mathcal{N}_i} f(\sigma_i z_i) - \mathrm{sgn}(a_{ij}) f(\sigma_j z_j) \\ &= -\sigma_i \sum_{j\in\mathcal{N}_i} \sigma_i f(z_i) - \mathrm{sgn}(a_{ij})\sigma_j f(z_j) \\ &= -\sum_{j\in\mathcal{N}_i} f(z_i) - f(z_j),\end{aligned}$$

which is defined as the unsigned absolute nonlinear flow. Then, from Theorems 6 and 7 we conclude the system is inaccessible.

Now, suppose f is an even function. From (3.6) we have

$$\begin{aligned}F_i(\varphi'(x)) &= -\sum_{l\in N_r} f(\sigma_i\sigma_r x_r) - \mathrm{sgn}(a_{ij}) f(\sigma_j\sigma_l x_l) \\ &= -\sum_{l\in N_r} f(x_r) - \mathrm{sgn}(a_{ij}) f(x_l),\end{aligned}$$

where $r = \phi(i)$ and $l = \phi(j)$ and the property $f(\sigma_i\sigma_j x) = f(x)$ of even functions is used.

On the other hand,

$$F_{\phi(i)}(x) = F_r(x) = -\sum_{l\in N_r} f(x_r) - \mathrm{sgn}(a_{rl}) f(x_l).$$

Hence, F is φ'-invariant if $\mathrm{sgn}(a_{ij}) = \mathrm{sgn}(a_{rl})$. □

The condition on even functions in Theorem 9 can be interpreted as the sign symmetry of the graph, in that if the link between two nodes contains a negative weight, it will remain negative even after the signed automorphism. For instance, sign symmetry does not hold in the graph of Figure 3.2 since

$a_{13} \neq a_{23}$. This feature is in addition to the topological property of structural balance.

3.3.0.2 *Relative Nonlinear Flow*

The main result of this section shows that unlike the absolute nonlinear flow, structural balance on top of the signed variant of the conditions in Theorem 6 imply that the network flow is not accessible from the origin for both even and odd functions, without any additional constraints on edge weight permutations.

Theorem 10. *Consider a structurally balanced graph $\mathcal{G}$ with gauge transformation G_t and* relative nonlinear flow *dynamics. Further suppose $\mathcal{G}$ has a non-trivial automorphism φ'. Let $f : \mathbb{R}^n \to \mathbb{R}$ be a smooth odd or even function (for example, odd $f \in \mathcal{S}_0$ with f smooth). Then, for any vertex $j \in \mathrm{Fix}(\varphi')$ chosen as the leader, the leader-follower network is not accessible from the origin in $\mathbb{R}^{n-1}$.*

Proof. Let the same notations as in proof of Theorem 9 hold. We will show that both cases of odd and even functions f lead to φ'-invariance of the flow F and therefore the inaccessibility from the origin.

Let f be an odd function. Changing the coordinates by $z = G_t x$ yields

$$\begin{aligned}
\dot{z}_i &= -\sigma_i \sum_{j \in \mathcal{N}_i} f(\sigma_i z_i - \mathrm{sgn}(a_{ij})\sigma_j z_j) \\
&= -\sigma_i \sum_{j \in \mathcal{N}_i} f(\sigma_i (z_i - \sigma_i \mathrm{sgn}(a_{ij})\sigma_j z_j)) \\
&= -\sum_{j \in \mathcal{N}_i} f(z_i - z_j),
\end{aligned}$$

which is the unsigned relative nonlinear flow. Hence, F is φ'-invariant and inaccessibility from the origin follows from Theorems 6 and 7.

For even function f, from (3.7)

$$\begin{aligned}
F_i(\varphi'(x)) &= -\sum_{l \in \mathcal{N}_r} f(\sigma_i \sigma_r x_r - \sigma_j \sigma_l \mathrm{sgn}(a_{ij}) x_l) \\
&= -\sum_{l \in \mathcal{N}_r} f(\sigma_i \sigma_r (x_r - \sigma_r \sigma_l \sigma_i \sigma_j \mathrm{sgn}(a_{ij}) x_l)) \\
&= -\sum_{l \in \mathcal{N}_r} f(x_r - \sigma_r \sigma_l x_l) \\
&= -\sum_{l \in \mathcal{N}_r} f(x_r - \mathrm{sgn}(a_{rl}) x_l) \\
&= F_r(x),
\end{aligned}$$

where we have used the fact that $\sigma_i \sigma_j \mathrm{sgn}(a_{ij}) > 0$ hence $\sigma_i \sigma_j = \mathrm{sgn}(a_{ij})$ for all i and $j \in \mathcal{N}_i$. □

3.3.0.3 *Disagreement Nonlinear Flow*

Applying the same assumptions for this type of flow, we will prove similar results without proof for the sake of completeness.

Theorem 11. *Consider a structurally balanced graph $\mathcal{G}$ with gauge transformation G_t and* disagreement nonlinear flow *dynamics. Further suppose $\mathcal{G}$ has a non-trivial automorphism φ'. Let $f : \mathbb{R}^n \to \mathbb{R}$ be a smooth odd or even function (for example, odd $f \in \mathcal{S}_0$ with f smooth). Then, for any vertex $j \in \mathrm{Fix}(\varphi')$ chosen as the leader, the leader-follower network is not accessible from the origin in $\mathbb{R}^{n-1}$.*

Proof. The proof is almost identical to that of Theorem 10 with the same change of coordinates for the odd functions, and similar sign analysis for the even case. □

Remark 5. *The analysis of this section demonstrates that for all of the three nonlinear flows (3.6)-(3.8) structural balance in addition to φ'-invariance leads to system uncontrollability for even and odd functions f. The only exception is when the absolute nonlinear flow f is even. In this case, an edge-sign symmetry condition is also required.*

3.4 AN ASIDE ON STRUCTURAL BALANCE

As stated in the introduction, it is of interest to study the properties of large graphs by examining smaller subgraphs, and how the property composes as you build the graph up. For example, Chapman *et al.* has studied controllability under Cartesian products of graphs [45]. A comprehensive summary of graph products can be found in one of [46]–[48]; the latter if one has a strong grasp of the Russian language.

Suppose that $\mathcal{G}_1 = (\mathcal{V}_1, \mathcal{E}_1, \mathcal{W}_1)$ and $\mathcal{G}_2 = (\mathcal{V}_2, \mathcal{E}_2, \mathcal{W}_2)$. Then the *Cartesian product graph* $\mathcal{G}_1 \square \mathcal{G}_2$ has vertex set $\mathcal{V}_1 \times \mathcal{V}_2$, and edge set $\mathcal{E}_{1\times 2}$ such that $\{(v_1, v_2), (v_1', v_2')\} \in \mathcal{E}_{1\times 2}$ if and only if either $\{v_1, v_1'\} \in \mathcal{E}_1$ and $v_2 = v_2'$, or $\{v_2, v_2'\} \in \mathcal{E}_2$ and $v_1 = v_1'$. The weight of this edge is given by

$$w_{\{(v_1,v_2),(v_1',v_2')\}} = \delta_{v_1,v_1'} w_{v_2,v_2'} + \delta_{v_2,v_2'} w_{v_1,v_1'}.$$

The Cartesian product of graphs is commutative (there is an isomorphism between $\mathcal{G}_1 \square \mathcal{G}_2$ and $\mathcal{G}_2 \square \mathcal{G}_1$), and and associative (there is an isomorphism between $(\mathcal{G}_1 \square \mathcal{G}_2) \square \mathcal{G}_3$ and $\mathcal{G}_1 \square (\mathcal{G}_2 \square \mathcal{G}_3)$). We denote the Cartesian product of n graphs $\mathcal{G}_1, \ldots, \mathcal{G}_n$ as

$$\square_{i=1}^{n} \mathcal{G}_i := \mathcal{G}_1 \square \ldots \square \mathcal{G}_n.$$

We show below how structural balance is preserved under the composition of Cartesian products.

Theorem 12. *Let $\mathcal{G}_1, \mathcal{G}_2, \ldots, \mathcal{G}_n$ be signed graphs. Then, the graph product*

$$\mathcal{G}^{[n]} := \square_{i=1}^{n} \mathcal{G}_i \tag{3.9}$$

is structurally balanced if and only if for each $1 \leq i \leq n$, $\mathcal{G}_i$ is structurally balanced.

Furthermore, suppose that the $\mathcal{G}_i$'s are structurally balanced signed graphs with pairs of bipartition vertex sets $(\mathcal{V}_1^1, \mathcal{V}_2^1), (\mathcal{V}_1^2, \mathcal{V}_2^2), \ldots, (\mathcal{V}_1^n, \mathcal{V}_2^n)$. Then, the bipartition of the graph product in Equation (3.9) is given by $(\mathcal{V}_1^{[n]}, \mathcal{V}_2^{[n]})$ defined in the following way.

Let $l_n := a_1 a_2 \ldots a_n$ be a 2-ary sequence of length n consisting of integers $a_i \in \{1, 2\}$. There are $\#\{l_n\} := 2^n$ such sequences. We call l_n odd *if $\sum_{i=1}^{n} a_i$ is odd, and* even *otherwise. For each such sequence l_n, we identify a bijection with a sequence of sets $\mathcal{V}_{a_i}^i$ as follows:*

$$a_1 a_2 \ldots a_n \longleftrightarrow \mathcal{V}_{a_1}^1 \mathcal{V}_{a_2}^2 \ldots \mathcal{V}_{a_n}^n. \tag{3.10}$$

Lastly, let S_n^e and S_n^o be defined as the sets of even and odd such sequences respectively:

$$S_n^e = \{l_n \in \{1,2\}^n |\ l_n = a_1 \ldots a_n,\ l_n \text{ even}\}$$
$$S_n^o = \{l_n \in \{1,2\}^n |\ l_n = a_1 \ldots a_n,\ l_n \text{ odd}\}.$$

Then, the bipartition $(\mathcal{V}_1^{[n]}, \mathcal{V}_2^{[n]})$ is given by taking unions over products of bipartition vertex sets corresponding to even and odd sequences l_n as follows:

$$\begin{aligned} \mathcal{V}_1^{[n]} &= \bigcup_{l_n \in S_n^e} \left[\bigtimes_{i=1}^{n} \mathcal{V}_{a_i}^i \right] \\ &= \bigcup_{l_n \in S_n^e} \mathcal{V}_{a_1}^1 \times \mathcal{V}_{a_2}^2 \times \cdots \times \mathcal{V}_{a_n}^n \end{aligned} \tag{3.11}$$

$$\begin{aligned} \mathcal{V}_2^{[n]} &= \bigcup_{l_n \in S_n^o} \left[\bigtimes_{i=1}^{n} \mathcal{V}_{a_i}^i \right] \\ &= \bigcup_{l_n \in S_n^o} \mathcal{V}_{a_1}^1 \times \mathcal{V}_{a_2}^2 \times \cdots \times \mathcal{V}_{a_n}^n. \end{aligned} \tag{3.12}$$

Proof. The first statement can be proven by induction. The base case is given by Theorem 5 in [29]. For the inductive step, suppose that the graph product

$$\mathcal{G}^{[n]} := \square_{i=1}^{n} \mathcal{G}_i$$

is structurally balanced. Then, by Theorem 5 in [29], we know that if $\mathcal{G}_{n+1}$ is structurally balanced, then $\mathcal{G}^{[n+1]} := \mathcal{G}^{[n]} \square \mathcal{G}_{n+1}$ is structurally balanced. But, by the associative property of the Cartesian product, we can see that

$$\mathcal{G}^{[n]} \square \mathcal{G}_{n+1} = \square_{i=1}^{n+1} \mathcal{G}_i,$$

and so the result follows.

We can also prove Equations (3.11) and (3.12) by induction, using a bijective combinatorial proof. Consider the base case for $n = 3$: suppose that $\mathcal{G}_1$, $\mathcal{G}_2$ and $\mathcal{G}_3$ have bipartitions $(\mathcal{V}_1, \mathcal{V}_2)$, $(\mathcal{U}_1, \mathcal{U}_2)$ and $(\mathcal{T}_1, \mathcal{T}_2)$ respectively. Consider the graph product $\mathcal{G}_1 \square \mathcal{G}_2 \square \mathcal{G}_3$.

By the definition of the Cartesian product, we have that $\mathcal{G}_1 \square \mathcal{G}_2$ has bipartition

$$\begin{aligned}\mathcal{V}_1' &= (\mathcal{V}_1 \times \mathcal{U}_1) \cup (\mathcal{V}_2 \times \mathcal{U}_2)\\ \mathcal{V}_2' &= (\mathcal{V}_1 \times \mathcal{U}_2) \cup (\mathcal{V}_2 \times \mathcal{U}_1),\end{aligned}$$

and so the graph product $(\mathcal{G}_1 \square \mathcal{G}_2) \square \mathcal{G}_3 = \mathcal{G}_1 \square \mathcal{G}_2 \square \mathcal{G}_3$ has bipartition

$$\begin{aligned}\mathcal{T}_1' &= (\mathcal{V}_1' \times \mathcal{T}_1) \cup (\mathcal{V}_2' \times \mathcal{T}_2)\\ &= (\mathcal{V}_1 \times \mathcal{U}_1 \times \mathcal{T}_1) \cup (\mathcal{V}_2 \times \mathcal{U}_2 \times \mathcal{T}_1)\\ &\quad \cup (\mathcal{V}_2 \times \mathcal{U}_1 \times \mathcal{T}_2) \cup (\mathcal{V}_1 \times \mathcal{U}_2 \times \mathcal{T}_2) \qquad (3.13)\\ \mathcal{T}_2' &= (\mathcal{V}_1' \times \mathcal{T}_2) \cup (\mathcal{V}_2' \times \mathcal{T}_1)\\ &= (\mathcal{V}_1 \times \mathcal{U}_1 \times \mathcal{T}_2) \cup (\mathcal{V}_2 \times \mathcal{U}_2 \times \mathcal{T}_2)\\ &\quad \cup (\mathcal{V}_1 \times \mathcal{U}_2 \times \mathcal{T}_1) \cup (\mathcal{V}_2 \times \mathcal{U}_1 \times \mathcal{T}_1). \qquad (3.14)\end{aligned}$$

There are $2^3 = 8$ 2-ary sequence l_n, and notice that the terms in Equation (3.13) correspond by the bijection (3.10) to the 4 odd sequences and the terms in Equation (3.14) correspond to the 4 even sequences. This concludes the base case.

For the induction step, suppose for each $1 \leq m \leq n$ that the (structurally balanced) graph product

$$\mathcal{G}^{[m]} := \square_{i=1}^{m} \mathcal{G}_i$$

has bipartition $(\mathcal{V}_1^{[m]}, \mathcal{V}_2^{[m]})$ corresponding to Equations (3.11) and (3.12). Let $\mathcal{G}_{n+1}$ be structurally balanced with bipartition $(\mathcal{V}_1^{n+1}, \mathcal{V}_2^{n+1})$. Then, by the definition of the Cartesian product, the graph product $\mathcal{G}^{[n+1]} := \mathcal{G}^{[n]} \square \mathcal{G}_{n+1}$ has bipartition

$$\mathcal{V}_1^{[n+1]} = \left(\mathcal{V}_1^{[n]} \times \mathcal{V}_1^{n+1}\right) \cup \left(\mathcal{V}_2^{[n]} \times \mathcal{V}_2^{n+1}\right) \qquad (3.15)$$

$$\mathcal{V}_2^{[n+1]} = \left(\mathcal{V}_1^{[n]} \times \mathcal{V}_2^{n+1}\right) \cup \left(\mathcal{V}_2^{[n]} \times \mathcal{V}_1^{n+1}\right). \qquad (3.16)$$

Let's examine the two terms appearing on the right-hand-side of Equation (3.15). First, we can see that

$$\begin{aligned}\mathcal{V}_1^{[n]} \times \mathcal{V}_1^{n+1} &= \left[\bigcup_{l_n \in S_n^e} \mathcal{V}_{a_1}^1 \times \mathcal{V}_{a_2}^2 \times \cdots \times \mathcal{V}_{a_n}^n\right] \times \mathcal{V}_1^{n+1}\\ &= \bigcup_{l_n \in S_n^o} \mathcal{V}_{a_1}^1 \times \mathcal{V}_{a_2}^2 \times \cdots \times \mathcal{V}_{a_n}^n \times \mathcal{V}_1^{n+1}.\end{aligned}$$

Hence, every term in the union corresponds by the bijection (3.10) to a 2-ary sequence of length $n+1$ given by $a_1 a_2 \ldots a_n 1$. Since $\sum_{i=1}^{n} a_n$ is even,

$1+\sum_{i=1}^{n} a_i$ is odd. The second term on the right-hand-side of Equation (3.15) is similarly given by

$$\mathcal{V}_2^{[n]} \times \mathcal{V}_2^{n+1} = \bigcup_{l_n \in S_n^o} \mathcal{V}_{a_1}^1 \times \mathcal{V}_{a_2}^2 \times \cdots \times \mathcal{V}_{a_n}^n \times \mathcal{V}_2^{n+1},$$

whose terms correspond by the bijection (3.10) to 2-ary sequences of length $n+1$ given by $a_1 a_2 \ldots a_n 2$. Since $\sum_{i=1}^{n} a_n$ is odd, $2 + \sum_{i=1}^{n} a_i$ is odd. These two terms correspond to all the ways of getting odd, length-$(n+1)$, 2-ary sequences: by taking length-n sequences and concatenating the appropriate term in $\{1, 2\}$ to the end of them. It follows by the bijection (3.10) that

$$\mathcal{V}_1^{[n+1]} = \bigcup_{l_n \in S_{n+1}^o} \mathcal{V}_{a_1}^1 \times \mathcal{V}_{a_2}^2 \times \cdots \times \mathcal{V}_{a_{n+1}}^{n+1}.$$

A similar calculation by considering the two terms in the right-hand-side of Equation (3.16) yields

$$\mathcal{V}_2^{[n+1]} = \bigcup_{l_n \in S_{n+1}^e} \mathcal{V}_{a_1}^1 \times \mathcal{V}_{a_2}^2 \times \cdots \times \mathcal{V}_{a_{n+1}}^{n+1},$$

and so the result follows by induction.

For the converse direction, suppose that $\mathcal{G}_1 \square \mathcal{G}_2$ is structurally balanced. In order to derive a contradiction, suppose (without loss of generality) that $\mathcal{G}_1$ is not structurally balanced. Then, $\mathcal{G}_1$ has a negative cycle. By the definition of the Cartesian product, $\mathcal{G}_1$ appears as a subgraph in $\mathcal{G}_1 \square \mathcal{G}_2$, and so the negative cycle in $\mathcal{G}_1$ appears in $\mathcal{G}_1 \square \mathcal{G}_2$, a contradiction. A similar contradiction can be achieved for an induction step, yielding the converse direction.

□

4

KOOPMAN ANALYSIS ON SIGNED NETWORKS

4.1 KOOPMAN OPERATOR THEORY

In the early 1930s, Koopman showed that nonlinear dynamical systems associated with Hamiltonian flows could be analyzed with an infinite-dimensional linear operator on the Hilbert space of functions on the state space of that dynamical system. The resulting field, called Koopman analysis, has been at the heart of recent data-driven efforts to characterize complex systems and there is a considerable interest in obtaining finite-dimensional representations of the Koopman operator that offer high-fidelity approximation of nonlinear systems.

For an introductory example, we show one rigorous way how a finite-dimensional ordinary differential equation can be written as an infinite-dimensional partial differential equation [49]. Suppose we have the nonlinear system of ODEs

$$\frac{d}{dt}\phi(x,t) = R\left(\phi(x,t)\right),\ \phi(x,0) = x \tag{4.1}$$

and we want to write it as

$$u_t = Lu,\ u(x,0) = g(x)$$

for some choice of u, L, g. First, we need a lemma.

Lemma 12.

$$R\left(\phi(x,t)\right) = D_x\phi(x,t)R(x)$$

where $D_x\phi$ is the Jacobian of ϕ given by

$$D_{x_j}\phi_i(x,t) = \frac{\partial \phi_i}{\partial x_j}.$$

Proof. Let $F = R\left(\phi(x,t)\right) - D_x\phi(x,t)R(x)$. We want to shown that F is identically zero. First, at $t = 0$ we have

$$\begin{aligned} F(x,0) &= R\left(\phi(x,0)\right) - D_x\phi(x,0)R(x) \\ &= R(x) - IR(x) = 0, \end{aligned}$$

since $D_x\phi(x,0) = D_x x = I$. Now, look at

$$\begin{aligned}
\frac{\partial F}{\partial t} &= \frac{\partial R}{\partial t} - \frac{\partial}{\partial t}\left[D_x\phi(x,t)R(x)\right] \\
&= \left[D_x R\right] \underbrace{\left(\phi(x,t)\right)}_{\text{Argument of } D_x R} \frac{\partial \phi}{\partial t} - \left(D_x \frac{\partial \phi}{\partial t}\right) R(x) \\
&= \left[D_x R\right]\left(\phi(x,t)\right) R\left(\phi(x,t)\right) - D_x R\left(\phi(x,t)\right) R(x) \\
&= \left[D_x R\right]\left(\phi(x,t)\right) R\left(\phi(x,t)\right) - \left[D_x R\right]\left(\phi(x,t)\right) D_x\phi(x,t)R(x) \\
&= \left[D_x R\right]\left(\phi(x,t)\right) \underbrace{\left[R\left(\phi(x,t)\right) - D_x\phi(x,t)R(x)\right]}_{F}.
\end{aligned}$$

The IVP defined by

$$\frac{\partial F}{\partial t} = \left[D_x R\right]\left(\phi(x,t)\right) F,\ F(x,0) = 0$$

has the unique solution (given R, ϕ are smooth) of $F(x,t) = 0$. □

Now we can prove the main result.

Claim 1. *Let g be an arbitrary smooth function. Then, when $\phi(x,t)$ solves the problem (4.1), we have that $u(x,t) = g\left(\phi(x,t)\right)$ is the unique solution to*

$$u_t = Lu,\ u(x,0) = g(x)$$

where L is the Liouville operator given by

$$L = \sum_i R_i \frac{\partial}{\partial x_i}.$$

Proof. Note that $u(x,0) = g(x)$ immediately from the relation $u(x,t) = g\left(\phi(x,t)\right)$. Then,

$$\begin{aligned}
\frac{\partial u}{\partial t} &= \sum_i \frac{\partial g\left(\phi(x,t)\right)}{\partial x_i} \frac{\partial \phi_i(x,t)}{\partial t} \\
&= \sum_i R_i\left(\phi(x,t)\right) \frac{\partial g\left(\phi(x,t)\right)}{\partial x_i}.
\end{aligned}$$

Recall by the lemma that $R_i\left(\phi(x,t)\right) = D_x\phi(x,t)R_i(x) = \sum_j \frac{\partial \phi_i(x,t)}{\partial x_j} R_j(x)$, and so we have

$$\begin{aligned}
\frac{\partial u}{\partial t} &= \sum_i \left(\sum_j \frac{\partial \phi_i(x,t)}{\partial x_j} R_j(x) \right) \frac{\partial g\left(\phi(x,t)\right)}{\partial x_i} \\
&= \sum_j R_j(x) \left(\sum_i \frac{\partial g\left(\phi(x,t)\right)}{\partial x_i} \right) \frac{\partial \phi_x(x,t)}{\partial x_j} \\
&= \sum_j R_j(x) \frac{\partial g\left(\phi(x,t)\right)}{\partial x_j} \\
&= Lu
\end{aligned}$$

□

In summary, given a system of ODEs

$$\frac{d}{dt}\phi(x,t) = R\left(\phi(x,t)\right),\ \phi(x,0) = x$$

with solution $\phi(x,t)$, we can write it as

$$\frac{\partial u}{\partial t} = \sum_i R_i(x) \frac{\partial g\left(\phi(x,t)\right)}{\partial x_i},\ u(x,0) = g(x)$$

with solution $u = g\left(\phi(x,t)\right)$.

We can relate this to a probabilistic interpretation in the context of Hamiltonian mechanics.

Recall that the Hamiltonian $\mathcal{H}$ is roughly the total energy of the system. A system is called *Hamiltonian* if it obeys Hamilton's equations of motion, given by

$$\frac{dp}{dt} = -\frac{\partial H}{\partial q},\ \frac{dq}{dt} = \frac{\partial H}{\partial p}$$

where q denotes the position vector and p denotes the momentum vector.

Suppose we have a Hamiltonian system with n degrees of freedom, namely that $q = (q_1, \ldots, q_n)$ and $p = (p_1, \ldots, p_n)$. The system exists in a $2n$-dimensional phase space $\Gamma = \{q, p\}$. Since we cannot computationally hope to keep track of $2n$ equations of motion, what we will do is assume that the initial data $p(0), q(0)$ are drawn from some probability distribution $W(t)$ and look at the collection, or ensemble, of trajectories that are initially distributed by $W(t)$. To this end, we have a few definitions:

1. **Microstate**: A vector $[q(t), p(t)] \in \Gamma$; drawn from $W(t)$
2. **Macrostate**: $W(t)$; describes the ensemble at time t
3. **Sample Space**: Ω; the set of all macrostates

Now, we derive the equations of motion for the macrostate. Define $u = (\dot{q}_1, \ldots, \dot{p}_n)$. Then, u is an incompressible vector field:

$$\begin{aligned}\nabla u &= \sum_{i=1}^{n} \frac{\partial}{\partial q_i}\left(\frac{dq_i}{dt}\right) + \sum_{i=1}^{n} \frac{\partial}{\partial p_i}\left(\frac{dp_i}{dt}\right) \\ &= \sum_{i=1}^{n} \frac{\partial}{\partial q_i}\frac{\partial H}{\partial p_i} - \frac{\partial}{\partial p_i}\frac{\partial H}{\partial q_i} \\ &= \sum_{i=1}^{n} \frac{\partial^2 H}{\partial q_i \partial p_i} - \frac{\partial^2 H}{\partial p_i \partial q_i} = 0.\end{aligned}$$

Next, consider a volume V in the phase space Γ, with probability density W. Then, the number of microstates in V at time t is on average given by

$$\int_V W dq dp = \int_V W dV$$

where $dp = dp_1 \ldots dp_n$ and $dq = dq_1 \ldots dq_n$. Now, microstates do not spontaneously appear or disappear. Therefore, the change in the number of microstates only comes from the inflow and outflow at the boundary of V. Therefore, by Green's Theorem, we get

$$\frac{d}{dt}\int_V W dq dp = -\int_{\partial V} W(u \cdot n) ds = -\int_V \nabla (Wu)\, dV.$$

If the density W is smooth, then we get

$$\int_V \left(\frac{\partial W}{\partial t} + \nabla (Wu)\right) dq dp = 0.$$

This implies that

$$\begin{aligned}\frac{\partial W}{\partial t} + \nabla (Wu) &= 0 \\ &= \frac{\partial W}{\partial t} + W \cdot \nabla u + u \cdot \nabla W \\ &= \frac{\partial W}{\partial t} + u \cdot \nabla W.\end{aligned}$$

Now, we can specify the Liouville operator

$$L = -\sum_{i=1}^{n} \left(\frac{\partial H}{\partial p_i}\frac{\partial}{\partial q_i} - \frac{\partial H}{\partial q_i}\frac{\partial}{\partial p_i}\right)$$

which will give

$$\frac{\partial W}{\partial t} = LW.$$

Based on the previous discussion on converting a system of nonlinear ODEs with nonlinear right-hand-side function R into a linear system of PDEs, we

can see by the definition of the Liouville operator here that $R_i(x = (q,p)$ is given by

$$R_i(x) = \left[\frac{dq_i}{dt}, \frac{dp_i}{dt}\right].$$

In summary, given a (nonlinear) system of ODEs

$$\frac{d}{dt}\phi(x,t) = R\left(\phi(x,t)\right),\ \phi(x,0) = x$$

with solution $\phi(x,t)$, we can write it as the (linear) system of PDEs

$$\frac{\partial u}{\partial t} = \sum_i R_i(x)\frac{\partial g\left(\phi(x,t)\right)}{\partial x_i},\ u(x,0) = g(x)$$

with solution $u = g\left(\phi(x,t)\right)$. In more convenient notation, this is simply

$$\frac{\partial u}{\partial t} = Lu$$

where L is the Liouville operator

$$\sum_i R_i(x)\frac{\partial}{\partial x_i}.$$

To get the equations of motion for a probability distribution (or macrostate), we can specify the Liouville operator

$$\begin{aligned} L &= -\sum_{i=1}^{n}\left(\frac{\partial H}{\partial p_i}\frac{\partial}{\partial q_i} - \frac{\partial H}{\partial q_i}\frac{\partial}{\partial p_i}\right) \\ &= \sum_{i=1}^{n}\left[\frac{dq_i}{dt}, \frac{dp_i}{dt}\right]\begin{bmatrix} \frac{\partial}{\partial q_i} \\ \frac{\partial}{\partial p_i} \end{bmatrix}. \end{aligned}$$

In other words, the function $R_i(x)$ is simply the Hamiltonian equations of motion

$$R_i(x) = \left[\frac{dq_i}{dt}, \frac{dp_i}{dt}\right]$$

and the partial derivative with respect to x is over the phase space variables $x = (q,p)$:

$$\frac{\partial}{\partial x} = \begin{bmatrix} \frac{\partial}{\partial q_i} \\ \frac{\partial}{\partial p_i} \end{bmatrix}.$$

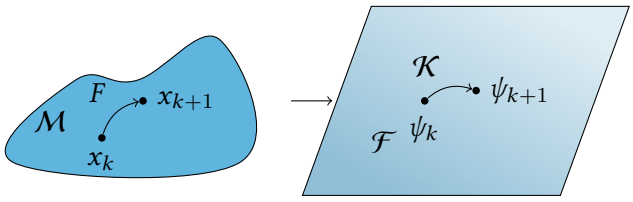

Figure 4.1: Cartoon of the Koopman operator approach: the composition operator 'lifts' a nonlinear manifold $\mathcal{M}$ into a linear, infinite-dimensional manifold on which observables of the state $x \in \mathcal{M}$ evolve

This will give the evolution of the probability density generating $x(t) = (q(t), p(t))$

$$\frac{\partial W}{\partial t} = LW.$$

In a manner analogous to the above discussion, the *Koopman operator* $\mathcal{K}$ 'lifts' a nonlinear ODE into a linear, infinite-dimensional PDE on the space of *observables*.

The Koopman operator is a powerful tool for the analysis and decomposition of nonlinear dynamical systems. This makes more sense if we assume that we have a linear approximation of a nonlinear dynamical system. Then, it becomes possible to not only investigate the behavior of the dynamical system as a linear system (where we know all the prominent definitions of controllability, stability, LQR, etc.), but also recover the state from the Koopman features in some cases.

Consider the following discrete-time nonlinear dynamical system

$$x_{k+1} = F(x_k),$$

where x_k is the state of the system at timestep k, and $F : \mathcal{M} \to \mathcal{M}$ is a nonlinear dynamical map propagating the state. Then, the Koopman operator $\mathcal{K}$, is defined on functions of states $\psi : \mathcal{M} \to \mathbb{R}$ as follows:

$$\begin{aligned} \mathcal{K}\psi = \psi \circ F \quad &\Rightarrow \quad \mathcal{K}\psi(x_k) = \psi(F(x_k)) = \psi(x_{k+1}) \\ &\Rightarrow \quad \psi(x_{k+1}) = \mathcal{K}\psi(x_k). \end{aligned} \tag{4.2}$$

We call the function ψ an *observable*, and the Koopman operator governs its evolution in time. Note that the action of the Koopman operator on ψ given in Equation ((4.2)) is linear.

Although the action of $\mathcal{K}$ is linear, the space of functions ψ is infinite-dimensional in general. Therefore, although one can envision some basis of functions describing all possible ψ on the manifold of the dynamical system, one cannot in general write, say, a finite-dimensional matrix representation of $\mathcal{K}$. Moreover, the dynamical framework adds some additional complexity in terms of decomposing the Koopman operator into algebraic quantities. By this, we mean that not only are there notions of "eigenvectors" of this operator, there are also *eigenfunctions*.

We call the function $\varphi(x)$ an *eigenfunction* of $\mathcal{K}$ corresponding to the *eigenvalue* μ if $\mathcal{K}\varphi(x) = e^{\mu t}\varphi(x)$. For an observable function ψ in the span of

Koopman eigenfunctions, one can write $\psi(x) = \sum_{k=1}^{\infty} v_k \varphi_k(x)$, where the v_k's are the *Koopman modes*. For the case of *full-state observable* $\psi(x) = x$ the states can be reconstructed

$$x(t) = g(x(t)) = \sum_{k=1}^{\infty} e^{\mu_k t} \varphi_k(x_0) v_k,$$

where we refer to $\{\mu_k, \varphi_k, v_k\}$ as the *Koopman triple*.

As stated before, the Koopman operator is linear, but can be infinite-dimensional. To make this operator computationally usable, a numerical approximation of Koopman operator can be obtained by EDMD, resulting in a finite-dimensional approximation $\mathbf{K}$ [43].

We describe the algorithm to find the Koopman finite-dimensional approximation $\mathbf{K}$. First, the required quantities to input into the algorithm are

- Pairs of snapshots gathered from data in the form of

  $$X = [x_1\ x_2\ \dots\ x_M] \quad , \quad Y = [y_1\ y_2\ \dots\ y_M]$$

  where $y_i = F(x_i)$ and M is the number of the measurements taken from the system.

- A clever choice of observables in the form of

  $$\Psi(x) = [\psi_1(x)\ \psi_2(x)\ \dots\ \psi_{N_K}(x)]$$

  where N_K is a number approximately denoting the 'order' of the approximation. For example, one can take polynomials up to order N_K.

- An appropriate weight matrix for constructing the modes later in the algorithm

  $$B = [b_1\ b_2\ \dots\ b_{N_K}]$$

Then, we can obtain the finite-dimensional approximation as follows

$$\mathbf{K} = G^{\dagger} A$$

where A and G are computed as

$$G = \frac{1}{M} \sum_{m=1}^{M} \Psi(x_m)^* \Psi(x_m)$$

$$A = \frac{1}{M} \sum_{m=1}^{M} \Psi(x_m)^* \Psi(y_m).$$

Then, the approximate Koopman modes $\{v_i\}_{i=1}^{N_K}$ are given by

$$v_i = (w_i^* B)^T,$$

where w_i is the ith left eigenvector of $\mathbf{K}$.

4.2 IDENTIFICATION OF BIPARTITION IN STRUCTURALLY BALANCED GRAPHS WITH THE KOOPMAN OPERATOR AND EDMD

In this section, we extend the data-driven approach by Pan *et al.* in using data-driven methods to identify the bipartite consensus for some of the nonlinear network flows considered in the preceding section. Our main result asserts that the Koopman mode corresponding to the zero eigenvalue of the Koopman operator contains the sign structure indicating the bipartite consensus.

Theorem 13. *Consider either the dynamics* (3.6) *with* $f \in \mathcal{S}$ *or the dynamics* (3.7) *with* $f \in \mathcal{S}_0$. *Recall that the full-state observable can be written in terms of the Koopman triple as*

$$x(t) = \sum_{j=1}^{\infty} e^{\lambda_j t} \varphi_j(x_0) v_j. \tag{4.3}$$

If the underlying graph is structurally balanced, then the following hold:

1. $\lambda_i \leq 0$ *with a unique zero eigenvalue.*
2. *Let* $\lambda_1 = 0$. *Then, the sign structure of the corresponding Koopman mode* v_1 *corresponds to the bipartition of nodes denoted in Lemma 1(5).*

Proof. By Theorem 8, if $\mathcal{G}$ is structurally balanced, then we have that

$$\lim_{t\to\infty} x(t) = \frac{1}{n}\left(\mathbf{1}^T G_t x_0\right) G_t \mathbf{1}.$$

Hence, $\lambda_i \leq 0$ since otherwise the RHS of Equation (4.3) does not converge.

The sign structure of the vector $G_t\mathbf{1}$ corresponds to bipartition of nodes denoted in Lemma 1(5). Since $\lambda_1 = 0$ is unique, by setting $\alpha = (1/n)\mathbf{1}^T G_t x_0$ we have that

$$\lim_{t\to\infty} x(t) = \lim_{t\to\infty} \sum_{j=1}^{\infty} e^{\lambda_j t} \varphi_j(x_0) v_j = \varphi_1(x_0) v_1 = \alpha G_t \mathbf{1}.$$

Since both α and $\varphi_1(x_0)$ are constants, we can see that $v_1 \propto G_t\mathbf{1}$, and the result follows. □

In §5.5, we show an example where we use EDMD to approximate the first mode of the Koopman operator to obtain the sign structure corresponding to the bipartite consensus.

5

EXAMPLES

In this section, we show some examples that highlight the necessity of combining φ-invariance, structural balance and leader-node symmetry for uncontrollability of signed networks. To see examples that show the necessity of combining φ-invariance and leader-node symmetry for unsigned graphs, we refer the reader to [33]. In particular, we show the difference between consensus under signed and unsigned consensus, for linear and nonlinear consensus. We then show an example of using EDMD to obtain the bipartite consensus structure of a nonlinear flow on a structurally balanced graph.

5.1 BIPARTITE CONSENSUS

Signed Laplacians considered in this section exhibit clustering when structurally balanced. Consider the signed network in Figure 5.3a, and its unsigned counterpart. Note that the signed network is structurally balanced, since the product of the edge weights over all three cycles is positive. The consensus dynamics (with no control input) beginning at $x_0 = [1, 2, 3, 4]^T$ for these two networks are shown in Figure 5.1. As one can see, the signed consensus converges to two clusters rather than a single equilibrium point.

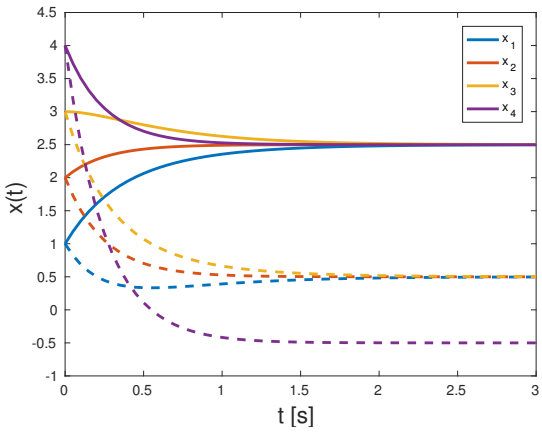

Figure 5.1: Solid lines: unsigned consensus. Dashed lines: signed consensus on structurally balanced graph

5.2 MIMO PERTURBED LAPLACIAN

In this example, we consider the MIMO case with two input signals injected onto nodes 4 and 5. The partition is equitable and $\pi = \{C_1, C_2, C_3, C_4\}$ and $\pi_f = \{C_1, C_2\}$. Moreover

$$A = \begin{bmatrix} 0 & -1 & -1 & 0 & -1 \\ -1 & 0 & 1 & 1 & 0 \\ -1 & 1 & 0 & 1 & 0 \\ 0 & 1 & 1 & 0 & 0 \\ -1 & 0 & 0 & 0 & 0 \end{bmatrix}, \; P' = \begin{bmatrix} -1 & 0 & 0 & 0 \\ 0 & 1 & 0 & 0 \\ 0 & 1 & 0 & 0 \\ 0 & 0 & 1 & 0 \\ 0 & 0 & 0 & 1 \end{bmatrix}$$

$$A(\mathcal{G}/\pi) = \begin{bmatrix} 0 & 2 & 0 & 1 \\ 1 & 1 & 1 & 0 \\ 0 & 2 & 0 & 0 \\ 1 & 0 & 0 & 0 \end{bmatrix}.$$

The system in figure 5.2a is structurally balanced and π_f contains the nontrivial cell C_2 in π and thus the system is uncontrollable. However, changing one negative sign to positive as depicted in figure 5.2 makes the system structurally unbalanced and the system becomes controllable.

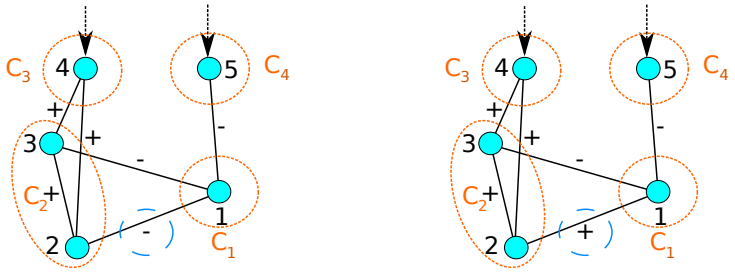

Figure 5.2: (a) Uncontrollable and structurally balanced graph with π_f containing nontrivial cells in π. (b) The same system with one change in the signs. No structural balance and controllable.

5.3 INFLUENCED CONSENSUS

Previously, we discussed that symmetry alone is not sufficient for uncontrollability. In this section we show an example of a symmetric signed network that is controllable.

Consider the influenced consensus networks in Figure 5.3. As one can see, the network in Figure 5.3a is structurally balanced, but the one in Figure 5.3b is not. The Laplacians for these two networks are, respectively,

$$L_1 = \begin{bmatrix} 2 & -1 & 0 & 1 \\ -1 & 3 & 1 & 1 \\ 0 & 1 & 2 & 1 \\ 1 & 1 & 1 & 3 \end{bmatrix}, \; L_2 = \begin{bmatrix} 2 & -1 & 0 & 1 \\ -1 & 3 & -1 & 1 \\ 0 & -1 & 2 & 1 \\ 1 & 1 & 1 & 3 \end{bmatrix}.$$

The controllability matrices for these two networks are, respectively:

$$C_1 = \begin{bmatrix} 0 & 1 & 4 & 16 \\ 0 & 1 & 4 & 16 \\ 0 & 1 & 4 & 16 \\ 1 & 3 & 12 & 48 \end{bmatrix}, \; C_2 = \begin{bmatrix} 0 & 1 & 4 & 14 \\ 0 & 1 & 6 & 32 \\ 0 & 1 & 6 & 30 \\ 1 & 3 & 12 & 52 \end{bmatrix}.$$

As one can see, the network in Figure 5.3a is uncontrollable since C_1 is rank-deficient, but the network in Figure 5.3b is controllable, and hence one can conclude that unsigned symmetry is not sufficient for uncontrollability.

5.4 UNSIGNED SYMMETRY IS NOT SUFFICIENT FOR UNCONTROLLABILITY

Here we show an example of a network flow on a signed graph which has a leader-node symmetry. We show that in one case, the graph is structurally balanced, and the induced flow is hence uncontrollable. By altering the sign on a single edge, structural balance is lost and the resulting network flow is controllable.

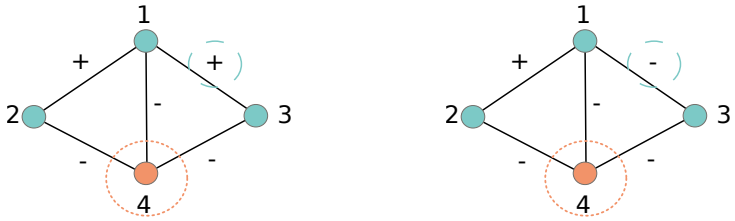

Figure 5.3: (a) Structurally balanced graph with a leader symmetry about node 4. (b) Structurally unbalanced graph with a leader symmetry about node 4.

Consider the structurally balanced graph in Figure 5.3a, and the structurally unbalanced graph in Figure 5.3b. These have respective dynamics

$$\dot{x} = -\mathcal{L}_{\mathcal{G}_1} x - \mathbf{1}u, \quad \dot{x} = -\mathcal{L}_{\mathcal{G}_2} x - \mathbf{1}u,$$

with Laplacians

$$L_1 = \begin{bmatrix} 2 & -1 & 0 \\ -1 & 3 & 1 \\ 0 & 1 & 2 \end{bmatrix}, \; L_2 = \begin{bmatrix} 2 & -1 & 0 \\ -1 & 3 & -1 \\ 0 & -1 & 2 \end{bmatrix}.$$

The controllability matrices of these dynamics are respectively,

$$C_1 = \begin{bmatrix} 1 & 1 & 1 \\ 1 & 1 & 1 \\ 1 & 1 & 1 \end{bmatrix}, \; C_2 = \begin{bmatrix} 1 & 1 & -1 \\ 1 & 3 & 11 \\ 1 & 3 & 9 \end{bmatrix}.$$

5.5 IDENTIFICATION OF BIPARTITE STRUCTURE

In this subsection, we consider a numerical method to identify the bipartite consensus structure of nonlinear dynamics on a structurally balanced graph. We do this by exploiting Theorem 13, and numerically approximating the Koopman mode corresponding to the zero eigenvalue. The goal is to take data from an unknown dynamical system and numerically identify the two groups of agents between which only exist antagonistic interactions. i.e. the bipartition of nodes in Lemma 1(5).

Consider the dynamics (3.7) with $f(\cdot) = \sin(\cdot)$. The underlying structurally balanced graph is pictured in Figure 5.4.

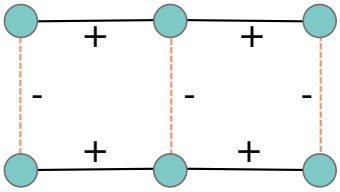

Figure 5.4: Underlying structurally balanced signed graph for EDMD example. Dashed edges indicate negative edges.

We use EDMD to approximate the first Koopman mode corresponding to the zero eigenvalue. We refer the reader to [43] for a detailed explanation of the EDMD algorithm; a summary of the relevant computations is shown in Algorithm 1.

Algorithm 1: Extended Dynamic Mode Decomposition

Input: Data $\{[X_i, Y_i]\}_{i=1}^{n-1} = \{[X_i, X_{i+1}]\}_{i=1}^{n-1}$
Dictionary $\Psi_i = \psi_i(x_1, \ldots, x_n)$, $1 \le i \le N_K$
Matrix $B \in \{0,1\}^{n \times N_k}$ s.t. $\Psi_j = x_i \Leftrightarrow B_{ij} = 1$
Result: Koopman Modes $\{v_i\}$
Compute
$G = 1/(n-1) \sum_{m=1}^{n-1} \Psi(X_m)^* \Psi(X_m)$
$A = 1/(n-1) \sum_{m=1}^{n-1} \Psi(X_m)^* \Psi(Y_m)$
$K = G^\dagger A$
Decompose K Into
Eigenvalues: μ_i
Right Eigenvectors: ξ_i
Left Eigenvectors: w_i
Compute
Koopman Modes: $v_i = (w_i^* B)^T$, $1 \le i \le N_K$

In particular, we use a dictionary of functions of the form $\psi_k = \prod_{i=1}^{6} H(x_i, j_i)$ where $H(x_i, j_i)$ is the j_ith order Hermite polynomial of x_i. We use all such possible ψ_k for Hermite polynomials up to order 2. Simple combinatorics indicates that there are 729 such functions ψ_k for a 6-node graph; hence $N_k = 729$ in Algorithm 1.

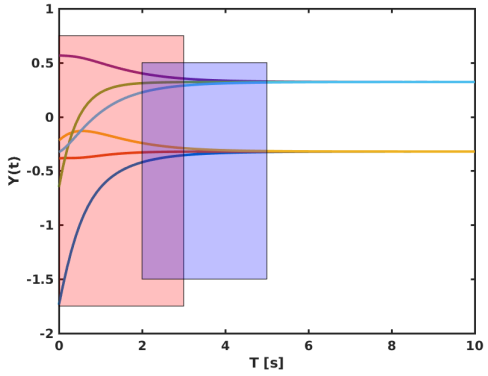

Figure 5.5: Evolution of Dynamics 3.7 with $f(\cdot) = \sin(\cdot)$ on the graph in Figure 5.4. Left (red) shaded region corresponds to $\bar{v}_1^2$ and the right (blue) shaded region corresponds to $\bar{v}_1^3$.

The dynamics are shown in Figure 5.5 for an initial condition of $x_0 = (-1.73, -0.38, -0.21, 0.56, -0.65, -0.32)$. The EDMD procedure in Algorithm 1 was applied to three sets of data with a time-step of 0.1, as depicted in Figure 5.5: the full data (from $0 \leq t \leq 10$), the data in the red shaded region ($0 \leq t \leq 3$) and the data in the blue shaded region $2 \leq t \leq 5$). The computed Koopman modes corresponding to $\bar{\lambda}_1 \approx 1$ for these regions respectively are

$$\bar{v}_1^1 = \begin{bmatrix} 0.018 \\ 0.026 \\ 0.016 \\ -0.020 \\ -0.020 \\ -0.011 \end{bmatrix}, \bar{v}_1^2 = \begin{bmatrix} 0.019 \\ 0.021 \\ 0.015 \\ -0.018 \\ -0.020 \\ -0.007 \end{bmatrix}, \bar{v}_1^3 = \begin{bmatrix} 0.016 \\ 0.023 \\ 0.015 \\ -0.018 \\ -0.016 \\ -0.012 \end{bmatrix},$$

which all contain sign structure corresponding to the bipartition depicted in Figure 5.4. Despite not using all available data, the EDMD procedure was able to extract the bipartition well before the dynamics converged (after which the bipartite structure is obvious from the data). This begs the question *how early can we detect the bipartite structure of the underlying dynamics?* We will address this question in future works.

6

DISTRIBUTED STATE ESTIMATION

6.1 MOTIVATION FOR DISTRIBUTED STATE ESTIMATION

In this section, we lay out the mathematical notation used for the remainder of the chapter, and summarize the essential background on Kalman filtering.

Consider the *noisy discrete-time controlled linear system*

$$\begin{aligned} x_{k+1} &= Ax_k + Bu_k + \Upsilon_k w_k \\ \tilde{y}_k &= C_k x_k + v_k, \end{aligned}$$

where $x_k \in \mathbb{R}^n$ denotes the *state vector*, $u_k \in \mathbb{R}^m$ denotes the *control vector*, $\tilde{y}_k \in \mathbb{R}^p$ is the *output vector* or *measurement*, and w_k, v_k are Gaussian white noise vectors of appropriate dimensions with covariances Q_k and R_k respectively. The subscript k refers to the timestep. The random vectors w_k and v_k represent system disturbances and sensor noise respectively, and the matrix Υ_k describes how the disturbance propagates into the system. Since most matrix quantities will have a subscript k denoting the timestep, we will refer to the ijth entry of a matrix A_k with bracketed superscripts: $A_k^{(ij)}$. Similarly, the ith entry of a vector a_k is denoted $a_k^{(i)}$, the ith column of a matrix A_k is denoted $A_k^{[i]}$ and the ith row is denoted $A_k^{\{i\}}$.

The purpose of Kalman filtering is to provide an accurate estimate $\hat{x}_k$ of the state x_k using the measurement $\tilde{y}_k$ and the known information about the system and noise. The standard *discrete-time linear Kalman filter* yields the estimate $\hat{x}_{k+1}$ and is given by

$$\begin{aligned} \hat{x}_{k+1} &= A\left(\hat{x}_k + K_k\left[\tilde{y}_k - C\hat{x}_k\right]\right) \\ K_k &= P_k C^T \left[CP_k C^T + R_k\right]^{-1} \\ P_{k+1} &= A\left(I - K_k C\right) P_k A^T + \Upsilon_k Q_k \Upsilon_k^T, \end{aligned}$$

where K_k is the *Kalman gain* and P_k is the *error covariance matrix*. The problem for high-dimensional systems is the inverse when computing K_k. In this paper, we assume that the sensor noise is uncorrelated, and so R_k is a diagonal positive-definite matrix. This leaves the term CP_kC^T; if this term is diagonal, then the matrix inverse becomes a series of n scalar divisions. We propose to replace P_k with a diagonal estimate $\hat{P}_k$, and one can also assume that C is a matrix that measures individual states of the system without redundancy. Therefore, a system with $1 \le p \le n$ outputs will have a measurement matrix of the form $C = [\mathrm{diag}(C^{(ii)})I_p\ \mathbf{0}_{n-p}]$. This assumption is common for networked systems where one measures the state of individual nodes of the network, see for example [18]. In the next few sections, we will formalize these assertions in the context of our algorithm.

6.2 GENERAL KALMAN FILTERING

In this section, we extend the gradient descent estimate for the error covariance proposed by [37]. In §6.2.1, we discuss the linear Kalman filter, and then extend the error covariance estimate to an accelerated gradient descent in §6.2.2. The accelerated gradient descent benefits from a clever adaptive learning rate, which is discussed in §6.2.3. The final algorithm combining all these methods is summarized in Algorithm 2.

6.2.1 *Gradient Descent for the Error Covariance Update: Linear Case*

Gradient descent is an iterative algorithm that seeks to find the local minimum of a function f by stepping in the direction of the largest gradient:

$$\beta_{k+1} = \beta_k - \mu \nabla f(\beta_k),$$

where μ is the *learning rate*. For the Kalman filter, we seek to find a diagonal matrix estimate $\hat{P}_k$ of P_k. We do this by assuming $\hat{P}_k$ is of the form $\hat{P}_k = \text{diag}(\hat{P}_k^{(ii)}) = \text{diag}(e^{\beta_k^i})$, where β_k is a parameter undergoing gradient descent attempting to minimize the norm of the error $\delta_k = \tilde{y}_k - C\hat{x}_k$:

$$\beta_{k+1}^{(i)} = \beta_k^{(i)} - \frac{1}{2}\mu \frac{\partial(\delta_k^T \delta_k)}{\partial \beta_k^{(i)}}.$$

Computing the gradient of $\delta_k^T \delta_k$ as outlined in Appendix 6.4 yields the following gradient descent equations for $\hat{P}$:

$$\begin{aligned}
\beta_{k+1}^{(i)} &= \beta_k^{(i)} + \mu \delta_k^T C^{[i]} h_k^{(i)} \\
h_{k+1}^{(i)} &= h_k^{(i)} \left(1 - k_k^{(i)T} C^{[i]}\right)^+ + \left(k_k^{(i)} - k_k^{(i)} k_k^{(i)T} C^{[i]}\right)^T \delta_k \\
\hat{P}_k^+ &= \text{diag}\left(\exp\left(\beta_{k+1}^{(i)}\right)\right)
\end{aligned} \tag{6.1}$$

The form of $\hat{P}^+$ guarantees that it remains positive-definite, which is required to preserve convergence of the Kalman filter.

6.2.2 *Nesterov-Accelerated Methods*

Nexterov acceleration is a method used to increase the convergence rate of gradient descent [[50]]. Although Nesterov-accelerated gradient descent converges in fewer timesteps, it does so by sacrificing monotonicity: the gradient descent trajectory will tend to oscillate as it converges towards the estimate.

In order to implement Nesterov acceleration, one must see that the quantity $h_k^{(i)}$ is a function of K_{k-1}, which in turn is a function of $\beta_k^{(i)}$:

$$\begin{aligned}\beta_{k+1}^{(i)} &= \beta_k^{(i)} - \frac{1}{2}\mu\nabla f\left(\beta_k^{(i)}\right) \\ &= \beta_k^{(i)} + \mu\delta_k^T C^{[i]} h_k^{(i)}\left(K_{k-1}\left(\beta_k^{(i)}\right)\right).\end{aligned}$$

Hence, we can get the form of the Nesterov-accelerated gradient descent by introducing the quantity α_k:

$$\begin{aligned}\beta_{k+1}^{(i)} &= \alpha_k^{(i)} - \frac{1}{2}\mu\nabla f\left(\alpha_k^{(i)}\right) \\ &= \alpha_k^{(i)} + \mu\delta_k^T C^{[i]} h_k^{(i)}\left(K_{k-1}\left(\alpha_k^{(i)}\right)\right)\end{aligned}$$

where $\alpha_k^{(i)}$ is given by

$$\alpha_k^{(i)} = \beta_k^{(i)} + \frac{k-1}{k+2}\left(\beta_k^{(i)} - \beta_{k-1}^{(i)}\right).$$

Therefore, the Nesterov-accelerated estimate $\hat{P}$ replaces the covariance update with the following equations:

$$\hat{P} = \operatorname{diag}\left(e^{\beta_{k+1}^{(i)}}\right),\ k_k^{(i)} = \exp\left(\alpha_{k+1}^{(i)}\right) D_k^{-1} C^{[i]}$$

$$\beta_{k+1}^{(i)} = \alpha_k^{(i)} + \mu\delta_k^T C^{[i]} h_k^{(i)}\left(K_{k-1}\left(\alpha_k^{(i)}\right)\right), \tag{6.2}$$

where h_k is as in Equation (6.1), but using this new expression for $k_k^{(i)}$ in Equation (6.2).

6.2.3 *Adaptive Learning Rate Methods*

Using a constant learning rate μ can lead to suboptimal performance, and therefore it is prudent to adapt μ on-the-fly as the gradient descent is run. A well-known method for adapting the learning rate is given by Barzilai and Borwein [51]. Suppose we have the gradient descent with learning rate μ:

$$\beta_{k+1}^{(i)} = \beta_k^{(i)} - \frac{1}{2}\mu\nabla f\left(\beta_k^{(i)}\right).$$

Let $\Delta\beta = \beta_k - \beta_{k+1}$ and let $\Delta g(\beta) = \nabla f\left(\beta_{k+1}\right) - \nabla f\left(\beta_k\right)$. Then, the Barzilai and Borwein method selects the learning rate parameter using a secant line approximation:

$$\frac{1}{2}\mu_k = \arg\min_{\lambda} \left\|\Delta\beta - \lambda\Delta g(\beta)\right\|.$$

For accelerated gradient descent, the updated learning rate μ is given by

$$\mu_k = 2\frac{\Delta g(\beta)^T \Delta\beta}{\Delta g(\beta)^T \Delta g(\beta)},\ \Delta\beta = \beta_k - \alpha_{k-1}.$$

Combining the accelerated gradient descent estimate of the error covariance with the adaptive learning rate μ_k yields the final algorithm as outlined in Algorithm 2.

Algorithm 2: Discrete Kalman Filter with Accelerated Gradient Descent on P and Adaptive Learning Rate μ

Initialize

$\hat{x}(t_1) = \hat{x}_0$

$P_0 = \mathbb{E}\left\{\tilde{x}(t_1)\tilde{x}(t_1)^T\right\}$

for $k = 1$ *to* $k = t_f$ **do**

Gain

$K_k = \hat{P}_k^- C^T (C\hat{P}_k^- C^T + R_k)^{-1}$

Accelerated Gradient Descent and Adaptive μ_k

$\Delta\beta = \beta_k - \alpha_{k-1}$

$\Delta g(\beta) = \nabla f\left(\beta_{k+1}\right) - \nabla f\left(\beta_k\right)$

$D_k = R_k + C\hat{P}_k C^T$

$\mu_k = 2(\Delta g(\beta)^T \Delta\beta)/(\Delta g(\beta)^T \Delta g(\beta))$

$\alpha_k^{(i)} = \beta_k^{(i)} + \frac{k+1}{k+2}\left(\beta_k^{(i)} - \beta_{k-1}^{(i)}\right)$

$\kappa_k^{(i)} = \exp\left(\alpha_k^{(i)}\right) D_k^{-1} C^{[i]}$

$\beta_{k+1}^{(i)} = \beta_k^{(i)} + \mu_k \delta_k^T C^{[i]} h_k^{(i)}$

$h_{k+1}^{(i)} = h_k^{(i)}(1 - \kappa_k^{(i)T} C^{[i]}) + (\kappa_k^{(i)} - \kappa_k^{(i)} \kappa_k^{(i)T} C^{[i]})^T \delta_k$

Update

$\hat{x}_k^+ = \hat{x}_k^- + K_k\left[\tilde{y}_k - C\hat{x}_k^-\right]$

Propagate

$\hat{x}_{k+1}^- = A_k \hat{x}_k^+ + B_k u_k$

$\hat{P}_{k+1}^- = \mathrm{diag}\left(\exp\left(\beta_{k+1}^{(i)}\right)\right)$

end

6.2.4 *Filter Properties*

In the standard Kalman filter, P_k is computed from an algebraic Ricatti equation. In order for this equation to have a positive-definite solution, a requirement for stable error dynamics, one must assume that (A^T, C^T) is stabilizable and $(A, \sqrt{Q})$ is detectable (see [52]). Therefore, since our estimate of P is positive definite by construction and not computed by an algebraic Ricatti equation, we do not need to have these assumptions. The next theorem shows that all one needs for stability of the error dynamics is for the system matrix A to be stable.

Theorem 14. *Suppose A is an asymptotically stable matrix, and so the eigenvalues of A satisfy $|\lambda(A)| \leq 1$. Then, the error dynamics*

$$\tilde{x}_k = x_k - \hat{x}_k^-$$

are stable, where $\hat{x}_k^-$ is the estimate computed according to Algorithm 1.

Proof. We can write the error dynamics as

$$\begin{aligned}\tilde{x}_{k+1} &= x_{k+1} - \hat{x}_{k+1}^- \\ &= (A - LC)\hat{x}_k^- + (w_k - Lv_k),\end{aligned}$$

where L is given by

$$L = A\hat{P}C^T(C\hat{P}C^T + R)^{-1}.$$

Hence, it suffices to show that $(A - LC)$ has eigenvalues in the unit disc. We can write $(A - LC)$ as

$$A - LC = A - A\hat{P}C^T(C\hat{P}C^T + R)^{-1}C = A(I - N),$$

where $N = \hat{P}C^T(C\hat{P}C^T + R)^{-1}C$. By the form of C and $\hat{P}$, if the system has p outputs, then N is a diagonal matrix with the form

$$N^{(ii)} = \begin{cases} \frac{e^{\beta_k^{(i)}}(C^{(ii)})^2}{e^{\beta_k^{(i)}}(C^{(ii)})^2 + R^{(ii)}} & \text{if } 1 \leq i \leq p \\ 0 & \text{if } p < i \leq n. \end{cases}$$

It is clear that $0 \leq N^{(ii)} < 1$ since R is a positive definite diagonal matrix. Therefore, $0 < (I - N)^{(ii)} \leq 1$, and so it follows that

$$\begin{aligned}|\lambda(L)| &= |\lambda(A(I - N))| \\ &\leq |\lambda_{\max}(A)||\lambda_{\max}(I - N)| \\ &\leq |\lambda_{\max}(A)|,\end{aligned}$$

and so by the asymptotic stability of A, the asymptotic stability of $(A - LC)$ follows. □

6.2.5 *Example*

Here, we show a simple numerical implementation of Algorithm 1 to see how the algorithm performs compared to the standard Kalman filter for different strengths of noise. Consider the linear system with matrices

$$A = \begin{bmatrix} 1.001 & 0.011 \\ -0.0301 & 0.98 \end{bmatrix}, B = \begin{bmatrix} 5\text{E}-5 \\ 1\text{E}-2 \end{bmatrix}, C = I$$

propagating with process noise of covariance $Q = 0.001$ and measurement noise of covariance $R = \alpha I$ for various values of α. The first and second plots of Figure 6.1 show the error and first state of the system for $R = 0.115I$ for

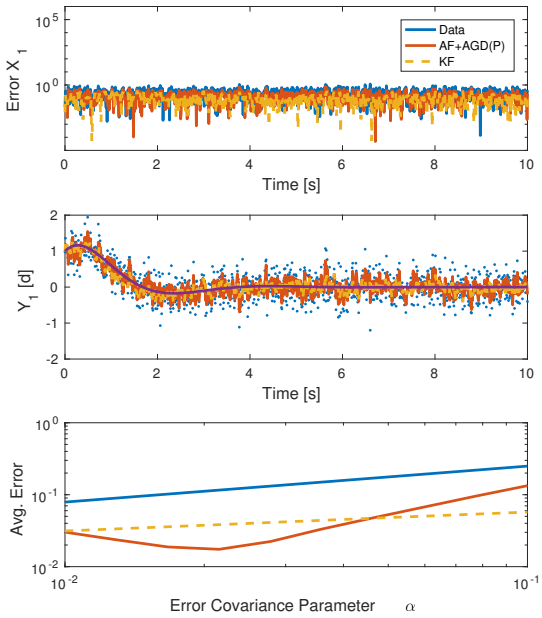

Figure 6.1: Numerical test of Algorithm 1. Top: Error from true state from data, accelerated filter and Kalman filter. Middle: $y_1 = x_1$ for data, accelerated filter and Kalman filter. Bottom: Average steady-state error.

the raw measurement data, and the filtered data using the accelerated gradient descent and the standard Kalman filter. The third plot shows the average steady state error computed on the time interval $t \in [6.6, 10]$ for various values of α indicating the covariance of the measurement error. Figure 6.1 shows that the filter in Algorithm 1 achieves similar performance as the standard Kalman filter.

6.3 DISTRIBUTED KALMAN FILTERING

[39] describes several methods of Kalman filtering using a network of sensors, with each nth sensor using a unique sensor model $\tilde{y}_{n,k} = C_{n,k}x_k + v_{n,k}$, to arrive at a global measurement of a system. The context of their system model is on a graph $\mathcal{G}$, which is an abstract representation of the connection structure of sensors, which are represented by nodes. An edge in the graph denotes a communication link between sensors by which they can exchange information about their current state estimate. One such information exchange algorithm is called *consensus*, where each node in the graph changes its estimated value by continuously averaging with the estimates of its neighbours:

$$\dot{\hat{x}}_i = \sum_{j \in N_i} (\hat{x}_j - \hat{x}_i) .$$

One particular algorithm in [39] utilizes a *Kalman-consensus filter* in which every node of the network computes an estimate of the state of the system and then performs consensus with its neighbours on this estimate. This al-

lows sensors that only see a portion of the system to collect a global state estimate over time.

For high-dimensional systems, implementing this filter is problematic again because each sensor has to invert a large matrix at each timestep in order to compute the Kalman filter gain. In Algorithm 2, we summarize the Kalman-consensus filter, where every node performs an accelerated gradient descent with adaptive learning rate, and shares its estimate with its neighbours. In the following section, we provide an example of such a high-dimensional system.

Algorithm 3: Discrete Distributed Kalman-Consensus Filter μ

Initialize
$\hat{x}(t_1) = \hat{x}_0$
$P_0 = \mathbb{E}\left\{\tilde{x}(t_1)\tilde{x}(t_1)^T\right\}$
$\epsilon = t_2 - t_1$
for $k = 1$ *to* $k = t_f$ **do**
  for *each node* $j \in V$ **do**
    Aggregate Data
    $S_j = |N_i|^{-1} \sum_{l \in N_j} C_i$
    $y_j = |N_i|^{-1} \sum_{l \in N_j} C_i^T \tilde{y}_i$
    Accelerated Gradient Descent and Adaptive μ_k
    $\Delta\beta = \beta_k - \alpha_{k-1}$
    $\Delta g(\beta) = \nabla f\left(\beta_{k+1}\right) - \nabla f\left(\beta_k\right)$
    $D_k = R_k + C\hat{P}_k C^T$
    $\mu_k = 2(\Delta g(\beta)^T \Delta\beta)/(\Delta g(\beta)^T \Delta g(\beta))$
    $\alpha_k^{(i)} = \beta_k^{(i)} + \dfrac{k+1}{k+2}\left(\beta_k^{(i)} - \beta_{k-1}^{(i)}\right)$
    $\kappa_k^{(i)} = \exp\left(\alpha_k^{(i)}\right) D_k^{-1} C^{[i]}$
    $\beta_{k+1}^{(i)} = \beta_k^{(i)} + \mu_k \delta_k^T C_n^{[i]} h_k^{(i)}$
    $h_{k+1}^{(i)} = h_k^{(i)}(1 - \kappa_k^{(i)T} C_n^{[i]}) + (\kappa_k^{(i)} - \kappa_k^{(i)} \kappa_k^{(i)T} C_n^{[i]})^T \delta_k$
    Update Kalman-Consensus Estimate
    $\hat{x}_{j,k}^+ = \hat{x}_{j,k}^- + D_k^{-1}\left[y_j - S_j \hat{x}_{j,k}^- + \epsilon \sum_{l \in N_j} (\hat{x}_{l,k}^- - \hat{x}_{j,k}^-)\right]$
    Propagate
    $\hat{x}_{k+1}^- = A_k \hat{x}_k^+ + B_k u_k$
    $\hat{P}_{k+1}^- = \operatorname{diag}\left(\exp\left(\beta_{k+1}^{(i)}\right)\right)$
  end
end

6.3.1 *Example*

Consider a physical phenomenon, such as weather, propagating on a planar surface according to the partial differential equation

$$\dot{u} = \left(\alpha \frac{\partial^2 u}{\partial x} + \beta \frac{\partial^2 u}{\partial y}\right).$$

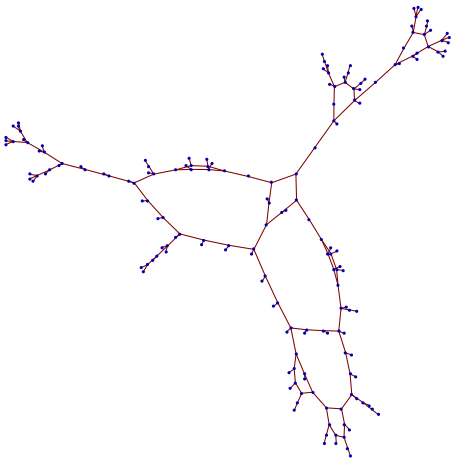

Figure 6.2: Sensor network graph with 178 nodes and 186 edges

As studied in [34], and [35], by discretizing the surface into an equally-spaced $n \times n$ grid in the x and y directions and the temporal dimension, thus obtaining a grid of values u_{ij}^k, one can construct the linear system representation

$$\dot{\vec{u}} = \frac{2}{\Delta x^2}\left[I_n \otimes (\alpha D) + (\beta D) \otimes I_n\right]\vec{u}, \;\; \vec{u} = \mathrm{vec}(u_{ij}^k)$$

where D is a tridiagonal matrix with 1's on the sub and superdiagonal, and -2's on the diagonal. The discrete-time state matrix A can be found using a matrix exponential, or a finite-order Taylor expansion. Periodic boundary conditions may be added by setting $D_{1n} = D_{n1} = 1$. Suppose that this phenomenon is being measured according to this discretization. We use a sensor model such that each node collects data from an $n_l \times n_l$ square portion of the grid u_{ij}^k so that each individual grid point is measured by at least one sensor. The sensor network by the graph in Figure 6.2 is used, with $n_l = 4$ for a 50×50 grid, and the sensor noise is given unit covariance. Five 2D Gaussian functions are used to set the initial conditions for the simulation, which was run over a time interval of 10 seconds. The true state of the system at 1.2s is shown in Figure 6.3, and an aggregate measurement of the entire system is shown in Figure 6.4. An estimate from a single sensor at this timestep is shown in Figure 6.5, and one can see that there is a substantial reduction of noise.

6.4 GRADIENT DESCENT FOR KALMAN FILTER COVARIANCE UPDATE

Sutton's Gradient Descent for updating the error covariance matrix approximation $\hat{P} = \mathrm{diag}\left(\hat{P}_k^{(ii)}\right) = \mathrm{diag}\left(\exp\beta_{k+1}^{(i)}\right)$ uses gradient descent on $\beta_{k+1}^{(i)}$:

$$\beta_{k+1}^{(i)} = \beta_k^{(i)} - \frac{1}{2}\mu\frac{\partial\left(\delta_k^T\delta_k\right)}{\partial\beta_k^{(i)}},$$

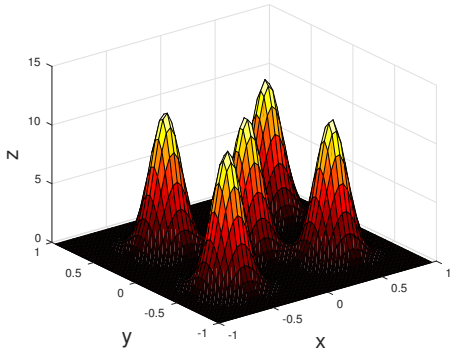

Figure 6.3: True state of system at $t = 1.2$s

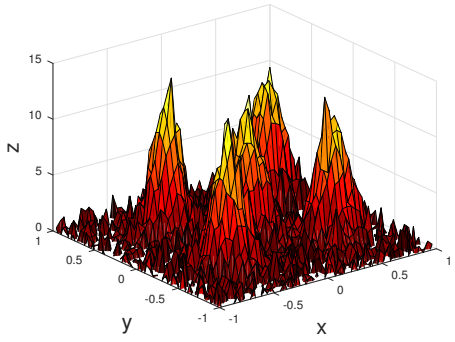

Figure 6.4: Sample measurement $\tilde{y}$ over the entire system at $t = 1.2$s

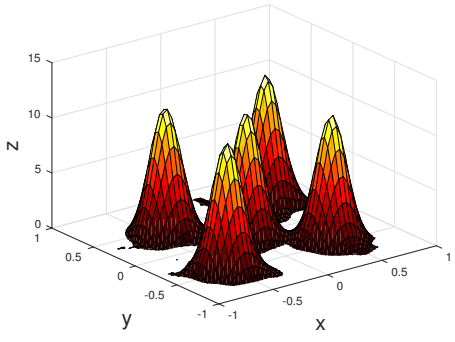

Figure 6.5: Sample system estimate at $t = 1.2$s from a single sensor

where $\delta_k = \tilde{y}_k - C\hat{x}_k^-$ is the error: To derive the exact form of the gradient descent on $\beta_k^{(i)}$, consider the following terms:

$$\frac{\partial\left(\delta_k^T\delta_k\right)}{\partial\hat{x}_k^{(i)}} = 2\delta_k^T\frac{\partial\delta_k}{\partial\hat{x}_k^{(i)}} = -2\delta_k^T C^{[i]}.$$

Next, we have

$$\frac{\partial\delta_k}{\partial\beta_k^{(i)}} = \frac{\partial}{\partial\beta_k^{(i)}}\left[\tilde{y}_k - C\hat{x}_k^-\right] = -\sum_{j=1}^{n} C^{[j]}\frac{\partial\hat{x}_k^{-(j)}}{\partial\beta_k^{(i)}}.$$

We assume that for $i \neq j$,

$$C^{[j]}\frac{\partial\hat{x}_k^{-(j)}}{\partial\beta_k^{(i)}} \cong \vec{0} \implies \frac{\partial\delta_k}{\partial\beta_k^{(i)}} \cong -C^{[i]}\frac{\partial\hat{x}_k^{-(i)}}{\partial\beta_k^{(i)}}.$$

Next, define the following two quantities:

$$\begin{aligned} D_k &:= R_k + C\hat{P}_k C^T = R_k + \sum_{i=1}^{n}\exp\left(\beta_{k+1}^{(i)}\right)C^{[i]}C^{[i]T} \\ k_k^{(i)} &:= \exp\left(\beta_{k+1}^{(i)}\right)D_k^{-1}C^{[i]}. \end{aligned}$$

Next, we compute the following derivatives:

$$\begin{aligned} \frac{\partial D_k}{\partial\beta^{(j)}} &= \sum_{i=1}^{n}\frac{\partial e^{\beta_{k+1}^{(i)}}}{\partial\beta^{(j)}}C^{[i]}C^{[i]T} = e_{k+1}^{\beta^{(j)}}C^{[j]}C^{[j]T} \\ \frac{\partial D_k^{-1}}{\partial\beta^{(j)}} &= -D_k^{-1}\frac{\partial D_k}{\partial\beta^{(j)}}D_k^{-1} = -k_k^{(i)}C^{[j]T}D_k^{-1} \\ \frac{\partial k_{k+1}^{(i)}}{\partial\beta^{(i)}} &= \left[\frac{\partial e^{\beta_{k+1}^{(i)}}}{\partial\beta^{(i)}}D_k^{-1} + e^{\beta_{k+1}^{(i)}}\frac{\partial D_k^{-1}}{\partial\beta^{(i)}}\right]C^{[i]} \\ &= \beta_{k+1}^{(i)}D_k^{-1}C^{[i]} - e^{\beta_{k+1}^{(i)}}k_{k+1}^{(i)}C^{[i]T}D_k^{-1}C^{[i]} \\ &= k_{k+1}^{(i)} - k_{k+1}^{(i)}\left(e^{\beta_{k+1}^{(i)}}\left(D_k^{-1}\right)^T C^{[i]}\right)^T C^{[i]} \\ &= k_{k+1}^{(i)} - k_{k+1}^{(i)}k_{k+1}^{(i)T}C^{[i]}. \end{aligned}$$

Now, we can write the gradient descent on $\beta^{(i)}$:

$$\begin{aligned}
\beta_{k+1}^{(i)} &= \beta_k^{(i)} - \frac{1}{2}\mu \frac{\partial(\delta_k^T \delta)}{\partial \beta^{(i)}} \\
&= \beta_k^{(i)} - \frac{1}{2}\mu \sum_j \frac{\partial(\delta_k^T \delta)}{\partial \hat{x}_k^{-(j)}} \frac{\partial \hat{x}_k^{-(j)}}{\partial \beta^{(i)}} \\
&\cong \beta_k^{(i)} - \frac{1}{2}\mu \frac{\partial(\delta_k^T \delta)}{\partial \hat{x}_k^{-(i)}} \frac{\partial \hat{x}_k^{-(i)}}{\partial \beta^{(i)}} \\
&= \beta_k^{(i)} + \mu \delta_k^T C^{[i]} \frac{\partial \hat{x}_k^{-(i)}}{\partial \beta^{(i)}}.
\end{aligned}$$

All that remains is to find an approximation to $\frac{\partial \hat{x}_k^{-(i)}}{\partial \beta^{(i)}}$. We denote this approximation with $h_{k+1}^{(i)}$:

$$\begin{aligned}
h_{k+1}^{(i)} &\cong \frac{\partial \hat{x}_{k+1}^{-(i)}}{\partial \beta^{(i)}} = \frac{\partial}{\partial \beta^{(i)}} \left[\hat{x}_k^{(i)} + k_k^{(i)T} \delta_k \right] \\
&= \frac{\partial \hat{x}_k^{(i)}}{\partial \beta^{(i)}} + \frac{\partial k_k^{(i)T}}{\partial \beta^{(i)}} \delta_k + k_k^{(i)T} \frac{\partial \delta_k}{\partial \beta^{(i)}} \\
&= \frac{\partial \hat{x}_k^{(i)}}{\partial \beta^{(i)}} + \left(k_k^{(i)} - k_k^{(i)} k_k^{(i)T} C^{[i]} \right)^T \delta_k - k_k^{(i)T} \frac{\partial \hat{x}_k^{(i)}}{\partial \beta^{(i)}} C^{[i]} \\
&= h_k^{(i)} \left(1 - k_k^{(i)T} C^{[i]} \right) + \left(k_k^{(i)} - k_k^{(i)} k_k^{(i)T} C^{[i]} \right)^T \delta_k.
\end{aligned}$$

This yields the final gradient descent update:

$$\beta_{k+1}^{(i)} = \beta_k^{(i)} + \mu \delta_k^T C^{[i]} h_k^{(i)}.$$

In conclusion, the Kalman filter with gradient descent error covariance update is given by the equations

$$\begin{aligned}
\hat{x}_{k+1} &= \hat{x}_k + K_k \left[\tilde{y}_k - C \hat{x}_k \right] \\
K_k &= \hat{P}_k C^T \left[C \hat{P}_k C^T + R_k \right]^{-1} \\
\hat{P} &= \operatorname{diag}\left(e^{\beta_{k+1}^{(i)}} \right) \\
\beta_{k+1}^{(i)} &= \beta_k^{(i)} + \mu \delta_k^T C^{[i]} h_k^{(i)} \\
h_{k+1}^{(i)} &= h_k^{(i)} \left(1 - k_k^{(i)T} C^{[i]} \right)^+ + \left(k_k^{(i)} - k_k^{(i)} k_k^{(i)T} C^{[i]} \right)^T \delta_k.
\end{aligned}$$

6.5 CONCLUSIONS AND FUTURE WORKS

In this part, we characterized the controllability and stabilizability of signed consensus networks in the linear and nonlinear settings. We showed that the topological notion of structural balance is the significant condition that appears when making statements on uncontrollability. In particular, structural

balance induces a gauge transformation that permits the extension of the classical controllability and stabilizability analysis of consensus networks to be applied to the signed Laplacian case.

We examined the role of structural balance both in the SISO and MIMO cases of the leader-follower consensus dynamics, and then extended this to the output controllability and stabilizability of the influenced consensus dynamics. We then looked at the task of identifying the bipartite consensus of certain classes of nonlinear network flows. In particular, We showed that the sign structure of the first Koopman mode corresponds to this bipartite consensus, and then used Extended Dynamic Mode Decomposition to numerically approximate this sign structure. Lastly, we considered estimation problems on large-scale consensus networks for the sensor fusion of high-dimensional data. Future work will determine bounds on the amount of data required to have an accurate approximation of the Koopman mode with respect to sign structure.

Part III

DESIGN

7

INTRODUCTION

Networked systems are pervasive in nature, and therefore in many fields of science and engineering. Such systems arise for example in robotic swarms [53], animal flocking [6], oscillator networks [54], infrastructure systems [55], and opinion dynamics [3]. The interplay between *modelling* and *synthesizing* such systems has led to the general area of networked dynamic systems–an active area of research in systems and control community. A great amount of effort has recently been focused on understanding how the connection structure, or topology, of a network affects the behaviour or performance of a dynamical process on that network. To that end, a natural question to ask is how one can systematically construct a network topology such that a certain performance metric defined over that behaviour is satisfied.

A well-known method for constructing networks is the method of preferential attachment, where nodes are added to the network and connected to already-existing nodes with a probability proportional to the degree of those nodes [56]. The advantage of this method is that it produces networks with power-law degree distributions[1] that resemble networks found in nature [57]. Another method for growing networks uses Kolmogorov-Sinai entropy as a heuristic parameter for evolving networks into ones with regular, random, scale-free or star topologies [58].

An area of recent focus is the study of controlling distributed systems. Networks arise naturally in the context of dynamics defined over distributed systems, and therefore the question of how the network topology affects network behaviour can be naturally extended to the question of how the network topology affects the controllability of the dynamics over that network. In particular, the consensus dynamics where agents perform distributed averaging over time, has attracted vigorous research [5], [33], [59]. Consensus has diverse applications in control and estimation, such as multi-agent systems [12], [13], distributed Kalman filtering [38], [60], and swarm deployment [61]. System-theoretic properties of the consensus algorithm have also been extensively examined in the literature. The fundamental algebraic object facilitating these studies is the *graph Laplacian* [5]. Using this setup allows one, for example, to draw connections between systems aspects of distributed algorithms and the graph structure, e.g., highlighting the role of symmetries in inducing uncontrollable modes [17]. Such a point of view has been extended to nonlinear variants of the protocol [33], and graphs admitting both positive and negative interactions [24], [62], [63]. Necessary and sufficient conditions for controllability and observability of linear consensus protocol have been explored using the notion of fractional automorphisms [18], [62]. O'Rourke and Touri discussed the controllability of random graphs in the context of adjacency dynamics [64].

1 So-called *scale-free* networks

More research has focused on how one may systematically construct a network that has favorable characteristics for consensus. Ghosh and Boyd developed an algorithm to select connections between agents in a network to maximize the connectivity of the network, and therefore reduce the time it takes for the agents to achieve consensus [65]. Chapman and Mesbahi showed how to construct large networks from graph products of smaller, atomic networks and discussed conditions under which these products preserve controllability [21], [66]. Yazicioglu and Egerstedt developed a method for decomposing and reconstructing graphs for leader-follower selection [67].

When designing a network graph, one has several objects to play with in order to achieve various performance characteristics. In particular, a graph consists of nodes connected by edges with weights, and input vectors indicating where one injects a control signal into the network. As discussed earlier, one example is an algorithm to select edges in a graph to maximize connectivity [65]. There has also been recent work in using submodular optimization for picking input vectors [68], [69]. An excellent summary of submodular optimization applications to the control of networked systems is given in [70]. Measures by which one may gauge network performance and specify network topologies have been suggested in [71], [72]. These include information-theoretic measures such as entropy [71], [73] and other so-called spectral measures [5], [71], as well as disturbance rejection cost in the form of the $\mathcal{H}_2$ norm and coherence [66], [74]–[78]. Since consensus is a distributed protocol over a graph, one can modify the topology of the network to adapt to disturbances and antagonistic influences. Algorithms for rewiring the network are proposed in [66], and those for reweighting the network for optimal noise rejection are discussed in [75]. ost of the existing literature on the control and performance analysis for consensus consider the case where each node in the network has a *scalar* state.[2]

Reasoning about the performance of agents operating over a network also requires consideration of the individual agent dynamics. The majority of literature on consensus systems focuses on the case where the agent dynamics are taken to be identical single or double integrators. The analysis of multi-scale problems has historically offered techniques for formal description and controller synthesis for complex system dynamics [79], which motivates us to consider agents operating on distinct, individual time scales as part of our consensus formulation. This extends the consensus formulation and the framework for distributed control into a specific class of heterogeneous agents, which has the potential to increase the applicability of the protocols previously developed, as well as the graph-theoretic performance metrics previously discussed.

The integration of multiple agent time scales into the consensus formualation is not seamless, and there is a growing body of literature that addresses various complications with the introduction of slow and fast agents. This started with the discussion of the consensus value for multi-rate integrators in [80]. Since then issues such as convergence [81], stability [82], [83], controller design [84], [85], as well as single-influenced consensus performance [86] for networks featuring multi-time scale behavior have been ad-

2 Or can be decomposed as such.

dressed. This existing literature has demonstrated that the inclusion of time scales can have a significant impact on the fundamental system-theoretic aspects of a networked system, but that in many cases it is still possible to analyze the system through a graph-theoretic lens.

Recently, several extensions to the case of *vector*-valued node states have been proposed; such consensus protocols are characterized by having graphs with *matrix-valued weights*. System-theoretic properties of matrix-valued weighted consensus networks, as well as applications to bearing-constrained formation control have been considered in [87]. A consensus-based model of opinion dynamics on matrix-valued weighted graphs was developed in [88], [89]. Further applications of matrix-valued weighted graphs are found in the control of coupled oscillators [90], spacecraft formation control [91], as well as in attitude estimation [92].

An interesting extension to the theory of electrical networks arises in the context of an estimation problem over a matrix-valued weighted graph. It is well-known that the graph Laplacian plays a central role in resistor networks; it is the fundamental object that encodes effective resistance across the network [93]. An extension of electrical networks to *matrix-valued* resistances, voltages and currents was examined in the aforementioned estimation problem with relative measurements between the agents [94]. In this line of work, the effective matrix-valued resistance was shown to be related to the covariance matrix of the estimation procedure; in a related work, the scalar effective resistance was shown to be related to the $\mathcal{H}_2$ performance of consensus [66], [75]. One of the contributions of this chapter is extending the resistor network formalism to the computation of $\mathcal{H}_2$ performance on matrix-valued weighted consensus-type networks.

The notions of performance and control of consensus rely on the underlying topology of the network. As such, it is desirable to devise algorithms for system theoretic analysis and synthesis that are scalable and modular. The combinatorics literature has developed several useful models for graph design, such as the scale-free network [56] and the Erdos-Renyi random graph model [95]. An axiomatic approach that can be adopted in this direction is to take smaller, atomic elements and build large-scale graphs from them; one can then use graph-growing operations that preserve properties such as controllability [22], [96]. In the similar vein, spectral properties of Cartesian product networks have proven useful for systems analysis, where certain properties of the atomic elements translate to the entire network [45], [55], [97]–[99].

In this chapter, one of our approaches to address the performance problem on leader-follower consensus utilizes the paradigm of *series-parallel networks*. This is a class of graphs characterized by the absence of a subgraph homeomorphic to K_4. An important property of series-parallel networks is that they can be sequentially decomposed into smaller networks via simple operations in linear [100] and sublinear [101] time. Many NP-hard problems on general classes of graphs become linear on series-parallel graphs, such as finding maximum matchings induced subgraphs and independent sets, and the maximum disjoint triangle problem [102]. The decomposition of series-parallel networks has been exploited in a number of other disciplines. For example, the Quadratic Assignment Problem is solvable in polynomial time on

series-parallel networks [103]. Efficient algorithms also exist for the discrete time-cost tradeoff problem [104], routing games and selfish routing [105], and resource allocation by dynamic programming [106]. As such, it is natural to conjecture that a number of difficult system-theoretic problems on networks can be solved or scaled efficiently on series-parallel networks. We do so in this chapter, focusing on the problem of efficiently computing the $\mathcal{H}_2$ performance of leader-follower consensus networks.

Whiskering is a process for growing graphs where at each iteration, a vertex and edge is connected to every node in the graph. In this chapter, we discuss using this process, and generalizations of this process, to construct large graphs that are controllable.

The contributions of this chapter are the following. We extend the use of submodular optimization in network science to problems involving adding *nodes* to the network. We present a graph-growth method that preserves controllability of consensus on the graph, and provide relevant bounds on the network performance. Furthermore, we develop a graph-growth algorithm, and formulate convex optimization problems which we then solve for specific test cases.

Next, by exploiting the structure of series-parallel networks, we present a way of computing the $\mathcal{H}_2$ norm of a leader-follower consensus network in best-case $O(k^\omega|\mathcal{R}|\log|\mathcal{N}|)$ (worst case $O(k^\omega|\mathcal{R}||\mathcal{N}|)$) complexity, where $|\mathcal{R}|, |\mathcal{N}|$ are the number of leaders and followers, respectively, and $O(k^\omega)$ is the complexity of inverting a $k \times k$ symmetric positive-definite matrix; the current best lower bound for ω is 2.3728639 [107]. We assume that the node state vector size k is small relative to the size of the network, and hence, the complexity of this computation is dominated by the number of nodes $|\mathcal{N}|$.

We also provide a gradient descent method for adaptively re-weighting the network to optimize $\mathcal{H}_2$ performance that utilizes computations of similar complexity. Using the matrix-valued resistances and currents extension of electrical networks, we show that the analogous notion of effective resistance is related to the $\mathcal{H}_2$ norm on a leader-follower consensus network with vector states. Again, the decomposition of series-parallel networks will be used to efficiently compute the parameters in the proposed gradient algorithm.

Additionally, we address the network design problem in the case where the agents have different time scales. Essentially, a time scale refers to how 'fast' an agent integrates information from its neighbours. We explore an optimal distribution of time scales over agents in the setting of the $\mathcal{H}_2$ performance problem. The issue arising from the introduction of time scales is that the effective system matrix (the Laplacian with time scales) is no longer symmetric – this means we cannot derive an analytic form of the $\mathcal{H}_2$ norm with standard techniques.

Instead, we utilize the notion of *edge consensus*. Instead of considering the 'performance' of the dynamics on the node states, we derive the dynamical system corresponding to information flow on edges between nodes. In the case of systems with time scales, this formulation has a symmetric edge Laplacian. We examine the design problem in this setting, and show that a separatation principle exists – one can optimize the edge weights and time scales separately to achieve good $\mathcal{H}_2$ performance.

Lastly, we examine notions of 'entropy' on networks. These are measures that related to the complexity of networks, and more 'complex' networks have higher entropy. We show that these measures have a system-theoretic interpretation, making them amenable to optimization.

The part is organized as follows. Mathematical preliminaries are discussed in §7.1. We examine whiskering and its generalizations in Chapter 8. In Chapter 9, we look at the $\mathcal{H}_2$ performance of matrix-weighted series-parallel networks, and then expand this to matrix-weighted networks with time scales in the edge consensus setting in Chapter 10. Network entropy is discussed in Chapter 12, and the part is concluded in § 12.6.

7.1 MATHEMATICAL PRELIMINARIES

A few of the main results of this chapter involve analyzing the *controllability* of the linear consensus dynamicsx. Theorem 15 provides a well-known and useful tool for testing controllability by looking at uncontrollable modes from the eigen-decomposition of the system.

Theorem 15 (Popov-Belevitch-Hautus Test [108]). *Consider the linear ordinary differential equation*

$$\dot{x} = Ax + Bu.$$

The system pair (A, B) is uncontrollable if and only if there is a non-zero left eigenvector of A orthogonal to the columns of B. In other words (A, B) is uncontrollable if and only if there exists $w \neq 0$ such that

$$w^T A = \lambda w^T, \; w^T B = 0.$$

7.1.1 *Submodular Optimization*

In this subsection, we outline some basic definitions from submodular optimization. Let $m \in \mathbb{Z}_+$, and $[m] := \{1, \dots, m\}$. We call a real-valued function $f : 2^{[m]} \to \mathbb{R}$ *nondecreasing* if for sets $J \subset K \subset [m]$,

$$f(J) \leq f(K).$$

The function f is *submodular* if for subsets $J, K \subset [m]$, we have that

$$f(K) + f(J) \geq f(K \cup J) + f(K \cap J).$$

Furthermore, f is *nonincreasing* if $-f$ is nondecreasing, and f is *supermodular* if $-f$ is submodular. f is *modular* if it is both supermodular and submodular.

A matrix H is *Hermitian* if $H = H^\dagger$, where '†' denotes the conjugate-transpose operation. Let Λ_E be a finite interval of $\mathbb{R}$, and thereby denote the set of $n \times n$ Hermitian matrices with eigenvalues contained in Λ_E as

$H_n(\Lambda_E)$. We say that f is *operator monotone* on Λ_E if for all $n \geq 1$ and for all $A, B \in H_n(\Lambda_E)$,

$$A \succeq B \implies f(A) \succeq f(B).$$

Lastly, let $A[K]$ denote the principal submatrix of A obtained by deleting the rows and columns of A corresponding to the elements in the set $[m] \setminus K$.

Recent work in submodular optimization has examined matrix functions (of say, A), such as the trace or the trace of powers of matrices, in the context of submodularity over a set $K \subseteq [n]$ on the principal submatrices $A[K]$ [109], [110]. We summarize the main general result of these works, as well as a more specific result about submodularity of functions over principle submatrices of M-matrices.

Theorem 16 ([109], [110]). *Let f be a real continuous function on an interval Λ_E of $\mathbb{R}$. Furthermore, let f' be operator monotone on the interior of Λ_E. Then, for all $A \in H_n(\Lambda_E)$, the map from $2^{[n]} \to \mathbb{R}$*

$$K \to \mathrm{Tr} f(A[K])$$

is supermodular.

Theorem 17 ([109]). *Let A be an M-matrix of size $n \times n$. Then, for all subsets $J, K \subset [n]$ we have that for $0 \leq p \leq 1$:*

$$\mathrm{Tr}A[K]^p + \mathrm{Tr}A[J]^p \geq \mathrm{Tr}A[K \cup J]^p + \mathrm{Tr}A[K \cap J]^p$$

and for $1 \leq p \leq 2$ and for $p < 0$,

$$\mathrm{Tr}A[K]^p + \mathrm{Tr}A[J]^p \leq \mathrm{Tr}A[K \cup J]^p + \mathrm{Tr}A[K \cap J]^p.$$

In particular, the map $K \to \mathrm{Tr}A[K]^{-1}$ is supermodular if A is an M-matrix.

8

GRAPH GROWING

8.1 GRAPH GROWING WITH SUBMODULAR OPTIMIZATION

In this section, we introduce a method of growing graphs that preserves controllability, by adding a leaf to every node of the graph. We then generalize this process to adding more complicated structures

Graph whiskering is a process for adding nodes to a graph, originally studied for the purpose of looking at monomial ideals [111], [112]. For each whiskering iteration, a single unique node is connected to an already existing node in the graph, for all nodes in the graph. This corresponds to concatenating the Laplacian in the following form:

$$\mathcal{L}_{\mathcal{G}} \longrightarrow \begin{bmatrix} \mathcal{L}_{\mathcal{G}} + I & -I \\ -I & I \end{bmatrix} = \mathcal{L}_{\mathcal{G}}', \tag{8.1}$$

where we denote the operation as $\mathcal{L}_{\mathcal{G}}' = W_1(\mathcal{L}_{\mathcal{G}})$. Figure 8.1 shows an example of whiskering a graph three times. This process is of great interest because of several properties that make it useful for control theory, namely it preserves controllability and provides guarantees on the performance of control exerted on the resulting network. The former property is captured in the following theorem.

Theorem 18. *Let $\mathcal{L}_{\mathcal{G}}' = W_1(\mathcal{L}_{\mathcal{G}})$. The pairs*

$$(\mathcal{L}_{\mathcal{G}}', [b^T, b^T]^T) \text{ and } (\mathcal{L}_{\mathcal{G}}', [b^T, \mathbf{0}^T]^T)$$

are controllable if and only if the pair $(\mathcal{L}_{\mathcal{G}}, b)$ is controllable.

Proof. We prove the contrapositive using the Popov-Belevitch Hautus test (Theorem 15). Suppose that $(\mathcal{L}_{\mathcal{G}}, b)$ is uncontrollable. Then, there exists w such that $w^T b = 0$ and $w^T \mathcal{L}_{\mathcal{G}} = \lambda \mathcal{L}_{\mathcal{G}}$. We show by construction that there exists a left eigenvector of $\mathcal{L}_{\mathcal{G}}'$ that is orthogonal to the columns of $[b^T, b^T]^T$ and of $[b^T, \mathbf{0}^T]$.

We claim that $[w^T, \ \alpha^T]^T$ is an eigenvector of $\mathcal{L}_{\mathcal{G}}'$ with eigenvalue Λ, where

$$\alpha = \frac{1}{1-\Lambda} w$$
$$\Lambda = \frac{1}{2}\left(\sqrt{\lambda^2 + 4} + \lambda + 2\right).$$

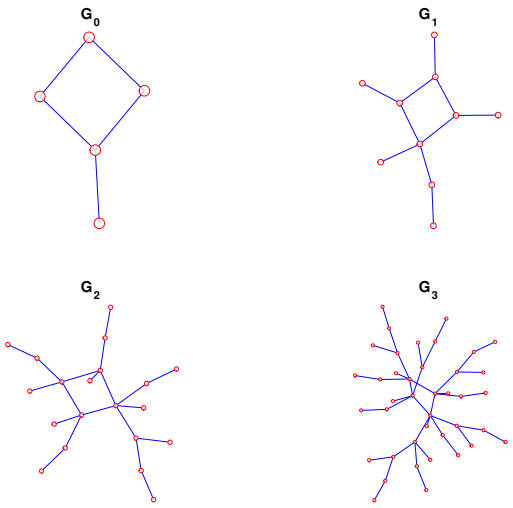

Figure 8.1: Whiskering a graph by adding a leaf to every node

The Laplacian is symmetric, and so its left eigenvectors are transposed right eigenvectors. Therefore, a computation yields

$$\begin{aligned}
\begin{bmatrix} \mathcal{L}_G + I & -I \\ -I & I \end{bmatrix} \begin{bmatrix} w \\ \alpha \end{bmatrix} &= \begin{bmatrix} (\mathcal{L}_G + I)w - I\alpha \\ I\alpha - Iw \end{bmatrix} \\
&= \begin{bmatrix} (\lambda + 1)w - \alpha \\ \alpha - w \end{bmatrix} \\
&= \begin{bmatrix} \dfrac{(1-\Lambda)(1+\lambda)-1}{1-\Lambda} w \\ \dfrac{1-(1-\Lambda)}{1-\Lambda} w \end{bmatrix} \\
&= \begin{bmatrix} \Lambda w \\ \dfrac{\Lambda}{1-\Lambda} w \end{bmatrix} \\
&= \begin{bmatrix} \Lambda w \\ \Lambda \alpha \end{bmatrix}.
\end{aligned}$$

This is orthogonal to the columns of $[b^T, b^T]^T$:

$$\begin{aligned}
[w^T, \alpha^T] \begin{bmatrix} b \\ b \end{bmatrix} &= \left[w^T, \ \frac{1}{1-\Lambda} w^T \right] \begin{bmatrix} b \\ b \end{bmatrix} \\
&= \left(1 + \frac{1}{1-\Lambda} \right) w^T b = \mathbf{0}.
\end{aligned}$$

$[w^T, \alpha^T]$ is also orthogonal to the columns of $[b^T, \mathbf{0}^T]^T$:

$$[w^T, \alpha^T] \begin{bmatrix} b \\ \mathbf{0} \end{bmatrix} = w^T b = \mathbf{0}.$$

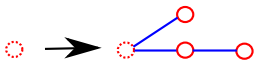

Figure 8.2: Adding a leaf and a path of length 2 to every node

For the reverse direction, assume that $(\mathcal{L}_\mathcal{G}', b = [b_1^T, b_2^T]^T)$ is uncontrollable. Then by Theorem 15 we have an eigenvector of $\mathcal{L}_\mathcal{G}'$ orthogonal to the columns of b:

$$\begin{aligned}\begin{bmatrix} \mathcal{L}_\mathcal{G} + I & -I \\ -I & I \end{bmatrix}\begin{bmatrix} w_1 \\ w_2 \end{bmatrix} &= \lambda \begin{bmatrix} w_1 \\ w_2 \end{bmatrix} \\ &= \begin{bmatrix} \mathcal{L}_\mathcal{G} w_1 + (w_1 - w_2) \\ w_2 - w_1 \end{bmatrix},\end{aligned}$$

$$[w_1^T, w_2^T]\begin{bmatrix} b_1 \\ b_2 \end{bmatrix} = \begin{bmatrix} w_1^T b_1 \\ w_2^T b_2 \end{bmatrix} = \begin{bmatrix} \mathbf{0} \\ \mathbf{0} \end{bmatrix}. \tag{8.2}$$

It follows that

$$\begin{aligned} w_2 &= \frac{1}{1-\lambda} w_1 \\ \mathcal{L}_\mathcal{G} w_1 &= \left(\frac{1-(1-\lambda)^2}{1-\lambda}\right) w_1, \end{aligned}$$

and so w_1 is an eigenvector of $\mathcal{L}_\mathcal{G}$ with eigenvalue $(1-(1-\lambda)^2)(1-\lambda)^{-1}$. It it is clear that from Equation (8.2) that $w_1^T b_1 = \mathbf{0}$, and so $(\mathcal{L}_\mathcal{G}, b_1)$ is uncontrollable. This result also holds when $b_2 = \mathbf{0}$, and the theorem follows. □

Theorem 18 therefore provides a useful way of ensuring that a large graph is controllable. Since rank controllability tests for very large graphs are often inaccurate due to machine precision or are computationally expensive, one can use this method by starting with a small graph on which a controllability test is easily performed and iterate this process several times until a sufficiently large network is obtained.

A natural question to ask is what other types of growth processes preserve controllability? For example, what if we attach a leaf to every node, but also attach a path of length 2 to every node (as shown in Figure 8.2)? This corresponds to concatenating the Laplacian as follows:

$$\mathcal{L}_\mathcal{G} \longrightarrow \begin{bmatrix} \mathcal{L}_\mathcal{G} + 2I & -I & -I & \mathbf{0} \\ -I & I & \mathbf{0} & \mathbf{0} \\ -I & \mathbf{0} & 2I & -I \\ \mathbf{0} & \mathbf{0} & -I & I \end{bmatrix} = \mathcal{L}_\mathcal{G}'. \tag{8.3}$$

We denote $\mathcal{L}_\mathcal{G}' = W_2(\mathcal{L}_\mathcal{G})$. It turns out that this growth process also preserves controllability.

Theorem 19.

Let $\mathcal{L}_\mathcal{G}' = W_2(\mathcal{L}_\mathcal{G})$. The pairs $(\mathcal{L}_\mathcal{G}', [b^T, b_i^T, b_i^T, b_i^T]^T)$ (where $b_i \in \{b, \mathbf{0}\}$) are controllable if and only if the pair $(\mathcal{L}_\mathcal{G}, b)$ is controllable.

Proof. We again prove the contrapositive using Theorem 15. Suppose that $(\mathcal{L}_\mathcal{G}, b)$ is uncontrollable. Then, there exists w such that $w^T b = 0$ and $w^T \mathcal{L}_\mathcal{G} = \lambda \mathcal{L}_\mathcal{G}$. We show by construction that there exists a left eigenvector of $\mathcal{L}_\mathcal{G}'$ that is orthogonal to the columns of $[b^T, b^T]^T$ and of $[b^T, \mathbf{0}^T]$. It can be verified in a similar calculation as in the proof of Theorem 18 that $[w^T, \alpha^T, \beta^T, \gamma^T]$ is a left eigenvector of $\mathcal{L}_\mathcal{G}'$ with eigenvalue Λ, where

$$\gamma = \frac{1}{1-\Lambda}\beta,\ \beta = \left(\frac{1}{1-\Lambda} - \Lambda - 2\right)^{-1} w,\ \alpha = \frac{1}{1-\Lambda} w$$

and where Λ satisfies the equation

$$\lambda + 2 = \frac{\Lambda\left(\Lambda^3 - 4\Lambda + 2\right)}{\Lambda^3 - 2\Lambda + 1}.$$

Note that α and β are simply scalings of w, and therefore γ is also a scaling of w. Therefore, α, β and γ are all orthogonal to the columns of b:

$$\alpha^T b = \beta^T b = \gamma^T b = w^T b = \mathbf{0},$$

and so it is clear that

$$[w^T, \alpha^T, \beta^T, \gamma^T][b^T, b_i^T, b_i^T, b_i^T]^T = \mathbf{0}$$

for $b_i \in \{b, \mathbf{0}\}$. It follows that $(\mathcal{L}_\mathcal{G}', [b^T, b_i^T, b_i^T, b_i^T]^T)$ is uncontrollable.

For the reverse direction, assume that the pair $(\mathcal{L}_\mathcal{G}', b = [b_1^T, b_2^T, b_3^T, b_4^T]^T)$ is uncontrollable. Then by Theorem 15 there exists an eigenvector $w = [w_1^T, w_2^T, w_3^T, w_4^T]^T$ of $\mathcal{L}_\mathcal{G}'$ orthogonal to the columns of b with eigenvalue λ such that

$$\begin{bmatrix} \mathcal{L}_\mathcal{G} + 2I & -I & -I & \mathbf{0} \\ -I & I & \mathbf{0} & \mathbf{0} \\ -I & \mathbf{0} & 2I & -I \\ \mathbf{0} & \mathbf{0} & -I & I \end{bmatrix} \begin{bmatrix} w_1 \\ w_2 \\ w_3 \\ w_4 \end{bmatrix} = \lambda \begin{bmatrix} w_1 \\ w_2 \\ w_3 \\ w_4 \end{bmatrix}$$

$$= \begin{bmatrix} \mathcal{L}_\mathcal{G} w_1 + 2w_1 - w_2 - w_3 \\ w_2 - w_1 \\ 2w_3 - w_1 - w_4 \\ w_4 - w_3 \end{bmatrix}$$

It follows from a simple calcuation that w_1 is an eigenvector of $\mathcal{L}_\mathcal{G}$ with eigenvalue

$$\lambda = \frac{\lambda^4 - 6\lambda^3 + 14\lambda^2 - 14\lambda + 4}{(\lambda - 1)(\lambda^2 - 3\lambda + 1)}.$$

Since w is orthogonal to the columns of b, it follows that $w_1^T b_1 = \mathbf{0}$, and the theorem follows. □

As Theorem 19 suggests, there are many ways to grow graphs such that they remain controllable. In this example, we showed that adding a *cluster* of nodes, namely a leaf and a path of length 2, to each node preserves controllability. It is a natural question to ask what types of node clusters in general one can place on each node to preserve controllability. The following theorem places some conditions on these clusters.

Theorem 20 (General Graph Growth). *Let $\mathcal{L}_\mathcal{G}$ be an $n \times n$ graph Laplacian, and let $\mathcal{L}_{\mathcal{G}_\delta}$ be $n \times n$, C be $r \times r$ and B be $n \times r$ (where $r = kn$ for $k \in \mathbb{Z}_+$) such that the matrix*

$$\mathcal{L}_\mathcal{G}{}' = \begin{bmatrix} \mathcal{L}_\mathcal{G} + \mathcal{L}_{\mathcal{G}_\delta} & B \\ B^T & C \end{bmatrix}$$

is a graph Laplacian. Since we are interested in adding the same cluster to each node, we can write $\mathcal{L}_{\mathcal{G}_\delta} = sI$, where s is the number of edges added to the node when attaching it to the cluster. We have the following results:

1. *Let $b_n, w_1 \in \mathbb{R}^n$ and $b_r, \beta \in \mathbb{R}^r$. Suppose $(\mathcal{L}_\mathcal{G}{}', b = [b_1, b_r])$ is uncontrollable. Then, there exists an eigenvector $W_1 \neq 0$ such that $\mathcal{L}_\mathcal{G}{}' W_1 = \Lambda w$, $W_1^T b = \mathbf{0}$ where, say $W_1 = [w_1^T, \beta^T]^T$. Then $(\mathcal{L}_\mathcal{G}, b_1)$ is uncontrollable when:*
   a) *$(\Lambda I - C)$ is invertible*
   b) *w_1 is an eigenvector of $B(\Lambda I - C)^{-1}B^T$.*
2. *Suppose $(\mathcal{L}_\mathcal{G}, b)$ is uncontrollable. Then, there exists $w \neq 0$ such that $\mathcal{L}_\mathcal{G} w = \lambda w$ with $w^T b = 0$. We thus have that $(\mathcal{L}_\mathcal{G}{}', [b, \mathbf{0}])$ is uncontrollable if*
   a) *There exists $\Lambda \geq 0$ such that:*
      i. *$(\Lambda I - C)^{-1}$ is invertible*
      ii. *w is an eigenvector of $B(\Lambda I - C)^{-1}B^T$ such that $B(\Lambda I - C)^{-1}B^T w = f(\Lambda)$*
      iii. *Λ satisfies $\Lambda - \lambda - s = f(\Lambda)$.*

Proof. We prove the two results separately.

1) Assuming the notation in Theorem 20-(1), suppose that $(\mathcal{L}_\mathcal{G}{}', b = [b_1, b_r])$ is uncontrollable. Then, by Theorem 15 there exists an eigenvector $W_1 = [w_1^T, \beta^T]^T \neq 0$ such that $\mathcal{L}_\mathcal{G}{}' W_1 = \Lambda w$, $W_1^T b = \mathbf{0}$ yielding:

$$\begin{aligned} \mathcal{L}_\mathcal{G}{}' W_1 &= \begin{bmatrix} \mathcal{L}_\mathcal{G} + \mathcal{L}_{\mathcal{G}_\delta} & B \\ B^T & C \end{bmatrix} \begin{bmatrix} w_1 \\ \beta \end{bmatrix} \\ &= \begin{bmatrix} (\mathcal{L}_\mathcal{G} + sI)w_1 + B\beta \\ B^T w_1 + C\beta \end{bmatrix} = \Lambda \begin{bmatrix} w_1 \\ \beta \end{bmatrix}. \end{aligned} \tag{8.4}$$

Therefore, if $(\Lambda I - C)$ is invertible, the lower entry of the vector in Equation (8.4) gives:

$$\beta = (\Lambda I - C)^{-1} B^T w_1.$$

Then, the first entry of the vector in Equation (8.4) gives

$$\mathcal{L}_{\mathcal{G}} w_1 = \left[(\Lambda - s)I - B(\Lambda I - C)^{-1}B^T\right] w_1.$$

This equation admits w_1 as an eigenvector of $\mathcal{L}_{\mathcal{G}}$ if the action of $B(\Lambda I - C)^{-1}B^T$ on w_1 is to scale w_1 by a fixed amount. In other words, if w_1 is an eigenvector of$B(\Lambda I - C)^{-1}B^T$, then it is an eigenvector of $\mathcal{L}_{\mathcal{G}}$, and since $w_1^T b_1 = \mathbf{0}$, the result follows.

2) Assuming the notation in Theorem 20-(2), suppose that $(\mathcal{L}_{\mathcal{G}}, b)$ is uncontrollable. Then, there exists $w \neq 0$ such that $\mathcal{L}_{\mathcal{G}} w = \lambda w$ with $w^T b = 0$. We seek an admissible solution for the equation

$$\begin{aligned}\begin{bmatrix} \mathcal{L}_{\mathcal{G}} + \mathcal{L}_{\mathcal{G}_\delta} & B \\ B^T & C \end{bmatrix} \begin{bmatrix} w \\ \beta \end{bmatrix} &= \begin{bmatrix} (\mathcal{L}_{\mathcal{G}} + sI)w + B\beta \\ B^T w + C\beta \end{bmatrix} \\ &= \Lambda \begin{bmatrix} w \\ \beta \end{bmatrix} \end{aligned} \tag{8.5}$$

in terms of the eigenvalue Λ of $\mathcal{L}_{\mathcal{G}}{}'$, and the lower part of the eigenvector, β. If $(\Lambda I - C)$ is invertible, we can write

$$\beta = (\Lambda I - C)^{-1}B^T w.$$

From the upper entry of the vector in Equation (8.5), we get the relation

$$(\Lambda - \lambda - s)Iw = B(\Lambda I - C)^{-1}B^T w.$$

Then, if w is an eigenvector of $B(\Lambda I - C)^{-1}B^T$, say $B(\Lambda I - C)^{-1}B^T w = f(\Lambda)w$, then we get an equation for Λ:

$$\Lambda - \lambda - s = f(\Lambda).$$

We add the stipulation that Λ must be *admissible*: $\Lambda \geq 0$ for Λ to be a Laplacian eigenvalue. Finally, it is clear that since $w^T b = 0$, we have that $[w^T, \beta^T][b^T, \mathbf{0}^T]^T = \mathbf{0}$. □

8.1.1 *Single Leaf Addition*

First, we will consider the addition of a single node to the graph. The new node is attached to an existing node with a single edge, see Figure 8.3 (a).

The operation for adding a single leaf to node i is algebraically represented by appending a row and column to the Laplacian in the following manner:

$$\mathcal{L}_{\mathcal{G}} \rightarrow \left[\begin{array}{c|c} \mathcal{L}_{\mathcal{G}} + e_i e_i^T & -e_i \\ \hline -e_i^T & 1 \end{array}\right] := \mathcal{W}_i(\mathcal{L}_{\mathcal{G}}).$$

where $\mathcal{W}_i$ denotes the Laplacian of the whiskered graph. In order to apply a PBH-style argument to analyze controllability, we need to look for eigen-

vectors V and eigenvalues Λ of the Laplacian. We separate the eigenvector into an n-dimensional vector v and a scalar part α:

$$\left[\begin{array}{c|c} \mathcal{L}_{\mathcal{G}} + e_i e_i^T & -e_i \\ \hline -e_i^T & 1 \end{array}\right] \begin{bmatrix} v \\ \alpha \end{bmatrix} = \Lambda \begin{bmatrix} v \\ \alpha \end{bmatrix}. \tag{8.6}$$

Equation (8.6) can be expanded into:

$$(\mathcal{L}_{\mathcal{G}} + e_i e_i^T)v - \alpha e_i = \Lambda v \tag{8.7}$$

$$\alpha - e_i^T v = \alpha.\Lambda \tag{8.8}$$

Equation (8.8) yields:

$$\alpha = \frac{e_i^T v}{1 - \Lambda},$$

and substituting this into Equation (8.7) yields:

$$\mathcal{L}_{\mathcal{G}} v = \left(\Lambda I + \left(\frac{1}{1-\Lambda} - 1\right) e_i e_i^T\right) v. \tag{8.9}$$

In the original whiskering process, V was shown to be described in terms of the eigenvectors of $\mathcal{L}_{\mathcal{G}}$. We will now derive expressions that show this is not the case for single leaf addition, with the exception of the consensus eigenvector. Rewriting Equation (8.9):

$$\begin{aligned} \mathcal{L}_{\mathcal{G}} v &= \left(\Lambda I + \left(\frac{1}{1-\Lambda} - 1\right) e_i e_i^T\right) v \\ &= \Lambda v + \left(\frac{1 - (1-\Lambda)}{1-\Lambda}\right) [v]_i e_i. \end{aligned} \tag{8.10}$$

If $\Lambda = 0$, then we get exactly that $\mathcal{L}_{\mathcal{G}} v = \Lambda v = \mathbf{0}_n$. Since $v = \mathbf{1}$ is the eigenvector of $\mathcal{L}_{\mathcal{G}}$ corresponding to $\Lambda = 0$, from Equation (8.8) we get that $\alpha = [v]_i = 1$. It follows that $[v^T,\ \alpha]^T = \mathbf{1}_{n+1}$.

Next, from Equation (8.10) we can write:

$$\begin{aligned} \mathcal{L}_{\mathcal{G}} v &= \Lambda v + \frac{\Lambda}{1-\Lambda} [v]_i e_i \\ &= \Lambda \begin{bmatrix} [v]_1 & \cdots & \dfrac{2-\Lambda}{1-\Lambda}[v]_i & \cdots & [v]_n \end{bmatrix}^T. \end{aligned}$$

For this to be an eigenvector of $\mathcal{L}_{\mathcal{G}}$, we need $(2-\Lambda)(1-\Lambda)^{-1} = 1$, but this equality has no solutions for finite Λ. It follows that v cannot be written in terms of an eigenvector of $\mathcal{L}_{\mathcal{G}}$, with the exception of the consensus eigenvector.

Without relying on the original eigenvectors, we have to find conditions on the new graph that guarantee controllability. Since the added node is always a leaf, we focus on finding conditions on the input matrix that leads to the desired guarantees.

Assuming that the original graph is controllable, by the PBH-test, there is no feasible solution to the linear equations given in Lemma 15; i.e. the

eigenvectors of the Laplacian satisfy the linear inequalities that follow from the infeasibility of the PBH Lemma.

It thus follows that to conserve controllability, the new eigenvectors and input matrix of the graph have to satisfy Lemma 15 and the linear inequalities described therein. The eigenvectors are directly given from the structure of the leaf addition. Therefore, we have only the new element of the extended input matrix $B = [b^T,\ \beta]^T$ to adjust the result and guarantee controllability of the grown graph.

Theorem 21 (Summary of Single Leaf Whiskering). *Consider the Laplacian-control vector pair $(\mathcal{L}_\mathcal{G}, b)$ and the corresponding single leaf whiskered pair $\left(\mathcal{W}_i(\mathcal{L}_\mathcal{G}), [b^T,\ \beta]^T\right)$ given by the operation*

$$\mathcal{L}_\mathcal{G} \to \left[\begin{array}{c|c} \mathcal{L}_\mathcal{G} + e_i e_i^T & -e_i \\ \hline -e_i^T & 1 \end{array}\right] := \mathcal{W}_i(\mathcal{L}_\mathcal{G}).$$

If $(\mathcal{L}_\mathcal{G}, b)$ is controllable, then $\left(\mathcal{W}_i(\mathcal{L}_\mathcal{G}), [b^T,\ \beta]^T\right)$ is controllable if and only if

$$\beta \neq [b]_i + \frac{v^T \mathcal{L}_\mathcal{G} b}{[v]_i - \alpha} \tag{8.11}$$

for all eigenvectors $V = \begin{bmatrix} v^T & \alpha \end{bmatrix}^T \neq \mathbf{1}_{n+1}$ of $\mathcal{W}_i(\mathcal{L}_\mathcal{G})$, and

$$\beta \neq -\sum_i [b]_i. \tag{8.12}$$

Proof. The conditions in Equation (8.11) and Equation (8.12) are derived using the PBH-test (Lemma 15). The pair $(\mathcal{W}_i(\mathcal{L}_\mathcal{G}), B)$ is controllable if and only if $V^T B \neq 0$ for all eigenvectors V of $\mathcal{W}_i(\mathcal{L}_\mathcal{G})$. Noting that the null space of $\mathcal{W}_i(\mathcal{L}_\mathcal{G})$ is $\operatorname{span}(\mathbf{1}_{n+1})$ and that $\mathbf{1}_{n+1}$ is an eigenvector of $\mathcal{W}_i(\mathcal{L}_\mathcal{G})$, this is equivalent to the conditions that

$$(\mathcal{W}_i(\mathcal{L}_\mathcal{G})V)^T B \neq 0 \ \text{ and } \ \mathbf{1}_{n+1}^T B \neq 0.$$

The latter condition gives

$$0 \neq \mathbf{1}_{n+1}^T B = \mathbf{1}_{n+1}^T \begin{bmatrix} b \\ \beta \end{bmatrix} = \beta + \sum_i [b]_i,$$

yielding the latter part of the theorem. The former condition gives

$$\begin{aligned} 0 &\neq (\mathcal{W}_i(\mathcal{L}_\mathcal{G})V)^T B \\ &= \left[\begin{array}{c|c} \mathcal{L}_\mathcal{G} + e_i e_i^T & -e_i \\ \hline -e_i^T & 1 \end{array}\right] \begin{bmatrix} v \\ \alpha \end{bmatrix} \\ &= v^T \mathcal{L}_\mathcal{G} b + ([v]_i - \alpha)([b]_i - \beta), \end{aligned}$$

yielding the first condition of the theorem. □

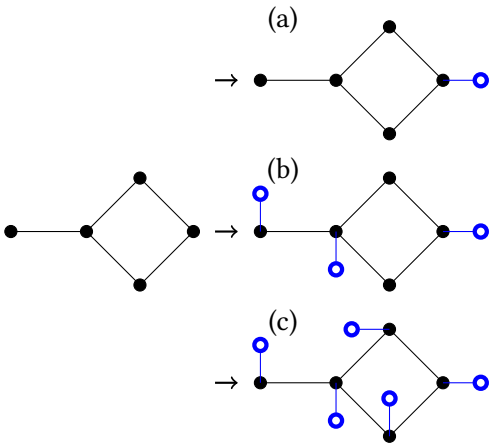

Figure 8.3: Three examples of graph whiskering, original graph is solid, added nodes are hollow. (a) Single leaf. (b) Multi-leaf. (c) Fully whiskered.

8.1.2 *Multi-Leaf Addition*

Extending the results of single leaf whiskering, we will now examine conditions on the grown graph when adding multiple nodes to it; see Figure 8.3 (b).

The operation of adding leaves to $1 < k < n$ distinct nodes in the graph (say the first k nodes, without loss of generality) is represented by:

$$\mathcal{L}_\mathcal{G} \to \left[\begin{array}{c|ccc} \mathcal{L}_\mathcal{G} + \sum_{i=1}^{k} e_i e_i^T & -e_1 & \cdots & -e_k \\ \hline -e_1^T & & & \\ \vdots & & I_k & \\ -e_k^T & & & \end{array}\right] := \mathcal{W}_{[k]}(\mathcal{L}_\mathcal{G}).$$

As in the preceding section, we search for eigenvectors $V = [v_1^T,\ v_2^T]^T$ of $\mathcal{W}_{[k]}(\mathcal{L}_\mathcal{G})$, where $v_1 \in \mathbb{R}^n$ and $v_2 \in \mathbb{R}^k$:

$$\left[\begin{array}{c|ccc} \mathcal{L}_\mathcal{G} + \sum_{i=1}^{k} e_i e_i^T & -e_1 & \cdots & -e_k \\ \hline -e_1^T & & & \\ \vdots & & I_k & \\ -e_k^T & & & \end{array}\right] \left[\frac{v_1}{v_2}\right] = \Lambda \left[\frac{v_1}{v_2}\right]$$

$$= \left[\begin{array}{c} \left(\mathcal{L}_\mathcal{G} + \sum_{i=1}^{k} e_i e_i^T\right) v_1 + \sum_{i=1}^{k} [v_2]_i\, e_i \\ v_2 - \left[\begin{array}{c} [v_1]_1 \\ \vdots \\ [v_1]_k \end{array}\right] \end{array}\right].$$

From the equation representing the $n+1, \ldots, n+k$ entries of V, we can see that

$$v_2 = \frac{1}{1-\Lambda} \begin{bmatrix} [v_1]_1 \\ \vdots \\ [v_1]_k \end{bmatrix} := \frac{1}{1-\Lambda} [v_1]_{[k]} .$$

Plugging this into the equation representing the first n entries of V, we obtain,

$$\left(\mathcal{L}_{\mathcal{G}} + \sum_{i=1}^{k} e_i e_i^T \right) v + \sum_{i=1}^{k} \frac{1}{1-\Lambda} [v_1]_i \, e_i = \Lambda v_1$$

$$\mathcal{L}_{\mathcal{G}} v_1 = \Lambda v_1 + \frac{\Lambda}{1-\Lambda} \sum_{i=1}^{k} [v_1]_i \, e_i .$$

Theorem 22 (Summary of Multi-Leaf Whiskering). *Consider the Laplacian-control vector pair $(\mathcal{L}_{\mathcal{G}}, b)$ and the corresponding multi-leaf whiskered pair*

$$\left(\mathcal{W}_{[k]}(\mathcal{L}_{\mathcal{G}}), [b^T \ \beta^T]^T \right)$$

given by the operation

$$\mathcal{L}_{\mathcal{G}} \rightarrow \left[\begin{array}{c|ccc} \mathcal{L}_{\mathcal{G}} + \sum_{i=1}^{k} e_i e_i^T & -e_1 & \cdots & -e_k \\ \hline -e_1^T & & & \\ \vdots & & I_k & \\ -e_k^T & & & \end{array}\right] := \mathcal{W}_{[k]}(\mathcal{L}_{\mathcal{G}}).$$

If $(\mathcal{L}_{\mathcal{G}}, b)$ is controllable, then $\left(\mathcal{W}_i(\mathcal{L}_{\mathcal{G}}), [b^T, \ \beta^T]^T\right)$ is controllable if and only if

$$v_1^T \mathcal{L}_{\mathcal{G}} b \neq \sum_{i=1}^{k} \left([v_1]_i - [v_2]_i \right) \left([b]_i - [\beta]_i \right)$$

for all eigenvectors $\mathbf{1}_{n+k} \neq \left[v_1^T, \ v_2^T\right]^T := V$ of $\mathcal{W}_i(\mathcal{L}_{\mathcal{G}})$, and

$$\sum_{i=1}^{n} [\beta]_i \neq - \sum_{j=1}^{k} [b]_j .$$

Proof. For all eigenvectors V of the multi-leaf whiskered graph $\mathcal{W}_{[k]}(\mathcal{L}_{\mathcal{G}})$, it has to be true that:

$$0 \neq V^T B.$$

Since the grown graph is fully connected, the vector of all ones $\mathbf{1}_{n+k}$ is still the consensus eigenvector related to the eigenvalue of 0. Thus all other eigen-

vector can be expressed by Laplacian multiplication without loss of generality. Then, the PBH-test yields:

$$\left(\mathcal{W}_{[k]}(\mathcal{L}_\mathcal{G})V\right)^T B \neq 0 \text{ and } \mathbf{1}_{n+k}^T B \neq 0$$

for all eigenvectors $V \neq \mathbf{1}_{n+k}$ of $\mathcal{W}_{[k]}(\mathcal{L}_\mathcal{G})$.

The first condition of the theorem is given by the inequality for all eigenvectors that are not the consensus eigenvector:

$$\begin{aligned}
0 &\neq \left(\mathcal{W}_{[k]}(\mathcal{L}_\mathcal{G})V\right)^T B \\
&= \left(\left(\mathcal{L}_\mathcal{G} + \textstyle\sum_{i=1}^k e_i e_i^T\right) v_1 - \sum_{i=1}^k [v_2]_i \, e_1\right)^T b + \left(v_2 - \begin{bmatrix} [v_1]_1 \\ \vdots \\ [v_1]_k \end{bmatrix}\right)^T \beta \\
&= v_1^T \mathcal{L}_\mathcal{G} b_1 + \sum_{i=1}^n \left([v_1]_i - [v_2]_i\right)[b]_i - \sum_{i=1}^k \left([v_1]_i - [v_2]_i\right)[\beta]_i \\
&= v_1^T \mathcal{L}_\mathcal{G} b + \sum_{i=1}^k \left([v_1]_i - [v_2]_i\right)\left([b]_i - [\beta]_i\right).
\end{aligned}$$

The second condition of the theorem follows directly from the second inequality given by the PBH Lemma:

$$0 \neq \mathbf{1}_{n+k}^T B = \sum_{i=1}^n [b]_i + \sum_{j=1}^k [\beta]_j .$$

□

This second inequality nicely describes an important effect in graph growing. Due to the fact that every new node is attached to a single original node, an equal but opposite input flow into these new nodes causes uncontrollability. This result is not constrained to an exactly opposite input in the nodes (i.e., $\beta = -b$), but already appears when the total sum of the new input coefficients is equal to the original.

8.1.3 *Fully Whiskered Graph*

Examining the result from multi-leaf addition we will briefly discuss the case when adding $k = n$ nodes to the graph, see Figure 8.3 (c). This case has been examined in [22] with consideration of the eigenvectors of the whiskered graph depending on the eigenvectors of the original graph. We will show that the results presented in the previous paragraph are generalizations to the approach in [22] and that the choice of input matrix coefficients can thereby be relaxed.

Given the graph Laplacian $\mathcal{L}_\mathcal{G}$ and input matrix b, for $k = n$ we are looking for the following whiskered Laplacian:

$$\mathcal{W}_{[n]}(\mathcal{L}_\mathcal{G}) = \left[\begin{array}{c|ccc} \mathcal{L}_\mathcal{G} + \sum_{i=1}^{n} e_i e_i^T & -e_1 & \cdots & -e_n \\ \hline -e_1^T & & & \\ \vdots & & I_n & \\ -e_n^T & & & \end{array}\right] = \begin{bmatrix} \mathcal{L}_\mathcal{G} + I & -I \\ -I & I \end{bmatrix} = \mathcal{W}(\mathcal{L}_\mathcal{G})$$

which is identical to the fully whiskered graph given in Theorem 18. The extended input matrix is $B = [b^T,\ \beta^T]^T$.

Given that the first half of the eigenvector of the new graph is identical to the eigenvector v of the original graph, the first condition of Theorem 22 becomes:

$$0 \neq \lambda v^T b + \sum_{i=1}^{k} \left([v_1]_i - [v_2]_i\right)\left([b]_i - [\beta]_i\right)$$

When choosing $\beta = b$, this inequality reduces to:

$$0 \neq \lambda v^T b$$

for all eigenvectors not equal to the consensus vector. Therefore, since the graph is fully connected, this inequality is always satisfied. In the second case, $\beta = \mathbf{0}_n$, the condition is:

$$0 \neq \lambda v^T b + \sum_{i=1}^{k} \left([v_1]_i - [v_2]_i\right)[b]_i = \lambda v^T b + (v_1 - v_2)^T b$$

From the original graph we know that $0 \neq \lambda v^T b$ and in [22] it is shown that $v = v_1$, the first element of the new eigenvector is equal to the original eigenvector. Furthermore, it is also shown that:

$$v_2 = \frac{1}{1-\Lambda} v, \quad l = \frac{1}{2}\left(\sqrt{\lambda^2 + 4} + \lambda + 2\right).$$

Thus, the following inequality has to be satisfied:

$$\begin{aligned} 0 &\neq \left(\lambda + 1 - \frac{1}{1-l}\right) v^T b \\ &= \frac{1}{2}\left(\sqrt{\lambda^2 + 4} + \lambda + 2\right) v^T b = l v^T b. \end{aligned}$$

Since the coefficient l does not have a root with respect to λ, this inequality is always satisfied.

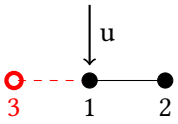

Figure 8.4: Original graph (solid) and added leaf (hollow) with control input to first node.

For either case of β, the second condition is obviously always satisfied. When $\beta = \mathbf{0}_n$, then:

$$0 \neq \sum_{i=1}^{n} [b]_i$$

is true if the original graph is controllable. And when $\beta = b$, we similarly get the condition:

$$0 \neq 2 \sum_{i=1}^{n} [b]_i \,.$$

This shows that both results can be used interchangeably. Furthermore, the new result proven in this section can be used to get more varied input matrices. So long as β does not violate the conditions given in Theorem 22, the whiskered graph will be controllable.

8.2 EXAMPLES

In this section we will give some examples of graph growing that rely on the presented results; as such, the graph growth process preserves network controllability. We will use the given inequalities to determine detrimental input matrices. Then, we will show that controllability is lost using the rank of the respective controllability matrix when selecting these undesirable input matrices.

Consider the Laplacian corresponding to the graph given in Figure 8.4 with control vector $b = [1\ 0]$. The controllability matrix is given by

$$\left(\mathcal{L}_{\mathcal{G}} = \begin{bmatrix} 1 & -1 \\ -1 & 1 \end{bmatrix}, \; b = \begin{bmatrix} 1 \\ 0 \end{bmatrix} \right) \rightarrow \; C = \begin{bmatrix} 1 & 1 \\ 0 & -1 \end{bmatrix},$$

which has two linearly independent columns, indicating that the system is controllable. This Laplacian has two eigenvectors with respective eigenvalue:

$$v_1 = \begin{bmatrix} 1 \\ 1 \end{bmatrix}, \; v_2 = \begin{bmatrix} -1 \\ 1 \end{bmatrix} \rightarrow \lambda_i = \{0, 2\},$$

where v_1 is the consensus eigenvector. In the next step we grow the graph by attaching a single leaf to the first node. It is obvious that this graph has inherent controllability issues due to the symmetry of the nodes with respect

to the original input node. We will use the results of Theorem 21 to give well stated constraints on the grown input matrix B.

The Laplacian, the input matrix, and the eigenvectors of the Laplacian of the single leaf whiskered graph are given by:

$$\mathcal{W}_1(\mathcal{L}_\mathcal{G}) = \begin{bmatrix} 2 & -1 & -1 \\ -1 & 1 & 0 \\ -1 & 0 & 1 \end{bmatrix}, \; B = \begin{bmatrix} 1 \\ 0 \\ \beta \end{bmatrix}$$

$$v_1 = \begin{bmatrix} -2 \\ 1 \\ 1 \end{bmatrix}, \; v_2 = \begin{bmatrix} 0 \\ -1 \\ 1 \end{bmatrix}, \; v_3 = \begin{bmatrix} 1 \\ 1 \\ 1 \end{bmatrix}.$$

Due to the consensus eigenvector we get the following condition given in equation (8.12) on β:

$$\beta|_{j=3} \neq -\sum_i [b]_i = -1$$

and from equation (8.11) for the eigenvectors v_1 and v_2 we get that:

$$\beta|_{j=1} \neq [b]_i + \frac{v^T \mathcal{L}_\mathcal{G} b}{[v]_i - \alpha} = 1 + \frac{1}{3}\begin{bmatrix} -2 & 1 \end{bmatrix}\begin{bmatrix} 1 & -1 \\ -1 & 1 \end{bmatrix}\begin{bmatrix} 1 \\ 0 \end{bmatrix} = 0$$

$$\beta|_{j=2} \neq 1 + \begin{bmatrix} 0 & -1 \end{bmatrix}\begin{bmatrix} 1 & -1 \\ -1 & 1 \end{bmatrix}\begin{bmatrix} 1 \\ 0 \end{bmatrix} = 2$$

So long as $\beta \neq \{-1, \; 0, \; 2\}$, the grown graph will be controllable.

The controllability matrix of $(\mathcal{W}_1(\mathcal{L}_\mathcal{G}), B)$ with respect to β is given by

$$C(\beta) = \begin{bmatrix} 1 & 2-\beta & 6-3\beta \\ 0 & -1 & \beta - 3 \\ \beta & \beta - 1 & 2\beta - 3 \end{bmatrix}.$$

When $\beta = -1$, we get that

$$C(-1) = \begin{bmatrix} 1 & 3 & 9 \\ 0 & -1 & -4 \\ -1 & -2 & -5 \end{bmatrix}.$$

The columns are not linearly independent: $-3c_1 + 2c_2 = c_3$, and so it is uncontrollable. For the other cases the rank deficiency of C is immediately obvious:

$$C(0) = \begin{bmatrix} 1 & 2 & 6 \\ 0 & -1 & -3 \\ 0 & -1 & -3 \end{bmatrix}, \; C(2) = \begin{bmatrix} 1 & 0 & 0 \\ 0 & -1 & -1 \\ 2 & 1 & 1 \end{bmatrix}.$$

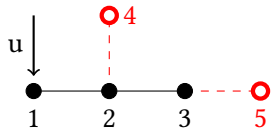

Figure 8.5: Multi-leaf whiskering example. Original graph (solid) and added leaves (hollow) with control input to first node.

In all cases the whiskered graph is uncontrollable.

Given the graph depicted in Figure 8.5 the Laplacian and the input matrix, where the only input is at the first node, are:

$$\mathcal{L}_{\mathcal{G}} = \begin{bmatrix} 1 & -1 & 0 \\ -1 & 2 & -1 \\ 0 & -1 & 1 \end{bmatrix}, \; b = \begin{bmatrix} 1 \\ 0 \\ 0 \end{bmatrix}.$$

This graph is controllable with the full rank controllability matrix:

$$C = \begin{bmatrix} 1 & 1 & 2 \\ 0 & -1 & -2 \\ 0 & 0 & 1 \end{bmatrix}.$$

Adding two leaves as shown in Figure 8.5 the whiskered Laplacian and input matrix are as follows:

$$\mathcal{W}_{[2]}(\mathcal{L}_{\mathcal{G}}) = \begin{bmatrix} 1 & -1 & 0 & 0 & 0 \\ -1 & 3 & -1 & -1 & 0 \\ 0 & -1 & 2 & 0 & -1 \\ 0 & -1 & 0 & 1 & 0 \\ 0 & 0 & -1 & 0 & 1 \end{bmatrix}, \; B = \begin{bmatrix} 1 \\ 0 \\ 0 \\ \beta_1 \\ \beta_2 \end{bmatrix}.$$

The second condition of Theorem 22 gives the following inequality:

$$\sum_{i=1}^{n} [\beta]_i \neq -\sum_{j=1}^{k} [b]_j \quad \Rightarrow \quad \beta_1 + \beta_2 \neq -1$$

As a counter-example, let $\beta_1 = 0$ and $\beta_2 = -1$. Then, the controllability matrix becomes:

$$C(0,-1) = \begin{bmatrix} 1 & 1 & 2 & 7 & 29 \\ 0 & -1 & -5 & -22 & -94 \\ 0 & 1 & 4 & 15 & 58 \\ 0 & 0 & 1 & 6 & 28 \\ -1 & -1 & -2 & -6 & -21 \end{bmatrix},$$

which does not have full rank. Thus, this choice of β will yield an uncontrollable graph.

8.2.1 *Optimization Algorithms: Adding Leaves*

In this section, we discuss optimization problems that are related to growing graphs. In particular, we consider when one wants to add node clusters to only a specific set of nodes in the graph.

Consider a connected graph $\mathcal{G}$ and its Laplacian matrix $L_{\mathcal{G}}$. The second-smallest eigenvalue $\lambda_2(L_{\mathcal{G}})$ is a measure of how interconnected the graph is. It is also an inverse measure of how long it takes for agents connected with graph $\mathcal{G}$ to achieve consensus by convergence to the agreement subspace. A well-known algorithm by Ghosh [65] adds edges between unconnected nodes in $\mathcal{G}$ to maximize $\lambda_2(L_{\mathcal{G}})$.

The algorithm considers a set of candidate edges between unconnected nodes in $\mathcal{G}$, and selects the k candidate edges that maximize $\lambda_2(L_{\mathcal{G}})$. For a set of m candidate edges $l = \{ij\}$, let a_l be the vector with all-zero entries except $a_{l_i} = 1$ and $a_{l_j} = -1$ when $\{ij\}$ is a candidate edge. The selection of k candidate edges from this set can be encoded with a $\{0,1\}^m$-vector x, where $x_l = 1$ if the algorithm selects candidate edge l, and zero otherwise. The optimization problem is then written in terms of the individual Laplacians $a_l a_l^T$ for each edge l as follows:

$$\begin{aligned} \text{maximize} \quad & \lambda_2\left(L_{\mathcal{G}} + \sum_{l=1}^{m} x_l a_l a_l^T\right) \\ \text{subject to} \quad & \mathbf{1}^T x = k \\ & x \in \{0,1\}^m. \end{aligned}$$

The standard relaxation of this problem into a semidefinite program (SDP) is of the form

$$\begin{aligned} \text{maximize} \quad & s \\ \text{subject to} \quad & s(I - \mathbf{1}\mathbf{1}^T/n) \preceq L(x) \\ & \mathbf{1}^T x = k \\ & 0 \le x \le 1 \\ & L(x) = L_{\mathcal{G}} + \sum_{l=1}^{m} x_l a_l a_l^T. \end{aligned}$$

We present a modification of this algorithm whereby one wants to add *nodes* to the graph $\mathcal{G}$ in such a way that the graph grows in order to maximize $\lambda_2(\mathcal{G})$. Suppose $\mathcal{G}$ has n nodes. We want to choose one of these n nodes to attach leaves to in order to 'grow' the graph to maximize $\lambda_2(\mathcal{G})$. Recall that $L_{\mathcal{G}}[I]$ is the principal submatrix of $L_{\mathcal{G}}$ obtained by deleting the rows and columns of $L_{\mathcal{G}}$ corresponding to the elements in the set $I \setminus [m]$. Let L_{tot} denote the graph that has every node whiskered:

$$L_{\text{tot}} = \begin{bmatrix} L_{\mathcal{G}} + I & -I \\ -I & I \end{bmatrix}.$$

We can write this problem as

$$\begin{aligned} &\text{maximize} && \lambda_2(L_{\mathcal{G}'}) \\ &\text{subject to} && L_{\mathcal{G}'} \in \left\{L_{\text{tot}}\left[[n] \cup \{i\}\right],\ i \in \{n+1, \dots, 2n\}\right\} \\ & && L_{\text{tot}} = \begin{bmatrix} L_{\mathcal{G}} + I & -I \\ -I & I \end{bmatrix}. \end{aligned} \tag{8.13}$$

This can be solved via exhaustive search over all possible whiskerings, however this becomes computationally intractable for large n. We can relax this problem to a modified Ghosh-Boyd Max-$\lambda_2(\mathcal{G})$ SDP as follows. Let e_i denote the ith standard basis vector in $\mathbb{R}^n$. Then, we introduce a single node into the system and create a set of n candidate edges potentially connecting the new node to any pre-existing node in the graph. The individual Laplacian for each candidate edge is $a_i a_i^T$, where $a_i \in \mathbb{R}^{n+1}$ is of the form $a_i = [e_i, -1]^T$. The SDP relaxation is then

$$\begin{aligned} &\text{maximize} && s \\ &\text{subject to} && s\left(I_{n+1} - \frac{(\mathbf{1}\mathbf{1}^T)_{n+1}}{n+1}\right) \preceq L(x) \\ & && \mathbf{1}^T x = 1 \\ & && 0 \le x \le 1 \\ & && L(x) = L'_{\mathcal{G}} + \sum_{l=1}^{n} x_l a_l a_l^T \\ & && L'_{\mathcal{G}} = \begin{bmatrix} L_{\mathcal{G}} & \mathbf{0}_n \\ \mathbf{0}_n^T & 0 \end{bmatrix},\ \mathbf{0}_n \in \mathbb{R}^n. \end{aligned} \tag{8.14}$$

Recall that $L[K]$ is the principal submatrix of L constructed by removing the rows and columns indexed by the set $[n] \setminus K$. For example, $L[[n] \setminus \{1\}] = L[\{2, \dots, n\}] := L[2 : n]$ is the principal submatrix of L with the first row and column removed. This matrix is positive-definite. We can also relate the inverse of this matrix to the *controllability Gramian* [71], [75] P, which is a measure of the steady-state covariance of the agent states. P is the positive-definite solution of the Lyapunov equation

$$-PL[2:n] - L[2:n]P^T = -I,$$

and is given by $P = \frac{1}{2}L[2:n]^{-1}$. Certain submodular functions of P (with respect to edge-addition) were studied in [69].

The trace of P can be interpreted as an average amount of energy expended to move the agent states around the controllable subspace, and therefore it is of interest to be able to bound the value of $\text{Tr}P$ on the results of our algorithms. We do this using the supermodularity properties of M-matrices from Theorem 17.

Theorem 23. *Let L' denote the whiskering process in Equation (8.1), where L is $n \times n$, and so L' is $2n \times 2n$. Let the controllability Gramian P' of L' be the solution to*

$$-P'L'[2:2n] - L'[2:2n]P'^T = -I.$$

Then,

$$\mathrm{Tr}P' \geq n + C,$$

where C is a constant depending on L.

Theorem 24. *Let L' denote the whiskering process in Equation (8.3), where L is $n \times n$, and so L' is $4n \times 4n$. Let the controllability Gramian P' of L' be the solution to*

$$-P'L'[2:4n] - L'[2:4n]P^T = -I.$$

Then,

$$\mathrm{Tr}P' \geq 4n + C,$$

where C is a constant depending on L.

We can prove Theorem 23 and 24 together.

Proof. First, we prove Theorem 23. We know that the solution to

$$-P'L'[2:2n] - L'[2:2n]P'^T = -I.$$

is given by $P' = \frac{1}{2}L'[2:2n]^{-1}$. From Theorem 17, using the fact that L' is an M-matrix, we have that

$$\begin{aligned}\mathrm{Tr}(P) &= \mathrm{Tr}(L'[2:2n]^{-1}) \\ &\geq \mathrm{Tr}(L'[2:n]^{-1}) + \mathrm{Tr}(L'[n+1:2n]^{-1}) \\ &= \mathrm{Tr}([L[2:n] + I]^{-1}) + \mathrm{Tr}(I) = C + n,\end{aligned}$$

where $C = \mathrm{Tr}([L[2:n] + I]^{-1})$ depends only on L. Theorem 24 follows from an identical calculation, noting that

$$\mathrm{Tr}\begin{bmatrix} I & \mathbf{0} & \mathbf{0} \\ \mathbf{0} & 2I & -I \\ \mathbf{0} & -I & I \end{bmatrix}^{-1} = 2\mathrm{Tr}(I) + \mathrm{Tr}(2I) = 4n.$$

□

We can use this result to bound the controllability Gramian when adding a single node to the system.

Theorem 25. *Consider the task of attaching a single node to the system with $n \times n$ Laplacian L to maximize λ_2, as denoted in Problem (8.13). Let L' be the subsequent Laplacian, and so $P = \frac{1}{2}L'[2:n+1]^{-1}$. Then, $\mathrm{Tr}P \geq C + 1$, where C is a constant depending only on L.*

Proof. Using Theorem 17 we can compute

$$\begin{aligned}\mathrm{Tr}(P) &= \mathrm{Tr}(L'[2:n+1]^{-1}) \\ &\geq \mathrm{Tr}(L'[2:n]^{-1}) + \mathrm{Tr}(L'[n+1:n+1]^{-1}) \\ &= \mathrm{Tr}([L[2:n] + e_i e_i^T]^{-1}) + 1 \geq C + 1,\end{aligned}$$

where i is the index of the attachment node chosen, and $C = \min_i(\mathrm{Tr}([L[2:n] + e_i e_i^T]^{-1}))$ is a constant depending only on L. □

In the next section, we will consider adding a cluster, and provide a similar result on the performance of TrP.

8.2.2 *Optimization Algorithms: Adding Clusters*

In the previous section, we considered the problem of optimally adding leaves to some nodes to optimize the algebraic connectivity of the graph. We will now consider the problem of adding a cluster of a node and a length-2 path, as depicted in Figure 8.2.

Let $\mathbf{0}_n \in \mathbb{R}^n$ and define $a_{3\to4} = [\mathbf{0}_n^T, 0, 1, -1]^T$, $a_{i,1} = [e_i^T, -1, 0, 0]^T$ and $a_{i,2} = [e_i^T, 0, -1, 0]^T$. Then, choosing an attachment node to maximize λ_2 can be written as

$$\begin{aligned}&\text{maximize} && \lambda_2(L_{\mathcal{G}'}) \\ &\text{subject to} && L_{\mathcal{G}'} \in \left\{L_{\mathrm{tot}}\left[[n] \cup \{i, i+n, i+2n\}\right], \right. \\ &&& \left. i \in \{n+1, \ldots, 2n\}\right\} \\ &&& L_{\mathrm{tot}} = \begin{bmatrix} L+2I & -I & -I & \mathbf{0} \\ -I & I & \mathbf{0} & \mathbf{0} \\ -I & \mathbf{0} & 2I & -I \\ \mathbf{0} & \mathbf{0} & -I & I \end{bmatrix}.\end{aligned} \tag{8.15}$$

We can write the SDP relaxation as:

$$\begin{aligned}&\text{maximize} && s \\ &\text{subject to} && s\left(I_{n+3} - \frac{(\mathbf{1}\mathbf{1}^T)_{n+3}}{n+3}\right) \preceq L(x) \\ &&& \mathbf{1}^T x = 1 \\ &&& 0 \leq x \leq 1 \\ &&& L(x) = L'_{\mathcal{G}} + a_{3\to4}a_{3\to4}^T \\ &&&\quad + \sum_{l=1}^{n} x_l(a_{i,1}a_{i,1}^T + a_{i,2}a_{i,2}^T) \\ &&& L'_{\mathcal{G}} = \begin{bmatrix} L_{\mathcal{G}} & \mathbf{0}_{n\times3} \\ \mathbf{0}_{3\times n} & \mathbf{0}_{3\times3} \end{bmatrix}.\end{aligned} \tag{8.16}$$

Lastly, we give a performance bound on the Gramian analogous to Theorem 25.

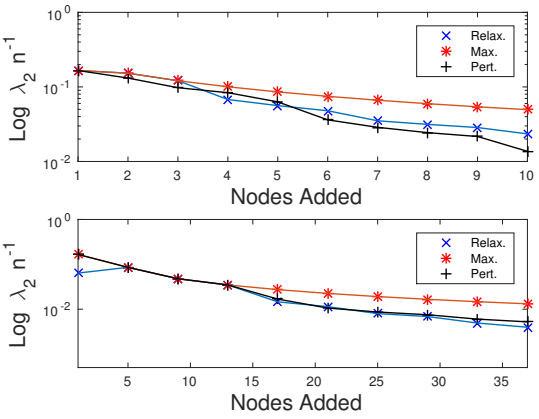

Figure 8.6: Max-λ_2 algorithm results for adding leaves (top) and path clusters (bottom), using the convex relaxation ($\times$), exhaustive search ($*$) and perturbation heuristic ($+$).

Theorem 26. *Consider the task of attaching a single node to the system with $n \times n$ Laplacian L to maximize λ_2, as denoted in Problem (8.15). Let L' be the subsequent Laplacian, and so $P = \frac{1}{2}L'[2:n+3]^{-1}$. Then, $\mathrm{Tr}P \geq C + 4$, where C is a constant depending only on L.*

Proof.

$$\begin{aligned}\mathrm{Tr}(P) &= \mathrm{Tr}(L'[2:n+3]^{-1}) \\ &\geq \mathrm{Tr}(L'[2:n]^{-1}) + \mathrm{Tr}(L'[n+1:n+3]^{-1}) \\ &= \mathrm{Tr}([L[2:n] + 2e_i e_i^T]^{-1}) + 4 \geq C + 4,\end{aligned}$$

where i is the index of the attachment node chosen, and $C = \min_i(\mathrm{Tr}([L[2:n] + 2e_i e_i^T]^{-1}))$ is a constant depending only on L. □

8.3 ALGORITHM IMPLEMENTATION

In this section, we show examples of the optimization problems discussed in the previous section.

The optimization problems (8.13) and (8.15) were implemented using CVX [113], [114]. An additional relaxation method used to solve problems (8.14) and (8.15) discussed in [65], known as the *perturbation heuristic*, was also implemented for the purposes of comparison. The perturbation heuristic works by considering the eigenvector v of L' corresponding to λ_2. At each iteration of the algorithm, the node cluster is attached to a single node in the graph. The attachment point is chosen by selecting the node with the largest value of $(v_i - v_{n+1})^2$ over all $i \in [n]$. Here, v_{n+1} is the entry of v corresponding to the node in the cluster attaching the cluster to the node i.

If there is more than one node attaching the cluster to the node in the graph (for example, the leaf and path addition displayed in Figure 8.2), then without loss of generality, denote these (say, l) nodes as $n+1, \ldots, n+l$. Then, the perturbation heuristic is to find the node $i \in [n]$ maximizing $\sum_{j=1}^{l}(v_i - v_{n+j})^2$ at each iteration.

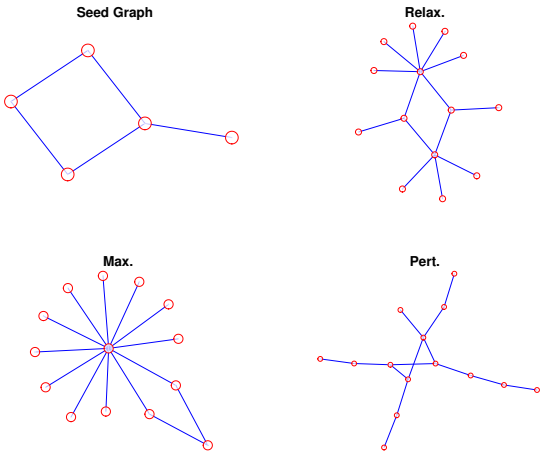

Figure 8.7: Seed graph, and final graph after 9 iterations of the leaf-adding problem using the SDP relaxation (8.14), exhaustive search over problem (8.13) and the perturbation heuristic.

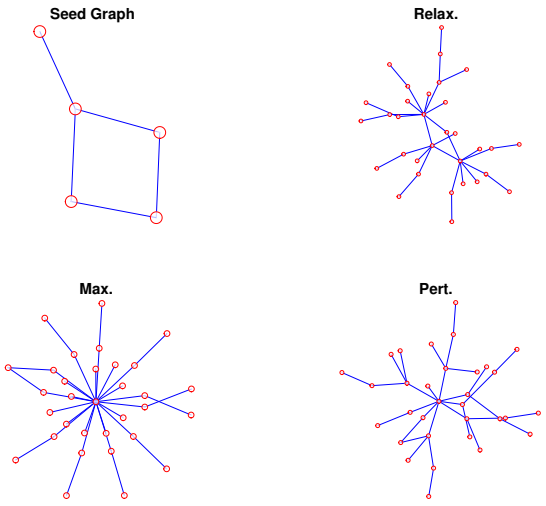

Figure 8.8: Seed graph, and final graph after 9 iterations of the path-cluster-adding problem using the SDP relaxation (8.16), exhaustive search over problem (8.15) and the perturbation heuristic.

The results of running these algorithms for 9 iterations are shown in Figures 8.6,8.7, and 8.8. The seed graphs, and final graphs after 9 iterations for each of the three techniques (exhaustive search, convex relaxation and perturbation heuristic) are shown in Figure 8.7 for adding a single leaf, and in Figure 8.8 for adding the path cluster. For both cases, the convex relaxations (problems (8.14) and (8.16)) perform reasonably well and pick out slightly suboptimal solutions, as seen in Figure 8.6. The perturbation heuristic performs worse than the convex relaxation for adding the leaves, but performs just as well for adding the path cluster despite yielding a different final graph as seen in Figure 8.8.

9

MATRIX-WEIGHTED GRAPHS

Next, we discuss consensus over vector-valued states, as well as consensus with different time scales. This requires the notion of *matrix-weighted graphs*.

This section considers dynamics governed by the interconnections of multi-rate, single integrator agents connected over connected, weighted communication graphs. Every agent has a vector-valued state $x \in \mathbb{R}^k$. In this formulation, we can consider a graph object defined by $\mathcal{G} = (\mathcal{V}, \mathcal{E}, \mathcal{W}, \mathcal{T})$, where $\mathcal{V}$ is the set of agents (nodes), $\mathcal{E}$ is the set of edges, $\mathcal{W}$ is a set of edge weights, and $\mathcal{T}$ a set of time scaling factors for each agent's state. This setup is expanded below.

Individual agents will be indexed by subscripts, e.g. $v_i \in \mathcal{V}$ to represent the i^{th} agent where $1 \leq i \leq |\mathcal{V}|$. If $(i,j) \in \mathcal{E}$, the i^{th} and j^{th} agents are connected by an edge ($i \sim j$), and they are referred to as adjacent agents. For a given agent, i, $N(i) = \{j \mid i \sim j \; \forall j \in \mathcal{V}\}$ denotes the neighbors of i, and $\deg(v_i) = |N(i)|$ denotes the unweighted degree of i.

Since we are considering vector-valued agent states, edges between agents are matrix-valued. This allows for a generalized notion of dynamical coupling between neighbouring agent states. Such matrix-valued weights will be denoted $W_e \in \mathcal{S}^k_{++}$, and so $\mathcal{W} = \{W_e \mid e \in \mathcal{E}\}$. The edge set can be ordered by a mapping, $\kappa(\cdot)$, such that $l = \kappa(ij)$ if and only if $(i,j) \in \mathcal{E}$. By this mapping, we can denote the weight on edge $\kappa(ij)$ by W_l or W_{ij}, interchangeably. Furthermore, we also assume that each individual state of each node can run on a separate timescale. Thus, for each node i and set of corresponding time scales $T_i = \{\epsilon_{i,1}, \ldots, \epsilon_{i,k}\} \in \mathcal{T}$, we associate the *time scale matrix* $E_i = \operatorname{diag}(\epsilon_{i,1}, \ldots, \epsilon_{i,k}) \in \mathcal{S}^k_+$. Note that the positive-definiteness of E_i is equivalent to requiring that each $\epsilon_{i,k} > 0$.

Next, we define some algebraic graph-theoretic objects.

The *incidence matrix* $D(\mathcal{G})$ is a $|\mathcal{N}| \times |\mathcal{E}|$ matrix where the rows are indexed by the nodes, and the columns are indexed by the edges of $\mathcal{G}$. Denote each column of $D(\mathcal{G})$ corresponding to edge $\{i,j\}$ by a_{ij}. For each edge $l := \{i,j\}$, where i is the tail and j is the head, $D(\mathcal{G})_{il} = 1$ and $D(\mathcal{G})_{jl} = -1$. If $\mathcal{G}$ is undirected, by convention we write that $D(\mathcal{G})_{il} = 1$ and $D(\mathcal{G})_{jl} = -1$ for $i > j$. Since we are dealing with matrix-valued weights, for defining the graph Laplacian below, we need the matrices $\mathbf{D}(\mathcal{G}) \triangleq D(\mathcal{G}) \otimes I_k$ and $\mathbf{a}_{ij} \triangleq a_{ij} \otimes I_k$, where I_k is the $k \times k$ identity matrix, and $\otimes$ denotes the Kronecker product. The *weight matrix* $\mathbf{W}$ is a $k|\mathcal{E}| \times k|\mathcal{E}|$ blockwise diagonal matrix containing the weights W_{ij} of each edge e.

The *graph Laplacian* $\mathcal{L}_\mathcal{G}$ of an undirected graph $\mathcal{G}$ can equivalently be defined by the incidence and weight matrix as $\mathcal{L}_\mathcal{G} \triangleq \mathbf{D}(\mathcal{G})\mathbf{W}\mathbf{D}(\mathcal{G})^T = \sum_{ij \in \mathcal{E}} \mathbf{a}_{ij} W_{ij} \mathbf{a}_{ij}^T$, and blockwise with the $k \times k$ block whose rows are associ-

ated with the ith node and whose columns are associated with the jth node given by

$$\begin{cases} \sum_{j\in\mathcal{N}_i} W_{ij} & i = j \\ -W_{ij} & ij \in \mathcal{E} \\ \mathbf{0}_{k\times k} & ij \notin \mathcal{E}. \end{cases}$$

Finally, a short aside on the terminology in this chapter, as the combination of scaling and weightings can become cumbersome at times. A *weighted* graph refers to a non-negative weighting on the edges of the graph. Matrices (such as the Laplacian) corresponding to weighted graphs will be denoted with w subscripts to differentiate them from an unweighted graph on the same topology. A *scaled* graph refers to a positive scaling on the nodes of the graph. The terminology is derived from the interpretation of the scaling parameters as indicators of the relative time scaling on the individual node dynamics, but they can equivalently be interpreted as a nodal weighting. Matrices associated with scaled graphs will be denoted with a tilde, and graphs with unity scaling on all states of nodes will be referred to as "mono-scale" graphs. In the course of our formulation, these descriptors may "stack" in certain scenarios, that is, we may consider scaled, weighted graphs in the most general cases.

We will also use some additional terminology from combinatorics and graph theory. A *tree* is a connected graph with no cycles, and a *leaf* is designated as a node of degree 1. A *binary tree* is a tree where one node is designated as the *root*, and all nodes of $\mathcal{T}$ are either leaves or *parents*. Each parent in a binary tree can have at most two *children* and one parent, except the root which has no parents. The *height* h of a binary tree is the length of the longest path from the root to a leaf. A *complete* (sometimes called *full*) binary tree is one where each node has either zero or two children.

Finally, the *parallel addition* of two symmetric matrices A, B is defined as $A : B \triangleq A(A+B)^{\dagger}B$; when A, B are nonzero scalars this reduces to the familiar formula of adding two resistances in parallel.

9.1 LEADER-FOLLOWER CONSENSUS NETWORK MODELS

In this chapter, we examine the leader-follower consensus problem on matrix-valued weighted series-parallel networks. Consider a connected weighted graph $\mathcal{G} = (\mathcal{N}, \mathcal{E}, \mathcal{W})$ with the Laplacian $\mathcal{L}_{\mathcal{G}}$. Each node i has a state $x_i \in \mathbb{R}^k$. Denote a set of *leaders* $\mathcal{R} \subset \mathcal{N}$ and a set of *followers* $\mathcal{N} \setminus \mathcal{R}$. Suppose that one is able to take over the state $x_i \in \mathbb{R}^k$ of a leader, and thereby exert control over the followers. Further, suppose that each leader is connected to a unique node in $\mathcal{N} \setminus \mathcal{R}$, that collectively will be called the *source* nodes and designated as the set R (see Figure 9.1 for a schematic of the setup). Then, using $\mathbf{B} := B \otimes I_k$, the graph Laplacian of $\mathcal{G}$ can be partitioned as,

$$\mathcal{L}_{\mathcal{G}} = \left[\begin{array}{c|c} \mathcal{L}_{\mathcal{R}} & -W_{\mathcal{R}}\mathbf{B} \\ \hline -\mathbf{B}^T W_{\mathcal{R}} & \mathcal{L}_{\mathcal{G}(\mathcal{N}\setminus\mathcal{R})} + \sum_{i\in R} \mathbf{e}_i W_i \mathbf{e}_i^T \end{array}\right], \tag{9.1}$$

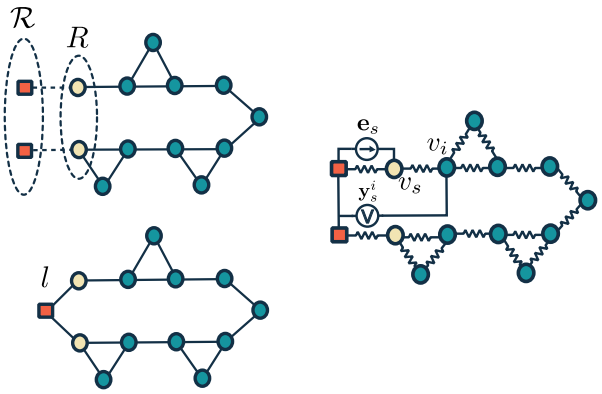

Figure 9.1: **Top**: leader-follower network setup. **Right**: electrical "grounding" of the leader set $\mathcal{R}$, and current vector $\mathbf{e}_s = e_s \otimes I_k$ injected into the network via node v_s; $\mathbf{y}_s^i$ is the voltage dropped from v_i to $\mathcal{R}$. **Bottom**: Identification of grounded leader set into a single node.

where $W_{\mathcal{R}}$ is a block-diagonal matrix containing the matrix-valued weights of the edges connecting $\mathcal{R}$ to R and $\mathbf{e}_i \triangleq e_i \otimes I_k$. Suppose that we can observe the full state of individual follower nodes. Thereby, the control and observation matrices are given by $B^T = [e_{i_1} \ \dots \ e_{i_m}]$ and $C = [e_{j_1} \ \dots \ e_{j_o}]$, where $R = \{i_1, \dots, i_m\}$ are the nodes attached to leaders, and $\{j_1, \dots, j_o\}$ are the nodes under observation.[1] Next, recall that one can write the graph Laplacian in terms of the incidence and weight matrices as

$$\begin{aligned}\mathcal{L}_{\mathcal{G}(\mathcal{N}\setminus\mathcal{R})} &= \mathbf{E}_{\mathcal{N}\setminus\mathcal{R}}\mathbf{W}\mathbf{E}_{\mathcal{N}\setminus\mathcal{R}}^T \\ &= \sum_{\{i,j\}\in\mathcal{E}(\mathcal{N}\setminus\mathcal{R})} \mathbf{a}_{ij} W_{ij} \mathbf{a}_{ij}^T,\end{aligned}$$

where $\mathbf{E}_{\mathcal{N}\setminus\mathcal{R}} = E_{\mathcal{N}\setminus\mathcal{R}} \otimes I_k$ and $E_{\mathcal{N}\setminus\mathcal{R}}$ is the result of removing the rows from E corresponding to the nodes in the leader set $\mathcal{R}$. The matrix $\mathbf{W}$ denotes the matrix consisting of W_e on the block-diagonal, denoted Blkdiag$[W_e]$. The corresponding leader-follower consensus dynamics are now given by,

$$\begin{aligned}\dot{\mathbf{x}} &= -\left(\mathcal{L}_{\mathcal{G}(\mathcal{N}\setminus\mathcal{R})} + \sum_{i\in R} \mathbf{e}_i W_i \mathbf{e}_i^T\right)\mathbf{x} + \mathbf{B}^T u \\ \tilde{y} &= \mathbf{C}\mathbf{x},\end{aligned}$$

where $\mathbf{C} = C \otimes I_k$, $\mathbf{x}$ is the vector containing the stacked states of the nodes, and u is the stacked vector of the leader node states–the control inputs to the followers. We note that the matrix $A \triangleq (\mathcal{L}_{\mathcal{G}(\mathcal{N}\setminus\mathcal{R})} + \sum_{i\in R} \mathbf{e}_i W_i \mathbf{e}_i^T)$ is positive definite if the underlying graph is connected.

We now introduce the paradigm of *series-parallel networks*, and how they can be utilized for the leader-follower consensus model. Building on connections to electrical networks and tools from the literature on series-parallel networks, we then proceed to show how one can–rather efficiently–compute

1 Note that the form of these matrices assumes that each leader is attached to a single, unique follower.

the $\mathcal{H}_2$ norm of leader-follower consensus, as well as devising efficient network-reweighting algorithms for this class of networks.

9.1.1 *Electrical Networks*

An insightful perspective on consensus comes from viewing the underlying graph as a resistive network [66], [115]. In the leader-follower setup, consider the graph $\mathcal{G} = (\mathcal{N}, \mathcal{E}, \mathcal{W})$ with scalar weights. For each edge $\{i, j\} \in \mathcal{E}$, consider placing a resistor between nodes i and j with conductance w_{ij} (resistance w_{ij}^{-1}). Then, the *effective resistance* between arbitrary nodes $k, l \in \mathcal{N}$ is given by

$$R_{kl} = (e_k - e_l)\mathcal{L}_{\mathcal{G}}{}^{\dagger}(e_k - e_l), \tag{9.2}$$

where $\mathcal{L}_{\mathcal{G}}{}^{\dagger}$ denotes the pseudoinverse of $\mathcal{L}_{\mathcal{G}}$.

Another perspective on effective resistance is the following. Consider 'grounding' all the leader nodes $r \in \mathcal{R}$, i.e., identifying them as one node, or electrically connecting them together by wires. Then, the diagonal entries of the matrix

$$\begin{aligned} A^{-1} &= \mathcal{L}_{\mathcal{G}(\mathcal{N}\setminus\mathcal{R})} + \sum_{i\in R} w_i e_i e_i^T \\ &= \left(\sum_{\{i,j\}\in\mathcal{E}} w_{ij} a_{ij} a_{ij}^T + \sum_{i\in R} e_i e_i^T \right)^{-1}, \end{aligned}$$

yield the effective resistances between the ith node in $\mathcal{N} \setminus \mathcal{R}$ to the leader node set, i.e., $[A^{-1}]_{ii}$ is the effective resistance from i to $\mathcal{R}$. If $x \in \mathbb{R}^{|\mathcal{N}|}$ denotes a vector of currents injected into nodes $\mathcal{N} \setminus \mathcal{R}$ from $\mathcal{R}$, then the quantity $[A^{-1}x]_i$ is the *voltage drop* from node v_i to the grounded leader node set. If $x = e_s$, then this corresponds to a 1 Amp current injected into the node $v_s \in R$; see Figure 9.1 for a schematic of this setup. In this case, we write $y_i^s \triangleq [A^{-1}e_s]_i$ as the voltage drop of node i; this quantity is used subsequently in the chapter.

One can generalize this electrical network interpretation to matrix-value weights [115]. Consider placing a *matrix-value resistor* on each edge ij with matrix-valued conductance W_{ij}. Such a construct is similar to that of an n-port network [116]. Then, the ith $k \times k$ block on the diagonal of the matrix,

$$\begin{aligned} A^{-1} &= \mathcal{L}_{\mathcal{G}(\mathcal{N}\setminus\mathcal{R})} + \sum_{i\in R} \mathbf{e}_i W_i \mathbf{e}_i^T \\ &= \left(\sum_{\{i,j\}\in\mathcal{E}} \mathbf{a}_{ij} W_{ij} \mathbf{a}_{ij}^T + \sum_{i\in R} \mathbf{e}_i W_i \mathbf{e}_i^T \right)^{-1} \end{aligned}$$

form the matrix-valued effective resistances from node $i \in \mathcal{N} \setminus \mathcal{R}$ to $\mathcal{R}$, denoted $R_u^{\text{eff}}(\mathcal{R})$. This generalization extends to other electrical quantities, such as power and current; one can obtain the following formalism from [115].

A *generalized current* from node u to v with *intensity* $\mathbf{i} \in \mathbb{R}^{k\times k}$ is an edge function $\mathbf{I} : \mathcal{E} \to \mathbb{R}^{k\times k}$ such that

$$\sum_{\substack{\{k,l\}\in\mathcal{E}\\ k=p}} \mathbf{I}_{\{k,l\}} - \sum_{\substack{\{l,k\}\in\mathcal{E}\\ k=p}} \mathbf{I}_{\{l,k\}} = \begin{cases} \mathbf{i} & p = u \\ -\mathbf{i} & p = v \\ \mathbf{0}_{k\times k} & \text{else} \end{cases} \quad \forall p \in \mathcal{N}$$

and there exists a node function $\mathbf{V} : \mathcal{N} \to \mathbb{R}^{k\times k}$ satisfying

$$R^{\text{eff}}_{\{u,v\}}\mathbf{I}_{\{u,v\}} = \mathbf{V}_u - \mathbf{V}_v, \quad \forall\{u,v\} \in \mathcal{E}.$$

In this setting, the *power* dissipated across an edge with a matrix weight R^{eff}_e and current $\mathbf{I}_e$ is given by the inner product,

$$P_e(i_e) = \operatorname{Tr}\left(\mathbf{I}_e^T R^{\text{eff}}_e \mathbf{I}_e\right).$$

In §9.2, we show that this notion of electrical power is consistent with adding matrix-valued resistances in series and parallel. We also note that when $x \in \mathbb{R}^{nk\times k}$ is a matrix of stacked $k \times k$ current matrices injected into n nodes of $\mathcal{G}$, then the matrix $A^{-1}x$ is the stacked matrix of the voltage drops from each node to the grounded leader node set. In particular, the sth $k\times k$ block of $A^{-1}x$ is denoted $\text{Blk}^{k\times k}_s[A^{-1}x]$, and if $x = (e_s \otimes I_k) = \mathbf{e}_s$, then this corresponds to a current of identity intensity injected into node s; again, this setup is shown in Figure 9.1.

Finally, we denote the quantity

$$\mathbf{Y}^s_i = \text{Blk}^{k\times k}_i[A^{-1}\mathbf{e}_s],$$

as the voltage drop from node i to $\mathcal{R}$ under identity current injected into node s; this reduces to the corresponding scalar definition when $k = 1$.

As a final remark, there is also an equivalent formulation of (9.2) in the case of matrix-valued resistances.

Proposition 1. *Let $\mathcal{G}(\mathcal{N}, \mathcal{E}, \mathcal{W})$ be a graph with matrix-valued weights. Consider the leader-follower setup in §9.1, with graph Laplacian $\mathcal{L}_\mathcal{G} = \mathbf{E}\mathbf{W}\mathbf{E}^T$. Then, the matrix-valued effective resistance between nodes i and j is given by*

$$\begin{aligned} R^{\text{eff}}_i(j) &= (e_i \otimes I_k - e_j \otimes I_k)^T \mathcal{L}_\mathcal{G}{}^\dagger (e_i \otimes I_k - e_j \otimes I_k) \\ &= (\mathbf{e}_i - \mathbf{e}_j)^T \mathcal{L}_\mathcal{G}{}^\dagger (\mathbf{e}_i - \mathbf{e}_j). \end{aligned}$$

In subsequent sections, we introduce series-parallel graphs. In particular, we show how y^s_i, and its matrix-valued generalization $\mathbf{Y}^s_i$, can be computed efficiently over series-parallel graphs, and how it is related to the $\mathcal{H}_2$ norm. We will then proceed to show how this setup can be utilized to provide a reweighting algorithm that results in optimal $\mathcal{H}_2$ performance of the leader-follower consensus network.

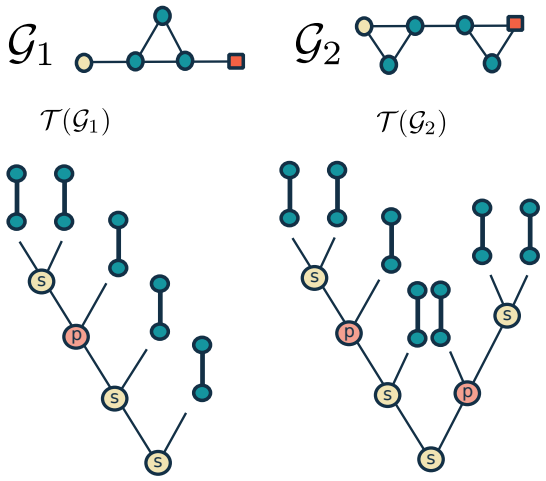

Figure 9.2: Decomposition trees of two graphs.

9.1.2 *Series-Parallel Networks*

In this chapter, we consider the class of graphs known as *series-parallel graphs*. This class has a number of interesting properties that can be utilized for their system-theoretic analysis. Given a series-parallel graph there exist rather efficient ($O(|\mathcal{N}| + |\mathcal{E}|)$, $O(\log|\mathcal{N}|)$ and $O(\log^2|\mathcal{N}|)$) algorithms that decompose the graph into atomic structures and simple composition operations on them [100], [101], [117]. This decomposition in turn facilitates efficient solutions to problems that are otherwise NP-hard on general classes of graphs, such as finding the minimum dominating set of a graph, maximum matchings and independent sets, and the maximum disjoint triangle problem [102], [118], [119].

Definition 3 (Two-Terminal Series-Parallel Graphs). *A directed acyclic graph is called* two-terminal series-parallel TTSP *if it can be defined recursively as follows:*

1. *The graph defined by two vertices connected by an edge (a* 1-path*) is a TTSP graph.*
2. *If $\mathcal{G}_1 = (\mathcal{N}_1, \mathcal{E}_1)$ and $\mathcal{G}_2 = (\mathcal{N}_2, \mathcal{E}_2)$ are TTSP where $\mathcal{S}_i = \{s_i\}, \mathcal{T}_i = \{t_i\}$ are the unique source and sink of $\mathcal{G}_i$, then the following operations produce TTSP graphs:*
   a) ***Parallel Addition**: $\mathcal{G}_p \leftarrow s_1 \sim s_2,\ t_1 \sim t_2$.*
   b) ***Series Addition**: $\mathcal{G}_s \leftarrow t_1 \sim s_2$.*

Denote the parallel join of $\mathcal{G}_1$ and $\mathcal{G}_2$ as $\mathcal{G}_1 \oslash \mathcal{G}_2$, and the corresponding series join as $\mathcal{G}_1 \odot \mathcal{G}_2$.

The two recursive operations defining the TTSP graph model allow for a simple constructive approach for defining graphs from atomic elements. Indeed, efficient algorithms exist that decompose TTSP graphs into a *decomposition tree* with the following structure [100], [101], [117].

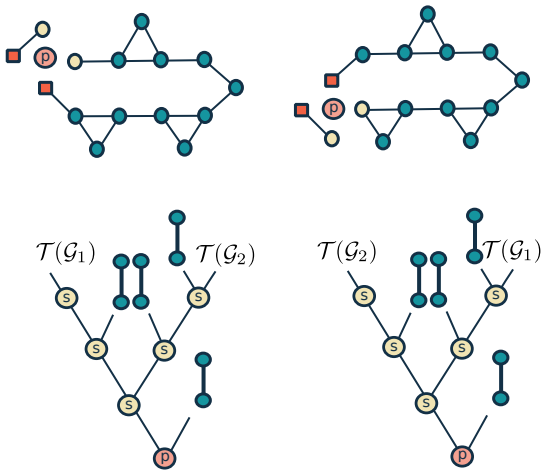

Figure 9.3: Decomposition trees of the all-input TTSP in Figure 9.5

Definition 4 (TTSP Decomposition Tree). *A* TTSP decomposition tree *of a TTSP graph $\mathcal{G}$ is a binary tree $\mathcal{T}(\mathcal{G})$ with the following properties:*

1. *$\mathcal{T}$ is a complete[2] binary tree, in that every node has either 2 or 0 children.*
2. *Every leaf of $\mathcal{T}$ corresponds to a 1-path.*
3. *Every parent of $\mathcal{T}$ corresponds to either a series or parallel addition operation from Definition 3 on its children.*

Remark 6. *In general, one can ignore the assumption of directed edges in Definition 3 and consider undirected TTSP graphs, see [101]. We consider undirected graphs (with symmetric Laplacians) in this chapter, as the notions of effective resistance require undirected graphs.*

Examples of TTSP graphs and their decomposition trees are shown in Figure 9.2. The graph is constructed by a reverse breadth-first-search: the deepest leaves combine with each other by the series or parallel join designated by their parent. At each layer of the decomposition tree, each operation can be performed independently of the other nodes in the layer. This means that the complexity of the reconstruction operation is limited by the height of the decomposition tree; it is this key insight that allows the efficient computation of system-theoretic measures in the remainder of the chapter.

In the following proposition, we quantify the height of the tree in terms of the size of the resulting graph.

Proposition 2 (Properties of $\mathcal{T}(\mathcal{G})$). *Let $\mathcal{G}$ be a TTSP graph with N nodes constructed from l 1-paths with p parallel joins and s series joins. Then,*

1. *$\mathcal{G}$ has $N = 2l - 2p - s$ nodes and $E = l$ edges.*
2. *The decomposition tree $\mathcal{T}(\mathcal{G})$ of $\mathcal{G}$ has $n = 2l - 1$ nodes.*

2 Some works refer to such a tree as *full*.

3. The height h of $\mathcal{T}(\mathcal{G})$ is bounded by

$$\log_2(N + 2p - s) \leq h \leq \frac{N + 2p + s}{2} - 2 \tag{9.3}$$

$$\log_2(E) \leq h \leq E - 1. \tag{9.4}$$

Proof. By definition, $\mathcal{T}(\mathcal{G})$ is a complete binary tree, meaning that each parent has either 2 or 0 children. If it has zero children, it is a leaf and therefore corresponds to a 1-path added to $\mathcal{G}$. Each leaf thus adds one edge to $\mathcal{G}$, and since series and parallel joins do not delete edges, it follows that $E \triangleq |\mathcal{E}| = l$.

Each leaf also adds two nodes to $\mathcal{G}$, but each series join identifies a pair of nodes, and each parallel join identifies two pairs of nodes, thus removing one and two nodes from $\mathcal{G}$ respectively. Hence,

$$N \triangleq |\mathcal{N}| = 2l - 2p - s. \tag{9.5}$$

It is well-known that a complete binary tree has $n = 2l - 1$ nodes. Using (9.5), it follows that

$$n = N + 2p + s - 1. \tag{9.6}$$

Furthermore, the number of nodes n of $\mathcal{T}(\mathcal{G})$ is bounded by its height by the relation $2h + 1 \leq n \leq 2^{h+1} - 1$, leading to

$$\log_2(n + 1) - 1 \leq h \leq \frac{n - 1}{2}. \tag{9.7}$$

Substituting (9.6) into the inequality (9.7) yields (9.3), and substituting $l = 2^{-1}(n + 1)$ into the inequality (9.7) yields the bounds in (9.4).

□

9.2 SYSTEM-THEORETIC ANALYSIS ON SERIES-PARALLEL GRAPHS

In this section, we examine how series-parallel graphs can be used to simplify 'hard' computational problems on networks by exploiting the structure of the decomposition tree. The basic ideas is that although some quantities are difficult to compute over the entire graph, they may be easy to compute over small "atomic" graphs (i.e., 1-paths or other atomic elements), and the quantities may propagate across simple graph compositions (i.e., series or parallel connections) by a recursive relation.[3] Given a decomposition tree, these quantities may in fact be computable in parallel in $O(h)$ time. We give an intuitive example here that directly relates to the $\mathcal{H}_2$ norm computation.

A natural use for series-parallel graphs is in electrical networks, as resistances add over a series connection of resistors, and conductances add over a parallel connection. Naïve methods for computing the effective resistances over general graphs can be expensive, such as the pseudoinverse-based formula in (9.2) which has complexity $O(|\mathcal{N}|^\omega)$ [120].

Recall that one can construct the tree by moving up the tree in a reverse breadth-first-search order and joining the graphs at each leaf via the opera-

3 Which is essentially a spatial dynamic programming.

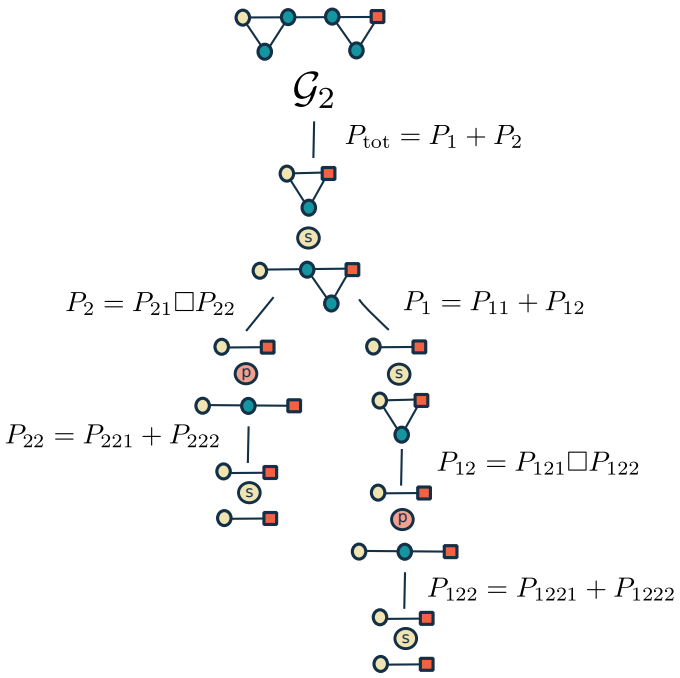

Figure 9.4: Nested infimal convolution/sum computations over a series-parallel graph. Beige circles (always on the left) denote sources, red squares (always on the right) denote sinks at each step.

tion prescribed by their parent. Similarly, given a TTSP network of resistors (edges with *scalar* weights corresponding to conductances) and its decomposition tree, one can start at the leaves (corresponding to 1-paths, i.e., individual resistors), and either add resistances together (if the join is series), or add their reciprocals (if the join is parallel). Hence, by performing this computation up the tree to the root, one yields the effective resistance across the TTSP graph from source to sink.

This is not the only useful electrical computation one can do on a TTSP graph. Suppose that a current is applied across the TTSP graph, from source to sink. Given measurements of currents across the resistors, it is possible to compute the total power dissipated across the graph without computing the effective resistance. Over a series connection of resistors R_1, R_2, the power dissipated is additive: $P_s = P_1 + P_2 = i^2(R_1 + R_2)$. Over a parallel connection of resistors, the total power dissipated is minimized over the resistors, subject to the conservation of current:

$$P_p(i) = \begin{array}{ll} \min & i_1^2 R_1 + i_2^2 R_2 \\ \text{s.t.} & i_1 + i_2 = i \end{array} \triangleq P_1 \square P_2;$$

the operation $P_1 \square P_2$ denotes the *infimal convolution*; an example of the power computation over a TTSP graph is shown in Figure 9.4.

In the case of matrix-valued edge weights, there is a natural generalization of the infimal convolution of powers for both vector-valued and matrix-valued currents. The key insight is in realizing that power is essentially an inner product-induced norm – for a vector-valued current $i \in \mathbb{R}^k$ across

a matrix-valued resistor R, $P = \langle i, Ri \rangle$, which reduces to $P = i^2 R$ when $k = 1$. Similarly, when we have a matrix-valued current $\mathbf{I} \in \mathbb{R}^{k \times k}$, as in §9.1.1, $P(\mathbf{I}) = \mathrm{Tr}(\mathbf{I}^T R \mathbf{I})$.

Proposition 3. *Let R_1 and R_2 denote two-matrix valued resistances in $\mathcal{S}^k_{++}$, and consider current $\mathbf{I} \in \mathbb{R}^{k \times k}$ across R_1 and R_2 in parallel. Then, the effective resistance across the join is given by*

$$R_{tot} = R_1 : R_2.$$

Proof. Recall that power with current i dissipates across a parallel join according to the infimal convolution

$$\begin{aligned} P_p(\mathbf{I}) = & \quad \min \quad \mathrm{Tr}(\mathbf{I}_1^T R_1 \mathbf{I}_1) + \mathrm{Tr}(\mathbf{I}_2^T R_2 \mathbf{I}_2) \\ & \quad \text{s.t.} \quad \mathbf{I}_1 + \mathbf{I}_2 = \mathbf{I} \\ & \triangleq (P_1 \square P_2)(\mathbf{I}). \end{aligned} \tag{9.8}$$

Applying the identity $(f \square g)^* = f^* + g^*$, where f^* denotes the Fenchel conjugate, to Problem (9.8) yields the minimum $P_p(\mathbf{I}) = \mathrm{Tr}(\mathbf{I}^T (R_1 : R_2)\mathbf{I})$. □

9.2.1 *Noise Rejection and Adaptive Weight Design*

Consider the leader-follower consensus dynamics setup from §9.1. In the scalar case (i.e., $k = 1$), the $\mathcal{H}_2$ performance of the system is characterized by the norm of the transfer matrix, and when all nodes are observed (i.e., $C = I$); it is given by [75],

$$\left(\mathcal{H}_2{}^{\mathcal{G},B}\right)^2 = \frac{1}{2}\mathrm{Tr}\left(B^T A^{-1} B\right).$$

In the case of matrix-valued edge weights, we have the following proposition.

Proposition 4. *Consider the leader-follower consensus dynamics setup for arbitrary $k \in \mathbb{Z}_{++}$. Suppose that all nodes are observed, i.e. $\mathbf{C} = C \otimes I_k = I \otimes I_k$. Then the $\mathcal{H}_2$ norm is given by*

$$\left(\mathcal{H}_2{}^{\mathcal{G},\mathbf{B}}\right) = \frac{1}{2}\mathrm{Tr}\left(\mathbf{B}^T A^{-1}(W)\mathbf{B}\right).$$

Proof. The $\mathcal{H}_2$ norm is given by $\mathrm{Tr}(\mathbf{B}^T P \mathbf{B})$, where P satisfies the Lyapunov equation

$$-A(W)P - PA(W)^T + \mathbf{C}^T\mathbf{C} = 0.$$

The ansatz $P = \frac{1}{2}A^{-1}(W)$ yields the solution. □

Consider the task of re-assigning positive weights to the edges of the network to minimize the $\mathcal{H}_2$ norm. This can be done via a gradient-descent method on the optimization problem,

$$\begin{aligned} \min \quad & \left(\mathcal{H}_2{}^{\mathcal{G},\mathbf{B}}\right)^2 = \tfrac{1}{2}\mathrm{Tr}\left(\mathbf{B}^T A(W)^{-1}\mathbf{B}\right) \\ \text{s.t.} \quad & W := \mathrm{Blkdiag}(W_e) \\ & W_e \in \mathcal{S}_{++}^{k\times k},\ \forall e \in \mathcal{E} \\ & U_e \succeq W_e \succeq L_e,\ \forall e \in \mathcal{E},\ L_e, P_e \in \mathcal{S}_{++}^{k\times k}. \end{aligned} \tag{9.9}$$

Remark 7. *In the unconstrained case of Problem (9.9) (i.e., the edge weights W_e are still positive-definite, but have no upper and lower bounds), the weights in the graph become can become unbounded in that an arbitrarily large weight W_e (in the sense of the Loewner order on W_e) close to an input node can make the $\mathcal{H}_2$ norm arbitrarily small. Hence, it is necessary to include bounds on the matrix weights; this also has the benefit of not allowing the edges to become effectively disconnected. Furthermore, this also motivates the modification of the cost function to include a penalty term $\frac{1}{2}h\sum_{e\in\mathcal{E}}\|W_e\|^2$ for some matrix norm $\|\cdot\|$ in order to reduce the large-weight blowup.*

The optimization problem (9.9) has several key features, highlighted in the following proposition.

Proposition 5. *Consider the setting of Problem (9.9). Then,*

1. *The objective function $\frac{1}{2}\mathrm{Tr}\left(\mathbf{B}^T A(W)^{-1}\mathbf{B}\right)$ is strongly convex on the cone of positive-definite matrices $W_e \in \mathcal{S}_{++}^k$.*
2. *The gradient of the objective function with respect to a single edge weight W_e at a point $H \in \mathcal{S}_{++}^k$ is given by $\nabla f_{W_e}[H] = -\frac{1}{2}Q^T Q$, where $Q = \mathbf{A}_f^T A^{-1}\mathbf{e}_s$, and so*

$$\nabla f_{W_e}[H] = -\frac{1}{2}\sum_{s\in\mathcal{R}}\left(\mathbf{Y}_i^s - \mathbf{Y}_j^s\right)^T\left(\mathbf{Y}_i^s - \mathbf{Y}_j^s\right), \tag{9.10}$$

where $\mathbf{Y}_i^s = \mathrm{Blk}_i^{k\times k}\left[A^{-1}\left(e_s \otimes I_k\right)\right]$, and A^{-1} is evaluated with H in place of W_e.

The proof is left to the appendix.

We can solve Problem (9.9) using a projected gradient descent algorithm:

$$x_{k+1} = \mathrm{Proj}_C\left(x_k + \frac{1}{h\sqrt{k}}\nabla_x f(x_k)\right),$$

where C is the cone generated by the constraints of Problem (9.9).

Following Remark 7, let us include a Frobenius norm penalty on the edge weights in the cost:

$$f(W) = \frac{1}{2}\mathrm{Tr}\left[\mathbf{B}^T A^{-1}\mathbf{B}\right] + \frac{h}{2}\sum_{e\in\mathcal{E}}\mathrm{Tr}\left(W_e^T W_e\right)^2.$$

The gradient of the penalty term with respect to W_e is simply hW_e, so each edge in the network updates its weight according to the dynamics given by the gradient update

$$W_{\{i,j\}}^{t+1} = \mathrm{Proj}_C \left[\left(1 - \frac{1}{\sqrt{t}}\right) W_{\{i,j\}}^t + \frac{1}{\sqrt{t}} \nabla f_{W_{\{i,j\}}}[W_{\{i,j\}}^t] \right]. \tag{9.11}$$

A centralized algorithm and a decentralized conjugate gradient algorithm for solving Problem (9.9) in the scalar edge weight case were presented in [75]. For scalar edge weights, the natural efficient projection onto the constraint set is via the $\|\cdot\|_\infty$ norm, as this consists of at most two comparisons and a copy operation per edge weight in each step of the dynamics (9.11) at time t. In the case of matrix edge weights, there is no such natural efficient projection. Instead, at each step one solves the problem

$$\mathrm{Proj}_C(X) = \min_{Y \in C \cap \mathcal{S}_{++}^n} \|Y - X\|$$

for some matrix norm $\|\cdot\|$. However, we assume that k is relatively small compared to the size of the overall network $\|\mathcal{E}\|$, and so this operation is not the most computationally expensive part of the setup.[4]

The main computational hurdle in solving Problem (9.9) is the computation of the gradient in (9.10), as it requires computing the voltage drops $\mathbf{Y}_i^s, \mathbf{Y}_j^s$ for each edge $\{i,j\} \in \mathcal{E}$. For the scalar case $k = 1$, the conjugate gradient algorithm is able to compute $y_i^s = [A(W)^{-1} e_s]_i$ in linear time (in $|\mathcal{N}|$ steps) for each edge [75]; the case of matrix-valued resistances has not been analyzed in previous work, and we do so here.

We now present a decentralized algorithm for computing this quantity on a certain class of two-terminal series-parallel graphs, and a characterization of its complexity. In this setup, for every input node $s \in R$, the graph is a TTSP with s as the sink, and a node representing the grounded leader set as the source.

Definition 5 (All-Input TTSP Graphs). *Consider a graph $\mathcal{G}$ in the setup of the leader-follower consensus dynamics. Identify each leader node $i_1, i_2, \ldots, i_r \in \mathcal{R}$ as one node l connected to all source nodes $s \in R$. The graph $\mathcal{G}$ is called an* all-input two-terminal series-parallel graph *if, for all source nodes $s \in R$, $\mathcal{G}$ is TTSP with s as the source and l as the sink.*

See Figure 9.5 for an example of an all-input TTSP graph.

Informally, the efficient algorithm that we will present subsequently proceeds as follows. For each source node s, the algorithm utilizes the decomposition tree of $\mathcal{G}$ with s as the source and the grounded leader set as the sink; this is why $\mathcal{G}$ needs to be TTSP with respect to all source nodes. The voltage drop can then be computed from resistances and currents across each join, and the currents can be extracted from the power dissipated across each

4 For example, in formation control one may desire to use consensus on position and velocity, so $k \leq 6$ depending on whether the formation is planar or 3D.

join. Hence, the effective resistances are computed first, as in Algorithm 4:

Algorithm 4: Effective Resistance over TTSP Graph

Input: Decomposition tree $\mathcal{T}(\mathcal{G})$
Edge weights $\mathcal{W}(\mathcal{G})$
Result: Effective resistances $\rho(\mathcal{G})$ over $\mathcal{T}(\mathcal{G})$
for *each leaf of* $\mathcal{T}(\mathcal{G})$ **do**
  Output $R_{\text{eff}} = W_e^{-1}$ to parent;
end
for *each parent* j *of* $\mathcal{T}(\mathcal{G})$ **do**
  if *received* R_{eff_i} *from both children* $i = 1, 2$ **then**
    if j *is a series join* **then**
      Output $R_{\text{eff}} = R_{\text{eff}_1} + R_{\text{eff}_2}$ to parent;
    else
      Output $R_{\text{eff}} = R_{\text{eff}_1} : R_{\text{eff}_2}$ to parent;
    end
  else
    wait;
  end
end

Once the effective resistance of each branch at each join is known, starting from the root of the decomposition tree, the currents at each join can be extracted from the power computations. This computation is summarized in Algorithm 5, and depicted in Figure 9.4:

Algorithm 5: Branch Currents over TTSP Graph

Input: Decomposition tree $\mathcal{T}(\mathcal{G})$
Effective resistances $\rho(\mathcal{G})$
Result: Currents $\mathcal{I}(\mathcal{G})$ over $\mathcal{T}(\mathcal{G})$
for *each parent* j *of* $\mathcal{T}(\mathcal{G})$ **do**
  if j *is root* **then**
    if j *is a series join* **then**
      Output $\mathbf{I}_{\text{out}} = I_k$ to children;
    else
      Output $(\mathbf{I}_1, \mathbf{I}_2) = \arg P_1 \square P_2$ to children;
    end
  else if *received* $\mathbf{I}_{in}$ *from parent* **then**
    if j *is a series join* **then**
      Output $\mathbf{I}_{\text{out}} = \mathbf{I}_{\text{in}}$ to children;
    else
      Output $(\mathbf{I}_1, \mathbf{I}_2) = \arg P_1 \square P_2$ to children;
    end
  else
    wait;
  end
end

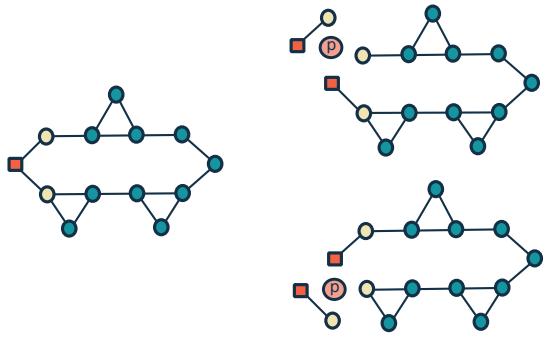

Figure 9.5: Left: An all-input TTSP graph. Right: Parallel joins across R to $\mathcal{R}$ used to compute $\mathbf{Y}_s^s$.

Lastly, once the currents through each join are known, the voltage drops over each branch are computed starting from the leaves of the decomposition tree, as seen in Algorithm 6.

Algorithm 6: Voltage Drops over TTSP Graph

Input: Decomposition tree $\mathcal{T}(\mathcal{G})$
Effective resistances $\rho(\mathcal{G})$ over $\mathcal{T}(\mathcal{G})$
Currents $\mathcal{I}(\mathcal{G})$ over $\mathcal{T}(\mathcal{G})$
Result: Voltage drops $\mathbf{Y}_i^s$ over $\mathcal{T}(\mathcal{G})$
for *each leaf of* $\mathcal{T}(\mathcal{G})$ **do**
  Output $\mathbf{V}_e = W_e^{-1}\mathbf{I}_e$ to parent;
end
for *each parent* j *of* $\mathcal{T}(\mathcal{G})$ **do**
  if *received* $\mathbf{V}_{e_i}$ *from both children* $i = 1, 2$ **then**
    if j *is a series join* **then**
      Output $\mathbf{V}_{\text{out}} = \mathbf{V}_{\text{in}_1} + \mathbf{V}_{\text{in}_2}$ to parent;
    else
      Output $\mathbf{V}_{\text{out}} = \mathbf{V}_{\text{in}_1} = \mathbf{V}_{\text{in}_2}$ to parent;
    end
  else
    wait;
  end
end

The computation of the voltage drops required for the gradient update scheme in (9.11) simply requires calling Algorithms 1,2 and 3 in succession for each $s \in \mathcal{R}$. We have the following result.

Theorem 27. *Consider the computation of the voltage drops* $\mathbf{Y}_i^s$ *in the gradient update scheme* (9.11). *The sub-algorithms have the following complexities:*

- *Algorithm 4: Best-case complexity of* $O(|\mathcal{R}|\log|\mathcal{N}|)$ *(worst-case complexity of* $O(|\mathcal{R}||\mathcal{N}|)$*) calls of a* $O(k^\omega)$ *matrix inversion.*
- *Algorithm 5: Best-case complexity of* $O(|\mathcal{R}|\log|\mathcal{N}|)$ *(worst-case complexity of* $O(|\mathcal{R}||\mathcal{N}|)$*) calls of a* $O(k^\omega)$ *matrix inversion.*
- *Algorithm 6: Best-case complexity of* $O(|\mathcal{R}|\log|\mathcal{N}|)$ *(worst-case complexity of* $O(|\mathcal{R}||\mathcal{N}|)$*).*

Proof. Algorithms 1,2 and 3 are computations done on a binary tree of height h, with each layer's computation done in parallel. Hence, the complexity is determined by h, which by Proposition 2 is $O(\log|\mathcal{N}|)$, and $O(|\mathcal{N}|)$ for best and worst-case, respectively. Each call of the three algorithms must be done $|\mathcal{R}|$ times. Algorithm 1 may perform an inversion of a $k \times k$ matrix, which has complexity $O(k^\omega)$. Algorithm 2 requires computing

$$\begin{aligned}(\mathbf{I}_1, \mathbf{I}_2) &= \arg P_1 \square P_2 \\ &= (R_{\text{eff}_1}^{-1}(R_{\text{eff}_1}^{-1} : R_{\text{eff}_2}^{-1})\mathbf{I}_{\text{in}}, R_{\text{eff}_2}^{-1}(R_{\text{eff}_1}^{-1} : R_{\text{eff}_2}^{-1})\mathbf{I}_{\text{in}}),\end{aligned}$$

over every parallel join, which also requires inverting 2 $k \times k$ matrices (the parallel addition of resistances is computed in Algorithm 1). The current best lower bound for ω is 2.3728639 [107]. □

9.2.2 *Synthesis of Optimal $\mathcal{H}_2$ Controllers*

The algorithm described above can be used to compute not only the terms required for the gradient update scheme for the edge weights, but also for an *a priori* synthesis calculation of the $\mathcal{H}_2$ norm.

First, let us examine the structure of the $\mathcal{H}_2$ norm in the context of the leader-follower consensus setup.

Lemma 13. *Consider the leader-follower consensus setup with $C = I \otimes I_k$. Then,*

$$\begin{aligned}\left(\mathcal{H}_2^{\mathcal{G},B}\right)^2 &= \frac{1}{2}\sum_{s\in R}\text{Tr}\left[\text{Blk}_s^{k\times k}\left[A^{-1}\mathbf{e}_s\right]\right] \\ &= \frac{1}{2}\sum_{s\in R}\text{Tr}\left[\mathbf{Y}_s^s\right] = \frac{1}{2}\sum_{s\in R}\text{Tr}\left[\rho_{s,\mathcal{R}}^{\text{eff}}\right].\end{aligned}$$

Proof. We note that,

$$\begin{aligned}\left(\mathcal{H}_2^{\mathcal{G},B}\right)^2 &= \frac{1}{2}\text{Tr}\left(\mathbf{B}^T A^{-1}\mathbf{B}\right) \\ &= \frac{1}{2}\text{Tr}\left(\sum_{i,s\in R}(e_i \otimes I_k)A_{is}^{-1}(e_s \otimes I_k)^T\right) \\ &= \frac{1}{2}\text{Tr}\left(\sum_{s\in R}(e_s \otimes I_k)A_{is}^{-1}(e_s \otimes I_k)^T\right) \\ &= \frac{1}{2}\sum_{s\in R}\text{Tr}\left[\text{Blk}_s^{k\times k}\left[A^{-1}\mathbf{e}_s\right]\right] \\ &= \frac{1}{2}\sum_{s\in R}\text{Tr}\left[\mathbf{Y}_s^s\right] = \frac{1}{2}\sum_{s\in R}\text{Tr}\left[\rho_{s,\mathcal{R}}^{\text{eff}}\right]. \qquad (9.12)\end{aligned}$$

□

Each quantity $\mathbf{Y}_s^s$ on the left side of the sum in (9.12) is the voltage drop from the source node $s \in R$ to the grounded leader node set $\mathcal{R}$. This is precisely the voltage dropped over the last parallel join of the series-parallel decomposition of an all-input TTSP graph; the join in question is exactly

the one depicted in Figure 9.5. We can utilize this observation to efficiently compute the $\mathcal{H}_2$ norm *a priori* knowing only the weights of the edges and the decomposition tree of $\mathcal{G}$.

We use the following setup. Consider a TTSP graph $\mathcal{G}$ with source node s and sink node t. Ground the source node s, and consider the grounded Laplacian A with respect to the grounded source s. This is a leader-follower system with a single leader.

Note that the parallel join depicted in Figure 9.5 effectively makes one of the terminals of the resulting graph an element of $\mathcal{R}$, and the other terminal (the sink) an element of R. The control matrix of the leader-follower consensus problem corresponds to exactly those elements in R, which are the 'sinks' of the TTSP graph used in that computation. Therefore, our choice of $\mathbf{B}$ must always select the state of the sink vector t; hence $\mathbf{B} = \mathbf{e}_t = e_t \otimes I_k$.

We now proceed in two steps. First, we need a lemma that essentially states that for an arbitrary TTSP graph, there exists an equivalent 1-path TTSP graph with the same effective resistance. Then, any composition rule on arbitrary TTSP graphs can be reduced to a composition on the equivalent 1-paths, simplifying the analysis. Afterward, we show that the series-parallel composition of graphs produces a similar series-parallel computation of the $\mathcal{H}_2$ performance.

Lemma 14. *Consider two graphs: an arbitrary TTSP graph $\mathcal{G}_1$ with source s_1 and sink t_1 with effective resistance $\rho^{eff}_{s_1,t_1}$, and a 1-path TTSP graph $\mathcal{G}_2$ with source s_2 and sink t_2 with effective resistance $\rho^{eff}_{s_2,t_2}$. Let their respective control matrices be $\mathbf{B}_1 = \mathbf{e}_{t_1}$ and $\mathbf{B}_2 = \mathbf{e}_{t_2}$. Further suppose that $\rho^{eff}_{s_1,t_1} = \rho^{eff}_{s_2,t_2}$. Then, $(\mathcal{H}_2{}^1)^2 = (\mathcal{H}_2{}^2)^2$.*

Proof. The setup of the graphs in the statement of the lemma is a leader-follower consensus with grounded (leader) nodes s_1, s_2. Therefore, we can invoke Lemma 13. Using Lemma 13, denoting the graphs' respective Dirichlet Laplacians as A_1, A_2 we can compute:

$$\begin{aligned}
(\mathcal{H}_2{}^1)^2 &= \frac{1}{2}\mathrm{Tr}\left[\mathbf{B}_1^T \left[A_1\right]^{-1} \mathbf{B}_1\right] \\
&= \frac{1}{2}\mathrm{Tr}\left[(e_{t_1}^T \otimes I_k)\left[A_1\right]^{-1}(e_{t_1} \otimes I_k)\right] \\
&= \frac{1}{2}\rho^{\mathrm{eff}}_{s_1,t_1} = \frac{1}{2}\rho^{\mathrm{eff}}_{s_2,t_2} \\
&= \frac{1}{2}\mathrm{Tr}\left[(e_{t_2}^T \otimes I_k)\left[A_2\right]^{-1}(e_{t_2} \otimes I_k)\right] \\
&= \frac{1}{2}\mathrm{Tr}\left[\mathbf{B}_2^T \left[A_2\right]^{-1} \mathbf{B}_2\right] \\
&= (\mathcal{H}_2{}^2)^2.
\end{aligned}$$

□

Lemma 14 will allow us to reduce the computation of the $\mathcal{H}_2$ norm of a composite TTSP graph to the computation of $\mathcal{H}_2$ norms of an equivalent 1-path. This allows us to prove the following theorem.

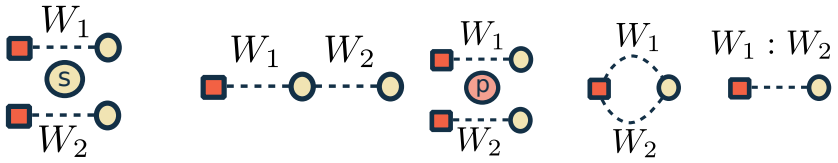

(a) Series join of 1-paths (b) Parallel join of 1-paths

Figure 9.6: Series and parallel joins of weighted 1-paths.

Theorem 28. *Consider two graphs: an arbitrary TTSP graph $\mathcal{G}_1$ with source s_1 and sink t_1, and a second arbitrary TTSP graph $\mathcal{G}_2$ with source s_2 and sink t_2. Let the Dirichlet Laplacian of $\mathcal{G}_i$ grounded with respect to its source s_i be A_i, and its control matrix be $\mathbf{B}_i = \mathbf{e}_{t_i} = e_i \otimes I_k$. Hence its $\mathcal{H}_2$ norm is given by $(\mathcal{H}_2{}^{\mathcal{G}_i})^2 = \frac{1}{2}\mathrm{Tr}[\mathbf{B}_i^T [A_i]^{-1} \mathbf{B}_i]$. Then,*

$$\left(\mathcal{H}_2{}^{\mathcal{G}_1 \odot \mathcal{G}_2}\right)^2 = \left(\mathcal{H}_2{}^{\mathcal{G}_1}\right)^2 + \left(\mathcal{H}_2{}^{\mathcal{G}_2}\right)^2 \tag{9.13}$$

$$\left(\mathcal{H}_2{}^{\mathcal{G}_1 \oslash \mathcal{G}_2}\right)^2 \leq \left(\mathcal{H}_2{}^{\mathcal{G}_1}\right)^2 : \left(\mathcal{H}_2{}^{\mathcal{G}_2}\right)^2, \tag{9.14}$$

with equality in the last display if and only if $\rho^{eff}_{s_1,t_1} = c\rho^{eff}_{s_2,t_2}$ for $c \in \mathbb{R}_{++}$.

Proof. By Lemma 13, the $\mathcal{H}_2$ norm of an arbitrary graph can be computed from an equivalent 1-path. Hence, we need to show (9.13) and (9.14) for series and parallel joins of 1-paths.

Consider the 1-paths in Figure 9.6, with weights $W_1, W_2 \in \mathcal{S}^k_{++}$ between the sources (square nodes) and sinks (circular nodes). The Dirichlet Laplacians of both with respect to the grounded source nodes are simply $\mathcal{L}_{\mathcal{G}\mathcal{G}_1} = [W_1]$, $\mathcal{L}_{\mathcal{G}\mathcal{G}_2} = [W_2]$, and their respective control matrices are $B_{\mathcal{G}_1} = B_{\mathcal{G}_2} = I_k$ and $\mathcal{H}_2$ norms are $(\mathcal{H}_2{}^{\mathcal{G}_1})^2 = \frac{1}{2}\mathrm{Tr}[W_1^{-1}]$, $(\mathcal{H}_2{}^{\mathcal{G}_2})^2 = \frac{1}{2}\mathrm{Tr}[W_2^{-1}]$.

Similarly, the Laplacians of the series and parallel joins in Figure 9.6 are,

$$\mathcal{L}_{\mathcal{G}\,\mathcal{G}_1 \oslash \mathcal{G}_2} = [W_1 + W_2], \; \mathcal{L}_{\mathcal{G}\,\mathcal{G}_1 \odot \mathcal{G}_2} = \begin{bmatrix} W_1 + W_2 & -W_2 \\ -W_2 & W_2 \end{bmatrix}.$$

The control matrices are $B_{\mathcal{G}_1 \oslash \mathcal{G}_2} = I_k$, $B_{\mathcal{G}_1 \odot \mathcal{G}_2} = [\mathbf{0}_{k\times k}\; I_k]$. Therefore, the $\mathcal{H}_2$ norm in the series join case is

$$\begin{aligned}
&\left(\mathcal{H}_2{}^{\mathcal{G}_1 \odot \mathcal{G}_2}\right)^2 \\
&= \frac{1}{2}\mathrm{Tr}\left[\begin{bmatrix}\mathbf{0}_{k\times k} & I_k\end{bmatrix}\begin{bmatrix} W_1 + W_2 & -W_2 \\ -W_2 & W_2 \end{bmatrix}^{-1}\begin{bmatrix}\mathbf{0}_{k\times k} \\ I_k\end{bmatrix}\right] \\
&= \frac{1}{2}\left(W_2 - W_2\left(W_1 + W_2\right)^{-1} W_2\right)^{-1},
\end{aligned} \tag{9.15}$$

where the formula in the last display follows from standard block matrix inversion formulae. Note that we can write

$$\begin{aligned}
&W_1(W_1+W_2)^{-1}W_2 \\
&= W_2(W_1+W_2)^{-1}W_2 - W_2(W_1+W_2)^{-1}W_2 \\
&\quad + W_1(W_1+W_2)^{-1}W_2 \\
&= (W_1+W_2)(W_1+W_2)^{-1}W_2 - W_2(W_1+W_2)^{-1}W_2 \\
&= W_2 - W_2\left(W_1+W_2\right)^{-1}W_2.
\end{aligned}$$

Inverting this expression and substituting into (9.15) yields,

$$\begin{aligned}
\left(\mathcal{H}_2{}^{\mathcal{G}_1\odot\mathcal{G}_2}\right)^2 &= \frac{1}{2}\left(W_1(W_1+W_2)^{-1}W_2\right)^{-1} \\
&= \frac{1}{2}W_1^{-1} + \frac{1}{2}W_2^{-1} \\
&= \left(\mathcal{H}_2{}^{\mathcal{G}_1}\right)^2 + \left(\mathcal{H}_2{}^{\mathcal{G}_2}\right)^2,
\end{aligned}$$

as desired. We can compute the $\mathcal{H}_2$ norm in the parallel join case by invoking Theorem 13 from [121], which states that for $A, B \in \mathcal{S}_{++}^k$,

$$\mathrm{Tr}(A:B) \leq \mathrm{Tr}(A):\mathrm{Tr}(B),$$

with equality if and only if $A = cB$ for some $c \in \mathbb{R}_{++}$. By this result, and by Lemma 13, we can compute:

$$\begin{aligned}
&\left(\mathcal{H}_2{}^{\mathcal{G}_1\oslash\mathcal{G}_2}\right)^2 = \frac{1}{2}\mathrm{Tr}\left[\rho_1^{\mathrm{eff}}:\rho_2^{\mathrm{eff}}\right] \\
&\leq \frac{1}{2}\left(\mathrm{Tr}\left[\rho_1^{\mathrm{eff}}\right]:\mathrm{Tr}\left[\rho_2^{\mathrm{eff}}\right]\right) \\
&= \left(\mathcal{H}_2{}^{\mathcal{G}_1}\right)^2 : \left(\mathcal{H}_2{}^{\mathcal{G}_2}\right)^2,
\end{aligned}$$

with equality if and only if $\rho^{\mathrm{eff}}_{s_1,t_1} = c\rho^{\mathrm{eff}}_{s_2,t_2}$ for $c \in \mathbb{R}_{++}$. □

We now propose the following Algorithm 7 for computing the $\mathcal{H}_2$ norm of a TTSP graph with control input e_s. If the matrix weights across the graph

are scalar multiples of each other, then Algorithm 7 computes precisely the $\mathcal{H}_2$ norm; otherwise it computes an upper bound.

Algorithm 7: $\mathcal{H}_2$ norm of TTSP Graph with $\mathbf{B} = \mathbf{e}_i$

Input: Decomposition tree $\mathcal{T}(\mathcal{G})$, weights $\mathcal{W}(\mathcal{G})$, $\mathbf{e}_i$
Result: $({\mathcal{H}_2}^{\mathcal{G}})^2$
for *each leaf* $\mathcal{L}$ *of* $\mathcal{T}(\mathcal{G})$ **do**
  Output $({\mathcal{H}_2}^{\mathcal{L}})^2 = \frac{1}{2}W_{\mathcal{L}}^{-1}$ to parent;
end
for *each parent* j *of* $\mathcal{T}(\mathcal{G})$ **do**
  if *received* ${\mathcal{H}_2}^{\mathcal{G}_i}$ *from both children* **then**
    if j *is a series join* **then**
      Output $(\mathcal{H}_2)^2 \leftarrow \left({\mathcal{H}_2}^{\mathcal{G}_1}\right)^2 + \left({\mathcal{H}_2}^{\mathcal{G}_2}\right)^2$ to parent;
    else
      Output $(\mathcal{H}_2)^2_{\text{est}} \leftarrow \left({\mathcal{H}_2}^{\mathcal{G}_1}\right)^2 : \left({\mathcal{H}_2}^{\mathcal{G}_2}\right)^2$ to parent;
    end
  else
    wait;
  end
end
return $(\mathcal{H}_2)^2$ *at root node of* $\mathcal{T}(\mathcal{G})$.

Remark 8. *Note that in the setting of Theorem 28, if we have* $k = 1$ *then* $\mathrm{Tr}(A : B) = \mathrm{Tr}(A) \cdot \mathrm{Tr}(B)$*, which is why Algorithm 7 computes the exact* $\mathcal{H}_2$ *norm.*

We now proceed to the final result of this section.

Theorem 29. *Consider a leader-follower consensus network on an all-input TTSP graph* $\mathcal{G}$*. Then, the* $\mathcal{H}_2$ *norm is given by*

$$\left({\mathcal{H}_2}^{\mathcal{G},\mathbf{B}}\right)^2 \triangleq -\frac{1}{2}\mathrm{Tr}\left[\mathbf{B}^T A^{-1}\mathbf{B}\right] = \sum_{s\in\mathcal{R}}\left({\mathcal{H}_2}^{\mathcal{G},\mathbf{e}_s}\right)^2,$$

and the best-case complexity of computing this $\mathcal{H}_2$ *norm is* $O(k^\omega|\mathcal{R}|\log|\mathcal{N}|)$*, and the worst-case complexity is* $O(k^\omega|\mathcal{R}||\mathcal{N}|)$*.*

Proof. We can compute:

$$\left({\mathcal{H}_2}^{\mathcal{G},\mathbf{B}}\right)^2 = -\frac{1}{2}\sum_{s\in\mathcal{R}}\mathrm{Tr}\left[\mathbf{e}_s^T A^{-1}\mathbf{e}_s\right] = \sum_{s\in\mathcal{R}}\left[{\mathcal{H}_2}^{\mathcal{G}_2,\mathbf{e}_s}\right]^2.$$

This is a sum of $|\mathcal{R}|$ $\mathcal{H}_2$ norms of leader-follower consensus networks with control input $\mathbf{e}_s$. Since at each layer of the decomposition tree $\mathcal{T}(\mathcal{G})$ each computation happens independently, the complexity depends on the height of the decomposition tree. The remainder of the proof is identical to that of Theorem 27. □

Remark 9. *The standard Lyapunov equation solution to the* $\mathcal{H}_2$ *norm is of complexity* $O(k^3|\mathcal{N}|^3)$*, or* $O(k^3|\mathcal{N}|^2)$ *if the system matrix is symmetric. Hence, the series-parallel method provides significant computational savings.*

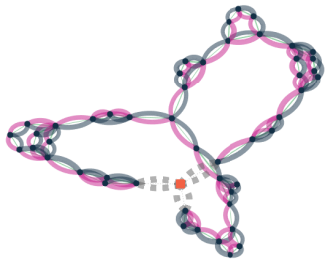

Figure 9.7: Edges weights for example at iteration 1

9.3 EXAMPLE

In this section, we provide a computational example for the adaptive reweighting algorithm. We perform the gradient descent on the TTSP graph in Figures 9.7-9.10 with 3 leader nodes, identified to a single node depicted as an orange square. The weights are assumed to be elements of $\mathcal{S}^2_{++}$, which are 2×2 symmetric matrices, and thus have 3 independent elements. The 3 independent elements of each weight $W_{\{i,j\}}$ are represented as a multi-edge, with 3 edges between each node i and its neighbour j. The edges connecting the leader nodes to the source nodes are identity weights, and the remaining weights were randomly initialized using the generator

$$W_{\{i,j\}} = \frac{G_{\{i,j\}} + G^T_{\{i,j\}}}{2} + 2I_2, \tag{9.16}$$

where $G_{\{i,j\}}$ is a 2×2 matrix with entries distributed according to a zero-mean standard Gaussian.

The weight penalty was set as $h = 0.05$, and upper/lower bounds for each weight were randomly generated according to Equation (9.16), with an additional scalar factor of 0.05 for the lower bound, and 10 for the upper bound.

The algorithm converges in a few steps, as shown in Figure 9.11.

9.4 PROOF OF PROPOSITION 5:

Recall that

$$\mathcal{H}_2{}^2 = \frac{1}{2} \sum_{s \in R} \mathrm{Tr}\left[\mathbf{e}_s^T A^{-1} \mathbf{e}_s\right] \tag{9.17}$$
$$A = \mathbf{A}_c W_c \mathbf{A}_c^T + \sum_{e \in \mathcal{E} \setminus c} \mathbf{A}_e W_e \mathbf{A}_e^T.$$

We want to find the gradient of the $\mathcal{H}_2$ norm with respect to W_c for each $c \in \mathcal{E}$, and we do this by computing the gradients of each individual term $\mathrm{Tr}\left[\mathbf{e}_s^T A^{-1} \mathbf{e}_s\right]$ in (9.17), for each $s \in R$.

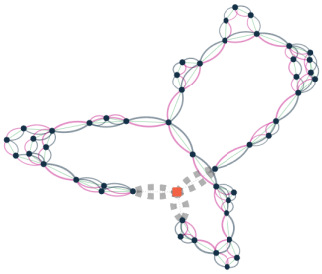

Figure 9.8: Edges weights for example iteration 3

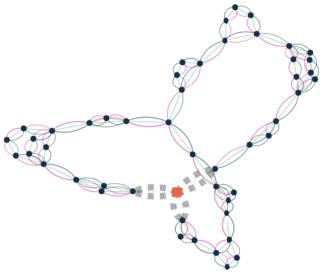

Figure 9.9: Edges weights for example iteration 5

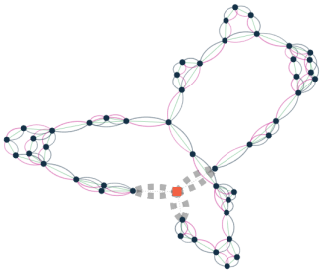

Figure 9.10: Edges weights for example iteration 7

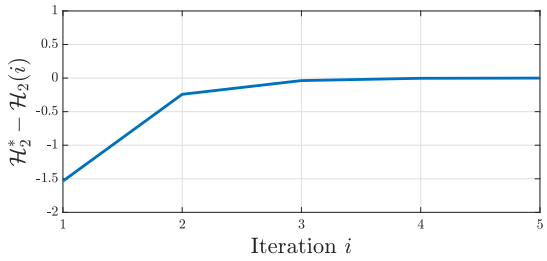

Figure 9.11: Convergence of gradient descent weight update for optimal $\mathcal{H}_2$ performance on the graphs in Figures 9.7-9.10

To this end, consider the functions

$$f(X) = \mathrm{Tr}(\mathbf{e}_s^T X \mathbf{e}_s)$$
$$g(X) = X^{-1}$$
$$h(X) = \mathbf{A}_c X \mathbf{A}_c^T + \sum_{e \in \mathcal{E} \setminus c} \mathbf{A}_e W_e \mathbf{A}_e^T.$$

These functions have differentials,

$$d_{f(X)}[H] = \mathrm{Tr}(\mathbf{e}_s^T H \mathbf{e}_s)$$
$$d_{g(X)}[H] = -X^{-1} H X^{-1}$$
$$d_{h(X)}[H] = \mathbf{A}_c H \mathbf{A}_c^T.$$

A single term of interest is given by

$$\mathrm{Tr}\left[\mathbf{e}_s^T A^{-1} \mathbf{e}_s\right] = f(g(h(W_c))) = (f \circ g \circ h)[W_c],$$

and the differentials are thus similarly composed. Note that g is strongly convex on the cone of PD matrices, and both f and h are linear functions in X. It follows that the objective function is strongly convex, proving the first part of the proposition.

Next, we have

$$d(g \circ h)[H] = -X^{-1} \left(\mathbf{A}_c H \mathbf{A}_c^T\right) X^{-1}$$
$$X = \left(\mathbf{A}_c H \mathbf{A}_c^T + \sum_{e \in \mathcal{E} \setminus c} \mathbf{A}_e W_e \mathbf{A}_e^T\right) = A,$$

and we also have that

$$d(f \circ g \circ h)[H] = -\mathrm{Tr}\left[\mathbf{e}_s^T A^{-1} \mathbf{A}_c H \mathbf{A}_c^T A^{-1} \mathbf{e}_s\right].$$

Let $Q = \mathbf{A}_c^T A^{-1} \mathbf{e}_s$. Then, we can identify the gradient at a point H as,

$$\begin{aligned} d(f \circ g \circ h)[H] &= -\mathrm{Tr}\left[Q^T H Q\right] \\ &= \langle -Q^T Q, H \rangle, \end{aligned}$$

and so the gradient at H is identifed as $-Q^TQ = -(\mathbf{A}_c^T A^{-1}\mathbf{e}_s)^T(\mathbf{A}_c^T A^{-1}\mathbf{e}_s)$. Let us examine the form of Q by letting $g = \{i, j\}$; in particular,

$$\begin{aligned} Q = \mathbf{A}_f^T A^{-1}\mathbf{e}_s &= \left(a_g^T \otimes I_k\right) A^{-1}\left(e_s \otimes I_k\right) \\ &= \left(e_i^T \otimes I_k - e_j^T \otimes I_k\right) A^{-1}\left(e_s \otimes I_k\right). \end{aligned}$$

This is precisely $\mathrm{Blk}_i^{k\times k}\left[A^{-1}e_s\right] - \mathrm{Blk}_j^{k\times k}\left[A^{-1}e_s\right] := \mathbf{Y}_i^s - \mathbf{Y}_j^s$, or the difference in matrix-valued voltage drops to the grounded leader node from node i to node j. Hence, the gradient with respect to weight W_c is given by

$$\nabla_{W_c}\mathcal{H}_2{}^2[H] = -\frac{1}{2}\sum_{s\in R}\left(\mathbf{Y}_i^s - \mathbf{Y}_j^s\right)^T\left(\mathbf{Y}_i^s - \mathbf{Y}_j^s\right),$$

where A^{-1} is computed with H in place of W_c.

Remark 10. *It is precisely this matrix inverse that we are able to avoid computing using the methods for series-parallel networks in §9.2.*

10

TIMESCALED CONSENSUS

10.1 LEADER-FOLLOWER CONSENSUS MODELS WITH TIME SCALES

In this section, we will describe a general formulation for consensus over a communication network with non-negative edge weighting, positive node time scaling, while accounting for possible measurement and process noise. The scaled consensus problem is derived from considering a group of n multi-rate integrators [80], with zero-mean Gaussian process noise, $\omega_i(t)$ such that $\mathbb{E}\left[\omega_i(t)\omega_i(t)^T\right] = \Gamma_i,\ \forall i \in \mathcal{N}$,

$$\begin{bmatrix} \epsilon_{i,1}\dot{x}_{i,1} \\ \vdots \\ \epsilon_{i,n}\dot{x}_{i,n} \end{bmatrix} = E_i\dot{x}_i(t) = u_i(t) + \omega(t), \tag{10.1}$$

where $\omega(t)$ is the stacked vector of process noises ω_i. Accounting for the communication between agents can be accomplished by representing the system as a graph with node set given by the agents, and edge set defined by the interconnections. Suppose that communication between agents i and j is corrupted by zero-mean Gaussian noise v_{ij}, and let v_i denote the sum of all noise inputted into agent i from the connections to its neighbours in $N(i)$. Without loss of generality, we can assume that the covariance of v_i is given by $\mathbb{E}[v_i(t)v_i(t)^T] = \Omega_i$. A weighted, decentralized feedback controller (corrupted by the above noise model) that seeks to bring agents into consensus is given by,

$$\begin{aligned} u_i(t) &= v_i(t) + \sum_{j\in N(i)} \left(W_{ij}(x_j(t) - x_i(t))\right) \\ \mathbf{u}(t) &= -\mathbf{W}\mathbf{D}(\mathcal{G})\mathbf{x}(t) + \mathbf{v}(t), \end{aligned} \tag{10.2}$$

where $\mathbf{W}$ is the block-diagonal matrix of edge weights with properties detailed in §13.1. The vector $\mathbf{u}$ is the stacked vector of control vectors u_i, and $\mathbf{v}$ is the stacked vector of all noises. The matrix version of applying (10.2) to (10.1) gives the general, time scaled and weighted consensus problem with process and measurement noise,

$$\begin{aligned} \dot{\mathbf{x}}(t) &= -\mathbf{E}^{-1}\mathcal{L}_{\mathcal{G}_w}(\mathcal{G})\mathbf{x}(t) + \begin{bmatrix} \mathbf{E}^{-1} & -\mathbf{E}^{-1}\mathbf{D}(\mathcal{G}) \end{bmatrix} \begin{bmatrix} \omega(t) \\ \mathbf{v}(t) \end{bmatrix} \\ \mathbf{z}(t) &= \mathbf{D}(\mathcal{G})^T\mathbf{x}(t), \end{aligned} \tag{10.3}$$

where $\mathcal{L}_{\mathcal{G}_w} = \mathbf{D}(\mathcal{G})\mathbf{W}\mathbf{D}(\mathcal{G})^T$ is the weighted Laplacian matrix, and $\mathbf{E} = \text{Blkdiag}(E_1, \ldots, E_n)$ is the time scale matrix of $\mathcal{G}$. The output, $\mathbf{z}(t)$ in (10.3), will be used to monitor the performance of the network and assess how the available system output impacts the network performance.

As noted by [122] (in the scalar-valued node state case), the zero eigenvalue of the Laplacian matrix (assuming $\mathcal{G}$ is connected) precludes reasoning about the $\mathcal{H}_2$ performance of (10.3). This property of the Laplacian matrix persists in the scaled, weighted case [86] (as well as the matrix-valued edge weight case), so as in [122] we will appeal to a similarity transform that separates out the zero eigenvalues, which is described in the following theorem.

Theorem 30. *The scaled and edge-weighted graph Laplacian for a connected graph with time scale matrix* $\mathbf{E}$ *and weight matrix* $\mathbf{W}$*, given by*

$$\mathcal{L}_{\mathcal{G}_w} = \mathbf{E}^{-1}\mathbf{D}(\mathcal{G})\mathbf{W}\mathbf{D}(\mathcal{G})^T,$$

is similar to

$$\begin{bmatrix} \tilde{\mathcal{L}}_{\mathcal{G}_e}\mathbf{R}\mathbf{W}\mathbf{R}^T & 0 \\ 0 & 0 \end{bmatrix},$$

where $\tilde{\mathcal{L}}_{\mathcal{G}_{e,s}} = \mathbf{D}(\mathcal{G}_\tau)^T\mathbf{E}^{-1}\mathbf{D}(\mathcal{G}_\tau)$ *is the edge Laplacian of* $\mathcal{G}$ *with time scales, and*

$$\mathbf{R}(\mathcal{G}) = \begin{bmatrix} I & \mathbf{T}_\tau^c \end{bmatrix} = R \otimes I_k$$

with,

$$\mathbf{T}_\tau^c = (\mathbf{D}(\mathcal{G}_\tau)^T\mathbf{D}(\mathcal{G}_\tau))^{-1}\mathbf{D}(\mathcal{G}_\tau)^T\mathbf{D}(\mathcal{G}_c).$$

and R *is is the basis of the cut space of* $\mathcal{G}$ *as defined as in [122]. Here, the* τ *and* c *subscripts on* $\mathcal{G}$ *denote the incidence matrices for a spanning tree and the complementary edges in* $\mathcal{G}$*, respectively.*

Proof. First, we prove a lemma.

Lemma 15 (Forms of $\mathbf{T}_\tau^c$ and $\mathbf{D}$). *The following hold:*

$$\begin{aligned} \mathbf{T}_\tau^c &= T_\tau^c \otimes I_k \\ \mathbf{D} &= \mathbf{D}_\tau\mathbf{R}. \end{aligned}$$

Proof. We can compute:

$$\begin{aligned} \mathbf{T}_\tau^c &= \left(\mathbf{D}_\tau^T\mathbf{D}_\tau\right)^{-1}\mathbf{D}_\tau^T\mathbf{D}_c \\ &= \left((D_\tau \otimes I_k)^T(D_\tau \otimes I_k)\right)^{-1}(D_\tau \otimes I_k)^T(D_c \otimes I_k) \\ &= \left(\left(D_\tau^T D_\tau\right) \otimes I_k\right)^{-1}\left(D_\tau^T D_c\right) \otimes I_k \\ &= \left(\left(D_\tau^T D_\tau\right)^{-1} D_\tau D_c\right) \otimes I_k \\ &= T_\tau^C \otimes I_k, \end{aligned}$$

and similarly,

$$\begin{aligned}\mathbf{D} &= D \otimes I_k \\ &= \begin{bmatrix} D_\tau & D_c \end{bmatrix} \otimes I_k \\ &= D_\tau \begin{bmatrix} I & T_\tau^c \end{bmatrix} \otimes I_k \\ &= (D_\tau R) \otimes I_k \\ &= (D_\tau \otimes I_k)(R \otimes I_k) \\ &= \mathbf{D}_\tau \mathbf{R}.\end{aligned}$$

□

Following [86], [122] , we define the similarity transforms

$$\begin{aligned} S_v(\mathcal{G}) &= \begin{bmatrix} \mathbf{E}^{-1}\mathbf{D}(\mathcal{G}_\tau)\left(\mathbf{D}(\mathcal{G}_\tau)^T\mathbf{E}^{-1}\mathbf{D}(\mathcal{G}_\tau)\right)^{-1} & \mathbf{1}_{n\otimes k} \end{bmatrix} \\ S_v(\mathcal{G})^{-1} &= \begin{bmatrix} \mathbf{D}(\mathcal{G}_\tau)^T \\ \Xi^{-1}F \end{bmatrix}, \end{aligned}$$

where

$$\begin{aligned} \mathbf{1}_{n\otimes k} &= \mathbf{1}_n \otimes I_k \\ F &= \begin{bmatrix} E_1 & \cdots & E_n \end{bmatrix} \\ \Xi &= \operatorname{diag}\left(\{\epsilon_{s,i}\}_{i=1}^k\right) \\ \epsilon_{s,i} &= \sum_{j=1}^n \epsilon_{j,i}. \end{aligned}$$

Note that $\epsilon_{i,s}$ is the sum of all the time scale parameters of the ith state over all nodes.

Lemma 16. *The similarity transforms are well-defined, in that* $S_v^{-1}S_v = I$.

Proof. Denote the product $S_v^{-1}S_v$ in block form:

$$S_v^{-1}S_v = \begin{bmatrix} \mathcal{A} & \mathcal{B} \\ C & \mathcal{D} \end{bmatrix}.$$

First, note that

$$F\mathbf{E}^{-1} = \begin{bmatrix} E_1 & \cdots & E_n \end{bmatrix}\mathbf{E}^{-1} = \begin{bmatrix} I & \cdots & I \end{bmatrix} = \mathbf{1}_n^T \otimes I_k.$$

Then, we can compute each term:

$$\begin{aligned}
\mathcal{A} &= \mathbf{D}_\tau^T \mathbf{E}^{-1} \mathbf{D}_\tau \left(D_\tau^T \mathbf{E}^{-1} \mathbf{D}_\tau \right)^{-1} = I \\
\mathcal{B} &= \mathbf{D}_\tau^T \mathbf{1}_{n \otimes k} \\
&= \left(\mathbf{D}_\tau \otimes I_k \right)^T \left(\mathbf{1}_k \otimes I_k \right) \\
&= \left(D_\tau^T \mathbf{1}_n \right) \otimes I_k = 0 \otimes I_k = \mathbf{0}. \\
\mathcal{C} &= \Xi^{-1} F \mathbf{E}^{-1} \mathbf{D}_\tau \left(\mathbf{D}_\tau^T \mathbf{E}^{-1} \mathbf{D}_\tau \right)^{-1} \\
&= \Xi^{-1} \left(\mathbf{1}_n^T \otimes I_k \right) \left(\mathbf{D}_\tau \otimes I_k \right) \left(\mathbf{D}_\tau^T \mathbf{E}^{-1} \mathbf{D}_\tau \right)^{-1} \\
&= \Xi^{-1} \left(\mathbf{1}_n^T \mathbf{D}_\tau \otimes I_k \right) \left(\mathbf{D}_\tau^T \mathbf{E}^{-1} \mathbf{D}_\tau \right)^{-1} \\
&= \mathbf{0}.
\end{aligned}$$

Lastly, we have

$$\begin{aligned}
\mathcal{D} &= \Xi^{-1} F \mathbf{1}_{n \otimes k} \\
&= \begin{bmatrix} \epsilon_{s,1}^{-1} & & \\ & \ddots & \\ & & \epsilon_{s,k}^{-1} \end{bmatrix} \begin{bmatrix} E_1 & \cdots & E_n \end{bmatrix} \left(\mathbf{1}_n \otimes I_k \right) \\
&= \begin{bmatrix} \epsilon_{s,1}^{-1} & & \\ & \ddots & \\ & & \epsilon_{s,k}^{-1} \end{bmatrix} \begin{bmatrix} \sum_{j=1}^n \epsilon_{j,1} & & \\ & \ddots & \\ & & \sum_{j=1}^n \epsilon_{j,k} \end{bmatrix} \\
&= \begin{bmatrix} \epsilon_{s,1}^{-1} \epsilon_{s,1} & & \\ & \ddots & \\ & & \epsilon_{s,k}^{-1} \epsilon_{s,k} \end{bmatrix} = I_k
\end{aligned}$$

□

Next, denoting for brevity $\mathbf{D}_\tau := \mathbf{D}(\mathcal{G}_\tau)$, $\mathbf{D} := \mathbf{D}(\mathcal{G})$, etc, and noting that $\mathbf{D}^T \mathbf{1}_{n \otimes k} = (D^T \mathbf{1}) \otimes I_k = \mathbf{0}$, we have

$$\begin{aligned}
&S_v^{-1} \mathcal{L}_{\mathcal{G}_w} S_v = \\
&\begin{bmatrix} \mathbf{D}_\tau^T \mathbf{E}^{-1} \mathbf{D} \mathbf{W} \mathbf{D}^T \mathbf{E}^{-1} \mathbf{D}_\tau \left(\mathbf{D}_\tau \mathbf{E}^{-1} \mathbf{D}_\tau \right)^{-1} & \mathbf{D}_\tau^T \mathbf{E}^{-1} \mathbf{D} \mathbf{W} \mathbf{D}^T \mathbf{1}_{n \otimes k} \\ \Xi^{-1} F \mathbf{D} \mathbf{D}^T \mathbf{D}_\tau \left(\mathbf{D}_\tau \mathbf{E}^{-1} \mathbf{D}_\tau \right)^{-1} & \Xi^{-1} F \mathbf{E}^{-1} \mathbf{D} \mathbf{D}^T \mathbf{1}_{n \otimes k} \end{bmatrix} \\
&= \begin{bmatrix} \mathbf{D}_\tau^T E^{-1} \mathbf{D}_\tau \mathbf{R} \mathbf{W} \mathbf{R}^T \mathbf{D}_\tau^T \mathbf{E}^{-1} \mathbf{D}_\tau \left(\mathbf{D}_\tau \mathbf{E}^{-1} \mathbf{D}_\tau \right)^{-1} & \mathbf{0} \\ \Xi^{-1} \mathbf{1}_{n \otimes k}{}^T \mathbf{D} \mathbf{D}_\tau \left(\mathbf{D}_\tau \mathbf{E}^{-1} \mathbf{D}_\tau \right)^{-1} & \mathbf{0} \end{bmatrix} \\
&= \begin{bmatrix} \tilde{\mathcal{L}}_{\mathcal{G}_{e,s}} \mathbf{R} \mathbf{W} \mathbf{R}^T & \mathbf{0} \\ \mathbf{0} & \mathbf{0} \end{bmatrix},
\end{aligned}$$

as desired. □

The model in (10.3) can now be transformed to edge variables with the scaled coordinate transformation introduced in Theorem 30, and noting that $S_v \mathbf{x}_e(t) = \mathbf{x}(t)$. The scaled, weighted consensus model with noise is then equivalent to,

$$\begin{aligned}\dot{\mathbf{x}}_e(t) &= \begin{bmatrix} -\mathcal{L}_{\mathcal{G}_{e,s}}(\mathcal{G}_\tau)\mathbf{R}(\mathcal{G})\mathbf{W}\mathbf{R}(\mathcal{G})^T & \mathbf{0} \\ \mathbf{0} & \mathbf{0} \end{bmatrix} \mathbf{x}_e(t) \\ &\quad + \begin{bmatrix} \mathbf{D}_\tau^T \mathbf{E}^{-1} & -\mathcal{L}_{\mathcal{G}_{e,s}}(\mathcal{G}_\tau)\mathbf{R}(\mathcal{G}) \\ \Xi^{-1}\mathbf{1}_{n\otimes k}{}^T & 0 \end{bmatrix} \begin{bmatrix} \omega(t) \\ \mathbf{v}(t) \end{bmatrix} \\ \mathbf{z}(t) &= \begin{bmatrix} \mathbf{R}(\mathcal{G}) & 0 \end{bmatrix} \mathbf{x}_e(t). \end{aligned} \tag{10.4}$$

where $\mathcal{L}_{\mathcal{G}_{e,s}}(\mathcal{G}_\tau) = \mathbf{D}_\tau^T \mathbf{E}^{-1} \mathbf{D}_\tau$ is the edge Laplacian for spanning tree $\mathcal{G}_\tau$ which is symmetrically "weighted" by the time scaling parameters. We can note that the form of (10.4) naturally suggests a partitioning of the edge state variable into a set of states in the spanning tree and those in the consensus space (span$(\mathbf{1} \otimes I_k)$), $\mathbf{x}_e(t) = \begin{bmatrix} \mathbf{x}_\tau(t) & \mathbf{x}_\mathbf{1}(t) \end{bmatrix}$. The resulting dynamics for the spanning tree states is taken from (10.4) as,

$$\Sigma_\tau := \begin{cases} \dot{\mathbf{x}}_\tau(t) = -\mathcal{L}_{\mathcal{G}_{e,s}}(\mathcal{G}_\tau)\mathbf{R}(\mathcal{G})\mathbf{W}\mathbf{R}(\mathcal{G})^T \mathbf{x}_\tau(t) \\ \qquad\qquad + \mathbf{D}_\tau^T \mathbf{E}^{-1} \Omega \hat{\omega} - \mathcal{L}_{\mathcal{G}_{e,s}}(\mathcal{G}_\tau)\mathbf{R}(\mathcal{G})\Gamma \hat{\mathbf{v}} \\ \mathbf{z}(t) = \mathbf{R}(\mathcal{G})^T \mathbf{x}_\tau(t), \end{cases} \tag{10.5}$$

where $\hat{\mathbf{v}}$ and $\hat{\omega}$ are normalized noise signals, $\Omega = \mathbb{E}\left[\omega(t)\omega(t)^T\right]$, and $\Gamma = \mathbb{E}\left[\mathbf{v}(t)\mathbf{v}(t)^T\right]$. An important note is that the output of (10.5) contains information of the cycle states due to the inclusion of $R(\mathcal{G})$ and the fact that the cycle states are linear combinations of the tree states. We can also consider the same edge state model with output given solely by the spanning tree states,

$$\hat{\Sigma}_\tau := \begin{cases} \dot{x}_\tau(t) = -\mathcal{L}_{\mathcal{G}_{e,s}}(\mathcal{G}_\tau)\mathbf{R}(\mathcal{G})\mathbf{W}\mathbf{R}(\mathcal{G})^T \mathbf{x}_\tau(t) \\ \qquad\qquad + \mathbf{D}_\tau^T \mathbf{E}^{-1} \Omega \hat{\omega} - \mathcal{L}_{\mathcal{G}_{e,s}}(\mathcal{G}_\tau)\mathbf{R}(\mathcal{G})\Gamma \hat{\mathbf{v}} \\ \mathbf{z}(t) = \mathbf{x}_\tau(t). \end{cases} \tag{10.6}$$

The $\mathcal{H}_2$ performance of (10.5) and (10.6) are given by $\mathbf{tr}(R^T X^\star R)$ and $\mathbf{tr}(X^\star)$, respectively, where $X^\star$ is the positive-definite solution to the Lyapunov equation,

$$\begin{aligned} &-\mathcal{L}_{\mathcal{G}_{e,s}^\tau}\mathbf{R}\mathbf{W}\mathbf{R}^T X - X\mathbf{R}\mathbf{W}\mathbf{R}^T \mathcal{L}_{\mathcal{G}_{e,s}^\tau} + \mathbf{D}_\tau^T \mathbf{E}^{-1}\Omega\Omega^T \mathbf{E}^{-1}\mathbf{D}_\tau + \\ &\mathcal{L}_{\mathcal{G}_{e,s}^\tau}\mathbf{R}\Gamma\Gamma^T \mathbf{R}^T \mathcal{L}_{\mathcal{G}_{e,s}^\tau} = 0. \end{aligned} \tag{10.7}$$

In general, the addition of the weighting and scaling precludes a closed form solution to (10.7) (which is desirable to find X's dependence on E, W), and numeric results yield a nonlinear mixing of weights and scaling param-

eters in the entries of X. However, in the following section we will outline a case when analytic solutions to (10.7) exist, their interpretations, and the insights they can give for design of edge weights and scaling parameters for optimal performance.

10.2 PERFORMANCE AND DESIGN PROBLEMS

10.2.1 $\mathcal{H}_2$ *Performance*

In this section, we discuss the $\mathcal{H}_2$ performance for the models of edge consensus in the cases of nodes with timescales, and weighted edges.

10.2.1.1 *Analytic Solutions to the Lyapunov Equation*

By appropriately selecting the covariance matrices Ω and Γ, we can find analytic solutions for (10.7) in line with those found in [122]. Specifically, if we take $\Omega = \sigma_\omega \mathbf{E}^{1/2}$ and $\Gamma = \sigma_\upsilon \mathbf{W}^{1/2}$, then by inspection (10.7) has the following solution,

$$X^\star = \frac{1}{2}\left(\sigma_w^2(\mathbf{R}\mathbf{W}\mathbf{R}^T)^{-1} + \sigma_\upsilon^2 \mathcal{L}_{\mathcal{G}^\tau_{e,s}}\right). \tag{10.8}$$

This selection of Ω and Γ may at first seem based in convenience, but there is actually strong justification for this choice. Consider a scaled node that is subject to process noise with a variance being controlled by an external influencer. As can be seen from the dynamics in (10.5) or (10.6), a input noise signal with unity variance will be scaled by the node's time scaling factor; intuitively we can see that slow (higher scaling parameter) will attenuate the input, while faster nodes act as an amplifier for the input. So in the case of a scaled network, to achieve a consistent value of σ_ω variance into each node, the input signal must be scaled by the scaling parameters over the network. The same reasoning applies to the measurement noise over the edges, which can be attenuated or amplified by the presence of non-unity weights. Thus, we can interpret the σ_ω and σ_υ parameters as the desired, effective variance to be applied to each node/edge, and the scaling/weighting matrices are then applied to ensure that all nodes/edges receive an appropriately adjusted input signal. Now that we have justified our choice of covariance matrices, let us consider the implications of this result.

Equation (10.8) is of particular interest because it shows by associating the covariances with the magnitudes of the edge weights and the time scale parameters, the edge and node weightings are completely separated in their effect on the $\mathcal{H}_2$ performance, save for the placement of the σ_ω and σ_υ parameters (that is, the effective covariance parameter of the process noise is a "node" parameter, but multiplies the term containing the edge weighting

in (10.8), and vice versa). To aid in the consideration of these independent contributions later, we can then define,

$$\begin{aligned}\mathcal{H}_2(\Sigma) &= \frac{\sigma_\omega^2}{2}\mathbf{tr}(\mathbf{R}^T(\mathbf{R}\mathbf{W}\mathbf{R}^T)^{-1}\mathbf{R}) + \frac{\sigma_v^2}{2}\mathbf{tr}(\mathbf{R}^T\mathcal{L}_{\mathcal{G}^\tau_{e,s}}\mathbf{R}) \\ &:= \mathcal{H}_2(\Sigma, \mathbf{W}) + \mathcal{H}_2(\Sigma, \mathbf{E}),\end{aligned} \tag{10.9}$$

and similarly,

$$\begin{aligned}\mathcal{H}_2(\hat{\Sigma}) &= \frac{\sigma_w^2}{2}\mathbf{tr}((\mathbf{R}\mathbf{W}\mathbf{R}^T)^{-1}) + \frac{\sigma_v^2}{2}\mathbf{tr}(\mathcal{L}_{\mathcal{G}^\tau_{e,s}}) \\ &:= \mathcal{H}_2(\hat{\Sigma}, \mathbf{W}) + \mathcal{H}_2(\hat{\Sigma}, \mathbf{E}).\end{aligned}$$

We will see in later sections that the minimization of $\mathcal{H}_2(\cdot, \mathbf{W})$ in comparison to $\mathcal{H}_2(\cdot, \mathbf{E})$ gives rise to different strategies. To enable this, we can further refine (10.9), considering the weighting term and scaling term separately. First, we start with the edge weight term,

$$\begin{aligned}&\mathcal{H}_2(\Sigma, \mathbf{W}) = \frac{\sigma_\omega^2}{2}\mathbf{tr}(\mathbf{R}^T(\mathbf{R}\mathbf{W}\mathbf{R}^T)^{-1}\mathbf{R}) \\ &= \frac{\sigma_\omega^2}{2}\mathbf{tr}\left(\begin{bmatrix} I \\ \mathbf{T}_\tau^c \end{bmatrix}(\mathbf{R}\mathbf{W}\mathbf{R}^T)^{-1}\begin{bmatrix} I & \mathbf{T}_\tau^c \end{bmatrix}\right) \\ &= \frac{\sigma_\omega^2}{2}\mathbf{tr}\left(\begin{bmatrix} (\mathbf{R}\mathbf{W}\mathbf{R}^T)^{-1} & (\mathbf{R}\mathbf{W}\mathbf{R}^T)^{-1}\mathbf{T}_\tau^c \\ (\mathbf{T}_\tau^c)^T(\mathbf{R}\mathbf{W}\mathbf{R}^T)^{-1} & (\mathbf{T}_\tau^c)^T(\mathbf{R}\mathbf{W}\mathbf{R}^T)^{-1}\mathbf{T}_\tau^c \end{bmatrix}\right) \\ &= \frac{\sigma_\omega^2}{2}\left(\mathbf{tr}\left((\mathbf{R}\mathbf{W}\mathbf{R}^T)^{-1}\right) + \mathbf{tr}\left((\mathbf{T}_\tau^c)^T(\mathbf{R}\mathbf{W}\mathbf{R}^T)^{-1}\mathbf{T}_\tau^c\right)\right) \\ &= \mathcal{H}_2(\hat{\Sigma}, \mathbf{W}) + \frac{\sigma_\omega^2}{2}\mathbf{tr}\left((\mathbf{T}_\tau^c)^T(\mathbf{R}\mathbf{W}\mathbf{R}^T)^{-1}\mathbf{T}_\tau^c\right).\end{aligned} \tag{10.10}$$

A similar relation can be found for the time scale term,

$$\begin{aligned}\mathcal{H}_2(\Sigma, \mathbf{E}) &= \frac{\sigma_v^2}{2}\mathbf{tr}(\mathbf{R}^T\mathcal{L}_{\mathcal{G}^\tau_{e,s}}\mathbf{R}) \\ &= \frac{\sigma_v^2}{2}\mathbf{tr}\left(\begin{bmatrix} \mathcal{L}_{\mathcal{G}^\tau_{e,s}} & \mathcal{L}_{\mathcal{G}^\tau_{e,s}}\mathbf{T}_\tau^c \\ (\mathbf{T}_\tau^c)^T\mathcal{L}_{\mathcal{G}^\tau_{e,s}} & (\mathbf{T}_\tau^c)^T\mathcal{L}_{\mathcal{G}^\tau_{e,s}}\mathbf{T}_\tau^c \end{bmatrix}\right) \\ &= \mathcal{H}_2(\hat{\Sigma}, \mathbf{E}) + \frac{\sigma_v^2}{2}\mathbf{tr}\left((\mathbf{T}_\tau^c)^T\mathcal{L}_{\mathcal{G}^\tau_{e,s}}\mathbf{T}_\tau^c\right).\end{aligned} \tag{10.11}$$

The simplifications to (10.9) show that the $\mathcal{H}_2$ performance of the Σ system, which has output containing information from the cycle edge states, predictably contains the $\mathcal{H}_2$ performance for the $\hat{\Sigma}$ system as an isolated term. Taken together, (10.10) and (10.11) illustrate how the output information differences between (10.4) and (10.5) influence the overall $\mathcal{H}_2$ performance for identical tree-edge-state dynamics.

As seen in [122], the cycle structure of arbitrary graphs makes closed-form solutions for terms containing $(RR^T)^{-1}$ difficult. In the case considered here, the consideration of edge weights allows us to consider terms containing $(\mathbf{R}\mathbf{W}\mathbf{R}^T)^{-1}$ instead. Unfortunately, this does not offer a reprieve from the

issues discussed for the unweighted case. For unity edge weighting, we can appeal to the results presented there for $\mathcal{H}_2(\Sigma, W)$ and $\mathcal{H}_2(\hat{\Sigma}, W)$ in the case of cycles and complete graphs. We reproduce those below for completeness and to bring them in line with our notation,

$$\mathcal{H}_{2,C_n}(\hat{\Sigma}, W = I) = \frac{\sigma_\omega^2}{2}\frac{(n-1)^2}{n}$$
$$\mathcal{H}_{2,K_n}(\hat{\Sigma}, W = I) = \sigma_\omega^2\frac{(n-1)}{n}.$$

In the case of tree graphs, however, the analysis simplifies even further as we will discuss in the next section.

10.2.1.2 *Tree Graphs*

When the underlying graph topology is a tree, $\mathbf{R} = I$, and (10.8) simplifies to,

$$X^\star = \frac{1}{2}\left(\sigma_\omega^2(\mathbf{W})^{-1} + \sigma_v^2\mathcal{L}_{\mathcal{G}_{e,s}^\tau}\right).$$

Furthermore, in this case $\mathcal{H}_2(\Sigma_\tau) = \mathcal{H}_2(\hat{\Sigma}_\tau) = \mathbf{tr}(X^\star)$. A closed form solution for the performance in this case is given in the following lemma.

Lemma 17. *For a tree graph, the $\mathcal{H}_2$ norm of the Σ_τ (10.6) system is given by,*

$$\begin{aligned}\mathcal{H}_2(\Sigma_\tau) &= \frac{1}{2}\mathbf{tr}\left(\sigma_\omega^2(\mathbf{W})^{-1} + \sigma_v^2\mathcal{L}_{\mathcal{G}_{e,s}^\tau}\right)\\ &= \frac{1}{2}\sum_{l=1}^{k}\left(\sigma_\omega^2\sum_{k=1}^{n-1}\frac{1}{w_{j,l}} + \sigma_v^2\sum_{i=1}^{n}\frac{deg(v_i)}{\epsilon_{i,l}}\right),\end{aligned} \tag{10.12}$$

where $deg(v_i)$ is the unweighted degree of agent v_i, and j is the index over the edges.

Proof. Consider a single layer of substates, denoted by l. We have that W_l is diagonal matrix of weights, so the trace of the inverse is simply the sum of the inverted weights. For the second term, consider one of the diagonal elements of $\mathcal{L}_{\mathcal{G}_{e,s}}$,

$$[L_{e,s}^\tau]_{(ql)(ql)} = a_q^T E_l^{-1} a_q = \epsilon_{i,l}^{-1} + \epsilon_{j,l}^{-1},$$

where a_q is the edge vector corresponding to the edge between nodes i and j, that is, $q = \kappa(ij)$. Now consider a single node, v_i. In the sum over all edges of the graph, $\epsilon_{i,l}^{-1}$ will appear once for every edge that connects v_i to its neighbors, which is the unweighted degree of v_i. Considering all other nodes gives the result for the second term.

Finally, the preceding argument holds for all the sub-state layers, which gives the sum over all sub-states. □

From this result, we can see that there exists a trade-off between the time scale parameters and the topology (in this case, the degree distribution)

which determines the overall performance of the network. Also, we can contrast the influence of time scale parameters and edge weights in this case. For a given distribution of scaling parameters and edge weights, changing the assignment of edge weights does not affect the $\mathcal{H}_2$ performance. However, the assignment of scaling parameters can have a significant effect on the performance of the network, which is in line with the similar results in the context of single-input influenced consensus [86]. We see this explicitly in the following example.

10.2.1.3 *Effect of Time Scale Distribution Example*

Consider a tree graph on six nodes with topology given in Figure 10.1. Assume that we have some distribution of edge weights and node scaling parameters such that $\sum_i w_i^{-1} = 2\alpha$, $\sum_i \epsilon_i = 1$, and further, that $\epsilon_i \in (0.1, 0.2, 0.4)$. Also, let $\sigma_v = \sigma_\omega = 1$.

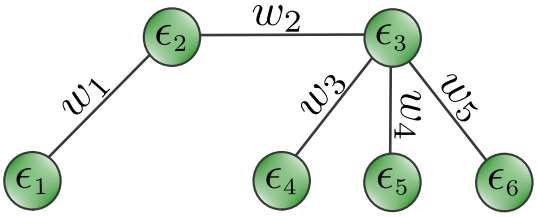

Figure 10.1: Tree graph for six agents, $\mathcal{T}$. Each agent has an associated scaling parameter, ϵ_i, with subscript denoting the agent number, and each edge is similarly labeled w_j. Agent 3 has the highest degree.

Now, for any assignment of weights, the first term in (10.12) will be 2α. However, the second term depends on the assignment of the scaling parameters. Consider the two following assignments:

- $\epsilon_{1,4,5,6} = 0.1$, $\epsilon_2 = 0.2$, $\epsilon_3 = 0.4$

  In this case, the second term is equal to $\sum_{i=1}^{6} \deg(i)/\epsilon_i = 60.0$ resulting in a combined $\mathcal{H}_2 = 30 + \alpha$. Now, consider a different distribution of scaling parameters.

- $\epsilon_{1,3,4,5} = 0.1$, $\epsilon_2 = 0.2$, $\epsilon_6 = 0.4$

  We can see that with agent 3 on a faster time scale, the second term suffers, $\sum_{i=1}^{6} \deg(i)/\epsilon_i = 82.5$, resulting in a comparatively higher performance value of $\mathcal{H}_2 = 41.25 + \alpha$.

Thus, we can see that high-degree nodes operating on slower time scales results in lower $\mathcal{H}_2$ performance, corresponding to better network resilience.

10.2.2 *Timescale Design For $\mathcal{H}_2$ Resilience*

The results of the previous section suggest a heuristic for minimizing the $\mathcal{H}_2$ performance is to identify high degree agents and ensure that they are operating on a slower time scale than the lower degree agents. However, it is not clear from the analysis for tree graphs if this holds in the presence of

cycles. To investigate this, we can note that the minimization of $\mathcal{H}_2(\Sigma)$ can be formulated as a convex problem,

$$\begin{aligned} \min_{\epsilon_1^{-1},\ldots,\epsilon_n^{-1}} \quad & \mathbf{tr}\left(\mathbf{R}X\mathbf{R}^T\right) \\ \text{s.t.} \quad & \frac{1}{\epsilon_{\max}} \leq \frac{1}{\epsilon_{i,l}} \leq \frac{1}{\epsilon_{\min}} \; \forall\, i \in \mathcal{N},\; l \in \{1,\ldots,k\} \\ & \mu_l \leq \sum_{i=1}^{n} \frac{1}{\epsilon_{i,l}} \forall\, l \in \{1,\ldots,k\} \\ & X = \frac{1}{2}\left((\mathbf{R}\mathbf{W}\mathbf{R}^T)^{-1} + \mathcal{L}_{\mathcal{G}^\tau_{e,s}}\right), \end{aligned} \tag{P1}$$

where we have taken the effective variances, σ_ω and σ_v, to be unity. The objective is convex in the optimization variables $(1/\epsilon_{1,1},\ldots,1/\epsilon_{n,k})$, and the constraints are linear. The design parameter of μ_l serves to ensure that not all the agents can operate on the slowest time scale, that is, it can be tuned to ensure that each layer of sub-states in the network has a requisite responsiveness that must be balanced with the desired resilience.

To investigate the effects of cycles on the distribution of time scales that minimizes the $\mathcal{H}_2(\Sigma)$, we generated a random graph for 10 agents (with probability of an edge between any two nodes as 0.15) that features multiple independent cycles. For $\epsilon_{\min} = 0.01$, $\epsilon_{\max} = 2.0$ and $\mu = 510.5$ (which can be interpreted as the value allowing up to half the nodes to be slow), the results and graph topology are presented Figure 10.2. These results (which appear to hold over a wide range of randomly generated graphs) suggest that the presence of cycles do not detract from the heuristic developed for tree graphs - that high degree nodes should be assigned slow time scales (high scaling parameters) to minimize $\mathcal{H}_2(\Sigma)$.

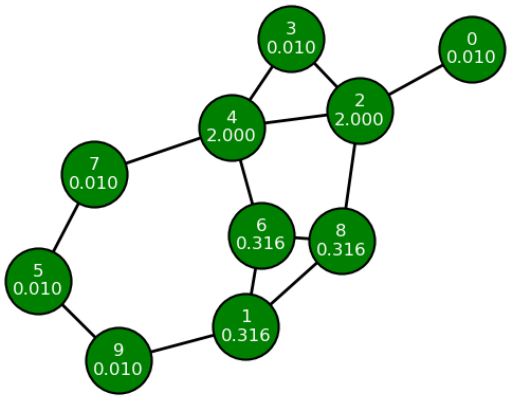

Figure 10.2: Random graph topology for 10 agents. The node number and time scale assigned by (P1) are printed in each node, which shows the slowest time scales are assigned to nodes with highest degree.

What is of further interest is that despite the fact that the time scales present in (P1) manifest through the edge Laplacian of the spanning tree (which may not reflect the degree distribution of the full graph that the heuristic is driven by), the optimal distribution appears to be independent of

the spanning tree chosen. We can see this by generating spanning trees with a variety of degree distributions, such as those in Figures 10.3 and 10.4. Both of these spanning trees generate the distribution presented in Figure. This suggests that the multiplication by $R(\mathcal{G})$ and its transpose in the objective function of (P1) grant the problem information about the full degree distribution of the graph containing the spanning tree. However, we can recall from (10.11) and (10.10) that the $\mathcal{H}_2$ performance for the Σ system can be viewed as the performance for the $\hat{\Sigma}$ system with an additive term that encompasses the contribution of the cycle states. Consider then, the quantity

$$K = \frac{\mathcal{H}_2(\hat{\Sigma}, \mathbf{E})}{\mathcal{H}_2(\Sigma, \mathbf{E})},$$

which is a measure of how well the performance as measured by the spanning tree states represents the graph performance including cycle information. For the spanning tree in Figure we have $K \simeq 0.66$, and for the spanning tree in Figure we have $K \simeq 0.24$. From these ratios we can make two observations pertaining to the performance of networks with cycles and their spanning trees. First, spanning trees that more accurately reflect the true degree distribution of the parent graph will have a higher K. Secondly, it is apparent that a significant portion of the $\mathcal{H}_2$ performance can come from the cycle contributions, so in general the performance of a given spanning tree may not be a good indicator of the full network performance. However, this result is suggestive that for graphs with few cycles, a spanning tree that reproduces the degree distribution of the full graph as closely as possible may be a good approximation for the full network performance.

The time scale assignment problem considered here demonstrates that while the heuristic developed from results on tree graphs appears to hold for more complex graph topologies, the performance of a given spanning tree does not necessarily reflect the performance of the full tree. In the next section, we will consider a reformulation of this problem that allows for a decentralized gradient update for achieving a similar time scale assignment scheme.

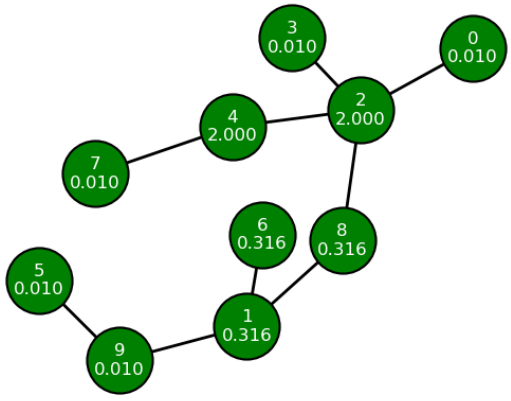

Figure 10.3: Spanning tree of the graph in Figure 10.2 used to calculate the optimal time scale distribution.

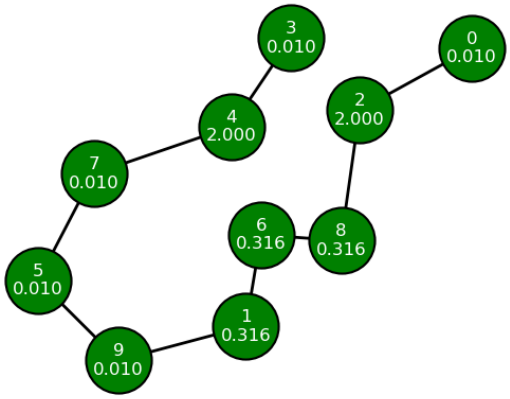

Figure 10.4: Spanning path graph of the graph in Figure 10.2. When used in place of the spanning tree in Figure 10.3, the same distribution of time scales results.

10.2.3 *Decentralized Gradient Updates for Optimal $\mathcal{H}_2$ Performance*

The main goal of this section is to motivate and discuss a decentralized update scheme on the network timescales to optimize the $\mathcal{H}_2$ norm. In cyber-physical systems, a chief concern is preventing system disruption by an antagonist - here, we have been considering this antagonist's choice of weapon to be noise injected into the system. This can take the form of signal jammers, corruption of measurements, GPS spoofing, etc. In response to such a disturbance, it is of interest for the network to be able to quickly, and autonomously, adapt parts of the network to minimize the effect of this influence. Consider Problem (P2),

$$\begin{aligned} \min_{\epsilon_1^{-1},\ldots,\epsilon_n^{-1}} \quad & \mathbf{tr}\left(R^T X R\right) + \frac{h}{2}\|E\|_2^2 \\ \text{s.t.} \quad & \frac{1}{\epsilon_{\max}} \leq \frac{1}{\epsilon_i} \leq \frac{1}{\epsilon_{\min}} \ \forall i \in \mathcal{N} \\ & X = \frac{1}{2} L_{e,s}^{\tau}. \end{aligned} \tag{P2}$$

This is an $\mathcal{H}_2$-norm minimization on the time scale portion of the separated $\mathcal{H}_2$ performance, discussed in §10.2.2. In lieu of the sum constraint $\mu \leq \sum_i \epsilon_i^{-1}$, we introduce a regularization term $2^{-1}h\|E\|_2^2$ which achieves a similar goal of penalizing large timescales which lead to the trivial result of all nodes at the slowest allowable time scale. As we will show below, this regularizer has the added benefit that it will be amenable to a decentralized gradient update scheme to solve Problem (P2).

Proposition 6 (Gradient Update Scheme). *Consider the setting of Problem* (P2). *Then, a decentralized algorithm to solve Problem* (P2) *is given by the projected gradient descent scheme on the solution variables* $\{\epsilon_1^{-1}, \dots, \epsilon_n^{-1}\}$

$$\frac{1}{\epsilon_i^{k+1}} = \text{Proj}_C\left(\frac{1}{\epsilon_i^k} - \frac{1}{h\sqrt{k}}\frac{\partial f}{\partial(\epsilon_i^k)^{-1}}\left(\frac{1}{\epsilon_i^k}\right)\right)$$

$$f\left(\frac{1}{\epsilon_i^k}\right) = \frac{1}{2}\left(\mathbf{tr}\left(R^T L_{e,s}^{\tau} R\right) + h\|E\|_2^2\right) \tag{10.13}$$

$$\frac{\partial f}{\partial(\epsilon_i^k)^{-1}}\left(\frac{1}{\epsilon_i^k}\right) = \left(\frac{\deg(v_i)}{2} - h\left(\epsilon_i^k\right)^3\right), \tag{10.14}$$

where the projection on the constraints C *is simply the projection onto the 'box constraints'* $\epsilon_{\max}^{-1} \le \epsilon_i^{-1} \le \epsilon_{\min}^{-1}$, *and the exponents of* ϵ_i*'s denote the update step.*

Proof. Noting that $E := E(\epsilon_i^k)$, we can write the objective function in Equation (10.13) as

$$f\left(\frac{1}{\epsilon_i^k}\right) = \frac{1}{2}\left(\mathbf{tr}\left(R^T D_\tau^T E^{-1}(\epsilon_i^k) D_\tau R\right) + h\sum_{i=1}^{n}\left(\epsilon_i^k\right)^2\right).$$

A standard matrix calculus identity [123] yields the gradient:

$$\begin{aligned}\frac{\partial f}{\partial(\epsilon_i^k)^{-1}}\left(\frac{1}{\epsilon_i^k}\right) &= \mathbf{tr}\left(DRR^T D^T E^{-1} e_i e_i^T\right) - h\left(\epsilon_i^k\right)^3 \\ &= \left[D_\tau RR^T D_\tau^T\right]_{ii} - h\left(\epsilon_i^k\right)^3.\end{aligned}$$

Next, since $D = D_\tau R$, we have that

$$D_\tau RR^T D_\tau^T = DD^T = L,$$

and so $\left[D_\tau RR^T D_\tau^T\right]_{ii} = L_{ii} = \deg(v_i)$. □

Remark 11. *The gradient update scheme in Proposition 6 is truly decentralized, because the gradient in Equation* (10.14) *only depends on the local node time scale parameter* ϵ_i^k, *and the degree of the* i^{th} *node. Both of these quantities are locally known to the* i^{th} *node at time step* k.

10.2.4 *Decentralized Gradient Updates on Weights for Optimal* $\mathcal{H}_2$ *Performance*

Consider Problem (P3),

$$\begin{aligned}\min_{\{W_i\}_{i=1}^{|\mathcal{E}|}} \ & \mathbf{tr}\left(\mathbf{R}^T(\mathbf{R}\mathbf{W}\mathbf{R}^T)^{-1}\mathbf{R}\right) + \frac{h}{2}\sum_{e\in\mathcal{E}}\mathbf{tr}\left[\mathbf{W}_e^T\mathbf{W}_e\right]^2 \\ \text{s.t. } & W_{\min} \preceq W_e \preceq W_{\max}, \forall e \in \mathcal{E} \\ & W = \text{blkdiag}(W_i).\end{aligned} \tag{P3}$$

Proposition 7 (Gradient Update for Edge Weights). *The gradient of the cost function with respect to the edge weight W_e in Problem (P3) is given by*

$$\nabla_{W_e} f[H] = -\text{deblk}_e^k \left[Q^T Q\right] + hW_e,$$

where $\text{deblk}_e^k[Q^T Q]$ *is the* e*th* $k \times k$ *diagonal block of* $Q^T Q$*, and* Q *is given by*

$$\begin{aligned} Q &= \mathbf{R}^T \left(\mathbf{R}\mathbf{W}_H^c \mathbf{R}^T\right)^{-1} R \\ \mathbf{W}_H^c &= \text{blk}_c^k(H) + \sum_{l \in \mathcal{E}\setminus c} \text{blk}_l^k(W_l), \end{aligned}$$

where

$$\text{blk}_c^k(H) = \mathbf{e}_c H \mathbf{e}_c^T = (e_c \otimes I_k)\, H \left(e_c^T \otimes I_k\right)$$

denotes the $kn \times kn$ *matrix with* H *on the* c*th* $k \times k$ *diagonal block, with zeros otherwise.*

A gradient update scheme for solving Problem (P3) is therefore

$$\begin{aligned} W_e^{k+1} &= W_e^k - \frac{1}{h\sqrt{k}} \nabla_{W_e} f[H] \\ &= W_e^k - \frac{1}{h\sqrt{k}} \left(hW_e - \text{deblk}_e^k \left[Q^T Q\right]\right). \end{aligned}$$

Proof. We first identify the gradient of the cost function with respect to W_c, the weight on the cth edge in $\mathcal{E}$. To this end, consider the functions

$$\begin{aligned} f(X) &= \mathbf{R} \left[\mathbf{e}_c X \mathbf{e}_c^T + \sum_{l \in \mathcal{E}\setminus c} \mathbf{e}_l W_l \mathbf{e}_l^T\right] \mathbf{R}^T \\ &= \mathbf{R} \left[\text{blk}_c^k(X) + \sum_{l \in \mathcal{E}\setminus c} \text{blk}_c^k(W_l)\right] \mathbf{R}^T \\ g(X) &= X^{-1} \\ h(X) &= \mathbf{tr}\left[\mathbf{R}^T X \mathbf{R}\right]. \end{aligned}$$

where

$$\text{blk}_l^k(W_l) = \mathbf{e}_l W_l \mathbf{e}_l^T = (e_l \otimes I_k)\, W_l \left(e_l^T \otimes I_k\right)$$

denotes the $kn \times kn$ matrix with W_l on the lth $k \times k$ diagonal block, with zeros otherwise. Then, the cost function with W_c as the argument, is given by

$$\text{tr}\left[\mathbf{R}^T \left(\mathbf{R}\mathbf{W}\mathbf{R}^T\right)^{-1} \mathbf{R}\right] = (h \circ g \circ f)\,(W_c).$$

These functions have differentials

$$\begin{aligned} df_X[H] &= \mathbf{R}\left[\mathrm{blk}_c^k(H)\right]\mathbf{R}^T \\ dg_X[H] &= -X^{-1}HX^{-1} \\ dh_X[H] &= \mathrm{tr}\left[\mathbf{R}^T H\mathbf{R}\right]. \end{aligned}$$

By the chain rule, we have that

$$\begin{aligned} d(g\circ f)_X[H] &= -Y^{-1}\mathbf{R}\mathrm{blk}_c^k(H)\mathbf{R}^T Y^{-1} \\ Y \triangleq f[H] &= \mathbf{R}\left[\mathrm{blk}_c^k(H) + \sum_{l\in\mathcal{E}\setminus c}\mathrm{blk}_l^k(W_l)\right]\mathbf{R}^T \\ &\triangleq \mathbf{R}\mathbf{W}_H^c\mathbf{R}^T, \end{aligned}$$

and so

$$d(g\circ f)_X[H] = -\left(\mathbf{R}\mathbf{W}_H^c\mathbf{R}^T\right)^{-1}\mathbf{R}\mathrm{blk}_c^k(H)\mathbf{R}^T\left(\mathbf{R}\mathbf{W}_H^c\mathbf{R}^T\right)^{-1}.$$

Similarly, we have

$$\begin{aligned} d(h\circ g\circ f)_X[H] &= -\mathrm{tr}\left[Q\mathrm{blk}_k^c(H)Q^T\right] \\ Q &\triangleq \mathbf{R}^T\left(\mathbf{R}\mathbf{W}_H^c\mathbf{R}^T\right)\mathbf{R}. \end{aligned}$$

Hence, we can write

$$\begin{aligned} d(h\circ g\circ f)_X[H] &= -\mathrm{tr}\left[Q\mathrm{blk}_k^c(H)Q^T\right] \\ &= -\mathrm{tr}\left[Q\mathbf{e}_c H\mathbf{e}_c^T Q^T\right] \\ &= -\mathrm{tr}\left[\mathbf{e}_c^T Q^T Q\mathbf{e}_c H\right] \\ &= \left\langle -\mathbf{e}_c^T Q^T Q\mathbf{e}_c, H\right\rangle, \end{aligned}$$

and so the gradient of the cost function with respect to the cth weight W_c is identified as the cth $k\times k$ diagonal block of $-Q^TQ$.

□

11

EXAMPLE: FLOCKING VIA SECOND-ORDER CONSENSUS

Flocking is a behaviour exhibited by certain multi-agent systems that are coordinating their motion into a cohesive formation, for example birds or stampeding buffalo. A consensus-type algorithm can be proposed that allows a system of n agents to agree on their velocity vector while maintaining a separation from their neighbours [75].

11.0.1 *Scalar State Case*

Consider the protocol

$$\epsilon_i \ddot{x}_i = -\sum_{j \in \mathcal{N}(i)} w_{ij}(x_i - x_j - d) - \sum_{j \in \mathcal{N}(i)} w_{ij}(\dot{x}_i - \dot{x}_j).$$

This is double-integrator consensus model that seeks to achieve a separation of distance d between neighbours i and j, as well as consensus on the velocity $\dot{x}_i$ and $\dot{x}_j$. In matrix form with disturbances and no constant separation input, this protocol is given by

$$\begin{bmatrix} \dot{x} \\ E\ddot{x} \end{bmatrix} = \begin{bmatrix} \mathbf{0} & I \\ -\mathcal{L}_{\mathcal{G}w} & -\mathcal{L}_{\mathcal{G}w} \end{bmatrix} \begin{bmatrix} x \\ \dot{x} \end{bmatrix} + \begin{bmatrix} \mathbf{0} & \mathbf{0} \\ I & -D_{\mathcal{G}} \end{bmatrix} \begin{bmatrix} \omega \\ v \end{bmatrix}.$$

As before, we take the covariance of ω to be $\Omega = \sigma_\omega E^{1/2}$ and the covariance of v to be $\Gamma = \sigma_v W^{1/2}$. We can examine the equivalent double-integrator edge consensus model.

Theorem 31. *The double-integrator edge consensus model is given by*

$$\begin{bmatrix} \dot{x}_e \\ \ddot{x}_e \end{bmatrix} = \begin{bmatrix} \mathbf{0} & 0 & I & \\ -\mathcal{L}_{\mathcal{G}e} RWR^T & \mathbf{0} & -\mathcal{L}_{\mathcal{G}e} RWR^T & \mathbf{0} \\ \mathbf{0} & 0 & \mathbf{0} & 0 \end{bmatrix} \begin{bmatrix} x_e \\ \dot{x}_e \end{bmatrix} + \begin{bmatrix} \mathbf{0} & \mathbf{0} \\ D_\tau^T E^{-1} & -\mathcal{L}_{\mathcal{G}e} R \\ \nu^{-1} \mathrm{diag}(E)^T & 0 \end{bmatrix} \begin{bmatrix} w \\ v \end{bmatrix},$$

and so the double-integrator consensus on the edge states of the chosen spanning tree τ is given by

$$\begin{bmatrix}\dot{x}_\tau \\ \ddot{x}_\tau\end{bmatrix} = \begin{bmatrix}\mathbf{0} & I \\ -\mathcal{L}_{\mathcal{G}_e} RWR^T & -\mathcal{L}_{\mathcal{G}_e} RWR^T\end{bmatrix}\begin{bmatrix}x_\tau \\ \dot{x}_\tau\end{bmatrix} + \begin{bmatrix}\mathbf{0} & \mathbf{0} \\ D_\tau^T & -\mathcal{L}_{\mathcal{G}_e} R\end{bmatrix}\begin{bmatrix}\omega \\ v\end{bmatrix}.$$

Proof. Applying the coordinate transform $x_e = S_v x$ and following a similar calculation as in Theorem 30 yields the result. □

We can also explicitly compute the form of the $\mathcal{H}_2$ norm for the double-integrator consensus.

Theorem 32. *The controllability gramian for the time scaled double-integrator consensus is given by*

$$\begin{aligned} X^* &= \frac{1}{2}\begin{bmatrix}X_1 & \mathbf{0} \\ \mathbf{0} & X_2\end{bmatrix} \\ X_1 &= \sigma_w^2\left[\left(RWR^T\right)^{-1}\mathcal{L}_{\mathcal{G}_e}^{-1}\left(RWR^T\right)^{-1}\right] + \sigma_v^2\left(RWR^T\right)^{-1} \\ X_2 &= \sigma_w^2\left(RWR^T\right)^{-1} + \sigma_v^2\mathcal{L}_{\mathcal{G}_e}. \end{aligned}$$

Furthermore, the blocks X_1, X_2 of X^* correspond to the position and velocity states, respectively. Hence, one can consider the $\mathcal{H}_2$ performance of the position and velocity states separately or aggregately by examining the $\mathcal{H}_2$ norms

$$\begin{aligned} {\mathcal{H}_2}^{(1)} &= \frac{1}{2}\mathbf{tr}\left[R^T X_1 R\right],\ {\mathcal{H}_2}^{(2)} = \frac{1}{2}\mathbf{tr}\left[R^T X_2 R\right] \\ {\mathcal{H}_2}^{(1)} &= \frac{1}{2}\mathbf{tr}\left[R^T(X_1 + X_2)R\right]. \end{aligned}$$

Proof. From the dynamics (9.3), the controllablity gramian is given by the positive semi-definite solution to the Lyapunov equation

$$AX^* + X^*A^T + BB^T = \mathbf{0},$$

where X^*, A, BB^T are given by

$$\begin{aligned} A &= \begin{bmatrix}\mathbf{0} & I \\ -\mathcal{L}_{\mathcal{G}_e} RWR^T & -\mathcal{L}_{\mathcal{G}_e} RWR^T\end{bmatrix} \\ BB^T &= \begin{bmatrix}\mathbf{0} & \mathbf{0} \\ \mathbf{0} & \sigma_w^2\mathcal{L}_{\mathcal{G}_e} + \sigma_v^2\mathcal{L}_{\mathcal{G}_e} RR^T\mathcal{L}_{\mathcal{G}_e}\end{bmatrix} \\ X^* &= \begin{bmatrix}X_1 & X_3 \\ X_3 & X_2.\end{bmatrix} \end{aligned}$$

Solving Equation (9.1) yields

$$\begin{aligned} X_3 &= \mathbf{0} \\ X_2 &= \sigma_w^2 \left(RWR^T\right)^{-1} + \sigma_v^2 \mathcal{L}_{\mathcal{G}_e} \\ X_2 &= X_1 RWR^T \mathcal{L}_{\mathcal{G}_e}, \end{aligned}$$

and solving for X_1 in the last display yields

$$X_1 = \sigma_w^2 \left[\left(RWR^T\right)^{-1} \mathcal{L}_{\mathcal{G}_e}^{-1} \left(RWR^T\right)^{-1} \right] + \sigma_v^2 \left(RWR^T\right)^{-1}.$$

To measure the position, velocity, or both states for consideration in the $\mathcal{H}_2$ norm, one can choose the observation matrices

$$\begin{bmatrix} R^T & \mathbf{0} \end{bmatrix}, \begin{bmatrix} \mathbf{0} & R^T \end{bmatrix}, \begin{bmatrix} R^T & \mathbf{0} \\ \mathbf{0} & R^T \end{bmatrix}$$

respectively. □

11.0.2 *Matrix-Valued Double Integrator Consensus*

In the case of vector-valued states, we can write the dynamics as

$$\begin{bmatrix} \dot{\mathbf{x}} \\ \mathbf{E}\ddot{\mathbf{x}} \end{bmatrix} = \begin{bmatrix} \mathbf{0} & I \\ -\mathcal{L}_{\mathcal{G}_w} & -\mathcal{L}_{\mathcal{G}_w} \end{bmatrix} \begin{bmatrix} \mathbf{x} \\ \dot{\mathbf{x}} \end{bmatrix} + \begin{bmatrix} \mathbf{0} & \mathbf{0} \\ I & -\mathbf{D}_{\mathcal{G}} \end{bmatrix} \begin{bmatrix} \omega \\ v \end{bmatrix}.$$

Theorem 33. *The double-integrator edge consensus model is given by*

$$\begin{aligned} \begin{bmatrix} \dot{\mathbf{x}}_e \\ \ddot{\mathbf{x}}_e \end{bmatrix} &= \begin{bmatrix} \mathbf{0} & 0 & I & \\ -\mathcal{L}_{\mathcal{G}_e}\mathbf{R}\mathbf{W}\mathbf{R}^T & \mathbf{0} & -\mathcal{L}_{\mathcal{G}_e}\mathbf{R}\mathbf{W}\mathbf{R}^T & \mathbf{0} \\ \mathbf{0} & 0 & \mathbf{0} & 0 \end{bmatrix} \begin{bmatrix} \mathbf{x}_e \\ \dot{\mathbf{x}}_e \end{bmatrix} \\ &\quad + \begin{bmatrix} \mathbf{0} & \mathbf{0} \\ \mathbf{D}_\tau^T \mathbf{E}^{-1} & -\mathcal{L}_{\mathcal{G}_e}\mathbf{R} \\ \Xi^{-1} \mathbb{K}^T & \mathbf{0} \end{bmatrix} \begin{bmatrix} \omega \\ v \end{bmatrix}, \end{aligned}$$

and so the double-integrator consensus on the edge states of the chosen spanning tree τ is given by

$$\begin{aligned} \begin{bmatrix} \dot{\mathbf{x}}_\tau \\ \ddot{\mathbf{x}}_\tau \end{bmatrix} &= \begin{bmatrix} \mathbf{0} & I \\ -\mathcal{L}_{\mathcal{G}_e}\mathbf{R}\mathbf{W}\mathbf{R}^T & -\mathcal{L}_{\mathcal{G}_e}\mathbf{R}\mathbf{W}\mathbf{R}^T \end{bmatrix} \begin{bmatrix} \mathbf{x}_\tau \\ \dot{\mathbf{x}}_\tau \end{bmatrix} \\ &\quad + \begin{bmatrix} \mathbf{0} & \mathbf{0} \\ \mathbf{D}_\tau^T & -\mathcal{L}_{\mathcal{G}_e}\mathbf{R} \end{bmatrix} \begin{bmatrix} \omega \\ v \end{bmatrix}. \end{aligned}$$

Proof. Appling the coordinate transform $\mathbf{x}_e = S_v \mathbf{x}$ and following a similar calculation as in Theorem 30 yields the result. □

We can also explicitly compute the form of the $\mathcal{H}_2$ norm for the matrix-weighted double-integrator consensus.

Theorem 34. *The controllability gramian for the time scaled double-integrator consensus is given by*

$$\begin{aligned}
\mathbf{X}^* &= \frac{1}{2}\begin{bmatrix} \mathbf{X}_1 & \mathbf{0} \\ \mathbf{0} & \mathbf{X}_2 \end{bmatrix} \\
\mathbf{X}_1 &= \sigma_w^2 \left[\left(\mathbf{R}\mathbf{W}\mathbf{R}^T\right)^{-1} \mathcal{L}_{\mathcal{G}_e}^{-1} \left(\mathbf{R}\mathbf{W}\mathbf{R}^T\right)^{-1} \right] + \sigma_v^2 \left(\mathbf{R}\mathbf{W}\mathbf{R}^T\right)^{-1} \\
\mathbf{X}_2 &= \sigma_w^2 \left(\mathbf{R}\mathbf{W}\mathbf{R}^T\right)^{-1} + \sigma_v^2 \mathcal{L}_{\mathcal{G}_e}.
\end{aligned}$$

Furthermore, the blocks $\mathbf{X}_1, \mathbf{X}_2$ of $\mathbf{X}^*$ correspond to the position and velocity states, respectively. Hence, one can consider the $\mathcal{H}_2$ performance of the position and velocity states separately or aggregately by examining the $\mathcal{H}_2$ norms

$$\begin{aligned}
{\mathcal{H}_2}^{(1)} = \frac{1}{2}\mathbf{tr}\left[\mathbf{R}^T\mathbf{X}_1\mathbf{R}\right], \; {\mathcal{H}_2}^{(2)} = \frac{1}{2}\mathbf{tr}\left[\mathbf{R}^T\mathbf{X}_2\mathbf{R}\right] \\
{\mathcal{H}_2}^{(1)} = \frac{1}{2}\mathbf{tr}\left[\mathbf{R}^T(\mathbf{X}_1+\mathbf{X}_2)\mathbf{R}\right].
\end{aligned}$$

Proof. From the dynamics (9.9), the controllablity gramian is given by the positive semi-definite solution to the Lyapunov equation

$$A\mathbf{X}^* + \mathbf{X}^*A^T + BB^T = \mathbf{0},$$

where $\mathbf{X}^*, A, BB^T$ are given by

$$\begin{aligned}
A &= \begin{bmatrix} \mathbf{0} & I \\ -\mathcal{L}_{\mathcal{G}_e}\mathbf{R}\mathbf{W}\mathbf{R}^T & -\mathcal{L}_{\mathcal{G}_e}\mathbf{R}\mathbf{W}\mathbf{R}^T \end{bmatrix} \\
BB^T &= \begin{bmatrix} \mathbf{0} & \mathbf{0} \\ \mathbf{0} & \sigma_w^2\mathcal{L}_{\mathcal{G}_e} + \sigma_v^2\mathcal{L}_{\mathcal{G}_e}\mathbf{R}\mathbf{R}^T\mathcal{L}_{\mathcal{G}_e} \end{bmatrix} \\
\mathbf{X}^* &= \begin{bmatrix} \mathbf{X}_1 & \mathbf{X}_3 \\ \mathbf{X}_3 & \mathbf{X}_2. \end{bmatrix}
\end{aligned}$$

Solving Equation (9.4) yields

$$\begin{aligned}
\mathbf{X}_3 &= \mathbf{0} \\
\mathbf{X}_2 &= \sigma_w^2 \left(\mathbf{R}\mathbf{W}\mathbf{R}^T\right)^{-1} + \sigma_v^2\mathcal{L}_{\mathcal{G}_e} \\
\mathbf{X}_2 &= \mathbf{X}_1\mathbf{R}\mathbf{W}\mathbf{R}^T\mathcal{L}_{\mathcal{G}_e},
\end{aligned}$$

and solving for $\mathbf{X}_1$ in the last display yields

$$\mathbf{X}_1 = \sigma_w^2 \left[\left(\mathbf{R}\mathbf{W}\mathbf{R}^T\right)^{-1} \mathcal{L}_{\mathcal{G}_e}^{-1} \left(\mathbf{R}\mathbf{W}\mathbf{R}^T\right)^{-1} \right] + \sigma_v^2 \left(\mathbf{R}\mathbf{W}\mathbf{R}^T\right)^{-1}.$$

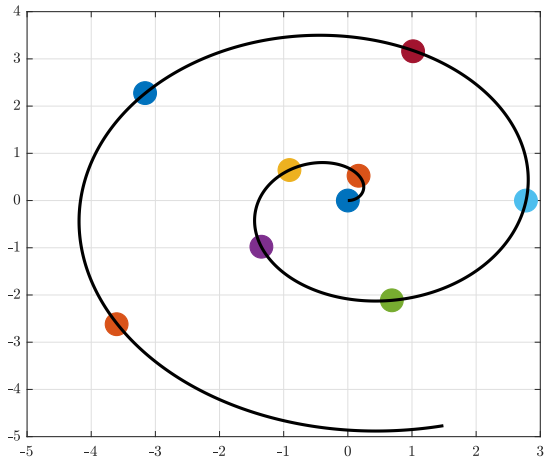

Figure 11.1: Relative formation of the agents, defined by discrete points on a spiral

To measure the position, velocity, or both states for consideration in the $\mathcal{H}_2$ norm, one can choose the observation matrices

$$\begin{bmatrix} \mathbf{R}^T & \mathbf{0} \end{bmatrix}, \begin{bmatrix} \mathbf{0} & \mathbf{R}^T \end{bmatrix}, \begin{bmatrix} \mathbf{R}^T & \mathbf{0} \\ \mathbf{0} & \mathbf{R}^T \end{bmatrix}$$

respectively. □

11.0.3 *Numerical Example*

The weight update scheme applied to the second-order consensus problem was implemented numerically. The task assigned to the agents was to use the second-order consensus protocol to achieve the formation shown in Figure 11.1 – a formation assigned by sampling discrete points on a 2D spiral.

Consensus on the formation is achieved by the second-order protocol with a constant signal $\mathbf{d}$ specifying the position in the formation:

$$\ddot{\mathbf{x}}_i = -\sum_{j \in \mathcal{N}(i)} \mathbf{W}_{ij}(\mathbf{x}_i - \mathbf{x}_j - \mathbf{d}) - \sum_{j \in \mathcal{N}(i)} \mathbf{W}_{ij}(\dot{\mathbf{x}}_i - \dot{\mathbf{x}}_j).$$

Since this is a constant signal, the $\mathcal{H}_2$ performance of the edge states remains the same as in the previous section.

The initial selection of weights was chosen at random using the generator

$$W_{\{i,j\}} = \alpha \left[\frac{G_{\{i,j\}} + G_{\{i,j\}}^T}{2} + 2I_2 \right]$$

where $G_{\{i,j\}}$ is a 2×2 matrix with entries distributed according to a zero-mean standard Gaussian, and $\alpha = 0.3$ was chosen arbitrarily to yield a suboptimal initial selection of weights. The upper and lower bounds on the weights were chosen with the same generator in Equation (9.7), but with $\alpha_l = 0.05$ and $\alpha_u = 10$. The penalty parameter was chosen as $h = 0.01$.

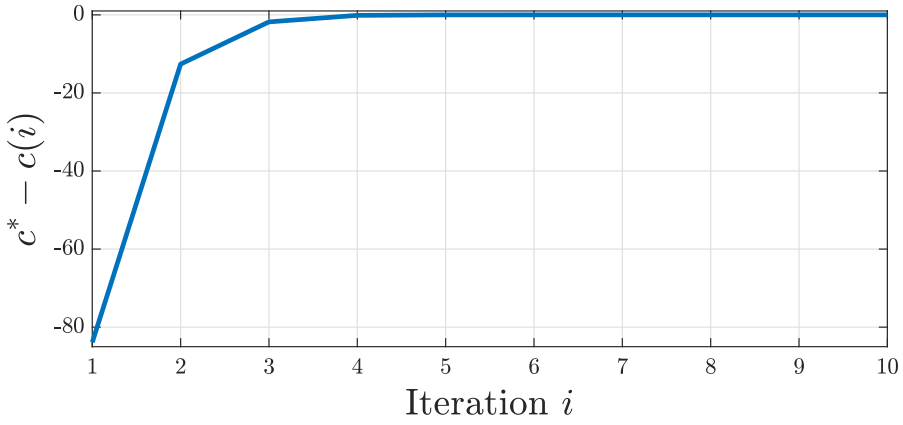

Figure 11.2: Cost of weight selection versus iteration

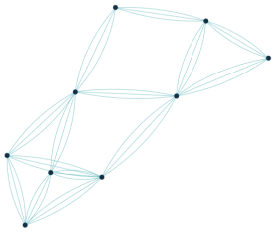

Figure 11.3: Visualization of edge weights at $k = 1$

The gradient descent algorithm from Proposition 7 converges in a few iterations, as shown in Figure 11.2, and intermediate graph weights are visualized in Figure 11.7. The 3 independent parameters of each weight are here visualized as 3 edges in a multigraph. None of the optimal edge weights saturated the upper and lower bounds in this setup.

These weights were then used in a simulation of the dynamics in Equation (9.11) over a time span of 30 seconds. At $10 \leq t \leq 20$, the formation is subject to a 'gust' of noise on the edges and self-dynamics of covariance $\sigma_w^2 I$ and $\sigma_v^2 \mathbf{W}$, with $\sigma_v = \sigma_w = 5$. In one simulation, no weight update was performed, and in the other, the updated weights were used during the wind gust. The edge states are shown in Figure 11.8, and the variance away from the consensus value $x_e(t_f)$

$$\mathrm{Var}[x_e(t)] := \left[x_e(t) - x_e(t_f)\right]^2$$

is shown in Figure 11.9. The updated weights clearly outperform the initial, suboptimal choice of weights

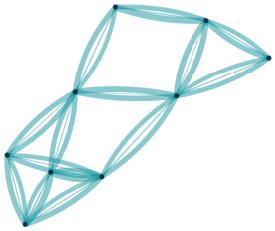

Figure 11.4: Visualization of edge weights at $k = 2$

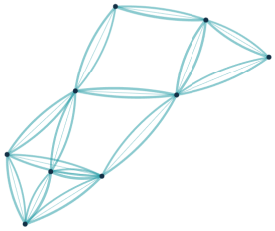

Figure 11.5: Visualization of edge weights at $k = 3$

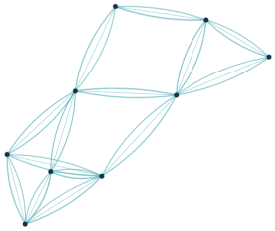

Figure 11.6: Visualization of edge weights at $k = 4$

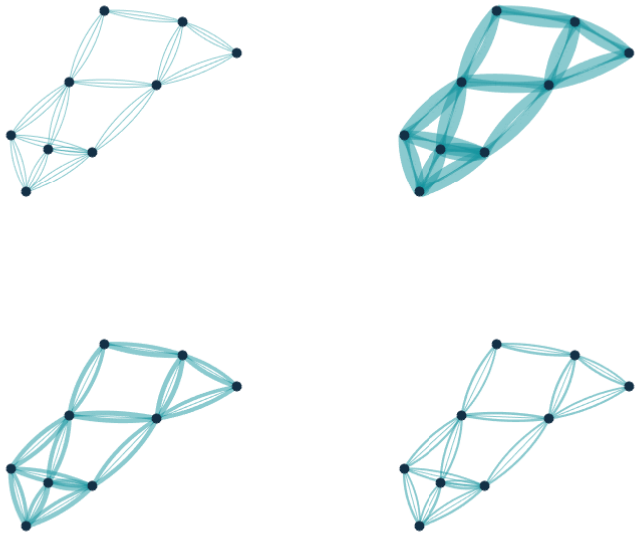

Figure 11.7: Visualization of edge weights over iterations $k = 1$ (top left), 2 (top right), 3 (bottom left) & 4 (bottom right). Each of the 3 independent parameters of the 2×2 matrix-valued weight is visualized in a multigraph.

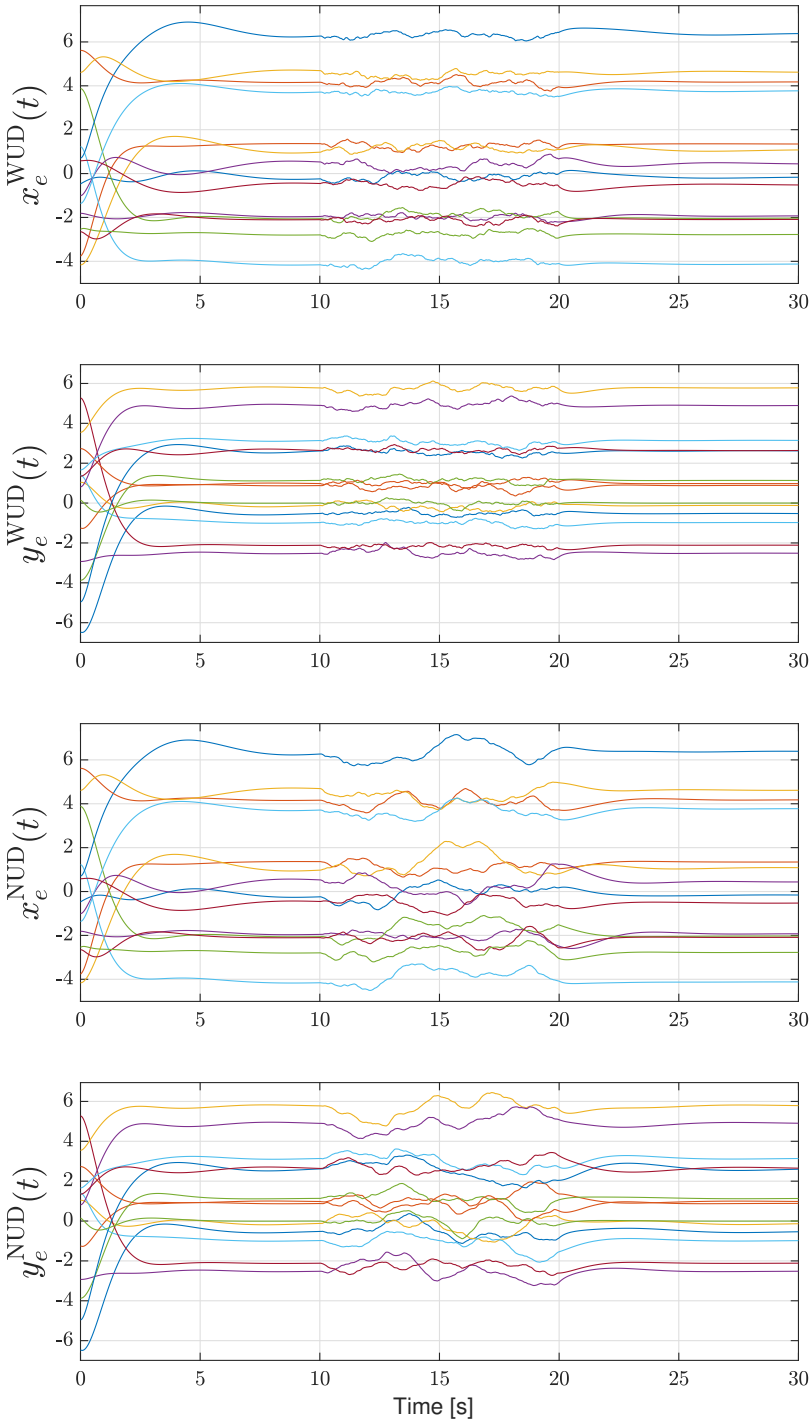

Figure 11.8: Edge states over time subjected to gust at $10 \leq t \leq 20$; top two plots are the edge states in the x, y directions respectively with the weight update, and the bottom two plots are the edge states in the x, y directions respectively with no weight update.

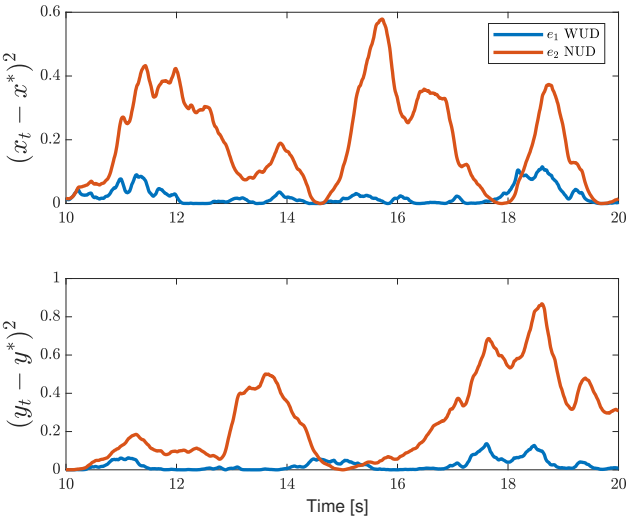

Figure 11.9: Variance from consensus for a representative edge $[x_e(t) - x_e(t_f)]^2$ for the case with the weight update and without.

12 NETWORK ENTROPY

12.1 INTRODUCTION

Networked dynamic systems are ubiquitous in many areas of engineering, and one can argue that they are of paramount importance for understanding complex phenomena in a wide range of disciplines including sociology (social networks [124], physics (quantum networks [125], [126]), and biology (gene networks [127]).

As such, there has been a surge of research activities in distinct scientific areas with two fundamental questions at their core. Firstly, what is the role of the network and its structure in characterizing the behavior that these networked systems exhibit? Secondly, to what extent can this structure be used for the purpose of control?

Furthermore, it is desired to provide such a characterization with an eye towards large networks. Some of the such open problems are: to what extent can these characterizations be done efficiently as the number of nodes and edges in the network grow? Do the computational requirements corresponding to this characterization depend on the local network structure? Does the study of system measures lead to a conceptual framework to examine dynamic networks and their system theoretic properties [66]?

In this chapter, we highlight the importance of two measures associated with the network that we believe have not been examined more thoroughly in the context of their system theoretic significance. These measures quantify a notion of "information content" in the network- and as such, they are referred to as the loop entropy and the Kolmogorov-Sinai (KS) entropy. Both measures have been extensively employed in the physics literature-however, we believe they should be more systematically studied in the networked dynamic systems due to their inherent connections with basic system theory of networks; a related work in this direction include that of Siami and Motee [72].

The contribution of the chapter is twofold. First, we examine the connection between loop entropy and noise propagation properties of networks. The loop entropy is defined separately for both the structure of the network, as well as for how the dynamics respond to a noise input. We show in Section 12.3 that these entropies are the same for the consensus dynamics. Secondly, we consider the KS entropy in Section 12.4 in the context of networks evolving via their adjacency matrix. Some examples of entropies are given in Section 12.5.

12.2 NETWORK MODEL

In this section, we provide the necessary background on the underlying model that will be considered in this chapter.

12.2.1 *Mathematical Notation and Graph Theory*

The identity matrix is defined as I and e_i is the column vector with all zeros except a 1 in the ith position. A symmetric matrix A is *positive semi definite* if for all $v \in \mathbb{R}^n$, $v^T A v \geq 0$. The *positive semi-definite ordering* is defined on two symmetric matrices A, B such that $A \succeq B$ if $A - B$ is positive semi-definite. The matrix $A^{\{n-1\}}$ is a matrix constructed from A by removing the first row and column.

The fundamental algebraic structure that represents a network is the graph $\mathcal{G}(V, E, W)$ with a vertex set V of cardinality $|V| = n$, an edge set E of cardinality $|E| = m$, and a set of weights W on the edges. The edge set consists of pairs of vertices i and j that are called *adjacent* if $\{i, j\} \in E \subseteq V^2$, and this edge has weight $w_{ij} \in W_{\mathcal{G}}$. The number of adjacent nodes to node i is called the *degree*, and is denoted by d_i. The *degree matrix* is denoted as $\Delta = \text{Diag}(d_i)$. The weights define an $m \times m$ *weight matrix* $W_{\mathcal{G}}$ with the lth edge $\{i, j\}$ having weight w_{ij} on the diagonal entry $(W_{\mathcal{G}})_{ll}$. The *adjacency matrix* A is defined such that a_{ij} has weight w_{ij} if there is an edge $\{i, j\}$ and 0 otherwise. The *graph Laplacian* $\mathcal{L}_{\mathcal{G}}$ is given by $\Delta - A$.

The graph is said to be *connected* if there exists a path of edges from every node to every other node. The graph Laplacian is a positive semi-definite matrix, and the multiplicity of the zero eigenvalue denotes the number of connected components of the graph. The eigenvalues of the Laplacian are ordered such that $0 = \lambda_1 \leq \cdots \leq \lambda_n$. Similary, we order the eigenvalues of the adjacency matrix such that $\mu_1 \leq \cdots \leq \mu_n$.

12.2.2 *Network Models*

In this chapter, we consider we consider four models. The first is the *controlled consensus dynamics* [5]:

$$\dot{x} = -\mathcal{L}_{\mathcal{G}} x(t) + Bu(t) + G\omega(t), \tag{12.1}$$

where $\omega(t)$ is a zero-mean Gaussian random vector depicting a random disturbance to the network, $x(t)$ is the states of the nodes of the network, and $u(t)$ is the control input. For compactness of presentation, the time t indication on the states will be henceforth removed.

The *single integrator leader-follower dynamics* can be interpreted as a leader agent x_l which provides an input signal to the set of follower agents x_f via their adjacent edges. This allows the graph Laplacian to be partitioned into two sub-Laplacians for the leaders and followers:

$$\mathcal{L}_{\mathcal{G}} = \left[\begin{array}{c|c} a & -B_{\mathcal{G}}^T \\ \hline -B_{\mathcal{G}} & \mathcal{A}_{\mathcal{G}} \end{array}\right] \tag{12.2}$$

with a perturbation matrix $B_{\mathcal{G}}$ encoding the connections between the leader and the followers:

$$\dot{x}_f = -\mathcal{A}_{\mathcal{G}} x_f + B_{\mathcal{G}} u + G\omega. \tag{12.3}$$

Here we take $G = I$.[1] The matrix $\mathcal{A}_{\mathcal{G}}$ is known as the Dirichlet matrix, or grounded Laplacian [128], [129]. It has the property of being strictly positive definite when the graph is connected, and hence is invertible unlike the original Laplacian $\mathcal{L}_{\mathcal{G}}$.

Similarly, we can define the *double integrator dynamics* as,

$$\begin{aligned}\begin{bmatrix} \dot{x}_f \\ \ddot{x}_f \end{bmatrix} &= \begin{bmatrix} 0 & I \\ -\mathcal{A}_{\mathcal{G}} & -\mathcal{A}_{\mathcal{G}} \end{bmatrix} \begin{bmatrix} x_f \\ \dot{x}_f \end{bmatrix} + \begin{bmatrix} 0 \\ B_{\mathcal{G}} \end{bmatrix} u + \begin{bmatrix} 0 \\ G \end{bmatrix} \omega \\ &:= -\bar{\mathcal{A}}_{\mathcal{G}} \begin{bmatrix} x_f \\ \dot{x}_f \end{bmatrix} + \bar{B}_{\mathcal{G}} u + \bar{G}\omega \end{aligned} \tag{12.4}$$

The *controlled adjacency dynamics* are given by

$$\dot{x} = Ax + Bu. \tag{12.5}$$

There has been a large body of work centered around finding connections between network structure and the system properties of the corresponding networked system. For example, it has been shown that symmetry structures in the graph topology undermine the controllability of the network [17]. Various notions of robustness measures have been introduced in an effort to describe the performance of networks, such as the convergence time $\tau = 1/\lambda_2$, and the utility of these measures often depends on the network topology [5], [66].

One quantity that captures system behavior with relation to system topology in other fields of science is that of entropy. Fundamentally, entropy is a measure that captures the randomness or disorder of a system. For example, a polymer can be modeled as a vector random walk where each iteration of the walk adds a monomer of some small length from tip-to-tail of the previous iteration [130]. If the polymer is extremely straight, its 'disorder' is very low and hence the entropy is small. On the other hand, a very disordered or loopy polymer has high entropy. The entropy of a polymer has a direct analytical effect on the dynamics of how the polymer behaves and evolves in a fluid at some temperature. In this chapter, we explore two notions of entropy defined for a network, and show that for the leader-follower dynamics we can indeed link the topological disorder to control-theoretic properties of the network.

12.3 LOOP ENTROPY AND SPANNING TREES

In this section, we define the standard notion for the entropy of a network. Using a well-known result by Kirchoff, we show that this notion of entropy is related to the number of spanning trees in the graph representing the Laplacian. Although a similar line of inquiry has been pursued in [72] (for a different notion of entropy) and [5], there are several interpretations of this result with respect to leader-follower dynamics that have not been explored in the literature.

1 This can be done without loss of generality since if G is non-identity, the effect of multiplying it with ω can be propagated into the covariance of the noise of ω.

Definition 6. *The* entropy *of a network $\mathcal{G}$ is given by the sum $S_{\mathcal{G}} = \sum_{i=2}^{n} \log \lambda_i$.*

The non-zero eigenvalues of $\mathcal{L}_{\mathcal{G}}$ are related to those of a submatrix $L_{\mathcal{G}}^{\{n-1\}}$ of $\mathcal{L}_{\mathcal{G}}$. For clarity, we will refrain from connecting $L_{\mathcal{G}}^{\{n-1\}}$ to $\mathcal{A}_{\mathcal{G}}$ as seen in the partition in (12.2) until we complete the exposition of the properties of $S_{\mathcal{G}}$. We will make this connection at the end of the section. The matrix $L_{\mathcal{G}}^{\{n-1\}}$ is constructed by removing an arbitrary ith row and column of $\mathcal{L}_{\mathcal{G}}$. The eigenvalues of $L_{\mathcal{G}}^{\{n-1\}}$ are strictly positive, and satisfy:

$$\begin{aligned}\frac{1}{n}\lambda_2(L_{\mathcal{G}}) \cdots \lambda_n(L_{\mathcal{G}}) &= \det L_{\mathcal{G}}^{\{n-1\}} \\ &= \lambda_1(L_{\mathcal{G}}^{\{n-1\}}) \cdots \lambda_{n-1}(L_{\mathcal{G}}^{\{n-1\}}).\end{aligned}$$

It is important to note that the eigenvalues of $L_{\mathcal{G}}^{\{n-1\}}$ are all positive because it is a Dirichlet matrix (or grounded Laplacian) of $\mathcal{L}_{\mathcal{G}}$. It should now be clear that

$$S_{\mathcal{G}} = \sum_{i=2}^{n} \log \lambda_i(L_{\mathcal{G}}) = \sum_{i=1}^{n-1} \log \lambda_i(L_{\mathcal{G}}^{\{n-1\}}) + \log n.$$

We can connect this definition to a well-known result by Kirchoff. First, recall that a *tree* is a connected undirected graph with no cycles. Furthermore, a *spanning tree* of a graph $\mathcal{G}$ is a tree containing every vertex of $\mathcal{G}$. Let $\tau(\mathcal{G})$ denote the number of unique spanning trees of $\mathcal{G}$. A well-known result by Kirchoff states that the $\det L_{\mathcal{G}}^{\{n-1\}} = \tau(\mathcal{G})$. The following observation is thus immediate.

Theorem 35. *Let $L_{\mathcal{G}}$ be the unweighted network Laplacian for the consensus dynamics. The network entropy is given by $S_{\mathcal{G}} = \log(n\tau(\mathcal{G}))$.*

Theorem 35 motivates a new paradigm in terms of interpreting the entropy measure of a networked system. We can now begin to view the entropy as being a fundamentally topological quantity. This formulation of entropy also has a very elegant analogy to Boltzmann entropy in statistical physics. Boltzmann defined the entropy of a physical system, say a gas, to be $S = k_b \log W_s$ where W_s is the number of microstates of the physical system and k_b is a constant [131]. The formula given in Theorem 35 is the number of possible paths a signal can take to propagate throughout the network. In this sense, we have a notion of systemic 'disorder' that captures the idea of enumerating possible states of the system, where in our case the quantity evolving the system is the control signal.

The system-theoretic interpretation motivating the examination of the determinant of the submatrix $L_{\mathcal{G}}^{\{n-1\}}$ in the entropy formula is the following. We take our system and designate a single node as the leader, and the rest of the nodes as followers. If we enumerate the leader node to correspond to the first vertex, then our Laplacian matrix is partitioned exactly according to:

$$\mathcal{L}_{\mathcal{G}} = \left[\begin{array}{c|c} a & \delta^T \\ \hline \delta & L_{\mathcal{G}}^{\{n-1\}} \end{array}\right]$$

where $\mathcal{A}_\mathcal{G} = L_\mathcal{G}^{\{n-1\}}$ in the dynamics (12.3), and the formula of entropy is $S_\mathcal{G} = \log\det\mathcal{A}_\mathcal{G}$. In the next section, we will motivate another graph-centric notion of this entropy, and then discuss how these notions relate to graph controllability.

12.3.1 *Counting Loops*

In this section, we describe a method of associating the notion of entropy to a notion of loops in the network. We do this indirectly: we identify the Dirichlet matrix of a network Laplacian to a non-unique flow graph. For the purposes in this chapter, we can consider a flow graph to be a directed graph with self-loops on each node. From this flow graph, the usual notion of the Coates Determinant is then examined; we will see that this will depend on the number of loops in the flow graph. This will shed light on a relation between the number of loops in the flow graph and the the number of spanning trees.

Definition 7. *A* connection *C of a flow graph $\mathcal{G}$ is a subgraph of $\mathcal{G}$ with the following properties:*

1. *Each node of C is in $\mathcal{G}$*
2. *Each node of C has a single edge originating from it and terminating at it.*

Definition 8. *A* directed loop *of $\mathcal{G}$ is a subgraph of $\mathcal{G}$ whose edges $b_1, \ldots, b_l$ can be ordered such that*

1. *The tip of b_k is the origin of b_{k+1}, for $k = 1, \ldots, l-1$*
2. *The origin of b_1 is the tip of b_l.*
3. *Each node tip along the loop is encountered only once.*

A fundamental result by Coates allows us to compute the determinant of $L_\mathcal{G}^{\{n-1\}}$ using a digraphic interpretation of this Dirichlet matrix. We can construct the flow graph corresponding to $L_\mathcal{G}^{\{n-1\}}$ as follows: Take each diagonal element $(L_\mathcal{G}^{\{n-1\}})_{ii}$ and identify it to a self-loop on the ith node with weight $(L_\mathcal{G}^{\{n-1\}})_{ii}$. Then, each node i is connected to node j in one direction with weight $(L_\mathcal{G}^{\{n-1\}})_{ij}$ and in the other direction with weight $(L_\mathcal{G}^{\{n-1\}})_{ji}$.

Lemma 18 (Coates Determinant). *Let $\mathcal{G}^{\{n-1\}}$ be the flow graph associated with the Dirichlet matrix $L_\mathcal{G}^{\{n-1\}}$. Let the subscript ρ denote a connection of the flow graph $\mathcal{G}$. Then, let the total gain $C(\mathcal{G})_\rho$ of the connection ρ be the product of all the edge weights $(L_\mathcal{G}^{\{n-1\}})_{ij}$ in the connection ρ. Finally, let L_ρ be the number of directed loops in the connection ρ. Then, the determinant of $L_\mathcal{G}^{\{n-1\}}$ is given by:*

$$\det L_\mathcal{G}^{\{n-1\}} = \Delta_c = (-1)^{n-1}\big(\textstyle\sum_\rho (-1)^{L_\rho} C(\mathcal{G}^{\{n-1\}})_\rho\big),$$

where the sum is taken over all connections ρ.

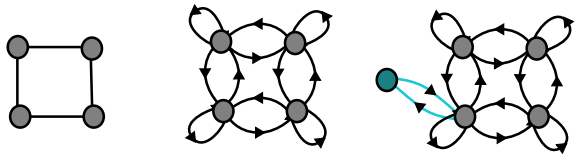

Figure 12.1: The two flow graphs of the transfer function of a 4-cycle controlled from a single node.

Proof. A proof of this lemma is given in [132]. □

This determinant formula is interesting because it depends on the number of directed loops in the flow graph - a topological feature.

Theorem 36. *Let $\mathcal{L}_\mathcal{G}$ be the Laplacian for the consensus dynamics; let $\mathcal{G}^{\{n-1\}}$ be the flow graph associated with the Dirichlet matrix $L_\mathcal{G}^{\{n-1\}}$. Then,*

$$S_\mathcal{G} = -\log\left[(-1)^n \sum_\rho (-1)^{L_\rho} C(\mathcal{G}^{\{n-1\}})_\rho\right].$$

An application of the Coates determinant formula is for computing the transfer function of the controlled consensus dynamics (12.1). Assuming the system output is given as $y = B_\mathcal{G}^T x$, the transfer function for the network assumes the form,

$$T(s) = \begin{vmatrix} sI + \mathcal{L}_\mathcal{G} & -B \\ B^T & 0 \end{vmatrix} / |sI + \mathcal{L}_\mathcal{G}|. \tag{12.6}$$

To use the Coates determinant formula, we must create two flow graphs corresponding to the numerator and denominator of $H(s)$. The flow graph of the denominator will have self-loops at each ith node with gain $s + \mathcal{L}_{\mathcal{G}ii}$, and each edge $\{i, j\}$ of $\mathcal{L}_\mathcal{G}$ will be replaced by a digon (pair of directed edges pointing in opposite directions) with gains $\mathcal{L}_{\mathcal{G}ij}$. The numerator will have an additional node for each column of B (corresponding to separate input channels) connected with a digon to each leader node with gains ± 1. An example is shown in Figure 12.1, where a 4-cycle is controlled,[2] with $B = [1, 0, 0, 0]^T$. The center and right flow graphs correspond to the denominator and numerator in (12.6), respectively. The Coates formula provides the coefficients of the polynomials in the transfer function, which in this case is

$$T(s) = \frac{4 + 10s + 6s^2 + s^3}{16s + 20s^2 + 8s^3 + s^4} = \frac{(2+s)(2+4s+s^2)}{s(2+s)^2(4+s)}.$$

12.3.2 *Loop Entropy and Network Gramians*

In this section, we highlight a result that connects the loop entropy to controllability properties of the consensus dynamics. Recalling the previous discussion highlighting the two interpretations of the loop entropy submatrix $L_\mathcal{G}^{\{n-1\}}$, without loss of generality let us assume that the loop entropy takes the form $S_\mathcal{G} = \log\det \mathcal{A}_\mathcal{G} = \sum_{i=1}^n \log \lambda_i(\mathcal{A}_\mathcal{G})$.

2 This system is uncontrollable to illustrate the pole-zero cancellation.

Definition 9 (Controllability Gramian). *Consider the full single integrator consensus dynamics driven by white noise. Then, the* controllability Gramian *is the unique positive semi-definite matrix* Σ *satisfying*

$$-\mathcal{A}_{\mathcal{G}}\Sigma - \Sigma{\mathcal{A}_{\mathcal{G}}}^T = -GG^T. \tag{12.7}$$

The controllability Gramian describes the mapping from inputs to steady state behavior of the internal states. In the meantime, it turns out that there is an intimate relationship between the controllability Gramian and the loop entropy of the system.

Theorem 37 (Controllability Gramian and Loop Entropy). *Let* $\mathcal{A}_{\mathcal{G}}$ *be the Dirichlet matrix of* $\mathcal{L}_{\mathcal{G}}$ *in the full single integrator dynamics* (12.3)*, let* Σ *be its controllability Gramian, and let* $G = I$*. Then, the loop entropy is given by* $S_{\mathcal{G}} = -\log\left(2^n \det \Sigma\right)$.

Proof. Since $\mathcal{A}_{\mathcal{G}}$ is positive definite, the controllability Gramian satisfies (12.7), and hence is given by $\Sigma = \frac{1}{2}{\mathcal{A}_{\mathcal{G}}}^{-1}$ and so $\left(2^n \det \Sigma\right)^{-1} = \det \mathcal{A}_{\mathcal{G}}$. Taking the logarithm of both sides yields the result. □

Theorem 38 (Loop Entropy for the Double Integrator). *Let* $\bar{\mathcal{A}}_{\mathcal{G}}$ *be the dynamics matrix from the full double integrator dynamics* (12.4)*:*

$$\bar{\mathcal{A}}_{\mathcal{G}} = \begin{bmatrix} 0 & -I \\ \mathcal{A}_{\mathcal{G}} & \mathcal{A}_{\mathcal{G}} \end{bmatrix}.$$

Next, let $\bar{\Sigma}$ *be the controllability Gramian satisfying*

$$-\bar{\mathcal{A}}_{\mathcal{G}}\bar{\Sigma} - \bar{\Sigma}\bar{\mathcal{A}}_{\mathcal{G}}^T = -\bar{G}\bar{G}^T,$$

where $\bar{G} = [0,\ I]^T$ (12.4)*. Then, the loop entropy satisfies*

$$S_{\mathcal{G}} = \log\left(2^{-2n} \det \bar{\Sigma}^{-1}\right).$$

Proof. The controllability Gramian for the double integrator dynamics is

$$\bar{\Sigma} = \frac{1}{2}\begin{bmatrix} I & 0 \\ 0 & {\mathcal{A}_{\mathcal{G}}}^{-1} \end{bmatrix},$$

and a similar computation as from the previous proof yields the result that $S_{\mathcal{G}} = \left(2^{-2n} \det \bar{\Sigma}^{-1}\right)$. □

The log determinant of the covariance matrix is proportional to the volume of the controllability ellipsoid. Recall that one interpretation of the controllability Gramian Σ is that it is the steady state covariance of $x(t)$ when the consensus dynamics is driven by white noise. Hence, when the steady state covariance of the state is small, the entropy is large, and vice versa. In this sense, a more disordered network is more robust to noise. Recalling our result linking the entropy to the number of spanning trees, a high entropy also corresponds to a large number of spanning trees, or a large number of possible paths noise can take as it propagates throughout the network.

Intuitively, one can think of the leader-node symmetries, described by Rahmani *et. al* [17], as being noise amplifiers, while disorder and large numbers of spanning trees act to dampen noise. Hence, when designing network topologies, it is beneficial to add edges between nodes such that entropy is maximized. In Section 12.5, we illustrate this with some examples.

Next, we will discuss solutions to the Lyapunov equation when $G \neq I$. Choose G to be $\sum_{i\in\mathcal{S}} e_i e_i^T$ for some set of indices $\mathcal{S}$ corresponding to follower nodes. To do this, we define the covariance entropy.

Definition 10 (Covariance Entropy). *Let $(-L_{\mathcal{G}}^{\{n-1\}}, G)$ be as before, and a controllable pair. Denote $\Sigma_{\mathcal{S}}$ to be the solution of the Lyapunov equation*

$$-L_{\mathcal{G}}^{\{n-1\}}\Sigma_{\mathcal{S}} - \Sigma_{\mathcal{S}}L_{\mathcal{G}}^{\{n-1\}} = -GG^T.$$

Define the covariance entropy *to be*

$$M_{\mathcal{S}} = \log 2^n \det \Sigma_{\mathcal{S}}^{-1}.$$

Clearly, when $G = I$, the covariance entropy is equal to the loop entropy. For a certain class of networks, the covariance entropy has a natural ordering property.

Theorem 39 (Covariance Entropy Ordering). *Construct $L_{\mathcal{G}}^{\{n-1\}}$ as before, but with the stipulation that $(-L_{\mathcal{G}}^{\{n-1\}}, G)$ be controllable for any $G = \sum_{i\in\mathcal{S}} e_i e_i^T$ with indices $\mathcal{S}$ corresponding to follower nodes. Let $M_{\mathcal{S}}$ and $M_{\mathcal{S}\cup\{k\}}$ denote the covariance entropies with input edge sets $\mathcal{S}$ and $\mathcal{S}\cup\{k\}$, respectively. Then, $M_{\mathcal{S}} \geq M_{\mathcal{S}\cup\{k\}}$. In particular, the loop entropy minimizes the covariance entropy.*

Proof. As before, choose G to be $\sum_{i\in\mathcal{S}} e_i e_i^T$ for some set of indices $\mathcal{S}$. Since $-L_{\mathcal{G}}^{\{n-1\}}$ is stable, it follows that the solution to the Lyapunov equation

$$-L_{\mathcal{G}}^{\{n-1\}}\Sigma_{\{i\}} - \Sigma_{\{i\}}L_{\mathcal{G}}^{\{n-1\}} = -GG^T$$

is given by

$$\Sigma_{\{i\}} = \int_0^\infty e^{-tL_{\mathcal{G}}^{\{n-1\}}} e_i e_i^T e_i e_i^T e^{-tL_{\mathcal{G}}^{\{n-1\}}} dt$$

and is positive semi-definite and so $\Sigma_{\mathcal{S}\cup\{k\}} - \Sigma_{\mathcal{S}} = \Sigma_{\{k\}}$ is positive semi-definite. It follows that $\Sigma_{\mathcal{S}\cup\{k\}} \geq \Sigma_{\mathcal{S}}$. Lastly, since the system is controllable, $\log 2^n \Sigma_{\mathcal{S}}^{-1} \geq \log 2^n \Sigma_{\mathcal{S}\cup\{k\}}^{-1}$. □

12.4 KOLMOGOROV-SINAI ENTROPY

In this section, we examine the Kolmogorov-Sinai entropy that is related to the adjacency matrix spectrum. We will also compute this entropy for a variety of simple graphs, which will elucidate the topological features it capture. Using results from [133], we will derive bounds on the value of this entropy and show that the bound is sharp for both regular and highly-irregular

graphs. At the end of this section, we will show the relation between the Kolmogorov-Sinai entropy and the stability of adjacency driven networks.

The Kolmogorov-Sinai entropy is a generalization of information-theoretic notion of the Shannon entropy on a network [134]. It characterizes the rate at which information is generated by the network. In the context of a network, information corresponds to a sequence of nodes visited by some Markov process on the network. The Kolmogorov-Sinai entropy is invariant under transformations that preserve the frequencies with which the network generates time-ordered sequences of nodes.

The stochastic process defining the information source is given by a Markov matrix M satisfying the properties

$$p_{ij} \geq 0,\ \textstyle\sum_j p_{ij} = 1,\ \text{and}\ \pi = \pi P$$

where π is the chain's stationary distribution. Consider the set of stochastic matrices M_A, where A is the adjacency matrix of the network graph, that have the property $a_{ij} = 0$ if and only if $p_{ij} = 0$. Let μ_n be the dominant eigenvalue of A with eigenvector v. Let M_A be a family of stochastic matrices with the property that $p_{ij} = 0$ if and only if $a_{ij} = 0$ in the network adjacency matrix. The *Kolmogorov-Sinai Entropy* defined presently is a measure that satisfies a variational principle analogous to that of the Gibbs principle in statistical mechanics [135]:

$$\log \mu_n = \sup_{P \in M_A} \left[-\textstyle\sum_{ij} \pi_i p_{ij} \log p_{ij} + \sum_{ij} \pi_i p_{ij} \log a_{ij} \right].$$

The supremum over all admissible stochastic matrices is given by the unique matrix P satisfying $p^*_{ij} = \frac{a_{ij} v_j}{\mu_n v_i}$, and hence we have

$$\log \mu_n = -\textstyle\sum_{ij} \pi_i p^*_{ij} \log p^*_{ij} + \sum_{ij} \pi_i p^*_{ij} \log a_{ij}. \tag{12.8}$$

By convention, $0 \log 0 = 0$. If the adjacency matrix is unweighted, in the sense that $a_{ij} = 1$ if there is an edge at $\{i, j\}$ and $a_{ij} = 0$ otherwise, then the term on the right hand side of (12.8) is zero. The term remaining is called the dynamical entropy of the Markov process, and is given by

$$H_P = -\textstyle\sum_{i=1}^{N} \pi_i \sum_j p^*_{ij} \log p^*_{ij}.$$

The Kolmogorov-Sinai Entropy is defined as follows [134]:

Definition 11 (Kolmogorov-Sinai Entropy). *The Kolmogorov-Sinai Entropy of a weighted adjacency matrix A is defined by*

$$H = \log \mu_n - \textstyle\sum_{ij} \pi_i p^*_{ij} \log a_{ij},$$

where $p^*_{ij} = \frac{a_{ij} v_j}{\mu_n v_i}$.

For an unweighted graph, the right-hand side vanishes:

$$H = \log \mu_n.$$

In the next part of this section, we will give some bounds on the value of the KS entropy. For the remainder of the chapter, we will assume unweighted adjacency matrices, and hence the KS-entropy is given by $H = \log \mu_n$.

12.4.1 *Bounds on the Kolmogorov-Sinai Entropy*

The Kolmogorov-Sinai entropy is difficult to compute in closed form for an arbitrary graph. Using results by Nikiforov [133], we can compute upper bounds on the Kolmogorov-Sinai entropy which is given in terms of topological quantities such as edge count and minimum degree. We can now recall the two theorems by Nikiforov.

Definition 12 (K_{p+1}-Free Graphs). *The $\mathcal{G}$ is called $p+1$-*free *if it does not contain a complete subgraph on $p+1$ vertices.*

Theorem 40 (Edge Bound). *Let $\mathcal{G}$ be $p+1$-free. Then, the largest eigenvalue μ_n of the adjacency matrix of $\mathcal{G}$ satisfies $\mu_n \leq \sqrt{2\frac{p-1}{p}|E|}$.*

Theorem 41 (Minimal Degree Bound). *Let $\mathcal{G}$ be $p+1$-free with minimal degree δ. Then, the largest eigenvalue μ_n of the adjacency matrix of $\mathcal{G}$ satisfies*

$$\mu_n \leq \frac{\delta - 1}{2} + \sqrt{2|E| - n\delta + \frac{(\delta+1)^2}{4}}.$$

By the definition of the Kolmogorov-Sinai entropy, we immediately have the following theorem:

Theorem 42 (Bounds on KS-Entropy). *Let $\mathcal{G}$ be $p+1$-free with minimal degree δ. Then, the Kolmogorov-Sinai entropy satisfies the two inequalities:*

$$H \leq \frac{1}{2}\log\left[2\frac{p-1}{p}|E|\right]$$
$$H \leq \log\left[\frac{\delta-1}{2} + \sqrt{2|E| - n\delta + \frac{(\delta+1)^2}{4}}\right]. \tag{12.9}$$

Equation (12.9) is in fact tight for regular graphs, and also highly irregular graphs in the sense of maximizing the degree variance. For example, let $n \geq k$, and let $H_{n,k}$ be the n-node complement of the complete graph on $n-k$ nodes K_{n-k}. Then, the maximal adjacency eigenvalue of $H_{n,k}$ is $\mu_n(H_{n,k}) = \frac{k-1}{2} + \sqrt{\frac{(k-1)^2}{4} + k(n-k)}$.

Now note that $\delta = k$ and $2|E| = kn - k^2 - k$ and so we get equality in (12.9). A result by Bell [136] states that $H_{n,k}$ maximizes the degree variance over all n-vertex graphs with the same edge count as $H_{n,k}$, where the degree variance is given by $V = \frac{1}{n}\sum_{i=1}^{n}\left(d_i - 2\frac{|E|}{n}\right)^2$. Hence graphs that maximize the KS-entropy include the regular graphs and the highly irregular graphs (namely the ones that maximize the degree variance over graphs with fixed vertex and edge counts).

A lower bound on the maximum eigenvalue follows from the Perron-Frobenius theorem. Let $\langle d \rangle$ denote the average degree of the graph and

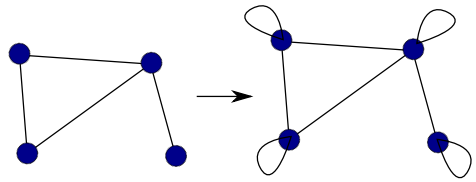

Figure 12.2: Adding self-loops to stabilize the adjacency dynamics.

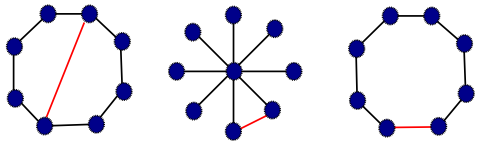

Figure 12.3: **Left**: Adding a edge in a cycle increases entropy by adding spanning trees. **Middle**: Adding an edge to a star graph adds two spanning trees. **Right**: Creating a cycle out of a path adds $n-1$ spanning trees.

let $d_{\max}$ denote its largest degree. Then, the following inequality holds [44], [137]:

$$\max\{\langle d\rangle, \sqrt{d_{\max}}\} \leq \mu_n \leq d_{\max}.$$

Hence, we can bound the entropy by

$$\max\{\log\langle d\rangle, 0.5 \log d_{\max}\} \leq H \leq \log d_{\max}.$$

Therefore increasing the average degree (say, by adding edges to every vertex) or increasing the maximum degree (adding many edges to a single vertex) will drive the entropy to increase from below.

12.4.2 *Kolmogorov-Sinai Entropy of Adjacency-driven Networks*

The system-theoretic interpretation of the Kolmogorov-Sinai entropy relates to the adjacency dynamics (12.5). Consider the dynamics where each node is driven by its neighbors as $\dot{x}_i = \sum_{\{i,j\}\in E} x_j$ on a connected network. In the matrix form, this is exactly the adjacency dynamics: $\dot{x} = Ax$.

Since $\mathrm{Tr}A = 0$ this dynamics is unstable as some eigenvalues are non-negative. One way of stabilizing the system is to add a self-loop with positive weights to each node that drives the system to stability, as show in Figure 12.2. This corresponds to the dynamics $\dot{x}_i = \sum_{\{i,j\}\in E} x_j - \delta x_i$, which in matrix form is $\dot{x} = (A - \delta I)x$. This is equivalent to taking $B = I$ in the controlled adjacency dynamics (12.5) in with a feedback gain of $u = -\delta x$. The minimum value that δ has to take in order to drive the system to stability is precisely the largest eigenvalue of A. Hence, the system is stable for any $\epsilon > 0$ when $\dot{x} = (A - (\epsilon + \mu_n)I)\, x = \left(A - (\epsilon + e^H)I\right) x$.

12.5 EXAMPLES OF ENTROPIES FOR SIMPLE GRAPHS

In Table 12.1, we show some examples of the loop entropy for some simple graphs.

In Figure 12.3, we show how adding edges increases the entropy of some example graphs. A cycle of n nodes has n spanning trees since removing any one of the n edges creates a path on n nodes and hence a spanning tree. Turning a path into a cycle greatly increases entropy as one goes from one spanning tree to n spanning trees. Clearly, creating larger cycles in a network increasing entropy. In the star graph, connecting any two non-center nodes induces a 3-cycle, which increases the number of spanning trees by two. The star graph is already low-entropy, and it is hence robust against edge perturbations in the sense that adding edges will not significantly increase the number of spanning trees, say compared to joining the ends of a path graph.

Table 12.1: Examples of Loop Entropies

Graph	Spectrum of $\mathcal{L}_\mathcal{G}$	Entropy $S_\mathcal{G}$
Cycle	$\left\{4\sin^2\left(\frac{\pi k}{2n}\right)\right\}$	$2\sum_{k=1}^{n-1}\log\left[2\sin\left(\frac{\pi k}{2n}\right)\right]$
Complete	$\{n, 0\}$	$(n-1)\log n$
Path	$\left\{4\sin^2\left(\frac{\pi k}{4n}\right)\right\}$	$\sum_{k=1}^{n-1}\log\left[2\sin\left(\frac{\pi k}{4n}\right)\right]$
Star	$\{0, 1, n\}$	$\log n$

Assuming an unweighted graph, we can write the Kolmogorov-Sinai entropy as $H = \log \mu_n$, where A is the adjacency matrix of the graph. Using results from the summary article by Brouwer *et al.* [138], we can write the entropy of some graph families, as shown in Table 12.2.

12.6 CONCLUSION

In this chapter, we examined the notion of *designing* networks that are amenable for control. First, we did this literally – we examined an algorithm, called whiskering, that preserves the controllability of networks as the graph is built up from scratch. We were able to derive some performance bounds on this algorithm using submodularity properties of the controllability gramian, and we also examined a graph-growing optimization setup that generated well-connected graphs.

Table 12.2: Examples of KS Entropies

Graph	Spectrum of A	Entropy H
Cycle	$\left\{2\cos\left(\frac{2\pi j}{n}\right)\right\}$	$\log 2$
Complete	$\{n-1, -1\}$	$\log(n-1)$
Path	$\left\{2\cos\left(\frac{2\pi j}{n+1}\right)\right\}$	$\log\left[2\cos\left(\frac{\pi}{n+1}\right)\right]$
Star	$\{-\sqrt{n-1}, 0, \sqrt{n-1}\}$	$\log\sqrt{n-1}$
Regular	$\lvert\mu(A)\rvert \leq k$	$\log k$
Complete Bipartite	$\{-\sqrt{nm}, 0, \sqrt{nm}\}$	$\log\sqrt{nm}$

Our focus then turned to *matrix-weighted graphs*, and notions of performance on those types of consensus models. For leader-follower consensus, we examined how series-parallel networks can be used to effciently reason about the performance of the system, as well to efficiently re-weight the network to optimize noise rejection.

In order to address the same question on matrix-weighted networks with time scales, we looked at *edge consensus* and the notion of $\mathcal{H}_2$ performance on that setup. We uncovered a separation principle allowing one to generate optimal time scales and optimal edge weights for consensus to achieve an optimal $\mathcal{H}_2$ performance.

Lastly, we examined two notions of network entropy, and discussed their respective system-theoretic interpretations.

Part IV

INTERACTION

13

INTRODUCTION

Networked dynamic systems arise in many synthetic and natural systems in science and engineering [5]; in particular multi-agent systems offer an interesting control paradigm. Each agent augments the system with an additional (local) computational resource, motivating the concept of *distributed controllers & estimators* [53], [60], [139], leading to a notion of *local* control versus *global* control. The latter seeks to design control laws to guide groups of agents to a desired objective, and the former seeks to design on-board controllers for each agent to facilitate their role in the global control law.

A class of the more widely used local control laws is called *consensus*, where each agent averages data from their neighbours to compute a parameter related to their objective – for example, heading, position or a formation center [5], [22], [80]. The attractive feature of consensus is how the interconnections between agents – the so-called *network* or *graph topology* – affect the performance and agreement characteristics of the algorithm [140], [141]. Graph-theoretic characteristics, such as symmetry, structural balance and graph spectra provide additional insights into the control-theoretic behaviour of consensus [17], [24], [62], [63], [71].

Global controllers for multi-agent systems take many forms [142], eg., potential field approaches [143], smoothed particle hydrodynamics [144] and density control [145]. In [146], [147], density control with only relative measurements of position between agents is considered, and mean-field control is used to tackle multi-agent interactions by considering a mass flow in the large-N limit [148]–[150].

The main interest area of the current paper is networked dynamic systems in which the underlying network is time-varying. Examples of such systems are switching and proximity-based consensus [5], [80], [151] and the Vicsek flocking model [152]. State-dependency refers to networks in which the underlying graph varies based on the state of the nodes. State-dependent networks have been considered in [83], [140], [148], [150], [153]–[155], but few underlying principles for designing controllers to account for this difficult nonlinearity has been proposed. A wide range of real-life networked systems are state-dependent.

To tackle this problem, we propose a twofold extension of the work in [145]. First, we consider state-dependent networked dynamic systems, instead of single-integrator dynamics. Second, we propose a control method for these systems by using a feedback-based density control law that utilizes *optimal mass transport* (OMT). OMT was considered for linear systems in [156], nonlinear systems in [157] and for density tracking of non-interacting agents in [158]. Our contribution considers OMT for multi-agent systems, in particular ones with state-dependent dynamics.

In the OMT problem, the initial and final densities ρ_0 & ρ_1 of the agents are specified. The solution to the problem yields a time-dependent density

profile with boundary conditions imposed by ρ_0, ρ_1, and a velocity field that together satisfy the continuity equation.

We aim to use this velocity field as a feedforward control input to the state-dependent multi-agent system, coupled with a density control feedback law. Using a modified form of *kernel density estimation* (KDE) that takes into account the state-dependent dynamics, we will show that the combination of the two control techniques will allow us to propose a physically realizable control strategy for state-dependent networked dynamic systems.

This chapter is organized as follows. The mathematical preliminaries, including notation, optimal mass transport, and density control with the KDE procedure are reviewed in §13.1. The problem statement and chapter contributions are outlined in §13.2. We present the feedforward controller based on OMT in §13.3, and the state-dependent KDE in §13.4. Examples are provided in §13.5, and the chapter is concluded in §13.6.

13.1 MATHEMATICAL PRELIMINARIES

13.1.1 *Mathematical Notation & Measure Theory*

A measure space $(\Sigma, \mathcal{A}, \mu)$ is a triple containing a *sample space* $\Sigma \subset \mathbb{R}^n$, a σ-algebra of subsets of Σ, and a *measure* μ that assigns the 'size' $\mu(A) \in \mathbb{R}_+$ to a set $A \in \mathcal{A}$. The *Borel σ-algebra* $\mathcal{B}$ is generated from the countable unions, intersections and complements of open subsets of $\mathbb{R}^n$. The *Lebesgue measure* λ assigns to a closed interval $[a, b] \subset \mathbb{R}$ the 'size' $b - a$; this can be extended to $\mathbb{R}^n$ by considering products of measures. A measure μ is called *absolutely continuous* with respect to a measure ν if $\nu(A) = 0 \implies \mu(A) = 0$ for $A \in \mathcal{A}$; μ is called *Lebesgue absolutely continuous* if $\nu = \lambda$. This is denoted $\mu \ll \nu$. If $\mu \ll \nu$, there exists a function $f : \mathbb{R} \to \mathbb{R}_+$ called a *Radon-Nikodym derivative*, or *density*, of μ with respect to ν. It is denoted $f := \frac{d\mu}{d\nu}$, and satisfies the property that for all $A \in \mathcal{A}$, $\mu(A) = \int_A f d\nu$. Let $\pi(x, y)$ be a joint measure on $\mathcal{X} \times \mathcal{Y}$. We denote the set of such joint measures π by $P(\mathcal{X}, \mathcal{Y})$. The *marginal* π_x of π on $\mathcal{X}$ is defined as the push-forward under the projection map X on $\mathcal{X}$: $\pi_x = X_\# \pi$, where $X(x, y) = x$. Similarly, the marginal π_y of π on $\mathcal{Y}$ is given by $\pi_y = Y_\# \pi$, where $Y(x, y) = y$. We denote the convolution of two functions f, g as $f \star g$, or the convolution of a function f and measure μ as $f \star \mu$.

13.1.2 *Optimal Mass Transport*

Informally speaking, the *optimal mass transport* problem is to find a mapping between two densities that minimizes some cost. Formally speaking, we consider two measures[1] μ_0, μ_1 on $\mathbb{R}^n$ with equal mass: $\int_{\mathbb{R}^n} d\mu_0 = \int_{\mathbb{R}^n} d\mu_1$.

1 If the measures are Lebesgue absolutely continuous, one can equivalently consider densities ρ_0, ρ_1.

The *optimal mass transport* problem [159], [160] is to find a measurable map $T : \mathbb{R}^n \to \mathbb{R}^n$ taking μ_0 to μ_1 via the following optimization problem:

$$\begin{aligned} &\text{minimize } \int_{\mathbb{R}^n} c\left(x, T(x)\right) d\mu_0(x) \\ &\text{s.t.} \qquad \int_{x\in A} d\mu_1(x) = \int_{T(x)\in A} d\mu_0(x), \forall A \subset \mathbb{R}^n, \end{aligned} \tag{13.1}$$

where c is a cost function depending on the initial and transported masses. The constraint in Problem (13.1) means that μ_1 is the *push-forward* measure of μ_0 under the map T, in that for each Borel set $B \in \mathcal{B} := \sigma(\mathbb{R}^n)$, we have that $\mu_1(B) = \mu_0\left(T^{-1}(B)\right)$. This is denoted as $T_{\#}\mu_0 = \mu_1$.

A generalization of Problem (13.1) by Kantorovich is able to pick out the optimal map T, if it exists, for a certain class of costs c under the assumption of absolute continuity of the measures [161]. Here, we consider a joint distribution $\pi(x, y)$ on $\mathbb{R}^n \times \mathbb{R}^n$ and solve for the optimal admissible measure π given some cost $c(x, y)$.

The set of admissible measures π are those whose marginals are μ_0 and μ_1: $X_{\#}\pi = \mu_0,\ Y_{\#}\pi = \mu_1$. This is equivalent to requiring

$$\pi(A \times \mathbb{R}^n) = \mu_0(A),\ \pi(\mathbb{R}^n \times B) = \mu_1(B) \tag{13.2}$$

for all measurable $A \subset \mathbb{R}^n$ and $B \subset \mathbb{R}^n$. The *Kantorovich relaxed optimal mass transport problem* [161] is given by

$$\begin{aligned} &\text{minimize} \quad \int_{\mathbb{R}^n \times \mathbb{R}^n} c(x, y) d\pi(x, y) \\ &\text{s.t.} \qquad \pi \in \left\{\pi \in P(\mathbb{R}^n, \mathbb{R}^n) \text{ s.t. (13.2) holds}\right\}. \end{aligned} \tag{13.3}$$

Proposition 8 ([159], [160]). *For quadratic costs $c(x, y) = \|x - y\|^2$, the support of the optimal joint measure $\pi^*(x, y)$ of Problem (13.3) is exactly the graph of the optimal map $T^*(x)$ minimizing Problem (13.1).*

For quadratic costs, Benamou and Brenier formulated an equivalent problem in terms of a constrained fluid mechanics model.

Proposition 9 ([162]). *Given Lebesgue absolutely continuous μ_0, μ_1 with Radon-Nikodym densities ρ_0, ρ_1 respectively, Problem (13.3) with quadratic costs is equivalent to*

$$\begin{aligned} &\inf_{\rho, v} \int_{\mathbb{R}^n} \int_0^1 \tfrac{1}{2}\|v(t, x)\|^2 \rho(t, x) dt dx \\ &\text{s.t.} \quad \frac{\partial \rho}{\partial t} + \nabla \cdot (v\rho) = 0 \\ &\qquad \rho(0, x) = \rho_0(x),\ \rho(1, y) = \rho_1(y). \end{aligned} \tag{13.4}$$

Furthermore, the solution to Problem (13.4) is of the form $v(t, x) = \nabla\varphi(t, x)$, where $\varphi(t, x)$ is the Lagrange multiplier of the constraints and the solution to the Hamilton-Jacobi equation $\partial_t\phi + \frac{1}{2}|\nabla\phi|^2 = 0$.

Remark 12. *The optimal map T^* of Problem (13.3) in the case of quadratic costs can be reconstructed from the variable $v(t, x)$ from the solution of Problem (13.4). This formally establishes the equivalence stated in Proposition 9 [162].*

13.1.3 *Density Control and Kernel Density Estimation*

In [145], a feedback control law to drive a group of single-integrator agents to a desired density profile $\rho_1(x,t)$ was analyzed. The following feedback law is proposed to compute the velocity field as a function of the error in density $\Phi(x,t) := \rho(x,t) - \rho_1(x)$ as

$$v(x,t) = -\alpha \frac{\nabla\Phi(x,t)}{\rho(x,t)} \,. \tag{13.5}$$

Density control of multi-agent systems is impacted by the ability of individual agents to discern the local density profile from measurements of their neighbours. Since the number of agents is finite, the local density profile must be approximated from finitely many samples $r_i(t)$.

This can be accomplished using *kernel density estimation* [163], [164]. The kernel density estimate $\hat{\rho}(t,x)$ at any point $x \in \mathbb{R}^n$ and time $t \in \mathbb{R}_+$ is given by

$$\hat{\rho}(t,x) = \int_{\mathbb{R}^n} \left[\prod_{k=1}^{d} \frac{1}{h_k} K\left(\frac{x^{[k]} - \xi^{[k]}}{h_k} \right) \right] dP_N(t,\xi). \tag{13.6}$$

Here, $K : \mathbb{R} \to \mathbb{R}$ is called the *smoothing kernel*, h_k is called the *smoothing parameter*, and $dP_N(t,\xi)$ is a sum of Dirac measures at sample points:

$$dP_N(t,\xi) = \frac{1}{N} \sum_{r(t)\in S(t)} \delta\left(\xi - r(t)\right) d\xi.$$

Since $\delta(\cdot)$ is the Dirac delta functional, Equation (13.6) can be written as

$$\hat{\rho}(t,x) = \frac{1}{N} \sum_{i=1}^{N} \left[\prod_{k=1}^{d} \frac{1}{h_k} K\left(\frac{x^{[k]} - r_i^{[k]}}{h_k} \right) \right].$$

The control law (13.5) then uses the estimate $\hat{\rho}(x,t)$ in place of knowledge of the true density $\rho(x,t)$, where the sample points $r(t)$ are taken to be the agent states:

$$v(x,t) = -\alpha \frac{\nabla(\hat{\rho}(x,t) - \rho_1(x))}{\hat{\rho}(x,t)}.$$

In [145], Gaussian kernels were used – this induces an all-to-all communication; every agent is able to sample the position every other agent. The control law (13.5) has a convergence guarantee listed in Theorem 6 of [145].

13.2 PROBLEM STATEMENT

In this chapter, we consider state-dependent networked dynamic systems with N agents on a bounded region $\mathcal{R} \subset \mathbb{R}^n$, where the ith agent's state evolves according to the dynamics

$$\dot{x}_i = f(\mathcal{G}(\mathbf{x}), \mathbf{x}) + Bu_i(\mathbf{x}, t), \ \mathbf{x} := (x_1, \ldots, x_n).$$

A prototypical example of such a system is *state-dependent consensus*

$$\dot{x}_i = \sum_{j \neq i} A(x_i, x_j) \cdot (x_i - x_j) + u_i, \tag{13.7}$$

where the edge weight $w_{ij} := A(x_i, x_j)$ changes depending on the state of the agent i and its neighbour j. In general, one can consider an *interaction kernel* $H(x)$ that generates a consensus-like dynamics by convolution with the Dirac measure supported at agent states [148], [150]:

$$\mu_N(x) = \frac{1}{N} \sum_{j=1}^{N} \mathbf{1}_{\{x_j\}}(x) = \frac{1}{N} \sum_{j=1}^{N} \delta(x - x_j). \tag{13.8}$$

Using Equation (13.8), we can write a general multi-agent system as

$$\dot{x}_i = (H \star \mu_N)(x_i) + u_i.$$

A simple example motivated by robotics is proximity-based edge switching, where $A(x_i, x_j) = 1$ if $\|x_i - x_j\| \leq r$ and 0 otherwise, where r is some communication radius. This corresponds to an interaction kernel $H(x) = x\mathbf{1}_{\|x\| \leq r}(x)$. One can also examine second-order systems, such as ones of the form

$$\begin{aligned} \dot{x}_i &= v_i \\ \dot{v}_i &= (H \star \mu_N)(x_i, v_i) + u_i \end{aligned}$$

If we let the interaction kernel be

$$H(x, v) = a(|x|)\, v, \ a \in C^1\big([0, +\infty)\big),$$

then this generates *Cucker-Smale-like flocking*:

$$\begin{aligned} \dot{x}_i &= v_i \\ \dot{v}_i &= \frac{1}{N} \sum_{j \neq i} a\big(|x_j - x_i|\big)(v_j - v_i) + u_i. \end{aligned}$$

As the number of agents N grows sufficiently large, one can consider the time-dependent *density* of agents $\rho(x, t)$ over a region of the state space. In

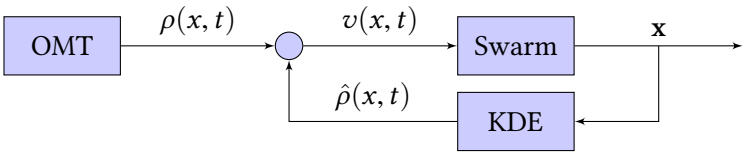

Figure 13.1: Block diagram of density control scheme

the context of mean-field control, the formal large-N limit of the dynamics (13.7) produces the *mean field dynamics* [148], [150],

$$\begin{aligned} &\frac{\partial \rho}{\partial t} + \nabla_x \cdot [(\mathcal{P}(\rho(x,t),t) + u)\,\rho] = 0 \\ &\mathcal{P}(\rho(x,t),x) = \int A(x,y)(y-x)\rho(y,t)dy. \end{aligned} \tag{13.9}$$

We now state the contributions of this chapter, namely the feedforward OMT scheme with kernel density estimation shown in Figure 13.1.

Contribution 1: Feed-Forward Density Control With Optimal Mass Transport.

We consider a generalization of the Brenier-Benamou OMT problem (13.4) with the continuity equation constraint replaced by the mean-field dynamics (13.9):

$$\begin{aligned} &\inf_{\rho,v} \int \int_0^1 \tfrac{1}{2}\|v(t,x)\|^2 \rho(t,x)dtdx \\ &\text{s.t.} \quad \partial_t \rho + \nabla_x \cdot [(\mathcal{P}(\rho(x,t),x) + v)\,\rho] = 0 \\ &\qquad \mathcal{P}(\rho(x,t),x) = \int A(x,y)(y-x)\rho(y,t)dy \\ &\qquad \rho(0,x) = \rho_0(x),\ \rho(1,y) = \rho_1(y). \end{aligned} \tag{13.10}$$

The solution to Problem (13.10) yields two variables with important physical interpretations. The time-varying density $\rho(t,x)$ represents the mass of agents with dynamics (13.7) with inputs $u_i(x,t) := v(x_i,t)$; the velocity field $v(x,t)$ is precisely the input u_i given to agent i at position x at time t.

Problem (13.10) assumes that the initial and final masses of agents are distributed in the mean-field limit according to densities ρ_0 and ρ_1, respectively. When considering finitely many agents, any initial density will take the form of Equation (13.8) - namely, it will be a Dirac measure supported at the agent states, also called the *empirical density*.

Hence, in general, the boundary conditions on the density in Problem (13.10) can be either *deterministic* (in the case of Dirac measures supported at the agent states), or *probabalistic* (in the sense that the initial/final agent states $x_i(0)$ and $x_i(1)$ are randomly distributed according to the densities ρ_0 and ρ_1). In the latter case, as $N \to \infty$, the Dirac measure supported at the agent states at time t converges in a formal sense to the density $\rho(\cdot,t)$ [148], [150].

In either case, we consider the velocity field $v(x,t)$ as a feed-forward input to the dynamics (13.7). Since the number of agents is finite, the empirical density at time t will only approximate the density $\rho(x,t)$ from the solution of Problem (13.10).

Contribution 2: Feedback Density Control with Kernel Density Estimation and State-Dependent Constraints.

In a state-dependent networked dynamic system, eg., Equation (13.7), the existence of an edge indicates some notion of information transfer between agents. Hence, a physical estimation scheme and density control law can only allow i to sample those agents j such that $A(x_i, x_j) \neq 0$. The second contribution of this chapter is to extend the KDE procedure in [145] by solving a quadratic program for an optimal kernel that takes into account the state-dependent communication constraints.

13.3 FEEDBACK CONTROL OF STATE-DEPENDENT NETWORKED DYNAMICAL SYSTEMS

Consider the state-dependent consensus dynamics (13.7). Let $v_1(x,t)$ denote the velocity field from the solution to Problem (13.10), and let $v_2(x,t)$ denote the velocity field from the control law (13.5). Our proposed control law is then given by the velocity field (with $\alpha > 0$),

$$u(x,t) = \begin{cases} v_1(x,t) - \alpha \dfrac{\nabla\left(\rho(x,t) - \rho_1(x)\right)}{\rho(x,t)} & 0 \leq t \leq 1 \\ v_2(x,t) - \mathcal{P}(\mu(x,t),x) & t \geq 1 \end{cases} \tag{13.11}$$

$$\mathcal{P}(\mu(x,t),x) = \int A(x,y)(y-x)\mu(y,t)dy.$$

Of course, the switch at $t = 1$ is completely arbitrary, and can be altered by changing the time horizon of Problem (13.10).

The main result of this section is the following theorem, an extension of Theorem 6 in [145]. Informally, it states that as the number of agents in the system tends as $N \to \infty$, the velocities of the agents performing the state-dependent control law (13.11) will vanish asymptotically.

Theorem 43. *Consider a system of N agents $\mathcal{S}(t)$ on a bounded region $\mathcal{R} \subset \mathbb{R}^n$ with individual dynamics given by (13.7) and with control law (13.11). Further suppose that the initial swarm density $\rho(x,t)$ and target density $\rho_1(x)$ satisfy the boundary condition $\nabla\Phi(x,t) = 0$ on $\partial\mathcal{R}$. As $t \to \infty$, for sufficiently large N the error density $\Phi(x,t)$ converges to zero: $\lim_{t\to\infty}\Phi(x,t) = 0$, for $x \in \mathcal{R}$ and so $\hat{\rho}(x,t) \to \rho_1(x)$. Furthermore, the velocities of all agents vanish asymptotically: $\lim_{t\to\infty}\dot{x}(t) = 0$, for $x \in \mathcal{R}$.*

Proof. First, recall the following theorem about consistency of the estimate $\hat{\rho}(x,t)$.

Theorem 44 ([165]). *Consider a kernel density estimation scheme for the target density $\rho(x)$. Suppose the smoothing parameter h is chosen as a function of the number of samples N: $\lim_{N\to\infty} Nh(N) = \infty$. Then, at each point of continuity x of ρ, the estimator $\hat{\rho}_N(x)$ is weakly consistent in that for all $\epsilon > 0$, $\lim_{N\to\infty}\mathbb{P}\left(|\rho_N(x) - \rho(x)| > \epsilon\right) = 0$.*

By Theorem 44, under the assumption on the smoothing parameter h, we have that as $N \to \infty$, $\hat{\rho}(t,x) \to \rho(t,x)$ with probability 1 for any finite t.

Consider the following Lyapunov function:

$$V(t) = \int_{\mathcal{R}} \left(\frac{\rho(x,t)}{\alpha} \right)^2 \dot{x}^T \dot{x} \, dx. \tag{13.12}$$

As $N \to \infty$, the velocity field $\dot{x}$ approaches the mean-field limit [148]: $\dot{x} = \mathcal{P}(\mu,t) + u(x,t)$, where $\mathcal{P}(\mu,x) = \int A(x,y)(y-x)\mu(y,t)dy$, and $\mu := \mu(y,t)$ is the measure satisfying $\partial t + \nabla \cdot ((\mathcal{P}(\mu,t) + u(x,t))\,\mu) = 0$. Under the control law (13.11), it follows that for sufficiently large t, the Lyapunov function (13.12) can be written as

$$V(t) = \int_{\mathcal{R}} \nabla\Phi(x,t)^T \nabla\Phi(x,t) dx.$$

The time derivative of $V(t)$ is then given by

$$\dot{V}(t) = \alpha \int_{\mathcal{R}} \xi(x,t)^T \Delta\xi(x,t) dx,$$

where $\xi(x,t) := \nabla\Phi(x,t)$. Since $\nabla\Phi(x,t) = 0$ on $\partial\mathcal{R}$, we have that $\xi(x,t) = 0$ on $\partial\mathcal{R}$ which is a Dirichlet boundary condition. It follows that $\dot{V}(t) < 0$ since the Dirichlet problem for the Laplace operator has strictly negative eigenvalues [166].

Therefore, by LaSalle's Invariance Principle, we can conclude that

$$\lim_{t\to\infty} \nabla\Phi(x,t) = 0,$$

and so $\lim_{t\to\infty} \Phi(x,t) =$ constant. However, since $\nabla\Phi(x,t) = 0$ on $\partial\mathcal{R}$, the mass $\int_{\mathcal{R}} \Phi(x,t)dx$ is conserved for all $t > 0$ (in that $\int_{\mathcal{R}} \Phi(x,t)dx = 0$) and so we have that $\int_{\mathcal{R}} \hat{\rho}(x,t)dx = \int_{\mathcal{R}} \rho(x,t)dx$. Consequently, it follows that $\lim_{t\to\infty} \Phi(x,t) = 0$, and hence $\lim_{t\to\infty} \rho(x,t) = \lim_{t\to\infty} \hat{\rho}(x,t)$ which completes the proof. □

13.4 DENSITY ESTIMATION FOR KERNELS WITH COMPACT SUPPORT

Consider a state-dependent consensus dynamics as in Equation (13.7) where $A(x_i, x_j)$ is a state-dependent edge weight. In order to implement the density control law, each agent must be able to estimate the density of nearby agents to generate the correct velocity field. In this section, we discuss optimal kernels designed to achieve this task that are subject to the state-dependent constraints imposed by $A(x_i, x_j)$.

The state-dependent constraints in some (informal) sense denote 'information transfer' between agents i and j. If $A_{ij} = 0$, then agents i and j cannot detect each other, and the KDE procedure should reflect this. To illustrate this notion, consider Figure 13.2.

In 1D kernel density estimation, there are two parameters selected *a priori* that influence the quality of the estimated probability density function, namely the kernel K and the smoothing parameter h. We consider an optimal selection of K subject to the state-dependent constraints; we leave the task

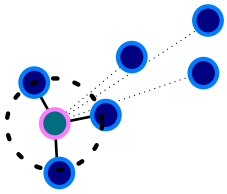

Figure 13.2: Illustration of (proximity-based) state-dependent constraints on the KDE procedure. Dotted lines indicate samples the center agent cannot measure.

of selecting h for future work. For now, we just need the following assumption on h as a function of the number of samples: $\lim_{N\to\infty} Nh(N) = \infty$. The standard metric for measuring the quality of the estimated probability density function is given by the *mean integrated square error* $E_{\text{MISE}} := \mathbb{E}\left[\int (\hat{\rho}(x) - \rho(x))\, dx\right]$.

By extracting out the dependence on the number of samples N, and the choice of smoothing parameter h, one can obtain the *asymptotic mean integrated square error* (AMISE) [163]: $E_{\text{MISE}} := E_{\text{AMISE}} + o\left((hn)^{-1} + h^4\right)$. One can factor the AMISE into a product of two terms, one depending on h and one depending on K: $E_{\text{AMISE}} = C_1(K)C_2(h)$, where

$$C_1(K) := \left[\left(\int K(x)^2 dx\right)^4 \left(\int x^2 K(x) dx\right)^2\right]^{1/5}.$$

Hence, by fixing $a := \int x^2 K(x) dx$ depending on the length of the boundary of our estimation horizon, the only parameter left to optimize is the *roughness* of $K(x)$: $\int K(x)^2 dx$. We can write an optimization problem as follows:

$$\begin{array}{ll} \text{minimize} & \int K(x)^2 dx \\ \text{s.t.} & \int K(x) = 1,\ \int xK(x) = 0 \\ & \int x^2 K(x) = a^2 < \infty,\ K(x) \geq 0. \end{array} \tag{13.13}$$

In one dimension, the solution to Problem (13.13) is given by [163],

$$K^a(x) = \frac{3}{4}\frac{1}{a\sqrt{5}}\left[1 - \left(\frac{x}{a\sqrt{5}}\right)^2\right] \mathbf{1}_{\{|x| \leq a\sqrt{5}\}}. \tag{13.14}$$

We wish to find the solution to a modified version of this problem where we enforce a compact support constraint of the form $\{K(x) = 0,\ x \in \mathcal{A},\ \mathcal{A}^c \text{ compact}\}$. To this end, notice that Problem (13.13) can be numerically solved by discretizing it as follows.

Denote the region of the problem as $X = \{x : |x| \leq B\}$. Discretize X into N points spaced dx apart. Let the vector $x := \{x_i\}_{i=1}^N \in [-B, B]^N$ consist of these points, and let $k := \{k_i\}_{i=1}^N$ be the vector of the kernel K evaluated

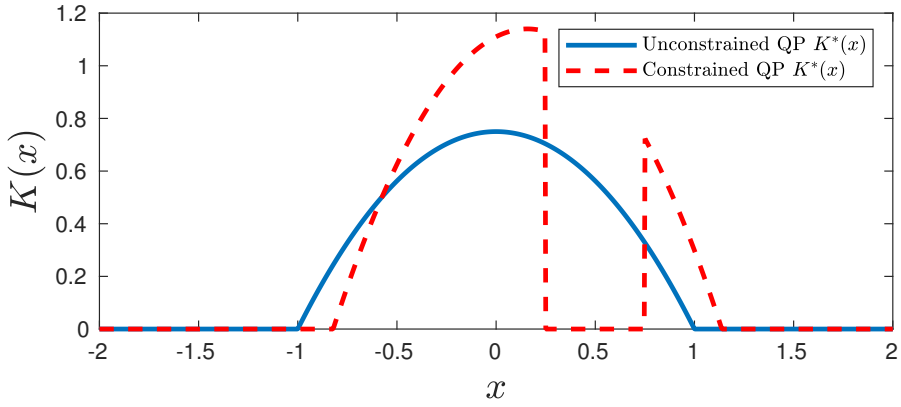

Figure 13.3: Optimal kernels with unconstrained support, and support constrained to $[-2, 2] \setminus [1/4, 3/4]$, with second moment $a = 5^{-1/2}$. The unconstrained kernel solution is exactly given by the Equation (13.14).

at these points, i.e. $k_i = K(x_i)$. Discretizing the integrals yields a quadratic program of the form:

$$\begin{aligned} &\text{minimize} && k^T k \\ &\text{s.t.} && \textstyle\sum_{i=1}^N k_i dx = 1,\ \sum_{i=1}^N x_i k_i = 0 \\ & && \textstyle\sum_{i=1}^N x_i^2 k_i dx = a^2,\ k_i \geq 0,\ 1 \leq i \leq N. \end{aligned} \tag{13.15}$$

As discussed before, an agent's state-dependent density estimate will depend on sampling points from agents that have an edge between them. Hence, in the density estimate for agent i, the kernel K will only depend upon the state of agent i and its neighbours $\mathcal{N}_i$. The density estimate of agent i is written as

$$\hat{\rho}_i(t, x(t)) = \frac{1}{Nh^d} \sum_{j \in \mathcal{N}_i} \left[\prod_{k=1}^{d} K_i \left(\frac{x_i(t) - x_j(t)}{h}, x_j \right) \right]$$

where the support of the kernel is restricted to the support of the state-dependent edge weight $A(x_i, x_j)$:

$$A(x_i, x_j) = 0 \implies K(h^{-1}(x_i - x_j), x_j) = 0.$$

To extend Problem (13.15) to multi-dimensional systems, we consider *multiplicative kernels* for $x_i \in \mathbb{R}^n$, where each dimension is estimated independently: $K(\mathbf{x}) = \prod_{k=1}^N K_k(x_k)$. This yields the final optimal kernel problem with compact support constraint. For brevity, we show the explicit form for

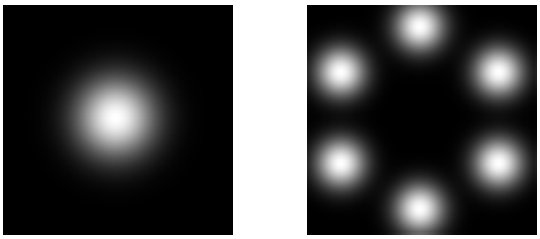

Figure 13.4: Left: Initial density ρ_0. Right: Target density ρ_1.

the 2D problem, as it is clear (yet notationally cumbersome) how to write the general ND problem:

$$\begin{aligned}
\text{minimize} \quad & \textstyle\sum_i^{N_x} \sum_j^{N_y} k_{ij}^2 \\
\text{s.t.} \quad & \textstyle\sum_{i=1}^{N_x} \sum_{j=1}^{N_y} k_{ij} dx dy = 1, \; k_{ij} \geq 0, \; \forall i, j \\
& \textstyle\sum_{i=1}^{N_x} x_i k_{ij} = 0, \; \sum_{i=1}^{N_x} x_i^2 k_{ij} dx = a^2, \; \forall j \\
& \textstyle\sum_{j=1}^{N_y} y_j k_{ij} = 0, \; \sum_{j=1}^{N_y} y_j^2 k_{ij} dx = a^2, \; \forall i \\
& k_{ij} = 0 \text{ if } (x_i, y_j) \in \mathcal{A}, \; \mathcal{A}^c \text{ compact.}
\end{aligned}$$

It is important to note that removing a compact interval from the kernel may bias the density estimate - this is unavoidable. The compact support constraint defines a *selection-biased distribution (SBD)*; each agent samples the distribution $g(x) = w(x)\rho(x)/\mu$, with $w(x) = \mathbf{1}_{\mathcal{A}^c}(x), \mu = \int w(x)\rho(x)dx$. The standard *unbiased* kernel density estimate of a SBD involves multiplying the kernel by a factor of $\mu/w(x)$ [167], [168], which is unbounded for our choice of $w(x)$. Techniques for unbiasing $\hat{\rho}(x)$ will be left for future work.

13.5 EXAMPLES

We numerically simulate $N = 200$ agents with interaction kernel $H(x) = x\mathbf{1}_{\|x\| \leq 0.01}(x)$. The velocity field $\mathcal{P}[\mu](x)$ is evaluated with the Dirac measure (13.8), effectively yielding N single-integrator agents that are able to only sample agents a short distance away from each other.

The optimal mass transport problem was solved using open-source code, utilizing a primal-dual algorithm [169], [170]. The density profile and velocity field was calculated over a $100 \times 100 \times 100$ grid in x, y and t space. The initial density $\rho_0(x)$ was a 2D Gaussian at the center of a $[0, 1]^2$ grid, and the target density was a ring of 2D Gaussians, as shown in Figure 13.4. The superimposed optimal density profile over time, and the states of the agents over time integrating the feedback and feedforward control law are shown in Figure 13.5. As one can see, the agents are more organized around the final density distributions when using the feedback law as opposed to just integrating the feedforward law, as shown in Figure 13.6.

13.6 CONCLUSION

In this chapter, we examined density control of state-dependent networked dynamic systems. We utilized the optimal mass transport problem to design

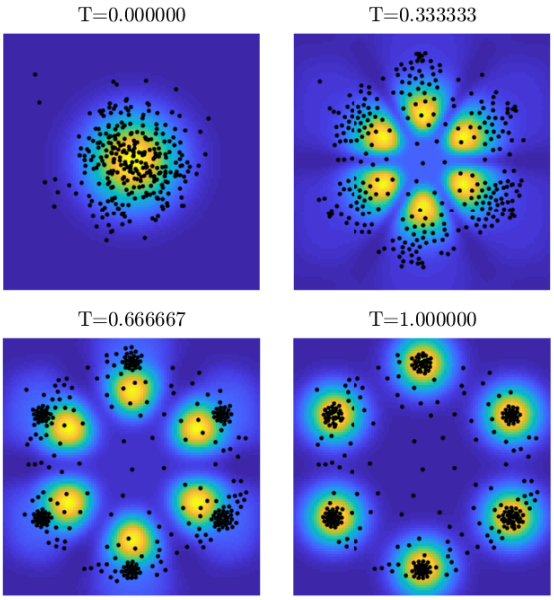

Figure 13.5: Optimal density profiles over time, and superimposed agent states using the feedback density control law.

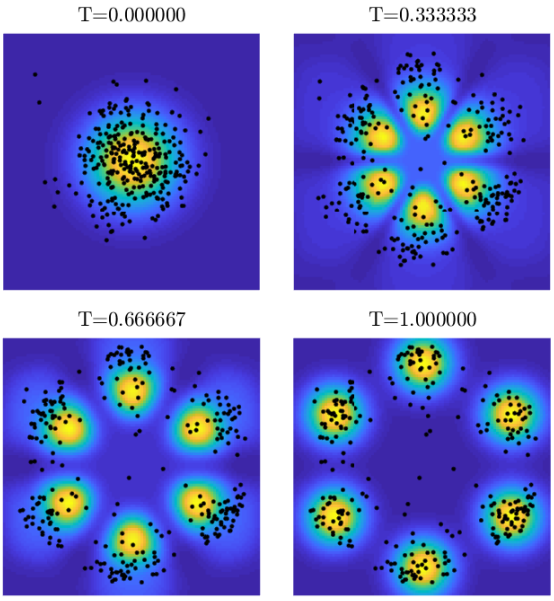

Figure 13.6: Optimal density profiles over time, and superimposed agent states with only the feedforward control.

a feed-forward velocity field propelling agents with initial conditions sampled from a density profile ρ_0 to some target density ρ_1. We then tackled the problem of using a density feedback control law with sparse measurements dictated by the state-dependent edge switching constraints of the agents. We utilized kernel density estimation to convert measurements of neighboring agents into a local estimate of the swarm density, which was then used to calculate a feedback density control law. In particular, a quadratic program was designed to find the optimal kernel subject to the state-dependent edge switching.

There are many open problems remaining, here we discuss several. First, the selection of an optimal interaction distance $r = h$ for proximity-based edge switching. This will depend on, for example, ρ_0, ρ_1 and N. If h is large, this will require more on-board computation and sensing capability; if h is small, agents will be isolated. Second, one can consider the task of determining a state-dependent kernel yielding an unbiased estimate of ρ.

Part V

CONCLUSION AND FUTURE WORK

14

CONCLUDING REMARKS

The purpose of this thesis was to examine various notions of how the underlying network structure affects the behaviour and performance of, and ability to control, networked dynamical systems. To this end, we examined three questions:

1. How does the network affect the control-theoretic properties of the underlying system?
2. How can one design a network *a priori* to achieve a certain performance criterion? Given an existing network, what metrics give us the correct notion of performance?
3. How does one interact with a networked dynamical system?

Each part of this thesis has addressed one of these three questions. In the first part, we examined how different types of interactions affect the controllability of the consensus protocol. We showed that a certain distribution of positive versus negative interactions between agents, coupled with network symmetries, causes the resulting protocol to be uncontrollable. We extended this to the nonlinear regime in the context of the accessibility problem.

The question of identifying communities of agents with friendly interactions was also addressed. Data-driven system identification techniques involving the Koopman operator were used to identify polarized clusters of agents – in each cluster, only positive interactions exist, and between clusters only negative interactions exist.

In the second part of this thesis, we examined the problem of measuring the performance of networks, and designing networks to achieve certain performance criteria. Algorithms for generating controllable and well-connected networks were considered. Next, the performance of matrix-weighted consensus networks were examined in the context of noise rejection and the $\mathcal{H}_2$ norm.

In two different contexts, we used the paradigm of series-parallel networks to address efficient $\mathcal{H}_2$ norm computation and fast, decentralized network re-weighting to optimize said norm. We considered edge consensus in order to analyze how the $\mathcal{H}_2$ norm behaves when considering systems with multiple time scales. In both cases, matrix-weighted networks were considered – these graphs have agents with vector-valued states, and more complex coupling between states.

Lastly, we examined notions of density control of networked dynamical systems. In cases where one allows some uncertainty in the agent states, or perhaps just wants the agent states to occupy some distribution, one can employ the field of *density control* to steer the agents from one distribution to another. We examined notions of feed-forward control (optimal mass transport) as well as feedback control (density control with kernel density estimation) in the case of edge-switching dynamics. This allowed us to design

control laws for systems where the network caries with time as a function of the states of the agents.

15 FUTURE WORK

In this chapter, we discuss the bright outlook for the future of research in networked dynamical systems, in particular pertaining to the extensions of work done in this dissertation. As in the spirit of this thesis, we outline open problems in the areas of control, design, and interaction with networked dynamical systems.

15.1 CONTROL

Controllability is one of the most important properties of the consensus algorithm, as it allows for single users to influence the overall behaviour of large networked dynamical systems by injecting signals at boundary nodes.

One interesting question is regarding matrix-weighted graphs. Suppose that the state of the ith node is $x_i(t) \in \mathbb{R}^k$:

$$x_i(t) = \begin{bmatrix} [x_i(t)]_1 \\ \vdots \\ [x_i(t)]_k. \end{bmatrix}$$

Then, the matrix weighted consensus protocol on the ith node in very explicit form is given by

$$\frac{d}{dt}\begin{bmatrix} [x_i(t)]_1 \\ \vdots \\ [x_i(t)]_k. \end{bmatrix} = -\sum_{j\in\mathbb{N}_i} W_{ij}\left(\begin{bmatrix} [x_i(t)]_1 \\ \vdots \\ [x_i(t)]_k. \end{bmatrix} - \begin{bmatrix} [x_j(t)]_1 \\ \vdots \\ [x_j(t)]_k. \end{bmatrix}\right).$$

If we designate a leader node l, and suppose that the ith node is connected to l, then we can write

$$\begin{aligned}\frac{d}{dt}\begin{bmatrix} [x_i(t)]_1 \\ \vdots \\ [x_i(t)]_k. \end{bmatrix} &= \begin{bmatrix} [x_j(t)]_1 \\ \vdots \\ [x_j(t)]_k. \end{bmatrix} + \begin{bmatrix} [x_l(t)]_1 \\ \vdots \\ [x_l(t)]_k. \end{bmatrix} \\ &\quad - \sum_{j\in\mathbb{N}_i\setminus\{l\}} W_{ij}\left(\begin{bmatrix} [x_i(t)]_1 \\ \vdots \\ [x_i(t)]_k. \end{bmatrix} - \begin{bmatrix} [x_j(t)]_1 \\ \vdots \\ [x_j(t)]_k. \end{bmatrix}\right)\end{aligned}$$

Here, the state of the leader node x_l is identified as our control input. A natural question is *can we steer the ath state of node i by driving the bth state of i via l?*

In other words, if we view the matrix-weighted graph as a network of k layers, then can we exert control over the ath layer by injecting a signal into the bth layer?

Another natural question to ask is the extension of signed networks into higher-order interactions. For example, a colour-charge type interaction where each node is assigned one of C colours, and nodes of the same colour interact cooperatively, or antagonistically otherwise. Formally, let $\chi : \mathcal{N} \to \{C_1, \dots, C_n\}$ be a *colouring function*. Then, for every edge $\{i, j\} \in \mathcal{E}$,

$$W_{\{i,j\}} = \begin{cases} 1 & \chi(i) = \chi(j) \\ -1 & \chi(i) \neq \chi(j). \end{cases}$$

This would be one way to generalize the bipartition corresponding to structural balance into a multipartite system.

Similarly, we can consider *complex phase interactions*, where the states of each node are now complex-valued, and the colouring function separates each node into a characteristic phase

$$\chi_\varphi(j) = e^{\chi(j)2\pi i/(N+1)}.$$

Then, the weight between two neighbours is given by

$$W_{\{l,m\}} = e^{\chi(l)2\pi i/(N+1)} e^{\chi(m)2\pi i/(N+1)}.$$

When the number of colours is two, this reduces down to the case of signed networks.

Another question is on the modeling usage of matrix-weighted graphs. The relevant chapters in this thesis discussed some applications from the literature on how matrix-weighted consensus protocols are used in practice, but it would be interesting to see if some interesting networked dynamical systems can be modelled by them, specifically oscillator dynamics. By extending the matrix weights to Hermitian matrices, and the node states to complex valued, one can view the matrix as a coupling between amplitude and phase over a network of oscillators. What specific oscillator models can be captured in such a setting is an open problem.

15.2 DESIGN

The network design problems in this paper were primarily focused on edge weight and time scale design for noise rejection in controlled consensus networks. A natural extension would be to consider similar design problems for the dual task of estimation. In particular, edge weight and time scale design has the potential to be useful for designing Kalman consensus filters over large sensor networks. Seminal work by Olfati-Saber has provided an angle for approaching this sort of design problem [38], [39], [41].

As seen in an earlier chapter of this dissertation, agents over a sensor network can achieve consensus on a state estimate of that system by adding a consensus step to their estimate propagation:

$$\hat{x}_i^{k+1} = \hat{x}_i^k + K_i^k(\tilde{y}_i^k - C_i\hat{x}_i^k)$$
$$\downarrow$$
$$\hat{x}_i^{k+1} = \hat{x}_i^k + K_i^k(\tilde{y}_i^k - C_i\hat{x}_i^k) + \sum_{j\in\mathcal{N}_i}(\hat{x}_j^k - \hat{x}_i^k).$$

What has not been explored is a weight assignment or weight update scheme of the form

$$\epsilon_k^i\hat{x}_i^{k+1} = \hat{x}_i^k + K_i^k\left(\tilde{y}_i^k - C_i\hat{x}_i^k\right) + \sum_{j\in\mathcal{N}_i} W_{ij}(\hat{x}_j^k - \hat{x}_i^k),$$

where the weights W_{ij}'s are chosen according to a gradient weight update on the minimization of an appropriate cost, perhaps related to the steady-state error covariance of the estimate, or a stability-based criterion, and similarly with the timescales ϵ_k^i.

Work by Barooah & Hespanha has shown that the electrical networks interpretation considered in the weight design section of this thesis has an interpretation in certain estimation tasks. In particular, the state estimate covariance of a certain type of (non-recursive) estimator is related to the matrix-valued effective resistance over a matrix-valued graph representing a sensor network [94], [115], [128]. If an analogous relation could be derived for a Kalman consensus filter setup, then it is very likely that a distributed series-parallel algorithm for adaptive weight design could be implemented in such a setting.

15.3 INTERACTION

Optimal transport has received a large amount of attention from both the mathematical and control theory communities. Two fields medalists in recent years, Cédric Villani and Alessio Figalli, have made substantial contributions to the field. The work in this dissertation has focused on applications of optimal transport theory in controlling distributions of agent states in networked dynamical systems, but there is a plethora of other questions one can pose that extends the results presented here.

One fundamental problem with the optimal transport approach, in particular when coupled with the gradient feedback, is the assumption of the mean-field approximation. In some formal sense, the continuity equation

$$\frac{\partial}{\partial t}\rho(x,t) + \nabla_x\cdot((\mathcal{P}(\rho,x) + v(x,t)\rho(x,t)) = 0$$

arises from a *mean-field limit* where we take the number of agents $n \to \infty$, yielding some notion of the following convergence of the empirical measure supported at agent states:

$$\lim_{n\to\infty} \frac{1}{n} \sum_{i=1}^{n} \delta(x - x_i(t)) = \rho(x,t).$$

Of course, real systems do not have infinitely many agents, and so the performance of the methods of the work presented in this dissertation will be affected by how many (or rather, how few) agents are in the system. The natural question to ask is what is the right "error metric" to use when comparing the vanilla continuum to the discrete counterpart. A naïve choice may be, for example

$$e(x,t) = \left\| n^{-1} \sum_{i=1}^{n} \delta(x - x_i(t)) - \rho(x,t) \right\|.$$

It would be of significant interest to identify what sort of "error metric" gives nice control-theoretic guarantees on the performance of these methods when applied to finitely many agents.

An alternate approach would be to explicitly discretize the optimal transport problem in such a way that the discretized density can be explicitly represented as the empirical measure supported at agent states. The issue with this approach is that then the discretized density is essentially a time-evolving grid when solving the continuity equation, and so care must be taken to make the solution nicely behaved.

When implementing these techniques on formation control of aerial or robotic agents, the task of collision avoidance becomes paramount. A natural question to ask is what conditions on $v(x,t)$ can be imposed that provide some bound on how two single-integrator particles solving the ODE

$$\dot{x}_1 = v(x_1(t),t),\ \dot{x}_2 = v(x_2(t),t)$$

will not come within some radius r from each other. For example, if $\|x_1(0) - x_2(0)\| \geq r$, what conditions on $v(x,t)$ will ensure that $\|x_1(t) - x_2(t)\| \geq r$ for all $0 \leq t \leq T$? Can these conditions be implemented in a convex optimization program compatible with optimal transport-type programs?

Lastly, hardware implementation of these methods will serve to both verify the mass transport techniques as well as expose the shortcomings and limitations of them. For example, actuator saturation and hardware speed limits will impair the ability of vehicles to properly track the velocity fields prescribed by the optimal transport and gradient feedback. Imposing constraints that solve these issues on the optimal transport optimization problem is certainly a topic of interest.

Another pressing issue related to hardware implementation is computational efficiency. Currently, the optimal transport control has to be solved offline, and in a rather computationally expensive way. The algorithm by [170] solves the vanilla Brenier-Benamou mass transport problem by changing to flux coordinates $F(x,t) = v(x,t)\rho(x,t)$ and then discretizing the problem

space in (x, t). The discretization of the Brenier-Benamou problem yields a cost function of the form

$$\min_{F,\rho} = \sum_{x,t} \frac{\|F(x,t)\|^2}{\rho(x,t)},$$

which is miraculously convex, as well as linear constraints arising from the discretization of

$$\frac{\partial}{\partial t}\rho(x,t) + \nabla_x \cdot F(x(t),t) = 0,$$

which yields a set of linear equality constraints. Unfortunately, the large solution space resulting from this discretization makes it computationally expensive. Research in online algorithms, or approximate solutions that are cheap, would be of significant interest.

BIBLIOGRAPHY

[1] R. Olfati-Saber, "Flocking for Multi-Agent Dynamic Systems: Algorithms and Theory," *IEEE Trans. on Automatic Control*, vol. 51, no. 3, pp. 401–420, 2004.

[2] M. H. Matheny, J. Emenheiser, W. Fon, A. Chapman, M. Rohden, A. Salova, J. Li, M. Hudoba de Badyn, L. Duenas-Osorio, M. Mesbahi, J. P. Crutchfield, M. C. Cross, R. M. D'Souza, and M. L. Roukes, "Exotic states in a simple network of nanoelectromechanical oscillators," *Science*, vol. 363, no. 6431, pp. 1–10, 2019. DOI: 10.1126/science.aav7932.

[3] R. Hegselmann and U. Krause, "Opinion dynamics and bounded confidence models, analysis and simulation," *Journal of Artificial Societies and Social Simulation*, vol. 5, no. 3, 2002.

[4] F. Cucker and S. Smale, "Emergent Behavior in Flocks," *IEEE Transaction on Automatic Control*, vol. 52, no. 5, pp. 852–862, 2007.

[5] M. Mesbahi and M. Egerstedt, *Graph-Theoretic Methods in Multiagent Networks*. Princeton University Press, 2010, p. 403, ISBN: 9780691140612. DOI: 10.1073/pnas.0703993104.

[6] T. Vicsek, A. Czirok, E. Ben-Jacob, I. Cohen, and O. Shochet, "Novel type of phase transistion in a system of self-driven particles," *New York*, vol. 75, no. 6, pp. 1226–1229, 1995, ISSN: 1079-7114. DOI: 10.1103/PhysRevLett.74.2248.

[7] M. A. Joordens and M. Jamshidi, "Underwater swarm robotics consensus control," in *Proc. IEEE International Conference on Systems, Man and Cybernetics*, San Antonio, USA, 2009, pp. 3163–3168, ISBN: 9781424427949. DOI: 10.1109/ICSMC.2009.5346165.

[8] P. Stone and M. Veloso, "Multiagent systems: a survey from a machine learning perspective," *Autonomous Robots*, vol. 8, no. 3, pp. 345–383, 2000, ISSN: 09295593. DOI: 10.1023/A:1008942012299.

[9] A. Acín, J. I. Cirac, and M. Lewenstein, "Entanglement percolation in quantum networks," *Nature Physics*, vol. 3, no. April, pp. 256–259, 2007, ISSN: 1745-2473.

[10] G. Fabrizio, L. Pollini, and M. Innocenti, "Autonomous Formation Flight," *IEEE Control Systems Magazine*, no. December, pp. 34–44, 2000.

[11] H. Yang and S. Yagar, "Traffic assignment and signal control in saturated road networks," *Transportation Research Part A*, vol. 29, no. 2, pp. 125–139, 1995, ISSN: 09658564. DOI: 10.1016/0965-8564(94)E0007-V.

[12] Y. Chen, J. Lu, X. Yu, and D. J. Hill, "Multi-agent systems with dynamical topologies: Consensus and applications," *IEEE Circuits and Systems Magazine*, vol. 13, no. 3, pp. 21–34, 2013, ISSN: 1531636X. DOI: 10.1109/MCAS.2013.2271443.

[13] R. Olfati-Saber and R. M. Murray, "Consensus protocols for networks of dynamic agents," *Proc. of the American Control Conference*, vol. 2, pp. 951–956, 2003, ISSN: 0743-1619. DOI: 10.1109/ACC.2003.1239709.

[14] M. K. S. Yeung, J. Tegnér, and J. J. Collins, "Reverse engineering gene networks using singular value decomposition and robust regression.," *Proceedings of the National Academy of Sciences of the United States of America*, vol. 99, no. 9, pp. 6163–6168, 2002, ISSN: 0027-8424.

[15] D. Cartwright and F. Harary, "Structural balance: A generalization of Heider's theory," *Psychological Review*, vol. 63, no. 5, p. 277, 1956.

[16] V. Srivastava, J. Moehlis, and F. Bullo, "On bifurcations in nonlinear consensus networks," *Journal of Nonlinear Science*, vol. 21, no. 6, pp. 875–895, 2011, ISSN: 09388974. DOI: 10.1007/s00332-011-9103-4.

[17] A. Rahmani, M. Ji, M. Mesbahi, and M. Egerstedt, "Controllability of multi-agent systems from a graph-theoretic perspective," *SIAM Journal on Control and Optimization*, vol. 48, no. 1, pp. 162–186, 2009.

[18] A. Chapman and M. Mesbahi, "State controllability, output controllability and stabilizability of networks : A symmetry perspective," in *Proc. 54th IEEE Conference on Decision and Control*, Osaka, Japan, 2015, pp. 4776–4781, ISBN: 9781479978854.

[19] M. Siami and N. Motee, "Tractable approximation algorithms for the NP-hard problem of growing linear consensus networks," in *Proceedings of the American Control Conference*, Boston, USA, 2016, pp. 6429–6434, ISBN: 9781467386821. DOI: 10.1109/ACC.2016.7526681.

[20] D. Zelazo, S. Schuler, and F. Allgöwer, "Performance and design of cycles in consensus networks," *Systems and Control Letters*, vol. 62, no. 1, pp. 85–96, 2013, ISSN: 01676911.

[21] A. Chapman and M. Mesbahi, "Kronecker product of networked systems and their approximates," in *21st International Symposium on the Mathematical Theory of Networks and Systems*, Groningen, 2014, pp. 1426–1431, ISBN: 9789036763219.

[22] M. Hudoba de Badyn and M. Mesbahi, "Growing controllable networks via whiskering and submodular optimization," in *Proc. 55th IEEE Conference on Decision and Control*, Las Vegas, USA, 2016, pp. 867–872, ISBN: 9781509018369. DOI: 10.1109/CDC.2016.7798376.

[23] M. Hudoba de Badyn, *On the Control of Consensus Networks: Theory and Applications*. Seattle, USA: Master's Thesis, 2017.

[24] C. Altafini, "Consensus problems on networks with antagonistic interactions," *IEEE Transactions on Automatic Control*, vol. 58, no. 4, pp. 935–946, 2013.

[25] ——, "Dynamics of opinion forming in structurally balanced social networks," *PloS one*, vol. 7, no. 6, pp. 5876–5881, 2012.

[26] J. Akiyama, D. Avis, V. Chvatal, and H. Era, "Balancing Signed Graphs," *Discrete Applied Mathematics*, vol. 3, pp. 227–233, 1981.

[27] E. Kaszkurewicz and A. Bhaya, *Matrix Diagonal Stability in Systems and Computation*. Springer Science & Business Media, 2012.

[28] L. Pan, H. Shao, and M. Mesbahi, "Laplacian dynamics on signed networks," in *Proc. 55th IEEE Conference on Decision and Control*, Las Vegas, USA, 2016, pp. 891–896, ISBN: 9781509018369. DOI: 10.1109/CDC.2016.7798380.

[29] ——, "Verification and prediction of structural balance: A data-driven perspective," in *Proc.of the American Control Conference*, Boston, USA, 2016, pp. 2858–2863.

[30] F. Harary and J. A. Kabell, "A simple algorithm to detect balance in signed graphs," *Mathematical Social Sciences*, vol. 1, no. 1, pp. 131–136, 1980.

[31] G. Facchetti, G. Iacono, and C. Altafini, "Computing global structural balance in large-scale signed social networks.," *Proceedings of the National Academy of Sciences of the United States of America*, vol. 108, no. 52, pp. 20 953–20 958, 2011, ISSN: 1091-6490.

[32] A. Clark, Q. Hou, L. Bushnell, and R. Poovendran, "A submodular optimization approach to leader- follower consensus in networks with negative edges," in *Proc. American Control Conference*, Seattle, USA, 2017.

[33] C. O. Aguilar and B. Gharesifard, "Necessary conditions for controllability of nonlinear networked control systems," in *Proc. American Control Conference*, Portland, USA, 2014, pp. 5379–5383, ISBN: 978-1-4799-3274-0. DOI: 10.1109/ACC.2014.6859170.

[34] U. A. Khan and J. M. F. Moura, "Distributing the Kalman filter for large-scale systems," *IEEE Transactions on Signal Processing*, vol. 56, no. 10, pp. 4919–4935, 2008.

[35] J. N. Kutz, *Data-driven modeling & scientific computation: Methods for complex systems & big data*. Oxford University Press, 2013, pp. 226–456.

[36] R. Furrer and T. Bengtsson, "Estimation of high-dimensional prior and posterior covariance matrices in Kalman filter variants," *Journal of Multivariate Analysis*, vol. 98, no. 2, pp. 227–255, 2007, ISSN: 0047259X.

[37] R. S. Sutton, "Gain adaptation beats least squares?" In *Proceedings of the Seventh Yale Workshop on Adaptive and Learning Systems*, 1992, pp. 161–166.

[38] R. Olfati-Saber, "Distributed Kalman filter with embedded consensus filters," in *Proceedings of the 44th IEEE Conference on Decision and Control and the European Control Conference*, Seville, Spain, 2005, pp. 8179–8184, ISBN: 0780395689.

[39] ——, "Distributed Kalman filtering for sensor networks," in *Proc. of the 46th IEEE Conference on Decision and Control*, New Orleans, USA, 2007, pp. 5492–5498, ISBN: 1424414989.

[40] R. Carli, A. Chiuso, L. Schenato, and S. Zampieri, "Distributed Kalman filtering based on consensus strategies," *IEEE Journal on Selected Areas in Communications*, vol. 26, no. 4, pp. 622–633, 2008, ISSN: 07338716.

[41] D. P. Spanos, R. Olfati-Saber, and R. M. Murray, "Approximate Distributed Kalman Filtering in Sensor Networks with Quantifiable Performance," in *Fourth International Symposium on Imformation Processing in Sensor Networks*, Los Angeles, USA, 2005, pp. 133–139, ISBN: 0780392027.

[42] M. Budišić, R. Mohr, and I. Mezić, "Applied Koopmanism," *Chaos*, vol. 22, no. 4, 2012, ISSN: 10541500. DOI: 10.1063/1.4772195.

[43] M. O. Williams, I. G. Kevrekidis, and C. W. Rowley, "A data-driven approximation of the Koopman operator: Extending dynamic mode decomposition," *Journal of Nonlinear Science*, vol. 25, no. 6, pp. 1307–1346, 2015.

[44] C. D. Godsil and G. F. Royle, *Algebraic Graph Theory*. Springer Science & Business Media, 2013, vol. 207.

[45] A. Chapman, M. Nabi-Abdolyousefi, and M. Mesbahi, "Controllability and observability of network-of-networks via Cartesian products," *IEEE Transaction on Automatic Control*, vol. 59, no. 10, pp. 2668–2679, 2014.

[46] W. Imrich and S. Klavžar, *Product Graphs: Structure and Recognition*. Wiley-Interscience, 2000.

[47] G. Sabidussi, "Graph Multiplication," *Mathematische Zeitschrift*, vol. 72, pp. 446–457, 1960.

[48] V. G. Vizing, "The Cartesian product of graphs," *Vyčisl. Sistemy*, vol. 9, pp. 30–43, 1963.

[49] A. J. Chorin and O. H. Hald, *Stochastic tools in mathematics and science*. Springer, 2009, vol. 3.

[50] Y. Nesterov, "A method of solving a convex programming problem with convergence rate O (1/k^2)," in *Soviet Mathematics Doklady*, vol. 27, 1983, pp. 372–376.

[51] J. Barzilai and J. M. Borwein, *Two-point step size gradient methods*, 1988.

[52] P. Dorato, V. Cerone, and C. Abdallah, *Linear-Quadratic Control: An Introduction*. Simon & Schuster, 1994.

[53] H. Li, C. Feng, H. Ehrhard, Y. Shen, B. Cobos, F. Zhang, K. Elamvazhuthi, S. Berman, M. Haberland, and A. L. Bertozzi, "Decentralized stochastic control of robotic swarm density: Theory, simulation, and experiment," in *Proc. IEEE International Conference on Intelligent Robots and Systems*, Vancouver, Canada, 2017, pp. 4341–4347, ISBN: 9781538626825. DOI: 10.1109/IROS.2017.8206299.

[54] J. Emenheiser, A. Chapman, M. Pósfai, J. P. Crutchfield, M. Mesbahi, and R. M. D'Souza, "Patterns of patterns of synchronization: Noise induced attractor switching in rings of coupled nonlinear oscillators," *Chaos*, vol. 26, no. 9, pp. 1–33, 2016, ISSN: 10541500. DOI: 10.1063/1.4960191.

[55] S. Alemzadeh and M. Mesbahi, "Influence models on layered uncertain networks: A guaranteed-cost design perspective," in *Proc. 57th IEEE Conference on Decision and Control*, 2018.

[56] R. Albert and A.-L. Barabási, "Statistical mechanics of complex networks," *Reviews of Modern Physics*, vol. 74, no. 1, pp. 47–97, 2002, ISSN: 1478-3967.

[57] A.-L. Barabási, "Scale-Free Networks: A Decade and Beyond," *Science*, vol. 325, no. 5939, pp. 412–413, 2009, ISSN: 0036-8075.

[58] L. Demetrius and T. Manke, "Robustness and network evolution - An entropic principle," *Physica A: Statistical Mechanics and its Applications*, vol. 346, no. 3-4, pp. 682–696, 2005, ISSN: 03784371. DOI: 10.1016/j.physa.2004.07.011.

[59] S. Boccaletti, V. Latora, Y. Moreno, M. Chavez, and D. U. Hwang, "Complex networks: Structure and dynamics," *Physics Reports*, vol. 424, no. 4-5, pp. 175–308, 2006, ISSN: 03701573. DOI: 10.1016/j.physrep.2005.10.009.

[60] M. Hudoba de Badyn and M. Mesbahi, "Large-scale distributed Kalman filtering via an optimization approach," *IFAC-PapersOnLine*, vol. 50, no. 1, pp. 10 742–10 747, 2017.

[61] M. Hudoba de Badyn, U. Eren, B. Açıkmeşe, and M. Mesbahi, "Optimal mass transport and kernel density estimation for state-dependent networked dynamic systems," in *Proc. 57th IEEE Conference on Decision and Control*, Miami Beach, USA, 2018.

[62] S. Alemzadeh, M. Hudoba de Badyn, and M. Mesbahi, "Controllability and stabilizability analysis of signed consensus networks," in *Proc. IEEE Conference on Control Technology and Applications*, Kohala Coast, USA, 2017, pp. 55–60.

[63] M. Hudoba de Badyn, S. Alemzadeh, and M. Mesbahi, "Controllability and data-driven identification of bipartite consensus on nonlinear signed networks," in *Proc. 56th IEEE Conference on Decision and Control*, Melbourne, Australia, 2017.

[64] S. O'Rourke and B. Touri, "On a conjecture of Godsil concerning controllable random graphs," *arXiv:1511.05080*, pp. 1–32, 2015.

[65] A. Ghosh and S. Boyd, "Growing well-connected graphs," in *Proc. 45th IEEE Conference on Decision and Control*, San Diego, 2006, pp. 6605–6611, ISBN: 1-4244-0171-2. DOI: 10.1109/CDC.2006.377282.

[66] A. Chapman and M. Mesbahi, "Semi-autonomous consensus: Network measures and adaptive trees," *IEEE Transactions on Automatic Control*, vol. 58, no. 1, pp. 19–31, 2013, ISSN: 00189286. DOI: 10.1109/TAC.2012.2205429.

[67] A. Y. Yazicioglu and M. Egerstedt, "Leader selection and network assembly for controllability of leader-follower networks," in *Proc. of the American Control Conference*, Washington, D.C., 2013, pp. 3802–3807, ISBN: 1479901776.

[68] F. L. Cortesi, T. H. Summers, and J. Lygeros, "Submodularity of Energy Related Controllability Metrics," in *Proc. 54rd IEEE Conference on Decision and Control*, Los Angeles, 2014, pp. 2883–2888, ISBN: 9781467360883. DOI: 10.1109/CDC.2014.7039832.

[69] T. H. Summers, F. L. Cortesi, and J. Lygeros, "On Submodularity and Controllability in Complex Dynamical Networks," *arXiv:1404.7665*, pp. 1–10, 2014, ISSN: 2325-5870. DOI: 10.1109/TCNS.2015.2453711.

[70] A. Clark, B. Alomair, L. Bushnell, and R. Poovendran, *Submodularity in Dynamics and Control of Networked Systems*. Springer, 2016.

[71] M. Hudoba de Badyn, A. Chapman, and M. Mesbahi, "Network entropy: A system-theoretic perspective," in *Proc. 54th IEEE Conference on Decision and Control*, Osaka, Japan, 2015, pp. 5512–5517.

[72] M. Siami and N. Motee, "Schur-Convex Robustness Measures in Dynamical Networks," in *Proc. of the American Control Conference*, Portland, 2014, pp. 5198–5203, ISBN: 9781479932719.

[73] ——, "Growing linear consensus networks endowed by spectral systemic performance measures," *IEEE Transaction on Automatic Control*, vol. 63, no. 7, pp. 2091–2106, 2018.

[74] ——, "Fundamental limits and tradeoffs on disturbance propagation in linear dynamical networks," *IEEE Transaction on Automatic Control*, vol. 61, no. 12, pp. 4055–4062, 2016, ISSN: 00189286. DOI: 10.1109/TAC.2016.2547982.

[75] A. Chapman, E. Schoof, and M. Mesbahi, "Online Adaptive Network Design for Disturbance Rejection," in *Principles of Cyber-Physical Systems*, Cambridge University Press, 2015.

[76] B. Bamieh, M. R. Jovanović, P. Mitra, and S. Patterson, "Coherence in Large-Scale Networks: Dimension-Dependent Limitations of Local Feedback," *IEEE Transactions on Automatic Control*, vol. 57, no. 9, pp. 2235–2249, 2012. DOI: 10.1109/TAC.2012.2202052.

[77] D. R. Foight, M. Hudoba de Badyn, and M. Mesbahi, "Time Scale Design for Network Resilience," in *Submitted to Proc. 58th IEEE Conference on Decision and Control*, Nice, France, 2019, pp. 1–8.

[78] M. Hudoba de Badyn, D. R. Foight, and M. Mesbahi, "Time Scale and Edge Weight Design for H2 Performance on Consensus Networks," *To be submitted to the IEEE Transactions on Control of Network Systems*, vol. XX, no. X, pp. 1–10, 2019.

[79] P. Kokotović, H. K. Khalil, and J. O'Reilly, *Singular Perturbation Methods in Control: Analysis and Design*. Philadelphia: Society for Industrial and Applied Mathematics, 1999, ISBN: 0898714443.

[80] R. Olfati-Saber and R. M. Murray, "Consensus problems in networks of agents with switching topology and time-delays," *IEEE Transactions on Automatic Control*, vol. 49, no. 9, pp. 1520–1533, 2004, ISSN: 00189286.

[81] F. Pedroche, M. Rebollo, C. Carrascosa, and A. Palomares, "Convergence of weighted-average consensus for undirected graphs," *International Journal of Complex Systems in Science*, vol. 4, no. 1, pp. 13–16, 2014.

[82] A. Chapman and M. Mesbahi, "Multiple Time-Scales in Network-of-Networks," in *Proc. American Control Conference*, Boston, USA, 2016, pp. 5563–5568, ISBN: 9781467386821.

[83] A. Awad, A. Chapman, E. Schoof, A. Narang-Siddarth, and M. Mesbahi, "Time-scale separation in networks: state-dependent graphs and consensus tracking," *IEEE Transactions on Control of Network Systems*, vol. 5870, no. c, pp. 1–1, 2018, ISSN: 2325-5870. DOI: 10.1109/TCNS.2018.2800401.

[84] J. B. Rejeb, I.-C. Morărescu, and J. Daafouz, "Synchronization in networks of linear singularly perturbed systems," in *Proc. American Control Conference*, Boston, USA: American Automatic Control Council (AACC), 2016, pp. 4293–4298, ISBN: 9781467386821. DOI: 10.1109/ACC.2016.7525597.

[85] ——, "Control design with guaranteed cost for synchronization in networks of linear singularly perturbed systems," *Automatica*, vol. 91, pp. 89–97, 2018.

[86] D. R. Foight and M. Mesbahi, "Influenced Consensus for Multi-Scale Networks," in *Proc. American Control Conference*, Philadelphia, USA, 2019.

[87] M. H. Trinh and H.-S. Ahn, "Theory and applications of matrix-weighted consensus," *arXiv preprint arXiv: 1703:00129v3*, no. 1, pp. 1–21, 2017.

[88] N. E. Friedkin, A. V. Proskurnikov, R. Tempo, and S. E. Parsegov, "Network science on belief system dynamics under logic constraints," *Science*, vol. 354, no. 6310, pp. 321–326, 2016, ISSN: 10959203. DOI: 10.1126/science.aag2624.

[89] S. E. Parsegov, A. V. Proskurnikov, R. Tempo, and N. E. Friedkin, "Novel multidimensional models of opinion dynamics in social networks," *IEEE Transactions on Automatic Control*, vol. 62, no. 5, pp. 2270–2285, 2017, ISSN: 00189286. DOI: 10.1109/TAC.2016.2613905.

[90] S. E. Tuna, "Synchronization under matrix-weighted Laplacian," *Automatica*, vol. 73, pp. 76–81, 2016, ISSN: 00051098. DOI: 10.1016/j.automatica.2016.06.012.

[91] J. L. Ramirez, M. Pavone, E. Frazzoli, and D. W. Miller, "Distributed control of spacecraft formation via cyclic pursuit: Theory and experiments," *Proc. American Control Conference*, pp. 4811–4817, 2019.

[92] B. H. Lee and H. S. Ahn, "Distributed formation control via global orientation estimation," *Automatica*, vol. 73, pp. 125–129, 2016, ISSN: 00051098. DOI: 10.1016/j.automatica.2016.06.030.

[93] F. Dörfler, "Electric networks and algebraic graph theory: Models, properties and applications," *Proceedings of the IEEE*, vol. 106, no. 5, pp. 997–1005, 2018.

[94] P. Barooah and J. P. Hespanha, "Estimation from relative measurements: Electrical analogy and large graphs," *IEEE Transactions on Signal Processing*, vol. 56, no. 6, pp. 2181–2193, 2008, ISSN: 1053587X. DOI: 10.1109/TSP.2007.912270.

[95] R. Diestel, *Graph Theory*. Springer Publishing Company, Incorporated, 2018.

[96] B. Barzgaran, M. Hudoba de Badyn, and M. Mesbahi, "Growing Controllable Networks via Single and Multi-Node Attachments," in *In prep*, Chicago, USA, 2019, pp. 1–6.

[97] A. Alaeddini, S. Alemzadeh, A. Mesbahi, and M. Mesbahi, "Linear model regression on time-series data: Non-asymptotic error bounds and applications," in *Proc. 57th IEEE Conference on Decision and Control*, Miami Beach, USA, 2018.

[98] M. Hudoba de Badyn and M. Mesbahi, "Efficient Computation of Performance on Series-Parallel Networks," in *Proc. American Control Conference*, Philadelphia, USA, 2019, pp. 1–6.

[99] ——, "H2 Performance of Series-Parallel Networks : A Compositional Perspective," *Submitted to the IEEE Transactions on Automatic Control*, vol. XX, no. X, pp. 1–13, 2019.

[100] J. Valdes, R. E. Tarjan, and E. L. Lawler, "The recognition of Series Parallel digraphs," *Proceedings of the eleventh annual ACM symposium on Theory of computing*, pp. 1–12, 1979, ISSN: 0097-5397. DOI: 10.1145/800135.804393.

[101] D. Eppstein, "Parallel Recognition of Series-Parallel Graphs," *Information and Computation*, vol. 98, pp. 41–55, 1992.

[102] K. Takamizawa, T. Nishizeki, and N. Saito, "Linear-time computability of combinatorial problems on series-parallel graphs," *Journal of the Association for Computing Machinery*, vol. 29, no. 3, pp. 623–641, 1986.

[103] E. Cela, *The Quadratic Assignment Problem: Theory and Algorithms*. Springer Science & Business Media, 2013, vol. 1.

[104] P. De, E. J. Dunne, J. B. Ghosh, and C. E. Wells, "Complexity of the discrete time-cost tradeoff problem for project networks," *Operations Research*, vol. 45, no. 2, pp. 302–306, 1997, ISSN: 0030-364X. DOI: 10.1287/opre.45.2.302.

[105] T. Roughgarden, "Selfish Routing," PhD thesis, Cornell University, 2012, p. 170, ISBN: 0-493-66069-0. DOI: 10.1145/506147.506153.

[106] S. E. Elmaghraby, "Resource allocation via dynamic programming in activity networks," *European Journal of Operational Research*, vol. 64, no. 2, pp. 199–215, 1993, ISSN: 03772217. DOI: 10.1016/0377-2217(93)90177-O.

[107] F. Le Gall, "Powers of Tensors and Fast Matrix Multiplication," in *Proc. of the 39th International Symposium on Symbolic and Algebraic Computation*, Kobe, Japan, 2014, pp. 296–303, ISBN: 9781450325011. DOI: 10.1145/2608628.2608664.

[108] V. Belevitch, *Classical network theory*. Holden-Day, 1968.

[109] S. Friedland and S. Gaubert, "Submodular spectral functions of principal submatrices of a hermitian matrix, extensions and applications," *Linear Algebra and Its Applications*, vol. 438, no. 10, pp. 3872–3884, 2013, ISSN: 00243795. DOI: 10.1016/j.laa.2011.11.021.

[110] K. Audenaert, F. Hiai, and D. Petz, "Strongly subadditive functions," *Acta Mathematica Hungarica*, vol. 128, no. 4, pp. 386–394, 2010, ISSN: 02365294. DOI: 10.1007/s10474-010-9222-7.

[111] R. H. Villarreal, "Cohen-Macaulay Graphs," *Manuscripta Mathematica*, vol. 66, no. 1, pp. 277–293, 1990.

[112] J. Biermann and A. Van Tuyl, "Balanced vertex decomposable simplicial complexes and their h-vectors," *Electronic Journal of Combinatorics*, vol. 20, no. 3, pp. 1–16, 2013, ISSN: 10778926.

[113] M. Grant and S. Boyd, "CVX: Matlab Software for Disciplined Convex Programming, version 2.1," in *Recent Advances in Learning and Control*, ser. Lecture Notes in Control and Information Sciences, V. Blondel, S. Boyd, and H. Kimura, Eds., Springer-Verlag Limited, Mar. 2014, pp. 95–110.

[114] ——, "Graph implementations for nonsmooth convex programs," in *Recent Advances in Learning and Control*, ser. Lecture Notes in Control and Information Sciences, V. Blondel, S. Boyd, and H. Kimura, Eds., Springer-Verlag Limited, 2008, pp. 95–110.

[115] P. Barooah and J. P. Hespanha, "Estimation on graphs from relative measurements," *IEEE Control Systems*, vol. 27, no. 4, pp. 57–74, 2007, ISSN: 1066033X. DOI: 10.1109/MCS.2007.384125.

[116] R. J. Duffin, "Network models," in *Mathematical Aspects of Electrical Network Analysis*, 1969, pp. 65–92.

[117] X. He and Y. Yesha, "Parallel recognition and decomposition of two terminal series parallel graphs," *Information and Computation*, vol. 75, no. 1, pp. 15–38, 1987, ISSN: 10902651. DOI: 10.1016/0890-5401(87)90061-7.

[118] M. W. Bern, E. L. Lawler, and A. L. Wong, "Linear-time computation of optimal subgraphs of decomposable graphs," *Journal of Algorithms*, vol. 8, no. 2, pp. 216–235, 1987, ISSN: 01966774. DOI: 10.1016/0196-6774(87)90039-3.

[119] T. Kikuno, N. Yoshida, and Y. Kakuda, "A linear algorithm for the domination number of a series-parallel graph," *Discrete Applied Mathematics*, vol. 5, no. 3, pp. 299–311, 1983, ISSN: 0166218X. DOI: 10.1016/0166-218X(83)90003-3.

[120] M. D. Petković and P. S. Stanimirović, "Generalized matrix inversion is not harder than matrix multiplication," *Journal of Computational and Applied Mathematics*, vol. 230, no. 1, pp. 270–282, 2009, ISSN: 03770427. DOI: 10.1016/j.cam.2008.11.012.

[121] W. N. Anderson Jr. and R. J. Duffin, "Series and parallel addition of matrices," *Journal of Mathematical Analysis and Applications*, vol. 26, pp. 576–594, 1969, ISSN: 10960813. DOI: 10.1016/0022-247X(69)90200-5.

[122] D. Zelazo and M. Mesbahi, "Edge agreement: Graph-theoretic performance bounds and passivity analysis," *IEEE Transactions on Automatic Control*, vol. 56, no. 3, pp. 544–555, 2011, ISSN: 00189286. DOI: 10.1109/TAC.2010.2056730.

[123] K. B. Petersen and M. S. Pedersen, *The Matrix Cookbook*. Technical University of Denmark, 2008.

[124] G. Robins, P. Pattison, Y. Kalish, and D. Lusher, "An introduction to exponential random graph (p^*) models for social networks," *Social Networks*, vol. 29, no. 2, pp. 173–191, 2007, ISSN: 03788733. DOI: 10.1016/j.socnet.2006.08.002.

[125] V. Vedral, A. Barenco, and A. Ekert, "Quantum Networks for Elementary Arithmetic Operations," *Physical Review A*, vol. 54, no. 1, pp. 147–153, 1996, ISSN: 1050-2947. DOI: 10.1103/PhysRevA.54.147. [Online]. Available: http://arxiv.org/abs/quant-ph/9511018.

[126] G. Mahler and R. Wawer, "Quantum Networks: Dynamics of Open Nanostructures," *VLSI Design*, vol. 8, no. 1-4, pp. 191–196, 1998.

[127] J. D. Allen, Y. Xie, M. Chen, L. Girard, and G. Xiao, "Comparing statistical methods for constructing large scale gene networks," *PLOS ONE*, vol. 7, no. 1, e29348, 2012, ISSN: 19326203. DOI: 10.1371/journal.pone.0029348.

[128] P. Barooah and J. P. Hespanha, "Graph effective resistance and distributed control: Spectral properties and applications," in *45th IEEE Conference on Decision & Control*, 2006, pp. 3479–3485, ISBN: 1424401712.

[129] S. Salsa, *Partial Differential Equations in Action: From Modelling to Theory*. Milano: Springer-Verlag Italia, 2008, ISBN: 9788847007512.

[130] G. S. Chirikjian, *Modeling Loop Entropy*. 2011, vol. 487, pp. 99–132, ISBN: 9780123812704. DOI: 10.1016/B978-0-12-381270-4.00004-4.Modeling.

[131] L. Boltzmann, *Lectures on Gas Theory*. Dover Publications, 2011.

[132] C. A. Desoer, "The Optimum Formula for the Gain of a Flow Graph or a Simple Derivation of Coates' Formula," *Proceedings of the IRE*, vol. 48, no. 5, pp. 883–889, 1960, ISSN: 0096-8390. DOI: 10.1109/JRPROC.1960.287625.

[133] V. Nikiforov, "Some Inequalities for the Largest Eigenvalue of a Graph," *Combinatorics, Probability and Computing*, vol. 11, no. 02, pp. 179–189, 2002, ISSN: 0963-5483. DOI: 10.1017/S0963548301004928.

[134] L. Demetrius and T. Manke, "Robustness and network evolution - An entropic principle," *Physica A: Statistical Mechanics and its Applications*, vol. 346, no. 3-4, pp. 682–696, 2005, ISSN: 03784371. DOI: 10.1016/j.physa.2004.07.011.

[135] L. Arnold, V. M. Gundlach, and L. Demetrius, "Evolutionary Formalism for Products of Positive Random Matrices," *The Annals of Applied Probability*, vol. 4, no. 3, pp. 859–901, 1994.

[136] F. K. Bell, "A Note on the Irregularity of Graphs," *Linear Algebra and its Applications*, vol. 161, pp. 45–54, 1992.

[137] D. Cvetković, P. Rowlinson, and S. Simić, *An introduction to the theory of graph spectra*. New York: Cambridge University Press, 2010. DOI: 10.5860/choice.48-0921.

[138] A. E. Brouwer and W. H. Haemers, *Spectra of Graphs*. New York; Dordrecht; Heidelberg; London: Springer, 2012, ISBN: 9781461419389.

[139] B. Açıkmeşe, M. Mandić, and J. L. Speyer, "Decentralized observers with consensus filters for distributed discrete-time linear systems," *Automatica*, vol. 50, no. 4, pp. 1037–1052, 2014, ISSN: 00051098. DOI: 10.1016/j.automatica.2014.02.008.

[140] Y. Kim and M. Mesbahi, "On maximizing the second smallest eigenvalue of a state-dependent graph Laplacian," *IEEE Transactions on Automatic Control*, vol. 51, no. 1, pp. 116–120, 2006, ISSN: 00189286. DOI: 10.1109/TAC.2005.861710.

[141] V. Krishnan and S. Martínez, "Identification of critical node clusters for consensus in large-scale spatial networks," in *IFAC-PapersOnLine*, vol. 50-1, 2017, pp. 14 721–14 726. DOI: 10.1016/j.ifacol.2017.08.2078.

[142] K. R. Harrison, A. P. Engelbrecht, and B. M. Ombuki-Berman, "Optimal parameter regions and the time-dependence of control parameter values for the particle swarm optimization algorithm," *Swarm and Evolutionary Computation*, pp. 1–40, 2018.

[143] L. Chaimowicz, N. Michael, and V. Kumar, "Controlling swarms of robots using interpolated implicit functions," in *Proc. 2005 IEEE International Conference on Robotics and Automation*, Barcelona, Spain, 2005, pp. 2487–2492, ISBN: 078038914X. DOI: 10.1109/ROBOT.2005.1570486.

[144] L. C. Pimenta, G. A. Pereira, N. Michael, R. C. Mesquita, M. M. Bosque, L. Chaimowicz, and V. Kumar, "Swarm coordination based on smoothed particle hydrodynamics technique," *IEEE Transactions on Robotics*, vol. 29, no. 2, pp. 383–399, 2013, ISSN: 15523098. DOI: 10.1109/TRO.2012.2234294.

[145] U. Eren and B. Açıkmeşe, "Velocity field generation for density control of swarms using heat equation and smoothing kernels," *IFAC-PapersOnLine*, vol. 50, no. 1, pp. 9405–9411, 2017, ISSN: 24058963. DOI: 10.1016/j.ifacol.2017.08.1454.

[146] V. Krishnan and S. Martínez, "Distributed Control for Spatial Self-Organization of Multi-Agent Swarms," *ArXiv preprint arXiv:1705.03109*, pp. 1–33, 2017.

[147] ——, "Self-Organization in Multi-Agent Swarms via Distributed Computation of Diffeomorphisms," in *Mathematical Theory of Networks and Systems*, Minneapolis, USA, 2016.

[148] G. Albi, Y.-P. Choi, M. Fornasier, and D. Kalise, "Mean field control hierarchy," *Applied Mathematics & Optimization*, vol. 76, no. 1, pp. 95–135, 2017, ISSN: 0095-4616. DOI: 10.1007/s00245-017-9429-x.

[149] P. E. Caines, *Mean field games*, 2013.

[150] M. Fornasier and F. Solombrino, "Mean-Field Optimal Control," *ESAIM: Control, Optimisation and Calculus of Variations*, vol. 20, no. 4, pp. 1123–1152, 2014, ISSN: 1292-8119. DOI: 10.1051/cocv/2014009.

[151] M. Nabi-Abdolyousefi and M. Mesbahi, "System theory over random consensus networks: Controllability and optimality properties," in *Proc. 50th IEEE Conference on Decision and Control*, Orlando, USA, 2011, pp. 2323–2328, ISBN: 9781612848006. DOI: 10.1109/CDC.2011.6161437.

[152] A. Tahbaz-Salehi and A. Jadbabaie, "On recurrence of graph connectivity in Vicsek's model of motion coordination for mobile autonomous agents," *Proceedings of the American Control Conference*, pp. 699–704, 2007, ISSN: 07431619. DOI: 10.1109/ACC.2007.4282958.

[153] M. Mesbahi, "On a dynamic extension of the theory of graphs," in *Proceedings of the American Control Conference*, vol. 2, Anchorage, USA, 2002, pp. 1234–1239, ISBN: 0780372980. DOI: 10.1109/ACC.2002.1023188.

[154] ——, "On state-dependent dynamic graphs and their controllability properties," *IEEE Transactions on Automatic Control*, vol. 50, no. 3, pp. 387–392, 2005, ISSN: 00189286. DOI: 10.1109/TAC.2005.843858.

[155] A. Awad, A. Chapman, E. Schoof, A. Narang-Siddarth, and M. Mesbahi, "Time-scale separation on networks: consensus, tracking, and state-dependent interactions," in *Proc. 54th IEEE Conference on Decision and Control*, Osaka, Japan, 2015, pp. 6172–6177, ISBN: 9781479978854.

[156] Y. Chen, T. T. Georgiou, and M. Pavon, "Optimal Transport Over a Linear Dynamical System," *IEEE Transactions on Automatic Control*, vol. 62, no. 5, pp. 2137–2152, 2017, ISSN: 00189286. DOI: 10.1109/TAC.2016.2602103.

[157] K. Elamvazhuthi and P. Grover, "Optimal transport over nonlinear systems via infinitesimal generators on graphs," *arXiv:1612.01193*, 2016.

[158] Y. Chen and J. Karlsson, "State tracking of linear ensembles via optimal mass transport," *IEEE Control Systems Letters*, vol. 2, no. 2, pp. 260–265, 2018.

[159] C. Villani, *Topics in Optimal Transportation*. American Mathematical Society, 2003, ISBN: 082183312X.

[160] ——, *Optimal Transport: Old and New*. Springer Science & Business Media, 2009, vol. 338, ISBN: 978-3-540-71049-3. DOI: 10.1007/978-3-540-71050-9.

[161] L. V. Kantorovich, "On a problem of Monge," *Uspekhi Matematicheskikh Nauk*, vol. 3, pp. 225–226, 1948.

[162] J. D. Benamou and Y. Brenier, "A computational fluid mechanics solution to the Monge-Kantorovich mass transfer problem," *Numerische Mathematik*, vol. 84, no. 3, pp. 375–393, 2000, ISSN: 0029599X. DOI: 10.1007/s002110050002.

[163] M. P. Wand and M. C. Jones, *Kernel smoothing*. Crc Press, 1994.

[164] E. Parzen, "On Estimation of a Probability Density Function and Mode," *The Annals of Mathematical Statistics*, vol. 33, no. 3, pp. 1065–1076, 1962, ISSN: 0003-4851. DOI: 10.1214/aoms/1177704472.

[165] D. Wied and R. Weißbach, "Consistency of the kernel density estimator: A survey," *Statistical Papers*, vol. 53, no. 1, pp. 1–21, 2012, ISSN: 09325026. DOI: 10.1007/s00362-010-0338-1.

[166] P. Li and S.-T. Yau, "On the Schrodinger Equation and the Eigenvalue Problem," *Commun. Math. Phys. Mathematical Physics*, vol. 88, no. 81, pp. 309–318, 1983, ISSN: 0010-3616. DOI: 10.1007/BF01213210.

[167] R. D. Gill, Y. Vardi, and J. A. Wellner, "Large Sample Theory of Empirical Distributions in Biased Sampling Models," *The Annals of Statistics*, vol. 16, no. 3, pp. 1069–1112, 1988.

[168] C. O. Wu and A. Q. Mao, "Minimax kernels for density estimation with biased data," *Annals of the Institute of Statistical Mathematics*, vol. 48, no. 3, pp. 451–467, 1996, ISSN: 00203157. DOI: 10.1007/BF00050848.

[169] N. Papadakis, G. Peyré, and E. Oudet, "Optimal Transport with Proximal Splitting," *SIAM Journal on Imaging Sciences*, vol. 7, no. 1, pp. 212–238, 2014, ISSN: 1936-4954. DOI: 10.1137/130920058.

[170] G. Peyré, "The Numerical Tours of Signal Processing," *Advanced Computational Signal and Image Processing IEEE Computing in Science and Engineering*, vol. 13, no. 4, pp. 94–97, 2011.

COLOPHON

This document was typeset using the `classicthesis` template developed by André Miede and Ivo Pletikosić. The style was inspired by Robert Bringhurst's seminal book on typography "*The Elements of Typographic Style*". The fonts used are `Linux Libertine` for prose, and `newtxmath` for mathematics.

Final Version as of June 20, 2019 ().